NON-LINEAR FINITE ELEMENT ANALYSIS OF ADHESIVELY BONDED JOINTS IN COMPOSITE STRUCTURES : A FRACTURE MECHANICS APPROACH

A Thesis Submitted
in Partial Fulfilment of the Requirements
for the Degree of

DOCTOR OF PHILOSOPHY

By

SURESH CHANDRA PRADHAN

to the

DEPARTMENT OF AEROSPACE ENGINEERING

INDIAN INSTITUTE OF TECHNOLOGY, KANPUR

SEPTEMBER, 1994

POST GRADUATE OFFICE
Submitted on 8/9/94

CERTIFICATE

It is certified that the work contained in the thesis entitled "NON-LINEAR FINITE ELEMENT ANALYSIS OF ADHESIVELY BONDED JOINTS IN COMPOSITE STRUCTURES : A FRACTURE MECHANICS APPROACH", by **Suresh Chandra Pradhan**, has been carried out under our supervision and that this work has not been submitted elsewhere for a degree

September, 1994

Prof N N Kishore
Department of Mechanical Engineering
Indian Institute of Technology, Kanpur

Prof N.G R. Iyengar
Department of Aerospace Engineering
Indian Institute of Technology, Kanpur

- 6 MAY 1996

RY

Acc. No. A. 121426

AE-1994-D-PRA-NON

A121426

POST GRADUATE OFFICE
Submitted on 30/9/94

CERTIFICATE

It is certified that the work contained in the thesis entitled "NON-LINEAR FINITE ELEMENT ANALYSIS OF ADHESIVELY BONDED JOINTS IN COMPOSITE STRUCTURES : A FRACTURE MECHANICS APPROACH", by **Suresh Chandra Pradhan**, has been carried out under our supervision and that this work has not been submitted elsewhere for a degree.

September, 1994

Prof N N. Kishore
Department of Mechanical Engineering
Indian Insititute of Technology, Kanpur

Prof N.G R Iyengar
Department of Aerospace Engineering
Indian Insititute of Technology, Kanpur

Acknowledgements

I have great pleasure in expressing my sincere gratitude to **Prof. N. G. R. Iyengar** and **Prof. N. N. Kishore** for their supervision, invaluable guidance, help and support. I am indebted to both of them. A special note of appreciation is extended to Mrs. Iyengar and Mrs. Kishore for their affection and encouragement.

I am grateful to Indian Space Research Organisation (ISRO) for sponsoring the present work under ISRO Respond Scheme. Financial supports received from Council of Scientific and Industrial Research (CSIR) New Delhi, ISRO and International Society of Photo-Optical Instrumentation Engineers (SPIE) to participate in International Conference on 'Adhesive Engineering' at San Deigo, California, U.S.A. during July 1993, are also gratefully acknowledged.

A personal note of gratitude goes to Dr. A.R. Acharya and Prof. N. Satyamurthy for their help and encouragement. A special note of gratitude goes to Profs. C.A. Fellipa, Ashwini Kumar, Prashant Kumar, A.S.D. Wang and D. Yadav for their technical help. A particular note of appreciation goes to the following Profs. R.D. Adams, H. Aglan, H.L. Groth, B. Dattaguru, V.K. Kinra, K.M. Liechti, J.K. Spelt, J.N. Reddy and J.D. Whitcomb for their help.

A special note of obligation goes to Profs. E. Reissner and S. Nemat-Nasser of University of California at San Deigo (UCSD) for the fruitful discussions, suggestions and encouragement. I owe, S. Prakash, Pradeep Jain, Vinod Sharma

and Dr. Sudhir Jain a personal debt of gratitude for their love, affection, care, help and hospitality during San Deigo trip

I am thankful to the Heads of Aerospace and Mechanical Engineering departments, Profs. Krishna Kumar and S. G. Dhande, respectively for their help and support.

The cooperation of the office staff of Aerospace Engineering, experimental stress analysis (ESA) Laboratory and Mr. V.K. Jain of ACMS, is cheerfully appreciated. My sincere thanks go to software engineers and operating staff of Computer Center and also to staff of Central Library for their help and cooperation. It has been a pleasure for me to work with Counseling Service (PG Wing) as the student coordinator and with Computer Centre as the students' representative.

My sincere thanks are to Dr. Raju Sethuraman, Dr. S. Mittal, Sri S.V. Sharma, Ashish, Jaleel, A.V. Rao, Sridhar and Deepak for their help, support and encouragement at various stages of this work. I am thankful to all my friends and colleagues for their help and encouragement. These include Dr. Gajbir Singh, Dr. C.A. Shankar, Salim, Ravi, Siva, Igi, Himansu, Srini, Manoj, Ashok, Mishra, Mohapatra, Kalyan Raman, Verma, Datta, Bajpai, Venkatesh, Vinod, Krishna Mohan, P. Manmohan, Venugopal, Venkat, Dr. Ravindra, Jagirdar, Jayatirtha, Harish, Nandy and many more.

Finally, i express my sincere gratitude to my beloved parents, relatives, well wishers and all the persons, who rendered their support and cooperation in making the cherished dream of Ph. D. a reality.

Dedicated to my Teachers

It is the peculiarity of knowledge that those who really thirst for it always get it

– Richard Jefferies

Synopsis

Joints are inevitable in structural applications. Adhesively bonded joints are being preferred to mechanical fasteners because of distinct advantages they offer, such as uniform stress distribution, stiff connection, smooth surface contour, sealing against corrosion, excellent fatigue properties, no fretting problems, relatively light weight, damage tolerance and stealthiness.

Use of composite materials in structural applications is also growing because of their excellent properties like high strength to weight ratio, stiffness to weight ratio, dimensional stability, electrical insulation, smooth outer surface etc. Composite materials provide a scope to the designer to tailor the material and/or structure to suit the applications. In addition, many complicated structural parts can easily be moulded using composites. Adhesive joints are found to be more suitable with composite materials particularly in case of the fibre reinforced plastics. With the development of various structural adhesives, these joints are being employed in a wide variety of structural applications ranging from aerospace, automobile components to those found in microelectronic components. In the primary adhesively bonded structures technology (PABST) programme, an expert group is working to promote the use of bonded structures in aircraft industry. Some of the important applications of adhesively bonded structural members are aircraft's rudder floor panel, engine cowling, elevator and flap, ceramic tyle of re-entry vehicles, integrated fuel tank, composite propeller blade, helicopters, launch vehicle attachment (LVA) ring, collapsible tube mast. For structural integrity, it is, therefore, important to assess their

strengths and durability a priori so that joints could be designed in a rational manner resulting in an improved strength and more reliable structure.

From a critical review of literature it is observed that polymeric adhesive materials generally exhibit material non-linearities (elasto-plastic and elasto-visco-plastic behaviour). In view of the versatility of finite element method this seems to be the best mathematical tool to analyse the bonded joints in presence of non-linearities. It is also a convenient tool for associated parametric studies. Furthermore, fracture mechanics approach results in better mathematical model to predict the joint strength. Most of these investigations reported are either purely theoretical or computational and very few have experimental data to support their results. Further, from a comparison of results of various researchers it is observed that there is a large amount of scatter in the results[1,2]. Thus, there is a need for a better technique with a suitable mathematical model representing crack propagation for the analyses of adhesively bonded joints. It is also necessary to conduct simple experiments to determine the joint strength and compare them with those obtained from the finite element analysis. This will be complementary to the results obtained by the finite element technique.

The thesis includes the studies of adhesive joint based on (i) linear elastic analysis (ii) elasto-plastic analysis and (iii) elasto-visco-plastic analysis. The adherend and adhesive materials are considered to be linear and non-linear, respectively. In all the above cases detailed parametric study is carried out. Experiments have been conducted on specially designed specimens to determine the fracture parameters and the strength of the joints.

In Chapter 1, various types of prevalent adhesively bonded joints are discussed. This Chapter provides an overview of the joints, composite materials, non-linear finite element analysis, fracture mechanics approach and experiments to determine the joint strength. Adams and Wake[3] have presented an excellent

review of the analyses, experiments and designs of these joints carried out by several researchers. Review of relevant literature carried out in this Chapter, includes (i) linear elastic analysis, (ii) material (elasto-plastic and elasto-visco-plastic) and geometrically non-linear analysis, (iii) fracture mechanics, (interface failure, fracture, delamination etc.), (iv) parametric study, (v) environmental effects, (vi) testing of bond quality and (vii) design of adhesively bonded joints (single lap, double lap, butt, scarf, tubular etc). The Chapter also summerises the various findings so far, the lacunae and the motivation to carry out the present research work.

In Chapter 2, the linear elastic finite element analysis of the joints, the modelling of crack opening is presented. Automatic mesh generation is adapted for the analysis of the joint. Chebyshev's function is employed to refine the mesh at the critical zones. Stress distribution in the adhesive across the overlap of single lap joint[4] is examined in detail. Stresses and strains distributions across the overlap and through the adhesive thickness of stepped lap joint[5] are also looked into. These results shows good agreement with corresponding results from the literature[4,5]. Crack is modelled with paired nodes. Employing Irwin's crack closure technique strain energy release rates are computed. A single edge notch (SEN) specimen is considered to determine the minimum refinement required to obtain reasonably accurate (close to exact value) strain energy release rate. Further, a cracked lap shear (CLS) specimen[6] is considered to validate the finite element code computing strain energy release rates.

Parametric study of the double lap joint is also presented in this Chapter. Seven possible fracture criteria are considered and the corresponding predicted failure loads are compared. Strengths predicted with the criterion ($G_I + G_{II} \geq G_{IC} + G_{IIC}$) are found to be closer to those obtained from the experiments than with the rest of the criteria. Hence, this criterion is considered in the rest of the analyses. Effect of use of the same and different adherend materials (stiffness) on joint strength are examined. Effect of equal and unequal adherends

(thickness) on joint strength is also investigated Response of the joint of metal to metal, composite to metal and composite to composite is discussed Effects of various parameters on the strength of composite to composite joint have been looked into These parameters include stacking sequence, boundary conditions, crack location, adhesive material properties, overlap length and adhesive thickness on joint strength are studied Some of the conclusions drawn on the basis of this study are

- Use of Chebyshev's function is found to be effective for automatic mesh generation with various refinements at critical zones
- In case of SEN specimen, with 2688 elements and proper mesh refinement near the crack-tip, error estimated in the value of fracture parameter is less than 1 6 percent
- Result based on two dimensional finite element analysis with fracture mechanics approach agreed well with the experimental result for CLS specimen and the difference is less than 2 7 percent
- Introduction of 0° ply in the immediate neighbourhood of adhesive results in a stronger joint

Elasto-plastic analysis of the adhesively bonded joint is presented in Chapter 3 The finite element model, flow chart and the algorithm for elasto-plastic analysis are also included Finite element code is validated on the cantilever beam problem[7] Spread of plastic zones based on elasto-plastic analysis for various boundary conditions and crack location are presented Effects of stacking sequence, adhesive material properties, overlap length and adhesive thickness on the joint strength are investigated

- The elastic analysis predicts a lower failure load as compared to the elasto-plastic analysis This might be due to the peak stresses of elasto-plastic analysis are reduced

Visco-plastic analysis of the adhesive joint is presented in Chapter 4 Finite element model, flow chart and the algorithm employed for the analysis are included Finite element code developed is validated on the perforated plate problem[8] The visco-plastic stress analysis results show good agreement with those available in literature for a single lap joint and a stepped lap joint Effects of stacking sequence, fracture toughness of the adhesive, overlap length and thickness of the adhesive on the joint strength are examined

- The elastic analysis predicts a lower failure load as compared to the visco-plastic analysis This might be due to the peak stresses of visco-plastic analysis are reduced

The evaluation of fracture properties requires the knowledge of critical strain energy release rates (fracture toughnesses) in mode I and II In Chapter 5, some simple experiments are performed to evaluate these values are discussed Joint strengths are measured from these experiments and are observed to be close to those obtained from the linear elastic finite element analysis Various possible fracture criteria are considered Among all possible fracture criteria, $(G_I + G_{II} \geq G_{IC} + G_{IIC})$ is found to be most appropriate

The thesis concludes with Chapter 6 Results and discussion of the present work are presented in this Chapter Some of the general conclusions drawn on the basis of the present work are

- The finite element approach with paired nodes modelling the crack provides a simple computational tool to predict joint failure However, fine grids

near the crack-tip are necessary for accurate estimation of strain energy release rates

- High Young's modulus of the adhesive, large overlap length and small adhesive thickness individually results in stronger bonded joint
- A proper choice of layup sequence results in an efficient bonded joint
- The computed bond strengths of double lap joint based on finite element analysis with fracture mechanics approach and those determined from the experiment show good comparison
- The finite element code developed predicts linear and non-linear behaviour of the adhesive lap joints fairly accurate[4,5]
- The elastic analysis predicts a lower failure load as compared to the elasto-plastic and elasto-visco-plastic analyses This might be due to the peak stresses of non-linear analysis are reduced
- The results obtained from parametric study are similar for linear elastic, elasto-plastic and elasto-visco-plastic analyses

Limitations of the present analyses are also indicated Finally few suggestions are made for further extension of the present work

References

1 Johnson, W S (1987), Stress analysis of the cracked-lap-shear specimen An ASTM Round-Robin, Journal of Testing and Evaluation, **15** (6) 303–324

2 Davies, P, Kausch, H. H, Williams, J G et al (1992), Round-robin interlaminar fracture testing of carbon-fibre-reinforced epoxy and PEEK composites, Composite Structures, **43** (2) 129–136

3 Adams, R D and Wake, W C (1984), Structural adhesive joints in engineering, Elsevier Applied Science Publishers London and New York

4 Hiregoudar, S (1993), Viscoplastic and geometric nonlinear finite element analysis of adhesively bonded lap joint, M Sc Thesis Report, Department of civil Engineering, Indian Institute of Science, Bangalore, India

5 Su, N and Mackie, R I, (1993), Two-dimensional creep analysis of structural adhesive joints, International Journal of Adhesion and Adhesives, **13** (1) 33–40

6 Fernlund, G and Spelt, J K (1991), Failure load prediction of structural adhesive joints part 2 experimental study, International Journal of Adhesion and Adhesives, **11** (4) 221–227

7 Zienkiewicz, O C, Valliappan, S and King, I S (1969), Elasto-plastic solutions of engineering problems 'initial stress', finite element approach, International Journal for Numerical Methods in Engineering, **1** 75–100

8 Zienkiewicz, O C, Owen, D R J and Cormeau, I C (1974), Analysis of visco-plastic effects in pressure vessels by the finite element method, Nuclear Engineering and Design, **28** 278–288

List of Publications

Following publications have come out of the present work

1 Pradhan, S C, Iyengar, N G R and Kishore, N N, Elasto-Plastic Analysis of Adhesive Bonded Joint, Mechanics Research Communication, Vol **20**, No 2, pp 155–163, 1993

2 Pradhan, S C, Iyengar, N G R and Kishore, N N, Parametric Study of Interfacial Debonding in Adhesively Bonded Composite Joints, Composite Structures, Vol **29**, No 1, pp 119-125, 1994

3 Pradhan, S C, Iyengar, N G R and Kishore, N N, Finite Element Analysis of Crack Growths in Adhesively Bonded Joints, accepted for publication in International Journal of Adhesion and Adhesives, 1994

4 Pradhan, S C, Kishore, N N, and Iyengar, N G R, Failure Analysis of Adhesively Bonded Composite Joint An Elasto-Plastic Approach, Proceedings of SPIE - The International Society of Optical and Instrument Engineering, International symposium on Adhesive Engineering, July 11–16, 1993, San Diego, California, U S A, Vol **1999**, pp 238–247

5 Pradhan, S C, Iyengar, N G R and Kishore, N N, Finite Element Analysis of Interfacial Debondings in Adhesively Bonded Composite Joints, Proceedings of national symposium on Structural Engineering and National Development, February, 26–28, 1993, I I T-Kanpur, India, pp 181–189

6 Pradhan, S C, Iyengar, N G R and Kishore, N N, Elasto-Plastic Analysis of Adhesively Bonded Joints in Composite Structures A Crack Closure Technique, Proceedings of national symposium Composites '94 on Composites technology and Applications, February 17–18, 1994, V S S C, Trivandrum, India, Vol **1**, pp 171–179

7 Pradhan, S C, Kishore, N N, and Iyengar, N G R, Failure Analysis of Composite Lap Joint An Elasto-Plastic Approach, Proceedings of Indo-German Workshop on Fracture Mechanics, March 28–31, 1994, I I Sc Bangalore, India, pp 130–135

Contents

Acknowledgements v

Synopsis ix

List of Publications xvi

List of Symbols xxiv

List of Tables xxviii

List of Figures xxxii

1 Introduction 1

1 1 Motivation 1

1 2 Review of literature 4

1 2 1 Elastic analysis 4

1 2 2 Non-linear (material) analysis 10

1 2 3 Non-linear (geometrical) analysis 17

1 2 4 Fracture mechanics approach 18

1 2 5 Parametric study 25

1 2 6 Environmental effects 28

1 2 7 Quality of adhesive bonding 30

1 2 8 Design 32

1 3 Objectives of the present work 33

1 4 Layout of the thesis 34

2 Elastic analysis 39

2 1 Introduction 39

2 2 Formulation 40

2 3 Validation of finite element code 46

2 3 1 Single lap joint 46

2 3 2 Stepped lap joint 47

2 4 Validation of crack closure technique 48

2 4 1 Single edge notch specimen 48

2 4 2 Cracked lap shear specimen 49

2 5 Mesh refinement 51

2 6 Parametric study 51

2 6 1 Crack location 52

2 6 2 Thickness and Young's modulus of the adherend 54

2 6 3 Stacking sequence 55

2 6 4 Young's modulus of adhesive 56

2 6 5 Overlap length 57

2 6 6 Adhesive thickness 59

2 7 Conclusions 61

3 Elasto-plastic analysis 116

3 1 Introduction 116

3 2 Formulation 117

3 2 1 Constitutive relations 117

3 2 2 Finite element technique 121

3 3 Validation of computer code 124

3 4 Growth of plastic zone 124

3 4 1 Boundary conditions 124

3 4 2 Crack propagation 125

3 5 Parametric study 125

3 5 1 Stacking sequence 126

3 5 2 Fracture toughness of adhesive 127

3 5 3 Overlap length 128

3 5 4 Adhesive thickness 128

3 6 Conclusions 128

4 Visco-plastic analysis 147

4 1 Introduction 147

4 2 Formulation 148

4 2 1 Finite element technique 152

4 3 Validation of computer code 154

4 3 1 Perforated plate 155

4 3 2 Single lap joint 155

4 3 3 Stepped lap joint 156

4 4 Parametric study 156

4.4.1 Stacking sequence 157

4.4.2 Fracture toughness of adhesive 158

4.4.3 Overlap length 158

4.4.4 Adhesive thickness 159

4.5 Conclusions 159

5 Experiments 182

5.1 Introduction 182

5.2 Strain energy release rate in mode I 183

5.3 Strain energy release rate in mode II 190

5.4 Strength of adhesively bonded joints 192

5.5 Conclusions 192

6 General Conclusions 199

6.1 Results and discussion 199

6.1.1 Comparison of results 199

6.2 Limitations of the present work 202

6.3 Suggestions for future work 203

References **205**

List of Symbols

A	new area created during crack growth
A_1, A_2	constants for a given specimen
$[B]$	elastic strain displacement matrix
$[B_0]$	elastic strain displacement matrix
$[B_{NL}]$	strain displacement matrix, non-linear component
$[B^n]$	strain displacement matrix for n^{th} iteration
C	compliance
C_0	prescribed constants
C^n	matrix
$[D]$	elastic constitutive relations
$[D_{ep}]$	elasto-plastic constitutive relations
$[D_{vp}]$	visco-plastic constitutive relations
E	Young's modulus
E_l	longitudinal modulus of fibre reinforced
E_T	stiffness of the adherend
E_S	stiffness of the adhesive
E_t	tangent modulus of fibre reinforced
F	flow rule expression
F_x, F_y, F_z	components of nodal forces in x,y and z directions
G	total strain energy release rate
G_C	critical strain energy release rate of standard adhesive (epoxy)
G'_C	assumed critical strain energy release rate of adhesive under consideration

G_I	strain energy release rate in mode I
G_{IC}	critical strain energy release rate in mode I
G_{II}	strain energy release rate in mode II
G_{IIC}	critical strain energy release rate in mode II
G_{III}	strain energy release rate in mode III
G_{cr}	strain energy release rate corresponding to a_{cr}
G_e	elastic shear modulus
G_{lt}	shear modulus of fibre reinforced composite
G_p	plastic shear modulus
G_x	strain energy release rate corresponding to a_x
G_{xy}	shear modulus
G_ϵ	strain energy release rate for plane strain
G_σ	strain energy release rate for plane stress
H	proportionality constant
$\bar{H}$	potential energy
H^n	matrix
I	second moment of area of cross section of the beam
J	J integral
$J_2^{'}$	second invariant of deviatoric stresses
$[K]$	elastic stiffness matrix
K_I	stress intensity factor in mode I
$[K^n]$	stiffness matrix in n^{th} iteration
L	length of the specimens
L_O	overlap length
L_t	total length
M	prescribed constants
N	prescribed constants
P	load
P_C	critical load corresponding to the fracture toughness G_C
P_f	failure load

$\bar{U}$	elastic strain energy stored in the body
$\hat{U}$	relative displacements between the mating crack surfaces
W	width of SEN, DCB and ENF specimens
$\bar{W}$	work done by the external forces
a	crack length
a_{cr}	critical crack length
a_x	crack length corresponding to G_I equals to G_{II}
$\hat{a}$	flow vector
$\mathbf{e}$	$\frac{E_s}{E_r}$
f^n	vector of equivalent nodal loads due to applied surface traction, body force, thermal loads etc
$\mathbf{g}$	$\frac{G_C'}{G_C}$
h	semi–height of the specimens
$\mathbf{l}$	$\frac{L_o}{L_t}$
$\mathbf{t}$	$\frac{t_s}{t_r}$
t_r	thickness of the adherend
t_s	thickness of the adhesive
u, v, w	components of nodal displacements in x,y and z directions
ΔW	work done to close the crack opening
Δa	incremental crack length
Δf^n	change in load during time interval Δt_n
Δt_n	time in seconds in n^{th} iteration
Δv	incremental displacement
$\{\Delta\delta\}$	incremental displacement vector
$\{\Delta\epsilon\}$	incremental strain vector
$\Delta\psi_{ep}$	elasto-plastic residual or out–of–balance force
$\Delta\psi_{vp}$	incremental pseudo–loads
$\{\Delta\sigma\}$	incremental stress vector

Ω	volume
Θ	prescribed constants
$\{\delta\}$	displacement vector
$\{\epsilon\}$	strain vector
ϵ_{ve}	visco-elastic strain
$\{\dot{\epsilon}\}$	strain rate vector
$\dot{\epsilon}_{ss}$	steady state strain rate
$\dot{\epsilon}_{ve}$	visco-elastic strain rate
$\dot{\epsilon}_{vp}$	visco-plastic strain rate
$\dot{\epsilon}_{vep}$	visco-elasto-plastic strain rate
$\bar{\dot{\epsilon}}_{vp}$	effective visco-plastic strain rate
γ	fluidity parameter
γ_{xy}	fluidity parameter in pure shear mode
κ	hardening parameter
λ	proportionality constant
ν	Poisson's ratio
ν_{lt}	Poisson's ratio of fibre reinforced composite
Φ	function controlling visco-plastic flow rate
ψ	residual or out–of–balance force
$\{\sigma\}$	stress vector
σ_0	yield stress
$\sigma_1, \sigma_2, \sigma_3$	principal stresses
$\sigma_x, \sigma_y, \sigma_z$	normal stresses
$\{\bar{\sigma}\}$	effective/generalised/equivalent stress
$\hat{\sigma}$	surface stress distribution
τ	pure shear stress
τ_0	yield stress in pure shear mode
$\tau_{xy}, \tau_{yz}, \tau_{zx}$	shear stresses

List of Tables

2 1 Seven fracture criteria considered in the finite element analysis 63

2 2 Specifications of single lap joint (Hiregoudar, 1993) 64

2 3 Specifications of stepped lap joint (thick adherend shear test specimen of Su and Mackie, 1993) 65

2 4 Physical dimensions and material properties of SEN specimen (Figure 2 15) 65

2 5 Physical dimensions and material properties of CLS specimen (Figure 2 16) 66

2 6 Specifications of the adhesively bonded joint (Figure 2 18) 67

2 7 Specifications of double lap joint 68

2 8 Description of eight different crack locations and their growth direction (Figure 2 20c) 69

2 9 Computed critical strain energy release rates for two different types of boundary conditions and eight different crack locations (Figure 2 20a-c) 69

2 10 Material properties of metal adherends 69

2 11 Material properties of composite adherends 70

2 12 Specifications of double lap joint 71

2 13 Computed failure loads in N/mm for joints of aluminium and various metals 72

2 14 Computed failure loads in N/mm for joints of steel and various metals 73

2 15 Computed failure loads in N/mm for joints of carbon fibre reinforced plastic (CFRP) composite and various metals 74

2 16 Computed failure loads in N/mm for joints of carbon fibre reinforced plastic (CFRP) composite and various fibre reinforced composites 75

2 17 Computed failure loads (P_f's) for various combinations of layups in different crack growths 76

2 18 Predicted failure loads of adhesively bonded joints with different Young's moduli of the adhesives (L_o/L_t= 1/2, t_s/t_r= 1/5, no of elements employed = 1816) 76

2 19 Computed failure loads (P_f's) for various adhesive stiffnesses and different combinations 77

2 20 Predicted failure loads of adhesively bonded joints with different overlap lengths (t_s/t_r= 1/5, E_s/E_r= 1/20, no of elements employed = 1816) 77

2 21 Computed failure loads (P_f's) for various overlap lengths and laminae combinations 78

2 22 Predicted failure loads of adhesively bonded joints with different thicknesses of the adhesives (L_o/L_t= 1/2, E_s/E_r= 1/20, no of elements employed = 3376) 78

2 23 Computed failure loads (P_f's) for various adhesive thicknesses and laminae combinations 79

3 1 Specifications of double lap joint 130

3 2 Specifications of double lap joint 130

3 3 Specifications of double lap joint 131

3 4 Computed failure loads (P_f's) for various g (= G_C'/G_C) values and different laminae combinations 132

3 5 Computed failure loads (P_f's) for various l (= L_o/L_t) values and different laminae combinations 132

3 6 Computed failure loads (P_f's) for various t (= t_s/t_r) values and different laminae combinations 133

4 1 Specifications of the perforated plate problem (Zienkiewicz, et al , 1974) 161

4 2 Specifications of single lap joint (Hiregoudar, 1993) 162

4 3 Specifications of stepped lap joint (thick adherend shear test specimen) of Su and Mackie (1993) 163

4 4 Specifications of double lap joint 164

4 5 Computed failure loads (P_f's) for various **g** (= G_C'/G_C) values and different laminae combinations 165

4 6 Computed failure loads (P_f's) for various **l** (= L_o/L_t) values and different laminae combinations 165

4 7 Computed failure loads (P_f's) for various **t** (= t_s/t_r) values and different laminae combinations 166

5 1 Experimental results for mode I critical strain energy release rate G_{IC} 193

5 2 Experimental results for mode II critical strain energy release rate G_{IIC} 193

5 3 Various dimensions of double lap joint specimens (Figure 5 5) 194

5 4 Comparison of experimental and finite element technique (elastic analysis) results for various fracture criteria 195

6 1 Comparison of results obtained from linear elastic, elasto-plastic and elasto-visco-plastic analyses 204

List of Figures

1 1 Joints of equivalent load capacity with various fastenings, (**a**) overlap 5 in, resorcinol-formaldehyde adhesive joint (**b**) overlap 9 in, four $\frac{1}{2}$ in bolts (**c**) overlap 11 in, two $2\frac{1}{2}$ in split ring connectors and one $\frac{1}{2}$ in bolt and (**d**) overlap $12\frac{1}{2}$ in, twenty-four 4 in 7 gauge nails driven in double shear into drilled holes 38

1 2 Schematics of some common adhesively bonded joints (**a**) single lap (**b**) double lap (**c**) butt with straps (**d**) stepped (**e**) scarf and (**f**) tubular lap joints 38

2 1 Finite element mesh at crack-tip illustrating the crack closure technique 79

2 2 Schematic representation of crack closure technique 80

2 3 Flow chart of linear elastic finite element analysis for crack growth 81

2 4 Variation of failure load and crack length for different possible fracture criteria (Table 2 1) 82

2 5 Schematic of single lap joint considered by Hiregoudar (1993) and the present finite element mesh consists of 1816 elements with an enlarged view of the edge region 83

2 6 Comparison of stress distributions along the overlap length of the single lap joint considered by Hiregoudar (1993) 84

2 7 Schematic of the stepped lap joint (thick adherend shear test TAST specimen of Su and Mackie, 1993) and the finite element mesh with an enlarged view of the stepped portion 85

2 8 Comparison of stress distribution along the overlap length at interface of adherend and adhesive of the stepped lap joint 86

2 9 Comparison of strain distribution along the overlap length at interface of adherend and adhesive of the stepped lap joint 87

2 10 Comparison of stress distribution along the overlap length at midline of adhesive of the stepped lap joint 88

2 11 Comparison of strain distribution along the overlap length at midline of adhesive of the stepped lap joint 89

2 12 Normal stress σ_x, and strain ϵ_x, distributions along the overlap length and across the adhesive thickness of the stepped lap joint 90

2 13 Normal stress σ_y, and strain ϵ_y, distributions along the overlap length and across the adhesive thickness of the stepped lap joint 91

2 14 Shear stress and strain distributions along the overlap length and across the adhesive thickness of the stepped lap joint 92

2 15 Error estimation in strain energy release rate for single edge notch (SEN) specimen and the finite element mesh consists of 1360 elements 93

2 16 Schematic representation of cracked lap shear (CLS) specimen under four-point bending and the finite element mesh consists of 2180 elements 94

2 17 Variation of strain energy release rates with crack length for plane stress and plane strain models of the cracked lap shear (CLS) specimen 95

2 18 Schematic of adhesively bonded double lap joint and the finite element mesh showing the crack location at '3' 96

2 19 Comparison of strain energy release rates for three different refined meshes 97

2 20 Schematic of (a) free edge boundary condition (in double lap joint), (b) constrained edge boundary condition and (c) eight different crack locations 98

2 21 Variation of strain energy release rate with crack length for crack growths at eight different locations (Figure 2 20c) for free side type boundary condition 99

2 22 Variation of strain energy release rate with crack length for crack growths at eight different locations (Figure 2 20c) for constrained side type boundary condition 100

2 23 Schematic of double lap joint of composite adherends [1324_S, 1324_S] with a magnified section view 101

2 24 Variation of failure load with crack length for symmetric combinations of $0°, 45°, 90°$ and $-45°$ layups in composite adherends, and for crack location at '3' 102

2 25 Variation of failure load with crack length for various symmetric combinations of 0°, 45°, 90° and −45° layups in composite adherends, with 0° layups being present in the immediate neighbourhood of the adhesive and, for crack location at '3' 103

2 26 Variation of failure load with crack length for $[0^\circ_{4S}, 0^\circ_{4S}]$, $[90^\circ_{4S}, 90^\circ_{4S}]$, $[0^\circ_{4S}, 90^\circ_{4S}]$, $[90^\circ_{4S}, 0^\circ_{4S}]$ laminate pairs for crack location at '1' 104

2 27 Variation of failure load with crack length for $[0^\circ_{4S}, 0^\circ_{4S}]$, $[90^\circ_{4S}, 90^\circ_{4S}]$, $[0^\circ_{4S}, 90^\circ_{4S}]$, $[90^\circ_{4S}, 0^\circ_{4S}]$ laminate pairs for crack location at '3' 104

2 28 Variation of failure load with crack length for $[0^\circ_{4S}, 0^\circ_{4S}]$, $[90^\circ_{4S}, 90^\circ_{4S}]$, $[0^\circ_{4S}, 90^\circ_{4S}]$, $[90^\circ_{4S}, 0^\circ_{4S}]$ laminate pairs for crack location at '4' 105

2 29 Variation of failure load with crack length for most likely interface edge crack growths in CFRP unidirectional (0°_{4S} and 90°_{4S}) laminate pairs 105

2 30 Variation of total strain energy release rate with crack length for crack initiation at location '3' and different e (= E_s/E_r) values in aluminium to aluminium joints 106

2 31 Variation of failure load with crack length for crack initiation at location '3' and different e (= E_s/E_r) values in $[0^\circ_{4S}, 0^\circ_{4S}]$ CFRP laminates 107

2 32 Variation of failure load with crack length for crack initiation at location '3' and different e (= E_s/E_r) values in $[1324_S, 1324_S]$ (optimal) CFRP laminates 108

2 33 Variation of total strain energy release rate with crack length for crack initiation at location '3' and different l (= L_o/L_t) values in aluminium to aluminium joints 109

2 34 Variation of failure load with crack length for crack initiation at location '3' and different l (= L_o/L_t) values in $[0^\circ_{4S}, 0^\circ_{4S}]$ CFRP laminates 110

2 35 Variation of failure load with crack length for crack initiation at location '3' and different l (= L_o/L_t) values in $[1324_S, 1324_S]$ (optimal) CFRP laminates 111

2 36 Variation of total strain energy release rate with crack length for crack initiation at location '3' and different t (= t_s/t_r) values in aluminium to aluminium joints 112

2 37 Variation of total strain energy release rate with crack length for crack initiation at location '3' and different t (= t_s/t_r) values in aluminium to aluminium joints with very fine mesh refinement 113

2 38 Variation of failure load with crack length for crack initiation at location '3' and different t (= t_s/t_r) values in $[0^\circ_{4S}, 0^\circ_{4S}]$ CFRP laminates 114

2 39 Variation of failure load with crack length for crack initiation at location '3' and different t (= t_s/t_r) values in $[1324_S, 1324_S]$ (optimal) CFRP laminates 115

3 1 Flow chart of elasto-plastic finite element analysis 134

3 2 Schematic of convergence of failure loads for various tolerance values 135

3 3 Schematic of hardening parameter κ 135

3 4 Comparison of deflections at location 'C' of cantilever beam (Zienkiewicz, et al , 1969) 136

3 5 Boundary conditions and the corresponding growth of plastic zones in the adhesive material 137

3 6 Schematic of adhesively bonded double lap joint and the finite element mesh showing the crack location '3' 138

3 7 Growth of plastic zone with crack propagation 139

3 8 Variation of failure load with crack length for crack initiation at location '3' and different **g** (= G_C'/G_C) values in $[0°/0°/\overset{90°}{0°}/\overset{90°}{0°}]_S$ CFRP laminates 139

3 9 Variation of failure load with crack length for crack initiation at location '3' and different **g** (= G_C'/G_C) values in $[0°/45°/90°/-45°]_S$ (optimal) CFRP laminates 140

3 10 Variation of failure load with crack length for crack initiation at location '3' and different **g** (= G_C'/G_C) values in $[0°/0°/\overset{0°}{90°}/\overset{0°}{90°}]_S$ CFRP laminates 141

3 11 Variation of failure load with crack length for crack initiation at location 3 and different **l** (= L_o/L_t) values in $[0°/0°/0°/0°]_S$ CFRP laminates 142

3 12 Variation of failure load with crack length for crack initiation at location 3 and different **l** (= L_o/L_t) values in $[0°/45°/90°/-45°]_S$ (optimal) CFRP laminates 143

3 13 Variation of failure load with crack length for crack initiation at location 3 and different l (= L_o/L_t) values in $[0°/0°/90°/90°]_S$ CFRP laminates 144

3 14 Variation of failure load with crack length for crack initiation at location '3' and different t (= t_s/t_r) values in $[0°/0°/0°/0°]_S$ CFRP laminates 144

3 15 Variation of failure load with crack length for crack initiation at location '3' and different t (= t_s/t_r) values in $[0°/45°/90°/-45°]_S$ (optimal) CFRP laminates 145

3 16 Variation of failure load with crack length for crack initiation at location '3' and different t (= t_s/t_r) values in $[0°/0°/90°/90°]_S$ CFRP laminates 146

4 1 Adhesive material models (a) the three parameter solid model, (b) the Bingham visco-plastic model, and (c) the five parameter viscoelastic-viscoplastic model 166

4 2 Flow chart of visco-plastic finite element analysis 167

4 3 Schematic of perforated plate under uniform tension (Zienkiewicz, et al , 1974) showing the plastic element $\mathcal{P}$ and the finite element mesh of the plate 168

4 4 Variation of stress with time for plastic element $\mathcal{P}$ of the perforated plate (Figure 4 3) 169

4 5 Schematic of single lap joint considered by Hiregoudar (1993) 169

4 6 Comparison of elastic and visco-plastic stress distribution along the overlap length of single lap joint (Hiregoudar, 1993) 170

4 7 Comparison of peel stress distribution along the overlap length of single lap joint (Hiregoudar, 1993) 171

4 8 Schematic of the stepped lap joint (thick adherend shear test TAST specimen considered by Su and Mackie, 1993) 171

4 9 Comparison of shear stress and strain distribution along the overlap length at interface of adherend and adhesive of the stepped lap joint 172

4 10 Schematic of adhesively bonded double lap joint and the finite element mesh showing the crack location '3' 173

4 11 Variation of failure load with crack length for crack initiation at location '3' and different **g** (= G_C'/G_C) values in $[0°/0°/0°/0°]_S$ CFRP laminates 174

4 12 Variation of failure load with crack length for crack initiation at location '3' and different **g** (= G_C'/G_C) values in $[0°/0°/90°/90°]_S$ CFRP laminates 175

4 13 Variation of failure load with crack length for crack initiation at location '3' and different **g** (= G_C'/G_C) values in $[0°/45°/90°/-45°]_S$ (optimal) CFRP laminates 176

4 14 Variation of failure load with crack length for crack initiation at location '3' and different **l** (= L_o/L_t) values in $[0°/0°/0°/0°]_S$ CFRP laminates 177

4 15 Variation of failure load with crack length for crack initiation at location '3' and different I (= L_o/L_t) values in $[0°/0°/90°/90°]_S$ CFRP laminates 177

4 16 Variation of failure load with crack length for crack initiation at location '3' and different I (= L_o/L_t) values in $[0°/45°/90°/-45°]_S$ (optimal) CFRP laminates 178

4 17 Variation of failure load with crack length for crack initiation at location '3' and different t (= t_s/t_r) values in $[0°/0°/0°/0°]_S$ CFRP laminates 179

4 18 Variation of failure load with crack length for crack initiation at location '3' and different t (= t_s/t_r) values in $[0°/0°/90°/90°]_S$ CFRP laminates 180

4 19 Variation of failure load with crack length for crack initiation at location '3' and different t (= t_s/t_r) values in $[0°/45°/90°/-45°]_S$ (optimal) CFRP laminates 181

5 1 Load-displacement behaviour for a cracked body under constant load and constant displacement 196

5 2 Double cantilever beam (DCB) specimen under mode I loading 196

5 3 A schematic of load-displacement (crack opening displacement) responses of double cantilever beam (DCB) specimen under mode I loading 197

5.4 End notch flexure (ENF) specimen under mode II loading 197

5.5 Double lap joint under tensile loading 198

Chapter 1

Introduction

1.1 Motivation

Joints are inevitable in structural applications Though, they constitute a small fraction of the total weight of a structure, they are important as load transfer and stress diffusion takes place through these joints Therefore, a good design could result in better utilisation of bulk materials Adhesively bonded joints are being preferred to mechanical fasteners because of distinct advantages such as

- uniform stress distribution
- stiff connection,
- smooth surface contour,
- sealed against corrosion,
- excellent fatigue properties,
- no fretting problem,
- relatively light weight,

- damage tolerance,
- stealthiness etc

An adhesively bonded joint and various mechanical fasteners, which could carry same amount of load (15 kN) are shown in Figure 1 1 Outer members of these timber joints, were $3\frac{1}{2}$ X 1 inch and the inner $3\frac{1}{2}$ X 2 inch These figures clearly shows that adhesive bonding saves significant amount of materials and in addition has same strength as the mechanical fasteners

With the development of high performance structural adhesives, these joints are being employed in a wide variety of structural applications ranging from aerospace, aircraft, automobile components to those found in microelectronic components In the aerospace industry extensive applications of adhesively bonded joints are found These include, honeycomb sandwich floor panel, rudder floor panel, engine cowling, elevator, flap, ceramic tyle of re-entry vehicle, integrated fuel tank, composite propeller blade, helicopter blade, launch vehicle attachment (LVA) ring, collapsible tube mast etc

A group of researchers are working in the primary adhesively bonded structures technology (PABST) programme in USA with the objective to develop a light transport aircraft, whose most parts will be of composite materials and adhesively bonded joints This is expected to result in less maintenance and operational costs and also the required runway length will be significantly short as compared to the present ones

Non-aerospace applications of adhesive bonds includes, Rolls-Royce carbon fibre reinforced plastic (CFRP) cowl door, storage barrel, lamp post, tire reinforcement, abrasive wheel, brake lining, safety glass, William Honda grand prix car shaft, decking, furnitures, magnets, yacht etc

Composite materials are now used extensively in a wide range of applications, because of specific properties like (i) high specific strength and stiffness, (ii) dimensional stability, (iii) electrical and thermal insulation, (iv) no corrosion, (v) smooth outer surface, and (vi) material could be tailored to suit the application Optimal use of the bulk material and desired redistribution of material properties result in 'engineered composite structure'

Adhesively bonded joints are also found to be more suitable with fibre reinforced plastic (FRP) composites because of the facts that conventional welding, brazing methods are not applicable for these composites Moreover, the adhesives used in the bonding are similar in nature as the basic matrix used for the reinforcement of the composites

There are large number of parameters, which affect the performance of the adhesively bonded joints of fibre reinforced plastics Following parameters

- relative stiffnesses of laminates (adherends)
- relative stiffnesses of adhesive and laminate (composite adherend)
- relative thicknesses of laminates (adherends)
- relative thicknesses of adhesive and laminate (adherend)
- overlap length
- employment of various types of joints such as
  single lap, double lap, stepped lap, butt, scarf, tubular etc
- displacement boundary conditions
- stacking sequence of layups in the laminates (adherends)
- surface preparation, use of primers, mechanical properties of the adhesive material, and shape of the adherends etc

are found to have strong influence on the performance of these joints Adhesives used in these joints are usually of polymeric materials, which exhibit non-linear material behaviour such as elasto-plastic and visco-plastic behaviour under high stress and/or high temperature Moreover, in adhesive bondings, mainly two types of failures are observed viz (i) cohesive type damage occurring in adhesive material, and (ii) adhesive type damage occurring at the interface of adhesive and adherend

The motivation for present study is, therefore, to study the response and fracture of the adhesively bonded joints of composite materials, in the presence of material non-linearities It has been observed that there is large amount of scatter in the experimental data Similar observations are also found in the theoretical results Hence, in order to confirm that the theoretical results are realistic, experiments need to be conducted on well designed specimens

1.2 Review of literature

1.2.1 Elastic analysis

- *Lap joints Figures 1 2a and 1 2b*

Shear lag analysis of adhesively bonded joints was carried out by Volkerson (1938) He observed that absolute maximum of shear stress was independent of overlap length However, bending moment caused by non-colinear forces was not accounted Further, adherends bending allowing the joint to rotate gave rise to geometrical non-linearity was also neglected Goland and Reissner (1944) determined stress distribution in the adhesively bonded joint under tensile load They also obtained solutions for thin and thick cement layers In this analysis,

the effect of flexibility of the joint was considered only for thick cement layer However, shear deformation and tensile stresses across the adherends were neglected Further, the joint was considered to be monolithic (zero glue line thickness)

Chen and Cheng (1983) obtained a closed-form solution, which was based on two-dimensional elasticity theory in conjunction with the variational principle of complementary energy and was adaptable for various possible adhesive layer flexibility Using an impact test, Harris and Adams (1985) measured strength and energy absorption of bonded single lap joints with four different epoxy adhesives and three different aluminium alloy adherends Static joint strength was found to be not significantly affected by loading rate Energy absorption observed to be large when joint strength was significant for plastic deformation to occur in the adherends prior to failure From the crush tests of bonded and spot welded cylinders, they found that bonded joints were superior in performance as compared to spot welded ones Adams and Harris (1987) investigated the effect of local geometry at the edges of the overlap in single lap joints Three types of joints viz (i) joints with square edged adhesive layer, (ii) joints with fillet of adhesive and (iii) joint with an adhesive fillet and tapered adherend for joint strength were analysed They found that finite element analysis was capable of predicting the significant strength increase, which was achieved in single lap joints by filleting the adhesive at the edges of the overlap and rounding the ends of the adherends

Pindera and Wang (1990) obtained the three dimensional stress distribution in a symmetric adhesively bonded joint using techniques of analytical and optical isodynes Cheng, *et al* (1991) studied the behaviour of the adhesively bonded single lap joints with non-identical adherends under the action of tensile forces Their results showed that the intensities of the stresses were always much greater in a small zone at both ends of overlap region of the joint ARALL laminates are a family of structural composite materials, which consist of thin aluminium

alloy sheets alternating with aramid fibre/epoxy prepreg These laminates are developed for layers developed for fatigue applications Using finite element modelling and shear lag analysis failure of the adhesive in ARALL was predicted by Long (1991) He inferred that the failure load was a function of joint configuration and overlap length

Dorn and Weiping (1993) studied the influences of spew fillets, different adhesives and metal adherends on the stress and strain states in adhesively bonded plastic/metal single lap joints the strength and failure properties of these structures were undertaken by finite element technique (ADINA software) and experimental approaches They observed that the introduction of spew fillets lead to significant reduction in peak values of adhesive shear and peel stresses Further, the use of aluminium adherend instead of steel in plastic/metal bonded joint could decrease the adhesive stiffness imbalance and hence improve the symmetry of adhesive stress distribution They also found that the failure occurred in the plastic adherend in the spew end region and suggested non-linear analysis for the accurate prediction of joint strength

■ *Butt joint Figure 1 2c*

Using linear elastic finite element method, adhesive butt joints were investigated by Alwar and Nagaraja (1976) They concluded that there were significant variation in stress pattern across the adhesive thickness particularly near the adhesive-air interface Further, they observed that, there were surface layers at the interface, whose characteristics were different from the bulk adhesive material However, this work did not include the influences of these surface layers and the viscous behaviour of these layers Sawa, et al (1989b) extended their earlier work to include three dimensional stress analysis of the adhesive butt joints Temma, et al (1990a) studied the three dimensional stress analysis

of adhesive butt joints subjected to tensile loads The effect of debonded area and a spew fillet on the principal stress distributions were numerically calculated It was shown that, the joint strength decreased considerably when the joint had a debonded area and got increased when the joint had a spew fillet

Temma, et al (1990b) carried out two dimensional stress analysis of adhesive butt joints, in which two dissimilar finite strips were joined by an adhesive subjected to cleavage loads Effects of elastic moduli ratio of adherend and adhesive, Poisson's ratio, thickness of the adhesive and the cleavage load on the stress distribution at the interface were studied They measured strains produced at the adherends with strain gauges and stresses by photoelastic techniques These results were comparable with those obtained from numerical methods Temma, et al (1991) examined the stress distribution of an adhesive butt joint having a circular hole in the adhesive when the joint was subjected to an external bending moment and also the influence of the hole size on the strength of the joint They also conducted photoelastic experiments to measure the stress distribution in the adhesive

▮ *Scarf joint Figure 1 2e*

Stress distributions, in a plane scarf joint with arbitrary angle of scarf and various material (elastic) parameters associated with adherends and adhesives, were analysed by Chen and Cheng (1990) The analysis was based on the two dimensional elastic theory in conjunction with the principle of complementary energy Some typical features of the stress distribution were shown Using elastic finite element analysis, Ikegami, et al (1990) investigated the strength of adhesively bonded scarf joints comprised of an epoxy adhesive and two adherends namely glass cloth laminated plastics and metal They also examined the effects of scarf length and elastic imbalance on the deformation and strength

of the joint

Marcolefas, et al (1991) suggested a method for the analysis of adhesive bonded metal to composite scarf joint, in which both the metal and the adhesive exhibited non-linear behaviour A failure criterion was proposed for this type of scarf joint and for a given joint this method calculated the bond strength as a function of overlap length Further, they observed that thermal mismatch of adherends and adhesive had a severe effect for intermediate overlaps only However, even with elasto-plastic adhesive behaviour reliability of this analysis was limited, because of complexities due to non-identical adherends and non-uniformities in the adhesive shear stress distribution

- *Tubular joint Figure 1 2f*

Using interface finite elements Habib, et al (1988) carried out stress analysis in axisymmetric structures, which took into account the interface conditions due to geometrical continuity and interface equilibrium Further, stress distribution in tubular lap joints under internal pressure and influence of the material properties of the adherends on the interfacial stress distribution were investigated They observed significant variation of the stresses across the adhesive thickness, specially near the two edges of the joint The stress variation was observed to be non-uniform across the thickness Further, the edge effect was significant up to a distance of 15 times the thickness of the adhesive from the edge Imanaka, et al (1989) conducted fatigue tests and also investigated analytically adhesive bonded joints in shafts. They found that the maximum normal and shear stresses are the key parameters for estimating fatigue strength under pulsating tensile and torsional loading conditions, respectively These maximum stresses under tensile or torsional load conditions increased with the increase of coupling (overlap) length Further, it was observed that shorter coupling

lengths resulted in a higher fatigue life and proper tapering in the coupling zone improved the fatigue strength

Harj-Rabab, et al (1990) employed rectangular and axisymmetric interface finite elements for the analysis of adhesive bonded joints The stress distributions were compared with the results of closed-form solution and of displacement finite elements The influence of defects on the stress distribution was also studied Though this method provided accurate stress distribution at the interface and solved local effect problems, the drawbacks of these elements were (i) a large number of degrees of freedom per node were needed, (ii) difficulties to solve resulting equations and (iii) computation time was more Further, this analysis was limited to linear elastic behaviour of the constituents of the bonded joint

Sawa, et al (1992) investigated the strength of the joints combining adhesives with bolts The stress distribution in the adhesives and a variation of axial bolt force were analysed using the theory of elasticity for axisymmetrical structures They found that the strength of the combined joint was greater than that of conventional adhesive joints, and the strength increases with decrease in the bolt pitch diameter They also performed experiments to determine joint strength, maximum stress in blots for various loading conditions Sawa and Kobayashi (1988) described the strength characteristics of a combined joint consisting of an adhesive with bolts Hollow cylinders were considered as adherends and stress distribution at the boundary of adhesive layer, the force ratio and the strength of the joints were examined They found that the strength of the combination joint was greater than that of an purely adhesive joint

Using finite element technique Davies and Khalil (1990) analysed double containment joint made up of steel and epoxy, and based on overall stiffness of the corner joint designs were recommended With modest increase in elastic modulus of adhesive, they observed substantial increase in joint stiffness Chen and Cheng (1992) analysed the stress distribution in adhesive-bonded tubular

lap joints subjected to torsion The analysis was based on the elasticity theory in conjunction with the variational principle of complementary energy Adherends with different thicknesses and different adhesive materials were considered in the analysis

1.2.2 Non-linear (material) analysis

- *Elasto-plastic analysis*

By means of elastic-plastic analytical technique, adhesively bonded double lap joints were analysed by Hart-Smith (1973) On the basis of the study, he concluded that (i) there was a definite limit to the bond strength that could develop between specified adherends and a particular adhesive (ii) the maximum potential bond shear strength was determined by the adhesive strain energy i e shear stress per unit bond area (iii) adhesive peel stresses were more critical at the ends of the overlap than those associated with shear stresses He also studied the effect of thickness on the strength of double lap joints Further, Hart-Smith (1981) analysed the adhesive-bonded joints using the continuum mechanics approach and concluded that (i) adhesive shear stress distribution was inherently non-uniform for single lap, double lap, stepped (Figure 1 2d) and scarf (Figure 1 2e) bonded joints (ii) the inclusion of adhesive non-linear (elasto-plastic) behaviour was vital if the bonded joints analyses were to predict failure (iii) very little portion of a typical bonded joint was actually loaded beyond the adhesive elastic compatibility, and plastic behaviour was confined to the immediate vicinity of the ends of the bonded overlap or to the ends of the steps in a stepped lap joint (iv) a precise representation of the adhesive non-linear behaviour was unnecessary, any model which was mathematically tractable could suffice (v) adhesive peel stresses, which occurred in conjunction with the shear stresses could be alleviated by suitable tapering of the adherend

or local thickening of the adhesive (vi) the strength of bonded joints of the simplest configuration was limited, so the use of adhesive bonding in thicker structure demands more complex geometries of the joints and (vii) bonded joints should always be designed in such a way that the adhesive was never the weak link

Ramamurthy and Rao (1984) analysed lap joints with elasto-plastic adhesive behaviour and uniform adherends This analysis also accounted for arbitrary adherend shapings They concluded that strength of a bonded joint depended on adhesive behaviour and the strength of adherend materials However, this work was limited to isotropic materials and did not consider the effects of other important parameters like adhesive thickness and overlap length etc on bond strength Czarnocki and Piekarski (1986) observed that the failure of an adhesive layer in a symmetric lap joint originated in the central plane of a joint at the front edge of an adhesive layer and was caused by the biaxial state of normal stresses Further, the most severe state of stresses existing in the central plane of a joint was not effected by joint width (within the range investigated) The load capacity of a joint per unit width was found to be constant They also found that use of weaker but sufficiently flexible adhesives resulted in a higher load capacity than that obtained with a strong but rigid adhesive, if the length of the joint was not restricted Further, application of a more flexible adhesive could significantly reduce stress concentration in adherends However, material non-linearity was not accounted in the analysis

Using non-linear (elasto-plastic) finite element analysis of both clad and unclad configurations Crocombe and Evan (1988) investigated the effect of the cladding layer on the strength of a bonded joints They found that for the unclad joints yielding occurred first at the tensile zone and spreads from the overlap region Analysis of clad joints showed a similar yielding in the overlap region but the adhesive fillet were stresses to a much higher level by the excessive deformation of the cladding layer Adams (1989) inferred that

finite element technique was one of the best way of treating the non-linear (joint rotation) mechanics, material properties, adhesive fillet and tapering of the corner in bonded joints He showed that the strength of the joint could be increased up to 500 percent by using composite adherends effectively Bassani and Qu (1989) calculated the crack-tip stress fields on the interface between two semi-infinite anisotropic elastic solids They estimated small scale yielding plastic zones surrounding the crack-tip They also found that crack-tip stress had the standard square-root singularity and the corresponding stress intensity factors were separable in the three modes of loading

Bigwood and Crocombe (1989a) carried out elastic and elasto-plastic analysis of general joint configurations and suggested a two parameter formula for preliminary design Lee, et al (1989) developed computer programs for analysis of adhesive joints in co-axial tubular structure This program took into account plasticity in adhesive and predicted the stress in a lap shear joint subjected to any combination of tensile, shear, bending and thermal loads They conducted tests to determine adhesive properties and the shear strength, stiffness and durability of structural joints Groth and Brottare (1989) carried out a finite element analysis for determination of the joint stiffness as function of the nominal strain Adhesive material was considered to exhibit elasto-plastic behaviour They observed that apparent stiffness of the adhesive layer kept on decreasing due to plasticity at the interface and saturates below a nominal strain level of 0 5 percent However, this work was limited to thick adhesives Additionally, Bigwood and Crocombe (1990) carried out the elasto-plastic finite difference analysis of adhesively bonded joint considering as a plane strain problem and compared these results with those obtained from elasto-plastic finite element analysis They assumed that the material behaviour of adherends and adhesive was linearly elastic and elasto-plastic, respectively The joint was modelled as an adherend-adhesive sandwich allowing the application of any combination of tensile, shear and moment loadings at the ends of the adherends They also studied the effect of adhesive thickness on the strength

of lap joint Schemes for estimation of J integral for predicting elastic-plastic fracture was explained by Brust, et al (1990) Edlund and Warbring (1990) carried out two-dimensional, elastic-plastic finite element analysis of a shear loaded adhesive joint Crocombe and Bigwood (1992) outlined an approach for including the adherend non-linearity into the adhesively bonded joint analysis A bi-linear elasto-plastic model incorporating strain hardening was used to model the adherend stress-strain behaviour However, this approach was complicated due to the complexities of the governing equations, involved in the analysis

Thomsen (1992) considered the problem of an adhesively bonded lap joint between two dissimilar orthotropic circular cylindrical laminated shells, which includes elasto-plastic behaviour of the adhesive He observed that the overlap length and stiffnesses of adhesive and adherends significantly influence the the stress distribution in the joint He also showed that with elasto-plastic analysis considerable reduction in peak stresses were achieved as compared with purely elastic analysis Adams and Mallick (1993) presented a method to predict the strengths of elasto-plastic adhesives at room temperature For most cases, predictions were within 5 percent variation from the experimental values However, these predictions were not accurate for the cases of brittle adhesives at low temperatures (−55°C) and high overlap lengths

Visco-elastic and visco-plastic analyses

Creep behaviour of structural adhesives used in lap joints with steel adherends was studied by Allen and Shanahan (1975) Adhesives employed were (i) a phenolic resin/polyvinyl formal composite Redux 775 and (ii) a modified epoxy novolac Redux BSL 906 It was shown that the separation of adherends due to adhesive shear creep should be associated with the maximum adhesive shear stresses found at the ends of the overlap. Due to the creep in adhesive bonded

lap joints, Allen and Shanahan (1976) observed reduction in stress concentrations at the ends of the overlap as compared with elastic solution They also found that creep curves obtained from the lap joints did not correspond directly to those obtained from experiments employing bulk adhesive material under similar loading conditions Further, they concluded that if creep was allowed, the long joint had a secondary safety factor in that stresses causing creep were reduced rapidly However, there was considerable amount of scatter reported in the experimental results

Devitt, et al (1980) suggested an approach for the determination of delamination fracture toughness in the opening mode, which was developed using a split beam and a non-linear visco-elastic analysis They determined the visco-elastic behaviour of the resin from creep/recovery tests They also showed that the measured range of energy release rates for a range of crack growth rates, was consistent with predictions from an idealised visco-elastic crack growth theory Using finite element program (SAAS III) Sen and Jones (1980a) determined the stresses and strains across the adhesive thickness in a double lap bonded joint, subjected to a quasi-static load Visco-elastic stress analysis was performed with the finite element program and Schapery's direct method of transform inversion Nagaraja and Alwar (1980) carried out finite element analysis of adhesively bonded plate lap joint considering the visco-elastic behaviour of the adhesive material They found that the decrease of stresses with time was of the order of 18 percent for normal stresses and 45 percent for shear stress Further, the variation of stresses across the adhesive thickness was confined only to the regions near the edges This method was also found applicable to study the response of solid propellants in rockets

Ratwani, et al (1982) discussed the importance of consideration of visco-elastic behaviour of adhesive for strength prediction of the bonded joint They showed that the maximum shear stress in the adhesive layer of a stepped lap joint was considerably reduced when the time dependent behaviour was

taken into consideration and the shear distribution becomes fairly uniform after about 2 hours Henriksen (1984) developed an algorithm for the analysis of non-linear visco-elastic adhesive materials This formulation also took into account high temperature, cyclic creep, finite and infinitesimal strains in adhesive joints Based on J integral, Schapery (1984) developed a method of quasi-static deformation and carried out fracture analysis for a non-linear visco-elastic material Their analysis, included crack growth, crack closing and crack healing and, was applicable to problems involving ablation, interfacial contact and interfacial separation Groth (1986) presented a general method to calculate the stresses in bonded joints using the substructuring technique, where large parts of structure were linearly elastic and remaining part exhibited non-linearity He also pointed out that visco-elasticity of the adhesive was very important because large redistributions of the stresses occurred during the period when the joint was loaded He also concluded that normal stresses changed rapidly at the terminus and more number of elements were required there in order to evaluate the stresses accurately Yadagiri, et al (1987) studied the visco-elastic analysis of adhesively bonded joints using finite element method with curved isoparametric elements Hereditary integrals used to represent the stress-strain relations resulted in a stiff model while the use of relaxation modulus resulted in a flexible model They found that the average of these two solutions resulted in a better approximation

Roy and Reddy (1988a) developed a general purpose finite element analysis software called NOVA to analyse bonded joint, which takes into account the visco-elastic adhesive behaviour and the geometrical non-linearity The effect of temperature and stress levels on the visco-elastic response was taken into account by a non-linear shift factor definition Penetration sorption was accounted by non-linear Fickean diffusion model, in which diffusion coefficient was dependent on the temperature, penetrant concentration and the dilatational strain The adhesive layer was modelled using Schapery's non-linear single integral constitutive law for uniaxial and multiaxial state of stress by Roy and

Reddy (1988b) The effects of temperature, stress level and penetrant absorption on the visco-elastic response were studied However, the effect of change in Poisson's ratio with time in the polymer was not taken into account, which had a significant bearing on the final response of the joint

Needleman (1990) discussed various issues associated with the analysis of interfacial failure phenomena and inferred that visco-plastic material behaviour was responsible for limiting the achievable stress level He also indicated that a key parameter controlling decohesion was the ratio of the strength of the interface to the strength of the ductile solid Chalkley and Chiu (1993) carried out experiments to study the shear stress-strain behaviour of FM 73 epoxy They found that FM 73 exhibited a more prominent visco-plastic behaviour than visco-elastic behaviour Based on the results of thick-adherend and short-overlap specimens, it was concluded that due to the time-dependent nature of the adhesive, true shear stress/strain testing could be accomplished only under strain control But, in practice thin adherends and long overlap lengths were employed to achieve higher strength

Fujii (1993) presented a numerical model using a one-dimensional approximation for analysing the dynamic response of adhesively bonded sandwich beams The visco-elastic characteristics of the adhesive damping layers were represented by generalised Maxwell model To determine the dynamic response, they proposed a new method which combines the transient analysis based on finite element method with the experimental modal analysis This approach was validated with an impact test on a sandwich beam bonded with chloroprene rubber adhesive damping layer Hiregoudar (1993) carried out finite element analysis of single lap joint This analysis included the geometrical and material (visco-plastic) non-linearities However, the analysis was limited to ideal bonded joint, having no defects at all Su and Mackie (1993) carried out two-dimensional creep analysis of structural adhesive joints They observed significant amount of viscous deformation even at room temperature. At elevated temperature (45^0C)

the Young's modulus was observed to be reduced substantially as compared with that at room temperature Both normal stresses and shear stress values got reduced because of the creep in the adhesive joints The reduction of shear stress was rather limited Further, with creep there was an increase in strains, and maximum increase was observed in shear strain

1.2.3 Non-linear (geometrical) analysis

Results of stress analysis of adhesively bonded joint and calculation of strain energy release rates for cracked lap shear (CLS) specimens at four different debond lengths were reported by Johnson (1987) The various numerical techniques considered were two- and three- dimensional finite element analyses, beam theory, plate theory, and a combination of beam theory The results were clustered into two groups, geometrically linear and geometrically non-linear analyses He suggested that care was needed to ensure proper modelling of the specimen in order to get correct result e g adhesive bondline must be modelled with proper grid density and full bondline and not just near crack-tip region, needed to be included in the model Further, he pointed out that, there was a small amount of contribution from out of plane shear deformation (mode III) of adherends Reddy and Roy (1988) developed a two-dimensional, finite element code using an updated Lagrangian formulation to account for the geometric non-linearity for the analysis of adhesively bonded joints. The effects of boundary conditions and mesh on the stress distributions in lap joints were also investigated It was observed that the type of boundary conditions assumed could significantly alter the stress distribution in a lap joint

1.2.4 Fracture mechanics approach

Using beam theory and J integral, Fernlund and Spelt (1991a) developed an numerical solution to calculate the strain energy release rate of adhesive layer, which included both geometrical and material non-linearities They observed that (i) double cantilever beam showed a predominant mode I fracture, (ii) end notch fracture (ENF) specimen produces almost pure mode II, and (iii) the cracked lap shear (CLS) specimen joint showed a mixed mode fracture Using modified crack closure integral and constant strain finite element stress analysis (AXISOL software), Rybicki and Kanninen (1977) evaluated stress intensity factors and applied to three configurations, (i) a double cantilever beam test specimen, (ii) a finite width plate containing an embedded crack and (iii) a bolt fastened double lap joint containing two radial cracks They observed that the results obtained with the use of higher order elements were less accurate as compared to those obtained with constant strain finite elements, which uses nodal forces and nodal displacements However, their work was limited to linear elastic analysis and isotropic materials

Using the finite element computer code NASTRAN, Ratwani and Kan (1986) carried out the analysis of delamination propagation in the composite layer of metal to composite stepped lap joints They found that the delaminations did not grow to be catastrophic in the composite layer for some resin material The presence of both debonding and step-end gaps in the adhesive layer represented a critical condition from the point of view of delamination initiation and propagation Janardhana, et al (1986) employed finite element model to study the effect of debond length on various lap joints They also examined the effects of delamination damage in composite to metal joints and conducted experiments on bonded double lap joints of graphite/epoxy and aluminium Mall and Johnson (1986) carried out experimental and analytical investigations on adhesively bonded composite joint to characterise both the static and fatigue

debond growth mechanisms under mode I and mixed-mode (I and II) loadings Failure occurred in the form of debond growth in all the specimens tested Total strain energy release rate appeared to be the driving parameter for cohesive debond growth under static and fatigue loadings Also the values of total strain energy release rates measured for debond growth were an order of magnitude below the static fracture toughness (critical strain energy release rate)

Groth (1988a) predicted fracture load of the single lap joint with failure criterion, which was based on material-induced singularities appeared at the terminus of the joint These results were compared with those obtained from the experiments Pilarski and Rose (1988) used an ultrasonic oblique-incidence technique to detect the interface quality in aluminium to aluminium adhesively bonded structure However, these measurements were sensitive to frequency range used, angle of incidence, attenuation and reflection coefficient Aivazzadeh, et al (1988) presented several triangular and rectangular mixed finite elements for the interface stress analysis in adhesive butt joints For two-dimensional interface problems such as sandwich structures and laminates they employed these elements and evaluated stress distributions in these structures However, these elements had the drawbacks of mixed elements and also it was difficult to extend this to non-linear analysis

Aivazzadeh and Verchery (1986) presented rectangular interface finite elements for the stress analysis of adhesive joints The results obtained from these elements showed that, stress distribution could be evaluated more accurately than those obtained from conventional displacement elements However, this work was limited to two-dimensional linear elastic and rectilinear interfaces Hattori, et al (1989) suggested a method which uses two stress singularity parameters for evaluating adhesive strength and applied to several kinds of moulded models, composed of epoxy resin and metal (Fe-Ni) alloy sheets, and plastic encapsulated large scale integration (LSI) models The initiation and extension of delamination were estimated theoretically Occurrence of

delamination and its propagation in the molded models were observed using scanning acoustic tomography Crompton and Clark (1989) examined the near crack tip stresses with finite element analysis and stress intensity calibration equations and found that for a 0 5 mm bond line thickness the stress singularity deviates from the conventional square root singularity

Groth and Brottare (1988) proposed a fracture parameter namely singular intensity factor equivalent of stress intensity factor (SIF) for the failure analysis of butt joint with various adhesive materials Sethuraman and Maiti (1989) developed an element with a constant shear strain field for the analysis of doubly bonded crack-stiffened panels serving as crack arresters They found that the stiffener accrued more benefits in the case of an edge crack than in the case of a centre crack, when both were subjected to the same mode I loading Further, increasing the shear modulus or reducing the thickness had a beneficial influence on the stress intensity factor of the stiffened structure Moreover, the stiffener was observed to be most effective when it was located close to the crack tip than on the side opposite to the ligament Crocombe, et al (1990) outlined various approaches applied in analyses of adhesively bonded joints to predict the strength of these joints The applications of the singularities at joint bimaterial interfaces were discussed and failure criteria were proposed

Kairouz and Matthews (1990) postulated various mechanisms of failure in bonded CFRP single lap joints These mechanisms were found to be dependent on the layup and stacking sequence of the adherends From the joints tested, strength of the joint was found not to be strongly dependent on stacking sequence, but failure mechanism was influenced by the direction of surface fibres and was determined by stresses induced by bending They concluded that for adherends with 0° ply/plies on the surface failure initiated as tensile fracture of the 0° fibres and was followed by delamination within 0° ply Further, they inferred that for adherends with $\mp 45°$ surface plies failure proceeded inwards from the surface layer and was manifested by intralaminar and interlaminar

shear cracking A numerical study of the coin-tap test was carried out by Mackie and Vardy (1990) Using a two-dimensional finite difference model of elastic waves in an adhesively bonded structures, they found a relationship between defect size and the frequency of vibration of the material However, this technique was effective for large civil structures only

Mecklenburg, et al (1990) applied the energy separation method for characterising the fracture resistance of adhesives and compared it with elastic and plastic fracture parameters such as strain energy release rate and J integrals of bonded half compact tension test specimens Suo (1990) discussed several mechanics problems of brittle adhesive joint in fracture testing of nominal toughness, configuration stability of mode-I in-layer fracture, tunnel crack and parallel debond due to residual stresses He concluded that parallel debonding was likely to take place for adhesives in residual compression than in tension, provided other conditions were the same Khalil and Bayoumi (1991) determined the fracture energy and fracture toughness of an epoxy adhesive material at different loading speeds with cleavage test specimens They observed that with increased loading speed the effect of loading rate on the fracture energy and toughness decreased Correlations between the fracture energy and fracture toughness were obtained for both aluminium and brass adherends Liechti and Chai (1991) developed a biaxial loading device, which produced steady crack propagation under all loading directions Energy release rates were extracted from linear elastic finite element solutions that matched with the measured normal crack opening displacements (NCOD) Zenkert (1991) investigated the debondings in foam core sandwich beams with cracks in the interface between the face and core Using fracture toughness criterion, he predicted the fracture loads for beams with simulated debondings subjected to four point bending He also inferred that interface debondings had significant influence on the load bearing capacity of foam core sandwich beams

Ishikawa, et al. (1991) investigated the mixed mode fracture criterion of

adhesive joint and carried out static fracture tests on acryl and epoxy adherends and epoxy resin adhesives From the experimental results, they concluded that total strain energy release rate was a dominant parameter, which characterise the fatigue crack propagation in adhesive joints Further, they inferred that the criteria for fatigue crack growth and static fracture toughness were different Using beam theory, Fernlund and Spelt (1991b) presented a method to predict failure load of structural adhesive joints in design application However, the calculation of the strain energy release rate and the analysis was limited to the linear relation of load and displacement Further, Fernlund and Spelt (1991c) conducted experiments for the study of crack propagation in cracked lap shear (CLS) specimen subjected to a range of loading conditions They concluded that the critical strain energy release rate was not a material property but increased with decrease in thickness of adhesive layer and with decrease in G_I/G_{II} ratio Further, they found that loads required to propagate a crack in a cracked joint for a specific adhesive system, provided a conservative estimate of the failure load for the corresponding uncracked joint

Miskioglu, et al (1991) proposed a linear elastic model for a bimaterial interface crack to determine the direction of crack propagation during surface-layer removal by scraping Photoelasticity method was used to determine the loading at which a scraper would need to be delivered to the surface layer for continued interfacial crack propagation and the results were compared with those obtained from finite element analysis In both the analyses frictionless contact between wedge and layer was assumed The data-collection region was restricted to a zone very close to the crack-tip There was discrepancies between the measured and calculated fringe orders far away from the crack-tip Similar discrepancies were observed in the very close proximity of crack-tip, where the solutions were influenced by material and geometrical non-linearities Stress and displacement fields for an interfacial crack opening in an anisotropic bimaterial were represented by two real matrices respectively by Qu and Li (1991) They found that interface could be characterised by the tractions along

the interface for dislocation and crack problems However, exact number of non-dimensional parameters needed to describe general anisotropic bimaterial system was not considered

Wassell, et al (1991) developed a test method, which measures the crack growth rate for an adhesive material in a bondline that contained a cohesive crack They used finite element technique to verify the experimental results (material properties) The test was found to be sensitive to crack propagation rates of the order of 10^{-7} mm/cycle However, this work was limited to linear elastic adhesive material Bishopp (1992) carried out experiments with equal adherends double cantilever beam (DCB) specimen, which generated mixed mode fracture data called as fatigue envelope He observed that the mode ratio and critical energy release rate (G_C) were independent of crack length and fracture toughness (G_{IC}) was independent of adherend thickness He also observed that critical energy release rate G_C was increased with increasing nominal phase angle of loading and G_{IIC} was approximately three times higher than G_{IC} Further, he found evidence of effects of crack-face friction in mode II However, these results were based on brittle nature of structural epoxy adhesive Davies, et al (1992) attempted to establish the reproductability of values for mode I and mode II tests on two materials in different laboratories Large amount of scatter was observed for the results obtained from end-loaded split (ELS) specimen They determined G_{IC} and G_{IIC} values from DCB and end notched flexure (ENF) specimen, respectively They also observed that the values of G_{IC} and G_{IIC} increased slightly with increase in specimen thickness

Dung (1992) introduced a numerical model of void growth and analysed the behaviour of a single cylindrical or spherical or ellipsoidal void in a plastic material containing a periodic array of voids The effects of the triaxiality on the void growth was accounted with the microscopic and macroscopic factors such as the stress components, the hardening exponent, the volume fraction, shape and spacing of the voids and the constitutive softening This model was applied

to a three-dimensional problem with the assumption of constant distribution of the stress and strain fields in solid throughout the process of deformation He found that the predicted results were satisfactory for volume fraction and yield stress However, estimated void aspect ratio did not show the flattening behaviour of the void In the analysis of adhesive joints Krenk (1992) modelled the adhesive layer as a continuous distribution of tension and shear springs He concluded that the stress concentration and the energy release rate depended on the adhesive thickness and stiffness This study revealed that large adhesive stiffness and small layer thickness resulted in a stiff bond with large localised stress concentrations Further, a double cantilever beam specimen under mode I and mode II loadings and a symmetric lap joint under mixed mode loading were analysed

Edde and Verreman (1992) carried out stress analysis using beam theory approach for a clamped crack lap shear (CLS) adhesively bonded joint They used a crack-closure technique to obtain the total energy release rate in various modes for a crack propagating along the bond line However, the results showed good agreement with finite element solution only for small crack lengths The fatigue growth of planar defects within adhesively bonded T-peel joints was modelled by Gilchrist and Smith (1993) In accordance with linear elastic fracture mechanics, crack growth was characterised by stress intensity factors and strain energy release rates It was assumed that defects within the adhesive were likely to be initiated cohesively within the adhesive fillet region, propagated to the surface, formed a through-width defect and rapidly grew through the remaining bond They found that the static and fatigue strength of joints were maximum, when the adhesive filled the fillet region This analysis was limited only to cohesive type of failure

Rossettos and Zang (1993) characterised stresses in single lap joints in the presence of a void by two non-dimensional parameters The influence of the location and size of the void on peak stress was also studied for identical and

non-identical adherends Whitcomb and Woo (1993) studied the debond growth in adhesively bonded tubular joints using geometrically non-linear finite element analyses They discussed behaviour of tubular and plate joints under tensile and flexural loads They also observed that the strain energy release rates converged rapidly with mesh refinement Richardson, et al (1993) assessed the validity of modelling adhesive joints as two-dimensional problems Comparison of both the adhesive stress distribution and the energy release rates associated with the crack growth from two- and three-dimensional analysis were made They suggested to carry out a three-dimensional analysis to obtain modified load distribution and apply these distributions to refined two-dimensional model, which would take care of non-uniform load transfer Refinement of three-dimensional mesh would influence the accuracy of the calculated load transfers and thus the final results This important aspect was not considered in their analysis

Using a high-magnification video camera Chai (1993) evaluated damage at the tip of cracks in adhesive bonds deforming in shear He concluded that ultimate shear strain was a key material property for controlling crack growth in brittle and ductile epoxy resin Qu and Bassani (1993) studied the aspects of fracture mechanics of interface cracks in anisotropic bi-materials A general discussion of the oscillatory nature of the crack-tip fields, crack-face contact, effects of specimen size, interfacial toughness and material properties were presented They concluded that there was a coupling of all three crack-tip fracture modes in the normal anisotropic bimaterials, whereas in isotropic case, mode III was decoupled from mode I and II

1.2.5 Parametric study

Influence of bond thickness on the stress distribution in single lap adhesive joints was investigated by Ojalvo and Eidinoff (1978) They found that its

effect was more pronounced for the joints with short overlaps, thick adherends and stiff adhesives Sen and Jones (1980b) carried out a parametric study and design of a double lap joint, which was bonded with a visco-elastic adhesive They studied the qualitative influences of the various geometrical, material parameters and creep strains on the possible failure modes of the joint They found that the most important parameters were (i) ratio of adherend modulus to equivalent property of visco-elastic adhesive and (ii) thickness of the adhesive Using the double cantilever beam (DCB) adhesive joint specimen and scanning electron microscope (SEM), Chai (1986) studied the effect of bond thickness on the fracture behaviour of ductile adhesive Depending on the thickness of the adhesive continuous crack growth, unstable crack growth and a combination of both were observed Qu and Bassani (1989) studied the two-dimensional problem of an interfacial crack between two anisotropic elastic solids and derived necessary and sufficient conditions such that the crack-tip fields were non-oscillatory However, this study was limited to perfect continuity of displacements across the interface

Using the theory of elasticity, Sawa, et al (1989a) analysed stress distributions of adhesive butt joints of dissimilar solid cylinders subjected to external tensile load The effects of adherend stiffness, adhesive thickness, ratio of adherend and adhesive Poisson's ratios, normal aspect ratio and shear stress distribution on the joint strength were studied by numerical calculations They found that the stress singularity became large at the edges of the interface where the adherend stiffness was large and fracture occurred at the interface Mall and Ramamurthy (1989) carried out experimental investigation on composite bonded joints to study the effect of bond thickness on debond growth rate under cyclic loading and critical strain energy release rate under static loading They observed that fracture and fatigue strengths were dependent on bondline thickness Using two stress singularity parameters Hattori (1991) investigated the shear strength of single lap bonded joints He studied the influence of adhesive layer thickness, overlap length and bonding edge angle on joint strength

He found that the shear strength of single lap joints got decreased when the overlap length was more than the substrate (adherend) thickness Further, he observed that fracture occurred at the upper bonding edge, when the bonding edge angle was less than $\pi/3$ and it occurred at the lower bonding edge, when the bonding edge angle was greater than $\pi/3$ It was suggested that shear strength could be improved by decreasing the bonding edge angle to less than $\pi/6$

Kim, et al (1992) employed small fatigue test specimens and investigated the effects of adhesive thickness and adherend surface roughness on the fatigue strength of the tubular single lap bonded joint These tests were performed on single lap joint, single lap joint with scarf, double lap joint and double lap joint with scarf Chai (1992) studied mixed mode fracture and interaction between fracture modes (opening and shearing modes) in adhesive joints with various adhesive thicknesses under combined loadings He found that fracture energy was largely controlled by plastic deformation in the adhesive material Munz and Yang (1992) examined stress singularity occurring at the free edge of the interface of dissimilar materials under mechanical and thermal loadings They inferred that size of the component had a significant effect on the stress at the free-edge of the interface, especially for thermal loading

Choi and Thangjitham (1993) presented a numerical method for analysing the steady state anisotropic thermo-elasticity problem of fibre reinforced composite laminate containing a crack embedded within a given matrix rich interlaminar region It was shown that the interlayer model provided a resulting crack-tip stress field with the standard order of square root singularity Owing to the unique structural characteristics of laminate stacking sequence, coupling effects could arise from material properties mismatch between adjacent fibre layers, leading to the simultaneous presence of all fracture modes This aspect was not considered and further his work was limited to linear elastic fracture mechanics (LEFM)

1.2.6 Environmental effects

Parker (1990) exposed carbon fibre reinforced epoxy composite joints bonded with epoxy adhesives to 50° C and 96 percent relative humidity for 3 years and tested them From the experiments, he concluded that strength reduction was dependent on exposure time, test temperature and changes in the adhesive properties rather than in adherends Depending on the adhesives used, he observed that the joints failed either in the composite adherend or in adhesive or both Rao and Crocker (1990) described a numerical model to predict the natural frequencies and the mode shapes of a bonded lap joint for free vibration They compared numerical and experimental results for natural frequencies of lap bonded joint in beam system They found that the natural frequencies of the system got increased with an increase in the overlap length Further, the damping ratio due to the presence of bonded joint in the system did not have significant effect on the system response Using numerical shape optimisation techniques, Groth and Nordlund (1991) performed shape optimisation of bonded joints By changing the profiling of the adherends, they obtained strong and light joints Types of joints studied were the single lap, double lap and double strap A console bonded to a rigid wall was also examined However, this analysis needed a suitable initial optimal geometry as the input, else the objective function could find a local (not necessarily global) minimum value

Adams, *et al* (1992) found significant changes in stress state of lap joints caused by thermal effects The stress/strain properties of the polymeric adhesive also got changed enormously with temperature resulting in variation of strength of single lap shear joints They observed that strain rate capability was high but the load capability was low The reverse occurred at low temperatures Cherry and Ye (1992) studied the behaviour of high temperature anaerobic (without oxygen) adhesives, which were cured at room temperature in the absence of oxygen Experimental results from a commercial high temperature anaerobic

adhesive showed that the adhesive polymer became brittle as a result of fully cured state, and the adhesive near the edges of the bond did not get cured properly because of penetration of oxygen inhibiting it from curing The size of this uncured zone was found to be a key factor affecting the strength of the joints at room temperature However, this work completely neglected the influence of interfaces and the adherend properties Conley, et al (1992b) measured subcritical crack growth behaviour along polymer/glass interfaces for various polymer adhesives at different relative humidities They used the power law relationship between crack velocity and the strain energy release rate to discuss the delamination of thin films under residual tensile stress The shell epoxy was found to be most resistant to delamination as compared to other epoxies Probable reason for this retarded crack growth was mentioned to be high fracture resistance and voids at the interface

Finger like crack growth behaviour in a urethane acrylate/glass interface was studied by Conley, et al (1992a) as a function of humidity and applied strain energy release rate G, for the study A four point flexure specimen consisted of two glass plates bonded together with a finger like crack introduced at the adhesive/glass interface They observed that finger spacing was independent of crack velocity Though crack growth at the interface was characterised by finger like perturbations along the crack front due to the viscous nature of this adhesive, calculation of G did not include viscous material behaviour of the adhesive Ritter and Conley (1992) carried out study of moisture assisted crack propagation at polymer/glass interfaces They concluded that, above a threshold value of applied G, moisture assisted crack growth at the interface was dependent on the applied G by a power law expression, where the proportionality constant depended on adhesive tested and the relative humidity Polymer adhesive tested were epoxy acrylate, urethane acrylate, Devcon epoxy and Shell epoxy They observed that high humidity enhanced the crack growth rate Su, et al (1992) studied the effects of aging and environment on the fatigue life of adhesively bonded joints They observed that those adhesives cured with

polyamine hardener showed improved fatigue life and had high initial strength and Young's modulus Further, the adhesive that had high moisture absorption, low initial Young's modulus and low heat deflection temperature, lost it's fatigue resistance completely Wingfield (1993) discussed the problems associated with the surface pretreatment of fibre reinforced composites of adhesive bonding To obtain a strong joint, they suggested removal of surface contamination such as silicones and flurocarbons However, the abrasive surface treatments like alumina glitblasting and silicon carbide abrasion would change the mechanical properties of the bulk composite

1.2.7 Quality of adhesive bonding

Various methods and specimens, for obtaining the mechanical characteristics of structural adhesives needed for the design and analysis of adhesively bonded structural joints, were described by Jeandrau (1986) Groth (1988b) designed a test specimen of double contoured cantilever beam, which resulted in a constant value of stress intensity factor in Mode I for a crack length up to 90 mm of the total specimen length 100 mm However, this test specimen was valid for mode I loading condition only The results obtained from five epoxy bases structural adhesives from single lap joints were presented by Jeandrau (1991) Thomson and Thomson (1991) attempted to develop a quantitative accept/reject methodology based on fracture mechanics, which considered elements of material characterisation, stress analysis, failure modelling (including time and temperature dependent features) and fractography They also reviewed the earlier research related to improvement of techniques to measure the bond strengths They concluded that the correlations between ultrasonic data and strengths for adhesive and cohesive types of failures persisted in complex adhesive structures

Jiao and Rose (1991) introduced an interface layer model for evaluation of adhesive bonding quality However, this process was sensitive to frequency range, angle of incidence, wave type, type of specimen and signal processing procedures employed during the experiment Using Acousto-ultrasonic (AU) non-destructive technique Tiwari, et al (1991) examined the quality of adhesively bonded sheet metal used for automobiles AU is a hybrid of acoustic emission and ultrasonic techniques This technique assured quality of bonded joint and requires access to only one side of the component They observed that bond quality was related to the attenuation of the energy content of the received signal for mixed mode failure However, surface roughness and cleanliness did affect the AU signals and thus influenced the results Hanneman and Kinra (1992a) proposed a technique for ultrasonic non-destructive evaluation of adhesively bonded joints, which was applicable to perfectly elastic and linear visco-elastic materials, and also for isotropic and anisotropic materials

Using piezoelectric transducers, transmissions of a plane longitudinal ultrasonic wave, through lap joint immersed in water, were measured by Hanneman and Kinra (1992b) to deduce the joint properties such as adherend and adhesive thicknesses However, these results were sensitive to frequency range used, resonance mode, adhesive material properties and attenuation Parker (1993) studied the environmental durability of aluminium joints with different pretreatments He compared the durabilities of bonded joints made with aluminium pretreated by ceramic pickle and anodizing pretreatment Considering time of failure under stress, residual strength and mode of failure, he concluded that anodizing pretreatment resulted in a longer life of the bonded joint under normal laboratory environment

1.2 8 Design

A method was developed by Findlater (1987), which enabled the effect of joint dimension to be compared with the load carrying capacity of a particular joint configuration However, these did not yield information about the levels of stress in a joint nor they were substitutes for numerical tool such as finite element analysis Bigwood and Crocombe (1989b) suggested a two parameter design formula which calculated the adhesive shear and tensile stresses in the overlap region However, the errors were introduced in case of adherends mismatch This design formula yielded accurate stress values and was valid for balanced joint configurations Hashim, *et al* (1990) studied the design and assessment methodologies for adhesively bonded structural connections They concluded that the use of hot cured epoxy adhesives was both technically and practically viable for replacing fillet welded connections in lightly loaded steel structures Depending on the specific application and requirement a limited experimental and numerical technique used with a reliability assessment method might be adequate and might not require a higher factor of safety However, this work did not provide enough case studies to support the new idea of reliability assessment in joint analysis

Adams (1992) discussed the importance of finite element analysis, reliable data (adhesive properties) for the joint analysis and the need to compare the results of finite element analysis with those obtained from experiments Lee and Selby (1992) devised a logical technique, which could be used to select most suitable adhesive for a purpose This was an implementation of expert system Therefore, this technique had the major limitations such as need of an excellent data bank and regular updating of data

1.3 Objectives of the present work

1 3 1 Status of the literature

From a critical review of the available literature following observations regarding the status of understanding of the response of adhesive joints could be made

- Various parameters like joint configuration (single lap, double lap, stepped lap, butt, scarf etc), adhesive thickness, overlap length, quality of surface preparation, bonding quality, material properties of the adhesive and adherend, and shape of adherends play an important role on the performance of the adhesively bonded joints

- Polymeric adhesives exhibit non-linear behaviour under high stress and/or extreme thermal conditions

- There is significant variation in the results based on elastic, elasto-plastic and visco-plastic analyses Results of non-linear responses of these joints are spread over a wide range

- Finite element technique appears to be one of the most versatile mathematical tool to handle the non-linear behaviour and the parametric study of the adhesively bonded joints

- Most of the analyses reported in literature are either completely theoretical or computational Very few of them have been corroborated by the experimental studies

1 3 2 Objectives of the present work

It is therefore felt that, there is a need to systematically develop a finite element technique to study the behaviour of adhesively bonded joints With this view, in this thesis an attempt is made to

- develop an automatic mesh generation program, which could locally refine the finite element mesh near the critical zones such as sharp edges, crack-tips, interfaces and discontinuities,
- be able to take into account various combination of adherend materials like metal-metal, composite-metal and composite-composite,
- incorporate fracture mechanics approach with possible failure criteria to predict the failure of the joint,
- include non-linear behaviour (elasto-plastic and visco-plastic) of the polymeric adhesive,
- study the effects of geometrical and material parameters on the performance and strength of these joints,
- examine the growth of plastic zones under different displacement boundary conditions and as the crack propagates,
- conduct some simple experiments to determine the strain energy release rates in pure modes I and II, respectively,
- determine the bond strength of the joint, and
- arrive at a simple theoretical fracture criterion, which fairly correlates well with the observed experimental results

1.4 Layout of the thesis

Present work includes (a) elastic analysis (b) elasto-plastic analysis (c) visco-plastic analysis and (d) experimental study of adhesively bonded joints

Chapter 1 serves to introduce the adhesively bonded joints Section 1 1 presents the motivation to carry out the present research work This Section provides brief introduction of adhesively bonded joints, composite material, non-linear finite element analysis, fracture mechanics approach and experiments to determine fracture parameters and the joint strength Section 1 2 contains the review of the literature In this Section literature related to (i) linear elastic analysis, (ii) non-linear (material) analysis (iii) non-linear (geometrical) analysis (iv) fracture mechanics approach (interface failure, fracture and delamination), (v) parametric study, (vi) environmental effects, (vii) quality of adhesive bonding and (viii) design of adhesively bonded joints (single lap, double lap, butt, scarf and tubular joints) are discussed Material non-linearity includes both elasto-plastic and visco-plastic behaviour Section 1 3 serves to focus on the objective of the present research work

Chapter 2 deals with the linear elastic finite element analysis of the joint and the fracture mechanics approach Section 2 1 provides a brief introduction of the linear elastic analysis of the bonded joints Section 2 2 presents the crack closure technique and finite element formulation Procedure followed to compute the failure loads and the automatic finite element mesh generation for bonded joints and the local refinement of mesh at critical zones of the joints are discussed Section 2 3 deals with the validation of computer code generated for the (linear elastic) finite element analysis Stress and strain distributions in the adhesive across the overlap length of single lap and stepped lap joints, are investigated in subsections 2 3 1 and 2 3 2, respectively Also, these distributions are investigated across the thickness of the adhesive

Section 2 4 intends to present the modelling of crack growth (quasi-static crack propagation) and validation of the finite element code computing strain energy release rates Crack is modelled with paired nodes Employing Irwin's crack closure technique strain energy release rates are computed In subsection 2 4 1 a single edge notch (SEN) specimen is considered to determine

the minimum refinement required to obtain accurate (close to the close form solution) strain energy release rate Moreover, in subsection 2 4 2, a cracked lap shear (CLS) specimen is considered to validate the finite element code calculating strain energy release rate Both plane stress and plane strain models of CLS specimen are investigated Effect of mesh refinement on the computation of strain energy release rates is investigated in Section 2 5 Parametric study is carried out in Section 2 6 These include effects of (i) crack location, (ii) thickness and Young's modulus of the adherend, (iii) stacking sequence in composite adherends, (iv) Young's modulus of the adhesive, (v) overlap length of the adhesively bonded joint, and (vi) thickness of the adhesive on the strength of the adhesively bonded joints These parameters are considered one at a time Conclusions of linear elastic analysis of these joints are discussed in Section 2 7

Elasto-plastic analysis is presented in Chapter 3 Section 3 1 provides a brief introduction of the non-linear elasto-plastic analysis Finite element model, flow chart and the algorithm for elasto-plastic analysis are illustrated in Section 3 2 In this Section stress-strain relation, convergence of the elasto-plastic analysis and effect of strain hardening on bond strength are also discussed In Section 3 3, finite element code is validated with a beam problem from literature Section 3 4 shows the spread of plastic zone based on elasto-plastic analysis Growth of plastic zone for three different boundary conditions and for crack propagation are illustrated in subsections 3 4 1 and 3 4 2, respectively In Section 3 5 the effects of various parameters (considered one at a time) on the strength of composite to composite joints are discusses Subsections 3 5 1, 3 5 2, 3 5 3 and 3 5 4 are dealt with influence of (i) stacking sequence in composite adherend, (ii) fracture toughness of adhesive (iii) overlap length and (iv) adhesive thickness on joint strength, respectively Conclusions related to the elasto-plastic analysis are discussed in Section 3 6

Visco-plastic analysis is presented in Chapter 4 Section 4 1 provides a

brief introduction of the non-linear visco-plastic analysis Strain rate, visco-elastic, visco-plastic, visco-elasto-plastic models of adhesive material, flow chart and the algorithm for visco-plastic analysis are illustrated in Section 4 2 In subsection 4 3 1, finite element code is validated with a perforated plate problem from literature Further, the visco-plastic stress analysis results are compared with those available from literature for single lap and stepped lap joints in subsections 4 3 2 and 4 3 3, respectively Section 4 4 discusses the effects of various parameters (considered one at a time) on the visco-plastic strength of composite to composite joints Subsections 4 4 1, 4 4 2, 4 4 3 and 4 4 4 are dealt with effects of (i) stacking sequence, (ii) fracture toughness of adhesive (iii) overlap length and (iv) adhesive thickness on joint strength, respectively Conclusions made from the visco-plastic analysis are discussed in Section 4 5

Experimental work is presented in Chapter 5 A brief introduction of experimental study is discussed in Section 5 1 Sections 5 2 and 5 3 describe the theories involved in determination of critical strain energy release rates in pure modes I and II, respectively Experimental determination of critical strain energy release rates in modes I and II are also reported In Section 5 4 determination of strength of the double lap carbon fibre reinforced plastic (CFRP) joints These results (bond strength) are compared with those obtained from the linear elastic finite element analysis considering various fracture criteria in Section 5 5

Concluding remarks are presented in Chapter 6 Section 6 1 contains the results and discussion of the present work Also comparison of elastic, elasto-plastic and elasto-visco-plastic results and the computation (execution) times are carried out and listed in this Section Section 6 2 presents the limitations of the present analyses Finally, in Section 6 3 few suggestions are listed for future extension of this work.

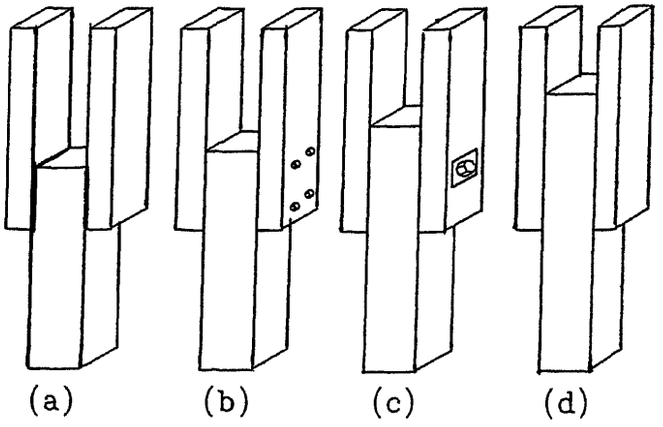

Figure 1 1 Joints of equivalent load capacity with various fastenings, (**a**) overlap 5 in, resorcinol-formaldehyde adhesive joint (**b**) overlap 9 in, four $\frac{1}{2}$ in bolts (**c**) overlap 11 in, two $2\frac{1}{2}$ in split ring connectors and one $\frac{1}{2}$ in bolt and (**d**) overlap $12\frac{1}{2}$ in, twenty-four 4 in 7 gauge nails driven in double shear into drilled holes

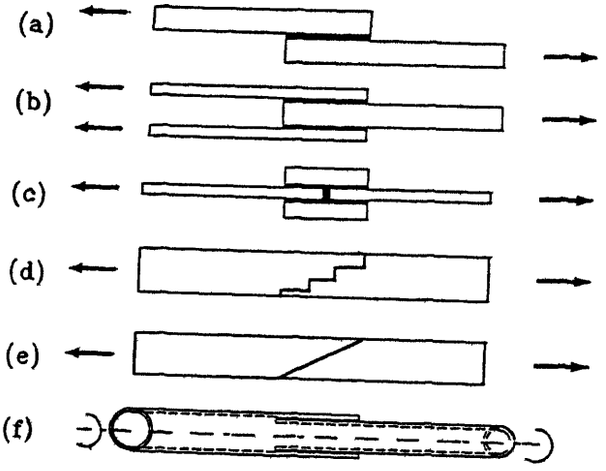

Figure 1 2 Schematics of some common adhesively bonded joints (**a**) single lap (**b**) double lap (**c**) butt with straps (**d**) stepped (**e**) scarf and (**f**) tubular lap joints

Chapter 2

Elastic analysis

2.1 Introduction

From a critical review of literature, it is observed that the finite element technique is found to be a suitable tool for the analysis of complex structures such as bonded joints In addition, fracture mechanics approach provides an accurate estimation of strength of these joints However, results, reported by various researchers in the literature, are found to be distributed over a wide range (Johnson, 1987 and Davies, et al , 1992) Therefore, it is important to estimate the strength of these joints accurately

Though, it is useful to include the material non-linearity of the adhesive, as a first step, in this Chapter, both adhesive and adherend are considered to be linear elastic in behaviour In addition, elastic analysis of the joints confirms the importance of various parameters and also forms the basis for non-linear analysis in the later Chapters Finite element code with fracture mechanics approach is developed and validated with existing results from the literature Elastic analyses of a single lap, a stepped lap and a double lap joints are carried out Various metals and fibre reinforced plastic (FRP) composites

are employed as adherends in the analyses In addition, seven fracture criteria are also considered Effect of mesh refinement on the computed strain energy release rates is investigated Influence of various parameters, such as (i) crack location, (ii) thickness of the adherend, (iii) Young's modulus of the adherend, (iv) stacking sequence in composite adherends, (v) Young's modulus of the adhesive, (vi) overlap length of the adhesively bonded joint, and (vii) thickness of the adhesive on the strength of the adhesively bonded joints, are also investigated

2.2 Formulation

Crack closure technique

Wang and Crossman (1982) discussed Griffith's strain energy release rate concept, Griffith's criterion, Irwin's crack closure integral and influence of shape of the body, loading, location, size and orientation of crack on the stress intensity factors They also emphasised the crack initiation and crack growth criteria

Griffith's criterion is employed to predict the crack growth (Broek, 1984) The stability of the crack growth is governed by the following conditions

$$G(a + \Delta a) < G_C \quad \text{stable crack growth} \tag{2 1}$$

$$G(a + \Delta a) > G_C \quad \text{unstable crack growth} \tag{2 2}$$

$$G(a + \Delta a) = G_C \quad \text{neutral crack growth} \tag{2 3}$$

where, G_C is the critical strain energy release rate and Δa represents an infinitesimal crack extension from the initial crack size 'a' as shown in Figure 2 1b

For isotropic materials the distributions of stresses near the crack-tip could be expressed in terms of stress intensity factors K_I, K_{II} and K_{III} (Broek, 1984) Strain energy release rates in mode I loading for plane stress and plane strain cases are expressed in terms of the crack-tip stress field and functional of the SIF's on the crack size

$$G_I(a) = \frac{K_I^2}{E} \qquad \text{(plane stress)} \qquad (2\,4)$$

$$G_I(a) = \frac{K_I^2}{E}(1-\nu^2) \qquad \text{(plane strain)} \qquad (2\,5)$$

a, E and ν represent the crack length, Young's modulus and Poisson's ratio, respectively For a general case of mixed mode fracture the total strain energy release rate is given by

$$G = G_I + G_{II} + G_{III} \qquad (2\,6)$$

where G_I, G_{II} and G_{III} denote the components of mode I, II and III fracture, respectively In general in fibre reinforced composite materials, fracture is a combination of all the three modes Irwin showed that the elastic strain energy released during an incremental crack extension is equal to the work done in closing the incremental crack (Wang and Crossman, 1982) This crack closure method provides an approach for the direct determination of strain energy release rates from only crack-tip stresses and displacements. When the

crack is opened as depicted in Figure 2.1b, the work done to close the crack opening could be written as

$$\Delta W = \frac{1}{2}\int_0^{\Delta a} \hat{\sigma}\,\Delta\hat{U}\,da \tag{2.7}$$

$\Delta\hat{U}$ is the relative displacements between the mating crack surfaces along Δa. $\hat{\sigma}$ is the surface stress distribution along infinitesimal crack extension Δa when the crack is closed as shown in Figure 2.1c. According to Irwin's crack closure equivalence, the available energy release rate G for a crack size a is expressed by

$$G(a) = \lim_{\Delta a \to 0} \frac{1}{2\Delta a}\int_0^{\Delta a} \hat{\sigma}\,\Delta\hat{U}\,da \tag{2.8}$$

Substituting the components of the surface stresses $\hat{\sigma}$ and the corresponding relative displacements $\Delta\hat{U}$ into Equation (2.8) yields components of G. The crack closure representation is convenient for adaptation in numerical computation. One among other methods to evaluate G is J integral technique, which is discussed by Johnson (1987).

Finite element technique

A numerical technique to calculate the strain energy release rate involves a finite element solution of Irwin's crack closure integral as given by Equation (2.8). In the finite element representation the continuous stress and displacement fields

of the solid are approximated by the nodal forces and nodal displacements, respectively Figure 2 2a represents the finite element modelling near a crack-tip region A crack of length a is shown with the crack tip at node c The finite element solution determines the displacement components (u, v, w) of the crack tip node c An incremental crack extension Δa is introduced replacing the crack tip node c with two separate nodes f and g as depicted in Figure 2 2b For the new crack geometry the finite element solution for the nodal displacements $(u, v, w)_f$ and $(u, v, w)_g$ are found for nodes f and g respectively The crack opening is then collapsed by applying equal and opposite forces at nodes f and g such that their common displacements match the displacements found earlier at c These forces correspond to the internal nodal forces which exist at node c before it opens The work required to close the crack opening (Figure 2.1c) is approximated by

$$\Delta W \simeq \frac{1}{2}[F_x(u_f - u_g) + F_y(v_f - v_g) + F_z(w_f - w_g)] \tag{2 9}$$

where F_x, F_y and F_z are normal components of nodal forces required to bring nodes f and g together The energy release rates for the three crack extension modes are approximated by

$$G_I = \frac{1}{2\Delta a}[F_y(v_f - v_g)] \tag{2 10}$$

$$G_{II} = \frac{1}{2\Delta a}[F_x(u_f - u_g)] \tag{2 11}$$

$$G_{III} = \frac{1}{2\Delta a}[F_z(w_f - w_g)] \tag{2 12}$$

This method does not require the calculation of the stresses and strains as stress and strain fields are approximated by nodal forces and displacements,

respectively Therefore, this method has the advantage of less computation and more accuracy as compared to other methods, where one needs to compute the stresses and strains

Prediction of failure load

A computer code is developed to predict the failure load, which is detailed in the following main algorithm and the flow chart is depicted in Figure 2 3 Though the algorithm and the flow chart are meant for linear elastic material, these are extended later to include elasto-plastic and visco-plastic materials by adding corresponding modules Details of these additional modules are explained in Chapters 3 and 4 The loads are updated in each iteration, strain energy release rate is computed for a pre-asigned crack path along the interface of the adhesive and adherend The computed strain energy release rate value is compared with its critical value within 1 percent tolerance Once this condition is satisfied paired node is opened (Wang, 1982) and the corresponding failure load and crack length are noted

The failure load is observed to be strongly influenced by the fracture criterion and the critical strain energy release rates Seven possible fracture (Table 2 1)
criteria are considered and the corresponding failure load vs crack length variations are compared in Figure 2 4 As will be shown later, in Section 5 4, the fracture criterion $G_I + G_{II} \geq G_{IC} + G_{IIC}$ is the most suitable one, among the seven criteria considered Therefore, in the present analysis this failure criterion is employed

Main algorithm

step 01 : read input data such as geometrical, material and mesh

parameters and various options

step 02 calculate stiffness matrix $[K]$

step 03 update applied load ΔP

step 04 solve for displacement
$\Delta\delta = [K]^{-1}\Delta P$

step 05 update displacement, strain and stress
$\delta = \delta + \Delta\delta$
$\epsilon = \epsilon + \Delta\epsilon$
$\sigma = \sigma + \Delta\sigma$

step 06 if plastic flow occurred
(i e a major portion of adhesive has become plastic)
or, maximum allowed load is achieved
or, all prescribed paired nodes are opened
(i e critical crack length is reached) then go to step 09

step 07 · compute the strain energy release rate (G)
and compare with its critical value (G_C)
if $1\ 01G_C \geq G \geq G_C$ then open the paired node and go to step 03
else go to step 03

step 08 if elastic analysis else go to step 07
if elasto-plastic analysis go to
step 01 of *elasto-plastic algorithm* in Section 3 2
if visco-plastic analysis go to
step 01 of visco-plastic *algorithm* in Section 4 2

step 09 · stop

- *Automatic mesh generation*

A finite element mesh generation computer code is developed, which automatically generates refined meshes for problems considered in the present work viz (i) a cantilever beam, (ii) a perforated plate, (iii) a cracked lap shear (CLS) specimen, (iv) single edge notch (SEN) specimen, (v) adhesively bonded single lap, double lap and stepped lap joints This makes use of Chebyshev's function to generate necessary mesh refinements at crack-tips and other stress concentration zones Thus, with less number of elements one could achieve reasonably accurate results A typical finite element mesh of adhesively bonded joint with more refinement at edges is shown in Figure 2 5 of next Section The code also generates data for the paired nodes at the interfaces and nodal forces and displacement boundary conditions The paired nodes, are opened in a sequence along a pre-defined (crack) path, simulating the crack growth, which facilitates calculation of the strain energy release rates

2.3 Validation of finite element code

To validate the computer code of finite element developed a single lap joint and a stepped lap joint are considered Stress and strain distributions along the overlap lengths are compared with those available in open literature

2.3.1 Single lap joint

To check the accuracy of computer code of finite element analysis, a single lap joint (Figure 2 5) is employed Details of the joint are listed in Table 2 2 In Figure 2 6 the computed peel stress and shear stress distributions along the

overlap are compared with those of Hiregoudar (1993) Results of the present analysis (with 1816 CST elements) are in good agreement with Hiregoudar (1993) The differences are of the order of 6 and 12 percent, for the peel and shear stresses along the overlap length, respectively (Figure 2 6) Maximum difference is observed near the end region of the overlap This difference is found to be minimum near the central portion of the overlap Because of the effective refinement in the finite element mesh near the edges and near the interfaces of adhesive and adherends, in the present analysis, predicted stress distributions are expected to be more accurate

2.3 2 Stepped lap joint

Further, validation of the computer code of finite element developed is carried out on a stepped lap joint Figure 2 7 illustrates the joint with a typical finite element mesh In this joint, thick adherends are employed and thus it is also called as thick adherend shear test (TAST) specimen Specifications of the joint are listed in Table 2 3 In Figures 2 8 and 2 9 the stress and strain distributions along the overlap at the interface of adherend and adhesive are compared with those of Su and Mackie (1993), respectively Similarly, in Figures 2 10 and 2 11 stress distributions along the overlap at the midline of adhesive are compared Results of the present analysis (with 1816 CST elements) are observed to be in good agreement with Su and Mackie (1993) Near both ends (edges) of the overlap there are ___ differences in these distributions Because of the effective refinement in the finite element mesh near the edges, the distributions obtained from Present analysis are expected to be more accurate The stress and strain distributions along the overlap and across the thickness of the adhesive are shown in Figures 2 12, 2 13 and 2 14, respectively Because of the antisymmetric joint configuration of the joint about the midline of the adhesive, stress and strain distributions in layers 1 and 5 are found to be antisymmetric Similar distributions are also observed

in layers 2 and 4

2.4 Validation of crack closure technique

2.4.1 Single edge notch specimen

A single edge notch (SEN) specimen (Figure 2.15) is considered as a sample problem to validate the proposed technique. The physical dimensions of the specimen and material properties are listed in Table 2.4 and a schematic of finite element mesh used, is illustrated in Figure 2.15.

Using modified crack closure integral and constant strain finite element stress analysis (AXISOL) Rybicki and Kanninen (1977) evaluated stress intensity factors and applied to three configurations (i) a double cantilever beam test specimen, (ii) a finite width plate containing an embedded crack and (iii) a bolt fastened double lap joint containing two radial cracks. They observed that the results computed employing higher order elements are less accurate as compared to those obtained with constant strain triangular (CST) elements, which uses nodal forces and nodal displacements. Therefore, a two-dimensional linear small displacement plane strain CST element (Zienkiewicz and Taylor, 1989) is employed for the present work.

Finite element mesh with fine grids near the crack tip and paired nodes on the line MN (Figure 2.15) are generated. A uniform far field stress σ is applied transverse to the crack to allow it to fail in mode I fracture. Material of the specimen is considered to be aluminium. Stress intensity factor is expressed as (Broek, 1984)

$$K_I(a) = \sigma\sqrt{a}\, f\left(\frac{a}{W}\right) \tag{2 13}$$

where

$$f\left(\frac{a}{W}\right) \simeq 1\,99 - 0\,41\left(\frac{a}{W}\right) + 18\,7\left(\frac{a}{W}\right)^2 - 38\,48\left(\frac{a}{W}\right)^3 + 53\,85\left(\frac{a}{W}\right)^4 \tag{2 14}$$

where a and W represent the crack length and width of the specimen, respectively

The exact solution of G_I is calculated with Equations (2 4) and (2 14) G_I is also computed using finite element analysis employing meshes of 520, 1360 and 2688 elements, respectively and the results are compared The error in the estimation of G_I is reduced rapidly as the grid is more and more refined The estimated error is observed to be less than 1 6 percent for a finite element mesh of 2688 elements (Figure 2 15)

2 4 2 Cracked lap shear specimen

A four-point bending cracked lap shear (CLS) specimen (Figure 2 16) is also considered for the analysis Adherends and adhesive are considered to be aluminium and epoxy resin, respectively and their material properties and physical dimensions are listed in Table 2 5 In the present analysis, a fine mesh, of 5786 CST elements, is generated with proper refinement near the interface lines and paired nodes along the bottom interface line Schematic representation of finite element mesh used is illustrated in Figure 2 16 This problem, is investigated treating it as plane stress and plane strain models and

the results (strain energy release rate) are compared with the corresponding experimental results of Fernlund and Spelt (1991c)

Ishikawa, et al (1991) investigated the mixed mode fracture criteria for adhesive joints and carried out fracture tests on acryl adherends and epoxy resin adhesive They concluded that total strain energy release rate is a dominant parameter, which characterise the crack propagation of the adhesive joints In the present work also, results based on the mixed mode fracture criterion ($G_I + G_{II} \geq G_{IC} + G_{IIC}$) shows better agreement with the results obtained from the experiment This is listed in Table 5 4, in Chapter 5

Therefore, the total energy release rate $G (= G_I + G_{II})$ is considered as the criterion for crack propagation Variations of G_I, G_{II} and G with crack length a, are plotted in Figure 2 17, for plane strain and plane stress cases and compared with the experimental result of Fernlund and Spelt (1991c) The difference is found to be less than 2 7 percent for plane strain model, while this is of the order of 5 5 percent for the plane stress model Therefore, the plane strain model represents the situation relatively better than the plane stress model It is also verified that the ratio of G_{II} and G_I remains constant for the same thickness of adherends as mentioned by Fernlund and Spelt (1991c) However, in the Figure 2 17, initially strain energy release rate increases with crack length (till a = 2 mm), which is mainly due to the edge effect For the failure load P_f (6 33 N per mm width), G is observed to be very close to the critical strain energy release rate (G_c = 0 366 kJm^{-2})

The finite element model predicts a value of $G_c \simeq 0\,35 kJm^{-2}$, while the results predicted from Figure 2 17 is 0 $366 kJm^{-2}$ The present results are likely to be more accurate as elasticity approach is employed in the present analysis, where as solid mechanics approach was used by Fernlund and Spelt (1991c)

2.5 Mesh refinement

To investigate the influence of the effect of mesh refinement on the computation of strain energy release rate, a double lap joint (Figure 2 18) is analysed with three different levels of refinements consisting of 680, 1184 and 1816 CST elements Because of symmetry only one half of the joint is considered for the analysis The problem is treated as one of plane strain model The joint specifications are listed on Table 2 6 The crack is introduced and allowed to grow and the corresponding strain energy release rates are computed for the above refined meshes Variations of strain energy release rates with crack length are shown in Figure 2 19

It is observed that the nature of the curves do not change with mesh refinement Refinement level does not have any significant change in the strain energy release rates values as well In the investigation of adhesively bonded joint, refined mesh with 1816 elements are considered However, more refined mesh is useful to analyse the free-edge effect particularly, when the thickness of the adhesive is very small A case study is presented in the subsection 2 6 6, where effect of adhesive thickness on joint strength is discussed

2.6 Parametric study

Acc. No. A. 121426

Effects of crack location, thickness of adherend, Young's modulus of adherend, stacking sequence of composite adherend, Young's modulus of adhesive, overlap length and thickness of adhesive on the strength of the double lap joint (Figure 2 18) are investigated Because of symmetry only one half of the joint is considered for the analysis The structure is treated as a plane strain model A finite element mesh consists of 1816 CST elements (Figure 2 5) is employed for

the analysis From the computation of strain energy release rate, it is observed that there exist a crack length a_x at which G_I and G_{II} values are equal This is indicated in Figure 2 19 Further, before crack length attains a value of a_x, mode I is found to be dominating and later mode II dominates

For convenience, three non-dimensional parameters are defined viz

$$\mathbf{e} = \frac{E_s}{E_r} \tag{2 15}$$

$$\mathbf{l} = \frac{L_o}{L_t} \tag{2 16}$$

$$\mathbf{t} = \frac{t_s}{t_r} \tag{2 17}$$

where, E_s and E_r are the elastic moduli of adhesive and adherend L_o and L_t denote the overlap length and the total length of the bonded joint In addition t_s and t_r represent the thicknesses of adhesive and adherend, respectively Assuming constant adherend thickness t_r, overlap length L_o and Young's modulus of adherend E_r, parametric study is carried out

The value of **e** is 1/20 for Epon VIII adhesive and aluminium adherend For convenience, this value is also mentioned to be 1/20 even for Epon VIII adhesive and various CFRP composite adherends For example, if **e** ($= E_s/E_r$) is 1/40 implies that, the adhesive considered has a Young's modulus of 1/2 times that of Epon VIII

2 6.1 Crack location

Effect of crack location on the strength of the double lap joint (Figure 2 18) is also investigated The adherends and adhesive of the joint, are considered to be aluminium and Epon VIII (Table 2 7), respectively

Eight different crack locations at the interfaces (Figure 2 20c) and corresponding crack growths are considered, which are described in Table 2 8 In the present work the criterion for failure is based on $G_I + G_{II} \geq G_C$ Finite element analysis is carried out for two different boundary conditions viz free side type and constrained side type (Figure 2 20a-b) Variation of strain energy release rate G, with crack length a, for the free side type boundary condition is plotted in Figure 2 21 For the crack location 3, it is found that the stresses are maximum as there is no constraint imposed on the adherend at this location and hence free to deform

In the constrained side type boundary condition (Figure 2 20b) mode II is found to be dominating For this boundary condition, variation of strain energy release rate with crack length is depicted in Figure 2 22 It is observed that crack growths at diagonally opposite locations 1 and 3 are equally prone to fail Similarly, crack growths at locations 2 and 4 show same variation of G with a Further, crack growths at locations 5, 6, 7 and 8 exhibit similar variations of G with a

For both the boundary conditions (free side and constrained side types) the crack propagation remains stable till the crack length reaches the critical value a_{cr} and beyond that the growth becomes unstable leading to failure The corresponding strain energy release rate is denoted as G_{cr} (Figure 2 21) This figure also indicates the a_{cr} and G_{cr} for this boundary condition For eight different crack locations considered for both the boundary conditions critical crack length a_{cr}'s and corresponding G_{cr}'s are listed in Table 2 9

From Figures 2 21 and 2 22, it may further be observed that G_I has increasing and decreasing nature initially for the cases of crack locations 1, 2, 3 and 4 and smooth increasing variation for crack locations 5, 6, 7 and 8 This complex behaviour at locations 1, 2, 3 and 4 can be attributed to free-edge effect The strain energy release rate G_{cr}, for the crack growth at location 3,

for the free side type boundary condition, is computed to be 19 5 kJ/m^2 This value is greater than that for crack growth at location 3 for the constrained side boundary condition The free side boundary condition results in a relatively weaker joint Thus, for the parametric study the crack location 3 and the free side type boundary condition are considered Further, the finite element mesh is refined near crack location 3 instead of refinement near all edge points viz 1, 2, 3 and 4

2.6 2 Thickness and Young's modulus of the adherend

Failure loads are computed for various crack locations in the double lap joint (Figure 2 20c and Table 2 8) and various combinations of adherends of different thicknesses and materials (Table 2 12) Four different thickness ratios are considered viz $t_r(upper)/t_r(lower) = 0\,5, 1, 2$ and 4 Thickness of the lower adherend was maintained constant Metal to metal, composite to metal and composite to composite joints are considered for the analysis In metals, aluminium, copper, brass and steel are considered In the case of composite materials glass-, kevlar-, carbon- and graphite-, fibre reinforced plastics are employed The elastic properties of the metal and composite adherends are listed in Tables 2 10 and 2 11, respectively Failure loads for metal to metal, composite to metal and composite to composite joints are listed in Tables 2 13–2 14, 2 15 and 2 16, respectively All the minimum (critical) failure loads among each set of the four locations considered are indicated with '†' It is found that in most of the cases location '3' is observed to be critical In the case of aluminium to brass and carbon fibre reinforced plastic (CFRP) to graphite fibre reinforced plastic (GFRP) joints (Tables 2 13 and 2 16) for the thickness ratio 0 5 crack locations '1' and '4' yield same failure load This result could be refined using reduced load steps in the analysis However, the difference may not be insignificant

For the thickness ratio 0 5 in aluminium to aluminium joint crack location '1' is found to be critical (Table 2 13) Location '4' yields minimum failure load for the thickness ratios 0 5 and 1 of aluminium to copper joint While, location '4' gives minimum failure load for the thickness ratios 0 5, 1 and 2 of aluminium to steel joint Further, location '4' yields minimum failure load for the thickness ratios 0 5, and, 0 5 and 1 of carbon composite to brass and carbon composite to steel, respectively (Table 2 15) Failure load is observed to be higher for thinner adherends For example the failure loads are in increasing order for thickness ratios, 0 5, 1, 2 and 4

2 6.3 Stacking sequence

Effect of stacking (layup) sequence of the composite adherends on the strength of the double lap joint (Figure 2 23) is investigated The adherends and adhesive of the joint, are considered to be carbon fibre reinforced plastics (CFRP) and Epon VIII (Table 2 7), respectively Unidirectional 0° and 90° layups and all symmetric combinations of 0°, 90°, 45°, and -45° layups are considered for the study The ordering of lamina is from top layer to bottom layer The plies corresponding to 0°, 90°, 45°, and –45° fibre orientations are identified as plies, 1, 2, 3 and 4, respectively, e g $[1324]_S$ implies $[0°/45°/90°/-45°]_S$ laminate Further, the transformed stiffness coefficients required for the analysis is obtained from the relations given in Jones (1975)

Variation of failure load with crack length for all the 24 different combinations of stacking sequences in composite adherend $[1324]_S$ are shown in Figures 2 24 and 2 25 Symmetric laminates of combinations 1324, 1342, 1234, 1243, 1423, and 1432 are found to have approximately equal and higher strength than rest of the combinations This study indicates that if one employs 0° plies in the immediate neighbourhood of adhesive one can achieve a stronger joint

(Figure 2 25) Out of total 24 possible combinations the maximum bond strength is observed for the laminate with $[1324]_S$ as ply sequence This is termed as optimal layup in the present work The joint with unidirectional laminates of 0° as the adherends is found to be strongest

The variations of failure load with crack length are discussed for the different crack locations (Figure 2 20c) in $[0^\circ_{4S}, 0^\circ_{4S}]$, $[90^\circ_{4S}, 90^\circ_{4S}]$, $[0^\circ_{4S}, 90^\circ_{4S}]$, $[90^\circ_{4S}, 0^\circ_{4S}]$ laminate pairs constituting the top and bottom adherends, e g $[0^\circ_{4S}, 90^\circ_{4S}]$ represents $[0°]_8$ and $[90°]_8$ unidirectional layups constitute bottom and top adherends, respectively Failure load vs crack length curves are illustrated for $[0^\circ_{4S}, 0^\circ_{4S}]$, $[90^\circ_{4S}, 90^\circ_{4S}]$, $[0^\circ_{4S}, 90^\circ_{4S}]$, $[90^\circ_{4S}, 0^\circ_{4S}]$ laminate pairs for crack locations at 1,3 and 4 in Figures 2 26, 2 27 and 2 28, respectively It is observed that the trend of load with crack length in $[0^\circ_{4S}, 0^\circ_{4S}]$ and $[90^\circ_{4S}, 90^\circ_{4S}]$ layups are opposite to those in $[0^\circ_{4S}, 90^\circ_{4S}]$ and $[90^\circ_{4S}, 0^\circ_{4S}]$ layups The failure loads for these combinations with for the most likely crack growth and the corresponding crack lengths are listed in Table 2 17 and shown in Figure 2 29

2.6 4 Young's modulus of adhesive

Effect of adhesive elastic properties on the strength of the double lap joint (Figure 2 18) is also investigated Strain energy release rate is plotted in Figure 2 30 as a function of crack length for various adhesive properties of double lap joint with aluminium adherend and Epon VIII adhesive, (Table 2 7) The values of a_x's and corresponding G_x's for different e (= E_a/E_r) values are listed in Table 2 18 Failure loads are calculated in terms of fracture toughness G_C of the adhesive material, for various values of e and are listed in Table 2 18 The dimension of G_C is kJ/m^2 As the adhesive Young's modulus E_a increases e also decreases This results in, decrease in G (Figure 2 30) and as a consequence corresponding failure load P_f increases For various e values, failure loads are

calculated in terms of fracture toughness G_C of the adhesive material and listed in Table 2 18 Critical crack length a_{cr}, is observed to remain constant for all values of **e** As the Young's modulus of the adhesive increases, **e** increases and slope of the curves G vs a decrease This indicates unstable crack growth and higher failure load are associated with higher adhesive Young's modulus Therefore, it is advantageous to use adhesive materials with higher Young's modulus values which leads to high Young's moduli ratio **e** resulting in a joint of high strength

Failure loads and the crack length variations are studied for the joint of carbon fibre reinforced plastics (CFRP) adherends and Epon VIII adhesive (Table 2 7), respectively For various **e** values and layups the predicted failure loads P_f's are shown in Table 2 19 It is observed that as **e** increases P_f increases appreciably for $[0^\circ_{4S}, 0^\circ_{4S}]$ laminates, while it is reversed for $[0^\circ_{4S}, 90^\circ_{4S}]$ and $[90^\circ_{4S}, 0^\circ_{4S}]$ laminates and remains fairly constant for $[90^\circ_{4S}, 90^\circ_{4S}]$ laminates Also crack growth is more stable in case of $[90^\circ_{4S}, 0^\circ_{4S}]$ layup In the case of optimal layup as **e** increases, strength increases Therefore, in order to obtain higher fracture strength, adhesive with higher elastic modulus (high value of **e**) for $[0^\circ_{4S}, 0^\circ_{4S}]$ and optimal layup laminate and lower elastic modulus (low value of **e**) for $[0^\circ_{4S}, 90^\circ_{4S}]$ and $[90^\circ_{4S}, 0^\circ_{4S}]$ laminates are suggested Variations of failure load with the crack length for different **e** values in $[0^\circ_{4S}, 0^\circ_{4S}]$ and optimal layup $[1324_S, 1324_S]$ are shown in Figures 2 31 and and 2 32, respectively

2.6.5 Overlap length

Effect of overlap length on the strength of the double lap joint (Figure 2 18) is studied Strain energy release rate is plotted in Figure 2 33 as a function of crack length for various overlap lengths in a double lap joint of aluminium adherend and Epon VIII adhesive, (Table 2 7) The values of a_x's and corresponding

G_x's for different l (= L_o/L_t) values are listed in Table 2 20 Failure loads are calculated in terms of fracture toughness (G_C) of the adhesive material, for various values of l and listed in Table 2 20 As the overlap length L_o increases l also increases As l increases strain energy release rate decreases (Figure 2 33a and 2 33b) and thus failure load P_f increases

With an increase in the overlap length l, a_x initially increases and then decreases But, with an increase in the overlap length l, a_{cr} initially decreases and later increases The failure load P_f is increased substantially as l is increased from 0 166 to 0 250 (Table 2 20) As l increases slope of the curves G vs a decrease This indicates faster and unstable crack growth and, low failure loads are associated with small overlap length Therefore, it is advantageous to use large overlap length, which leads to high overlap ratio l, resulting in a joint of more strength For various l ratios, failure loads are calculated in terms of fracture toughness G_C of the adhesive material and listed in Table 2 20

Failure loads and the crack length variations are studied for the joint of carbon fibre reinforced plastics (CFRP) adherends and Epon VIII adhesive (Table 2 7), respectively For various l values and laminate combinations the predicted failure loads P_f's are shown in Table 2 21 It is observed that as l increases P_f increases appreciably for all combination of 0°_{4S}, 90°_{4S} plies, and optimal layup For $[0^\circ_{4S}, 0^\circ_{4S}]$ layup P_f is almost double as compared to rest of the layups including optimal layup More stable growth is observed in the case of $[90^\circ_{4S}, 0^\circ_{4S}]$ layup In particular for $[0^\circ_{4S}, 0^\circ_{4S}]$ and optimal layup l preferably be more than 0 250 Variations of failure load with the crack length for different l values in $[0^\circ_{4S}, 0^\circ_{4S}]$ and optimal $[1324_S, 1324_S]$ laminates are shown in Figures 2 34 and 2 35, respectively As also revealed by these figures for higher fracture strength, large overlap length (high value of l) is suggested.

2.6 6 Adhesive thickness

Effect of adhesive thickness on the strength of the double lap joint (Figure 2 18) is investigated Strain energy release rate is plotted in Figure 2 36 as a function of crack length for various adhesive thickness ratios t (= t_s/t_r) in double lap joint of aluminium adherend and Epon VIII adhesive, (Table 2 7) Failure loads and the crack length variations are studied for the joints of unidirectional (0°) carbon fibre reinforced plastics (CFRP) adherends and Epon VIII adhesive (Table 2 7) With increase in t, adhesive thickness increases and the mesh refinement decreases in the adhesive region As the adhesive thickness t_s increases (t increases), G increases (Figure 2 36) and thus failure load P_f decreases Critical crack length (a_{cr}) is observed to decrease with adhesive thickness It is also found that variation of strain energy release rate with crack length for t = 0 0125 and t = 0 0100 is nearly same The slope of the curve (G vs a) increases as adhesive thickness increases

It is also observed that as the crack grows from the location 3 (Figure 2 20c) along the interface, strain energy release rate of mode I, initially increases to a maximum, then decreases and again increases It can be observed from the curves that this local free-edge effect is confined to a small crack length, which is of the order of size of the adhesive thickness (t_s) For the study of effect of adhesive thickness on bond strength and the free-edge effect, a more refined mesh consisting of 3376 elements and paired nodes at the interfaces is employed From Figure 2 37, it can be observed that there is an increase and then decrease in the value of G close to the free edge As the adhesive thickness increases (t value increases) this local variation diminishes and is confined to a small zone near the free-edge Further, for very small adhesive thickness (t = 0 0100) this local effect is found to be negligible Associated slope of G vs a curve monotonically decreases, as a consequence the crack growth is unstable

Present analysis indicates faster and unstable crack growth and, lower

failure loads are associated with large adhesive thicknesses Therefore, it is advantageous to use small adhesive thickness, which leads to low thickness ratio t resulting in a joint of high strength However, the value of t below 0 0125 has no extra advantage For various t ratios, failure loads are calculated in terms of fracture toughness (G_c) of the adhesive material and listed in Table 2 22

For various t values and laminate combinations the predicted failure loads P_f's are shown in Table 2 23 As t increases the failure load decreases for $[0^\circ_{4S}, 90^\circ_{4S}]$ and $[90^\circ_{4S}, 0^\circ_{4S}]$ layups In all the laminates, there is no significant change in the failure load for $t \leq 0\,0125$ For $t = 0\,2000$ and $t = 0\,1000$ the crack growths are found to be stable for $[90^\circ_{4S}, 90^\circ_{4S}]$, $[0^\circ_{4S}, 90^\circ_{4S}]$ and $[90^\circ_{4S}, 0^\circ_{4S}]$ layup sequence and unstable crack growth is observed in $[0^\circ_{4S}, 0^\circ_{4S}]$ layup and optimal layup One can therefore, conclude that for higher joint strength, small thickness of adhesive (low value of t) is preferable for $[0^\circ_{4S}, 0^\circ_{4S}]$, $[0^\circ_{4S}, 90^\circ_{4S}]$, optimal layup Variations of failure load with the crack length for different t values in $[0^\circ_{4S}, 0^\circ_{4S}]$ and $[1324_S, 1324_S]$ (optimal layup) are shown in Figures 2 38 and 2 39, respectively

Though the nature of G vs a curves are not affected by mesh refinement for e and l variations, it is observed that refined mesh is useful for the study of free-edge effect particularly for small adhesive thickness Further, it is observed that high adhesive stiffness e, high overlap length l and low adhesive thickness t are desirable for a strong double lap joint Critical crack length is found to be a function of geometrical parameters l, t and independent of material parameter e

2.7 Conclusions

On the basis of linear elastic analysis carried out in this Chapter, the following conclusions are drawn

- The finite element approach with paired nodes modelling the crack provides a simple computational tool to predict joint failure However, fine grids near the crack-tip are necessary for accurate estimation of strain energy release rates

- Use of Chebyshev's function is found to be effective for automatic mesh generation with various refinements at critical zones

- Stress distributions along the overlap length of the single lap joint are predicted by the present computer code and the results agree with the those reported by Hiregoudar (1993)

- Stress distributions are also predicted along the overlap length and across the adhesive thickness of thick adherend shear test (TAST) specimen and the results are observed to agree with the those reported by Su and Mackie (1993)

- In case of single edge notch (SEN) specimen, with 2688 elements and with fine mesh near the crack-tip, error estimated in the value of strain energy release rate is less than 1 6 percent (as compared to close form solution)

- Strain energy release rate computed by the present finite element analysis with fracture mechanics approach agrees well with the experimental result for cracked lap shear (CLS) specimens (Fernlund and Spelt, 1991c) The difference is less than 2 7 percent.

- Cracks located at the edges are more critical than those at the central part of the overlap region Further, in symmetric boundary conditions the diagonally opposite cracks are equally prone to failure
- Introduction of 0° ply in the immediate neighbourhood of adhesive results in a stronger joint In addition, a proper choice of layup sequence results in an efficient bonded joint
- Use of adhesives of high Young's moduli results in stronger bonded joint
- Employment of longer overlap length results in stronger bonded joint
- Use of small thickness of adhesive results in stronger bonded joint
- For bonded joints with very thin adhesives free-edge effects are found to be significant Moreover, for the analysis of bonded joints having very small adhesive thicknesses, more refined meshes are preferred to account for the free-edge effects

Table 2.1 Seven fracture criteria considered in the finite element analysis

Criterion type	Expression
1	$G_I + G_{II} \geq G_{IC} + G_{IIC}$
2	$G_I \geq G_{IC}$
3	$G_{II} \geq G_{IIC}$
4	$G_I + G_{II} \geq G_{IC}$
5	$G_I + G_{II} \geq G_{IIC}$
6	$\frac{G_I}{G_{IC}} + \frac{G_{II}}{G_{IIC}} \geq 1$
7	$\left(\frac{G_I}{G_{IC}}\right)^2 + \left(\frac{G_{II}}{G_{IIC}}\right)^2 \geq 1$

Table 2 2 Specifications of single lap joint (Hiregoudar, 1993)

Single lap joint

overlap length (L_o)	16 mm
total length (L_t)	80 mm
applied stress (σ)	200 MPa
adhesive thickness (t_s)	0 30 mm
adherend thickness (t_r)	1 60 mm

Adhesive (FM 73)

Young's modulus (E_s)	2 21 Gpa
Poisson's ratio (ν_s)	0 43
yield stress (σ_o)	40 Mpa

Adherend (Steel)

Young's modulus (E_r)	211 3 GPa
Poisson's ratio (ν_r)	0 33
yield stress (σ_o)	∞

Table 2 3 Specifications of stepped lap joint (thick adherend shear test specimen of Su and Mackie, 1993)

Joint configuration	
overlap length (L_o)	8 mm
total length (L_t)	125 mm
applied load (P)	3 5 kN
total joint thickness (t)	13 35 mm
width of the joint (W)	25 4 mm
Adhesive (rubber-toughened epoxy)	
Young's modulus (E_s)	6 60 Gpa
Poisson's ratio (ν_s)	0 38
thickness of adhesive (t_s)	0 65 mm
Adherend (Steel)	
Young's modulus (E_r)	210 Gpa
Poisson's ratio (ν_r)	0 3
thickness of adherend (t_r)	6 35 mm

Table 2 4 Physical dimensions and material properties of SEN specimen (Figure 2 15)

length (L)	100 mm
width (W)	50 mm
thickness	1 mm
crack length (a)	2 mm
Young's modulus (E)	70 GPa
Poisson's ratio (ν)	0 3
stress applied (σ)	0 1 GPa

Table 2 5 Physical dimensions and material properties of CLS specimen (Figure 2 16)

Adhesive (Cybond 4523 GB)	
Young's modulus	8 GPa
Poisson's ratio	0 35
thickness	0 21 mm
width	10 mm
length	180 mm

Adherend (Aluminium 6061–T6)	
Young's modulus	70 GPa
Poisson's ratio	0 3
thickness	3 06 mm
width	10 mm
lengths	180 mm and 240 mm
load (P_f)	6 33 N/mm

Table 2 6 Specifications of the adhesively bonded joint (Figure 2 18)

Joint specifications

total length (L_t)	80 mm
overlap length (L_0)	40 mm
load applied (P)	1000 N/mm
width (W)	1 mm

Adhesive (Epon VIII)

Young's modulus (E_s)	3 5 GPa
Poisson's ratio (ν_s)	0 41
thickness (t_s)	2 mm

Adherend (Aluminium)

Young's modulus (E_r)	70 GPa
Poisson's ratio (ν_r)	0 367
thickness (t_r)	10 mm

Table 2 7 Specifications of double lap joint

Double lap joint

overlap length (L_o)	40 mm
total length (L_t)	80 mm

Adherend (Aluminium)

Young's modulus (E_r)	70 GPa
Poisson's ratio (ν_r)	0 3
adherend thickness (t_r)	10 mm

Adherend (carbon fibre reinforced plastic)

longitudinal modulus (E_l)	137 GPa
transverse modulus (E_t)	7 GPa
shear modulus G_{lt}	4 5 GPa
Poisson's ratio (ν_{lt})	0 3
adherend thickness (t_r)	10 mm

Adhesive (Epon VIII)

Young's modulus (E_s)	3 5 GPa
Poisson's ratio (ν_s)	0 41
thickness (t_s)	2 mm
fracture toughness (G_C)	0 366 kJ/m^2

fracture criterion $G_I + G_{II} \geq G_C$

Table 2 8 Description of eight different crack locations and their growth direction (Figure 2 20c)

Crack Location	Interface	From	To
1	bottom	left edge	center
2	bottom	right edge	center
3	top	right edge	center
4	top	left edge	center
5	bottom	center	left edge
6	bottom	center	right edge
7	top	center	left edge
8	top	center	right edge

Table 2 9 Computed critical strain energy release rates for two different types of boundary conditions and eight different crack locations (Figure 2 20a-c)

crack growth	free side		constrained side	
location	a_{cr}(mm)	$G_{cr}(kJ/m^2)$	a_{cr}(mm)	$G_{cr}(kJ/m^2)$
1	1 72	7 5	1 72	14 2
2	0 98	0 5	0 98	0 5
3	1 72	19 5	1 72	14 2
4	0 98	5 7	0 98	0 5
5	2 1	6 2	2 1	6 5
6	2 1	6 2	2 1	6 5
7	2 1	5 8	2 1	6 5
8	2 1	5 8	2 1	6 5

Table 2 10 Material properties of metal adherends

	aluminium	**brass**	**copper**	**steel**
Young's modulus (GPa)	70	90	120	210
Poisson's ratio	0 3	0 25	0 25	0 25

Table 2 11 Material properties of composite adherends

glass fibre reinforced plastic	
longitudinal modulus (E_l)	39 GPa
transverse modulus (E_t)	10 GPa
shear modulus G_{lt}	7 GPa
Poisson's ratio (ν_r)	0 25
kevlar fibre reinforced plastic	
longitudinal modulus (E_l)	83 GPa
transverse modulus (E_t)	5 6 GPa
shear modulus G_{lt}	2 1 GPa
Poisson's ratio (ν_r)	0 34
carbon fibre reinforced plastic	
longitudinal modulus (E_l)	137 GPa
transverse modulus (E_t)	7 GPa
shear modulus G_{lt}	4 5 GPa
Poisson's ratio (ν_r)	0 3
graphite fibre reinforced plastic	
longitudinal modulus (E_l)	159 GPa
transverse modulus (E_t)	10 9 GPa
shear modulus G_{lt}	6 4 GPa
Poisson's ratio (ν_r)	0 38

Table 2 12 Specifications of double lap joint

Double lap joint	
overlap length (L_o)	120 mm
total length (L_t)	240 mm
lower adherend thickness (t_r)	2 mm
Adhesive (Epon VIII)	
Young's modulus (E_s)	3 5 GPa
Poisson's ratio (ν_s)	0 41
thickness (t_s)	0 1 mm
fracture toughness (G_C)	1 11 kJ/m^2

fracture criterion $G_I + G_{II} \geq G_C$

where $G_C = G_{IC} + G_{IIC}$

Table 2 13 Computed failure loads in N/mm for joints of aluminium and various metals

$\frac{t_r(upper)}{t_r(lower)}$	crack locations			
	1	2	3	4
	aluminium to aluminium			
0 5	144 99†	264 99	212 49	148 74
1	249 99	212 49	167 49†	242 49
2	459 99	182 49	141 24†	429 99
4	849 99	163 74	129 99†	774 99
	aluminium to copper			
0 5	129 99	422 49	339 99	126 24†
1	212 49	324 99	261 24	197 49†
2	369 99	268 74	212 49†	324 99
4	654 99	234 99	182 49†	564 99
	aluminium to brass			
0 5	137 49†	324 99	264 99	137 49†
1	234 99	257 49	204 99†	219 99
2	414 99	216 24	171 24†	377 49
4	744 99	193 74	152 49†	669 99
	aluminium to steel			
0 5	118 74	699 99	579 99	113 12†
1	186 25	534 99	429 99	167 49†
2	302 49	414 99	324 99	264 99†
4	519 99	347 49	272 49†	429 99

† minimum failure load among the four crack locations

Table 2 14 Computed failure loads in N/mm for joints of steel and various metals

$\frac{t_r(upper)}{t_r(lower)}$	crack locations			
	1	2	3	4
	steel to aluminium			
0 5	324 99	197 49	159 99†	339 99
1	594 99	174 99	141 24†	609 99
2	1134 99	163 74	129 99†	1134 99
4	–	156 25	124 37†	–
	steel to copper			
0 5	272 49	294 99	242 49†	272 49
1	474 99	253 74	204 99†	467 49
2	879 99	227 49	182 49†	849 99
4	–	216 25	171 24†	–
	steel to brass			
0 5	294 99	234 99	197 49†	302 49
1	534 99	208 74	167 49†	534 99
2	999 99	189 99	152 49†	984 99
4	–	182 49	144 99†	–
	steel to steel			
0 5	242 49	474 99	399 99	234 99†
1	414 99	399 99	324 99†	384 99
2	744 99	347 49	272 49†	654 99
4	1374 99	317 49	242 49†	1194 99

† minimum failure load among the four crack locations
– failure load is $\gg$ 1000 N/mm

Table 2 15 Computed failure loads in N/mm for joints of carbon fibre reinforced plastic (CFRP) composite and various metals

$\frac{t_r(upper)}{t_r(lower)}$	crack locations			
	1	2	3	4
CFRP to aluminium				
0 5	234 99	193 74	156 24†	208 74
1	399 99	163 74	133 74†	354 99
2	744 99	148 74	122 49†	654 99
4	1419 99	144 99	116 87†	1254 99
CFRP to copper				
0 5	294 99	234 99	197 49†	302 49
1	534 99	208 74	167 49†	534 99
2	999 99	189 99	152 49†	984 99
4	–	182 49	144 99†	–
CFRP to brass				
0 5	208 74	234 99	189 99	186 24†
1	354 99	197 49	159 99†	309 99
2	624 99	174 99	152 49†	984 99
4	–	182 49	144 99†	–
CFRP to steel				
0 5	159 99	474 99	384 99	144 99†
1	249 99	369 99	302 49	219 99†
2	407 49	309 99	257 49†	354 99
4	729 99	279 99	234 99†	624 99

† minimum failure load among the four crack locations
– failure load is $\gg$ 1000 N/mm

Table 2 16 Computed failure loads in N/mm for joints of carbon fibre reinforced plastic (CFRP) composite and various fibre reinforced composites

$\frac{t_r(upper)}{t_r(lower)}$	crack locations			
	1	2	3	4
CFRP to glass				
0 5	362 49	128 12	99 99†	377 49
1	654 99	113 12	88 74†	684 99
2	1149 99	105 62	83 12†	1269 99
4	1314 99	103 74	81 24†	1449 99
CFRP to kevlar				
0 5	291 24	223 74	167 49†	339 99
1	489 99	182 49	141 24†	579 99
2	834 99	159 99	124 37†	999 99
4	1449 99	148 74	114 99†	1449 99
CFRP to CFRP				
0 5	272 49	208 74	163 74†	178 74
1	452 49	163 74	129 99†	302 49
2	774 99	137 49	111 24†	527 49
4	1314 99	124 37	99 99†	924 99
CFRP to graphite				
0 5	249 99†	369 99	294 99	249 99†
1	429 99	287 49	231 24†	414 99
2	729 99	242 49	193 74†	729 99
4	1299 99	216 24	174 99†	1299 99

† minimum failure load among the four crack locations

Table 2 17 Computed failure loads (P_f's) for various combinations of layups in different crack growths

Crack location	Failure loads in N/mm				
	$[0^\circ_{4S}, 0^\circ_{4S}]$	$[90^\circ_{4S}, 90^\circ_{4S}]$	$[0^\circ_{4S}, 90^\circ_{4S}]$	$[90^\circ_{4S}, 0^\circ_{4S}]$	$[1324_S, 1324_S]$
1	45 0	26 0	242 0	15 0	63 2
3	28 5	15 0	12 0	48 0	26 8
4	130 0	42 0	162 0	42 0	56 8
1324	$[0^\circ/45^\circ/90^\circ/-45^\circ]$				

Table 2 18 Predicted failure loads of adhesively bonded joints with different Young's moduli of the adhesives ($L_o/L_t = 1/2$, $t_a/t_r = 1/5$, no of elements employed = 1816)

E_a/E_r	a_x(mm)	$G_x(kJ/m^2)$	$a_{cr}(mm)$	$G_{cr}(kJ/m^2)$	$P_f/\sqrt{G_C}(kN/m)$
0 0125	1 72	22 4	1 72	29 3	184 74
0 0250	1 91	14 9	1 72	28 2	188 31
0 0500	2 1	10 5	1 72	19 2	228 21
0 1000	2 42	7 8	1 72	14 5	262 61

Table 2 19 Computed failure loads (P_f's) for various adhesive stiffnesses and different combinations

	Failure loads in N/mm				
E_s/E_r	$[0^\circ_{4S}, 0^\circ_{4S}]$	$[90^\circ_{4S}, 90^\circ_{4S}]$	$[0^\circ_{4S}, 90^\circ_{4S}]$	$[90^\circ_{4S}, 0^\circ_{4S}]$	$[1324_S, 1324_S]$
0 0125	21 5	15 0	12 0	15 0	20 0
0 0166	23 5	15 5	13 0	16 75	22 3
0 0250	26 0	15 5	12 75	16 25	24 0
0 0500	28 5	15 0	12 0	15 0	26 8
0 1000	29 5	14 0	11 0	13 75	28 0

1324 $[0^\circ/45^\circ/90^\circ/-45^\circ]$

Table 2 20 Predicted failure loads of adhesively bonded joints with different overlap lengths (t_s/t_r= 1/5, E_s/E_r= 1/20, no of elements employed = 1816)

L_o/L_t	a_x(mm)	$G_x(kJ/m^2)$	a_{cr}(mm)	$G_{cr}(kJ/m^2)$	$P_f/\sqrt{G_C}(kN/m)$
0 083	2 0†	350†	1 37	610	40 48
0 125	2 6†	250†	1 32	452	47 03
0 166	4 0†	200†	1 11	312	56 61
0 250	2 35	50	1 32	48	144 33
0 500	2 15	10	1 72	19 2	228 21

† represents actual value is greater than the specified one

Table 2 21 Computed failure loads (P_f's) for various overlap lengths and laminae combinations

	Failure loads in N/mm				
L_o/L_t	$[0^\circ_{4S}, 0^\circ_{4S}]$	$[90^\circ_{4S}, 90^\circ_{4S}]$	$[0^\circ_{4S}, 90^\circ_{4S}]$	$[90^\circ_{4S}, 0^\circ_{4S}]$	$[1324_S, 1324_S]$
0 125	10 25	6 25	7 5	9 62	11 7
0 166	12 5	8 0	8 87	11 5	14 0
0 250	16 0	11 0	10 5	14 0	18 0
0 500	28 5	15 0	12 0	15 0	28 5

1324 $[0°/45°/90°/-45°]$

Table 2 22 Predicted failure loads of adhesively bonded joints with different thicknesses of the adhesives ($L_o/L_t = 1/2$, $E_s/E_r = 1/20$, no of elements employed = 3376)

t_s/t_r	a_x(mm)	$G_x(kJ/m^2)$	a_{cr}(mm)	$G_{cr}(kJ/m^2)$	$P_f/\sqrt{G_c}(kN/m)$
0 0100	0 16	4 1	0 03	6 85	382 072
0 0125	0 19	4 2	0 13	7 8	358 049
0 0250	0 32	4 5	0 23	8 65	321 908
0 0500	0 55	5 4	0 36	10 2	313 110
0 1000	1 00	7 0	0 67	12 7	280 607
0 2000	1 93	11 7	1 1	20 4	221 396

Table 2 23 Computed failure loads (P_f's) for various adhesive thicknesses and laminae combinations

	Failure loads in N/mm				
t_s/t_r	$[0^\circ_{4S}, 0^\circ_{4S}]$	$[90^\circ_{4S}, 90^\circ_{4S}]$	$[0^\circ_{4S}, 90^\circ_{4S}]$	$[90^\circ_{4S}, 0^\circ_{4S}]$	$[1324_S, 1324_S]$
0 0100	39 0	16 0	11 75	13 25	41 0
0 0125	38 0	16 0	11 75	13 25	40 0
0 0250	36 5	15 5	11 25	13 25	36 0
0 0500	34 0	15 5	11 25	14 0	33 0
0 1000	32 0	15 5	11 5	14 75	31 0
0 2000	28 5	15 0	12 0	15 0	28 5

1324 [0°/45°/90°/ − 45°]

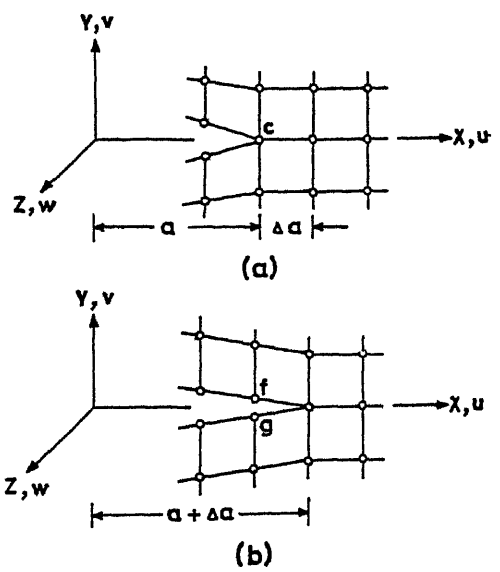

Figure 2 1 Finite element mesh at crack-tip illustrating the crack closure technique

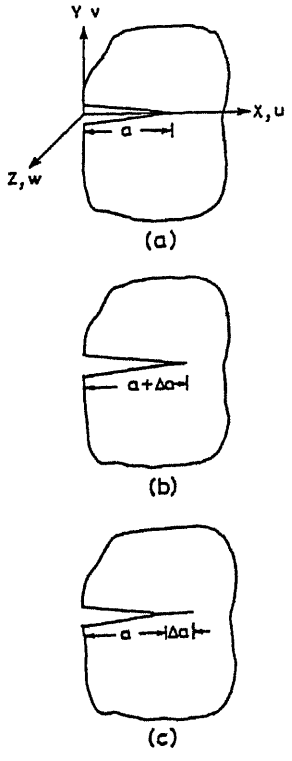

Figure 2 2 Schematic representation of crack closure technique

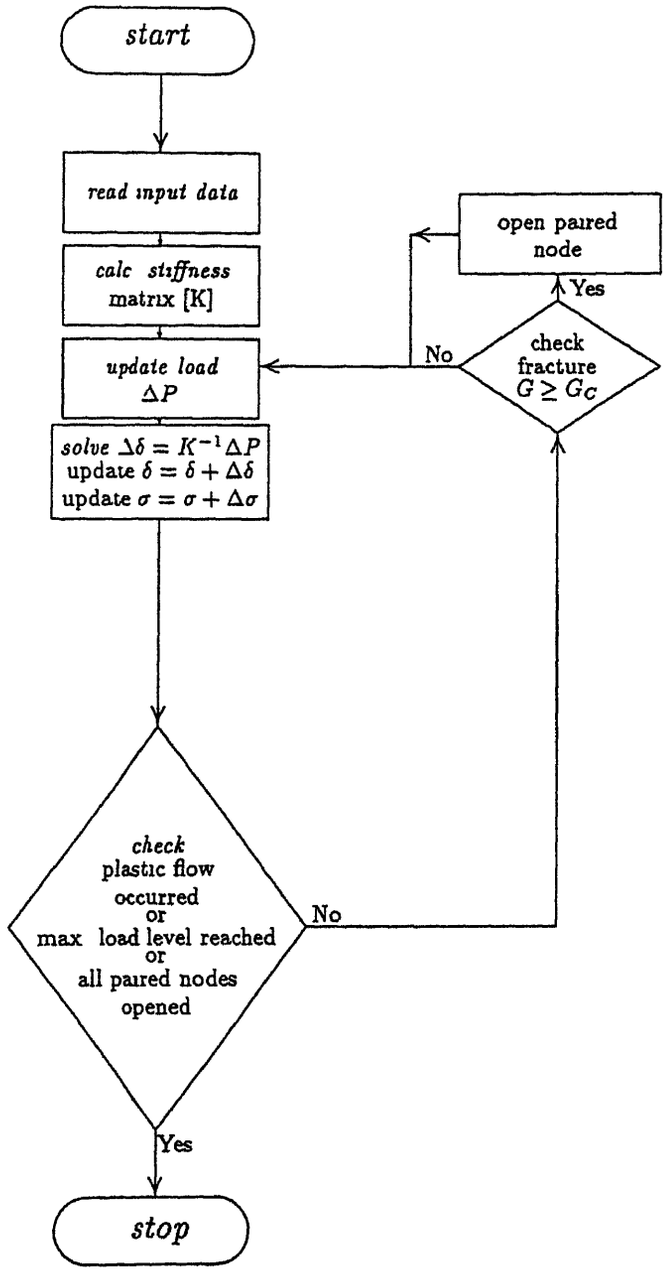

Figure 2.3 Flow chart of linear elastic finite element analysis for crack growth

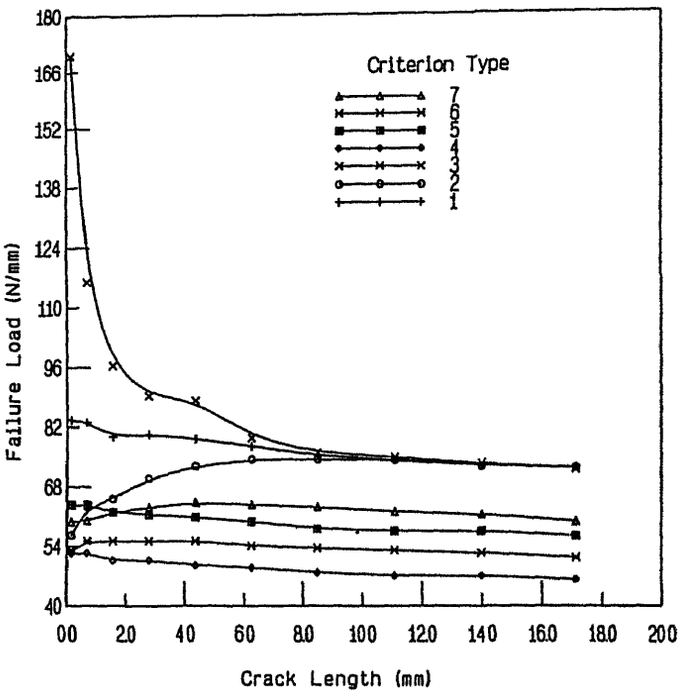

Figure 2 4 Variation of failure load and crack length for different possible fracture criteria (Table 2 1)

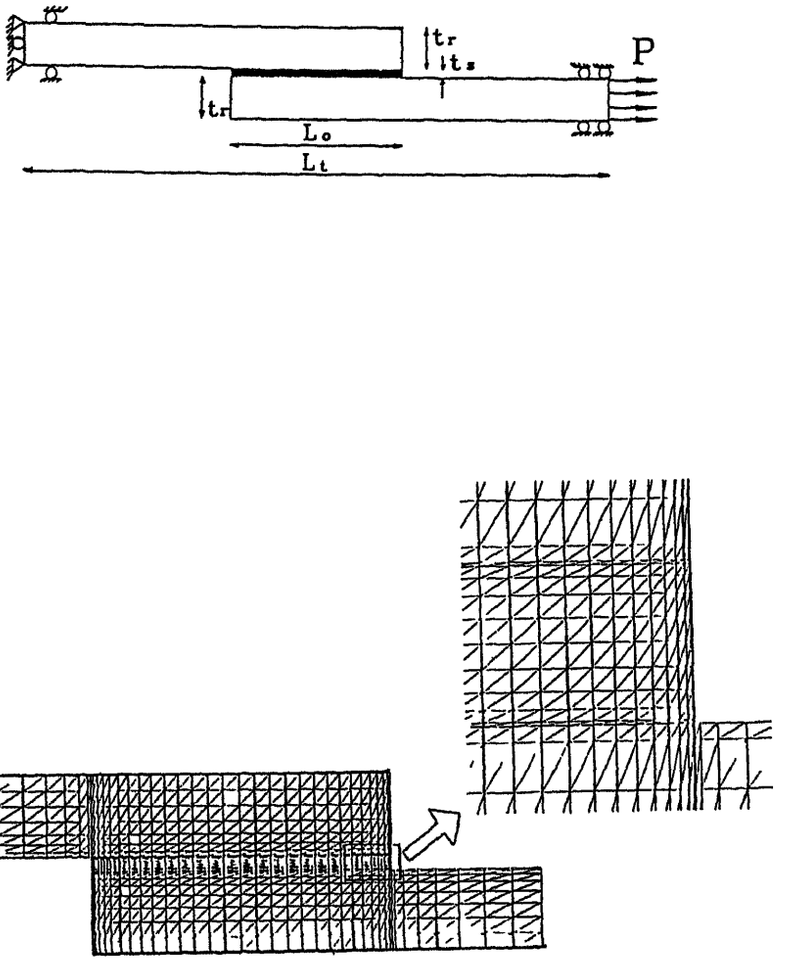

Figure 2 5 Schematic of single lap joint considered by Hiregoudar (1993) and the present finite element mesh consists of 1816 elements with an enlarged view of the edge region

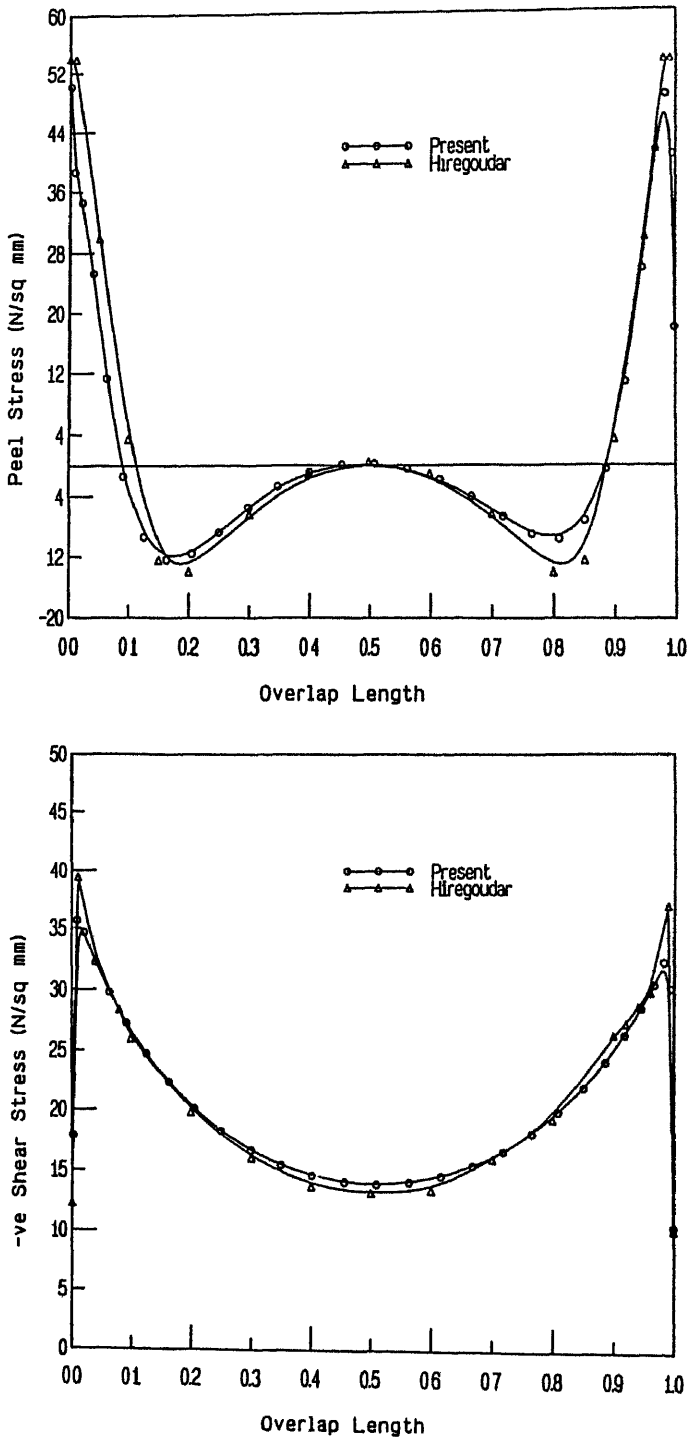

Figure 2 6 Comparison of stress distributions along the overlap length of the single lap joint considered by Hiregoudar (1993)

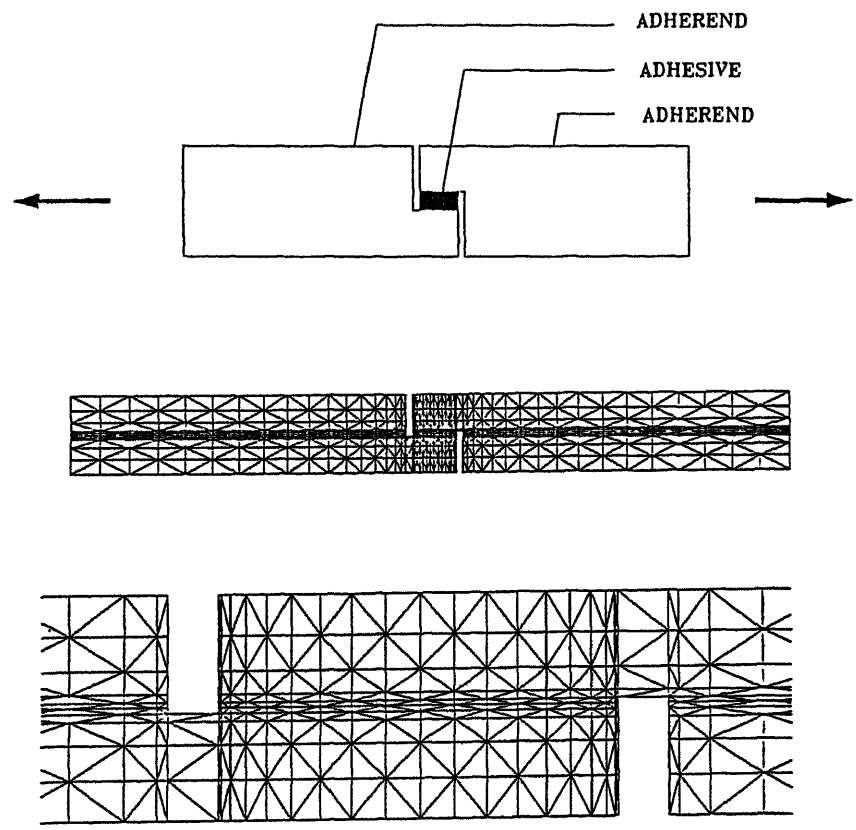

Figure 2 7 Schematic of the stepped lap joint (thick adherend shear test TAST specimen of Su and Mackie, 1993) and the finite element mesh with an enlarged view of the stepped portion

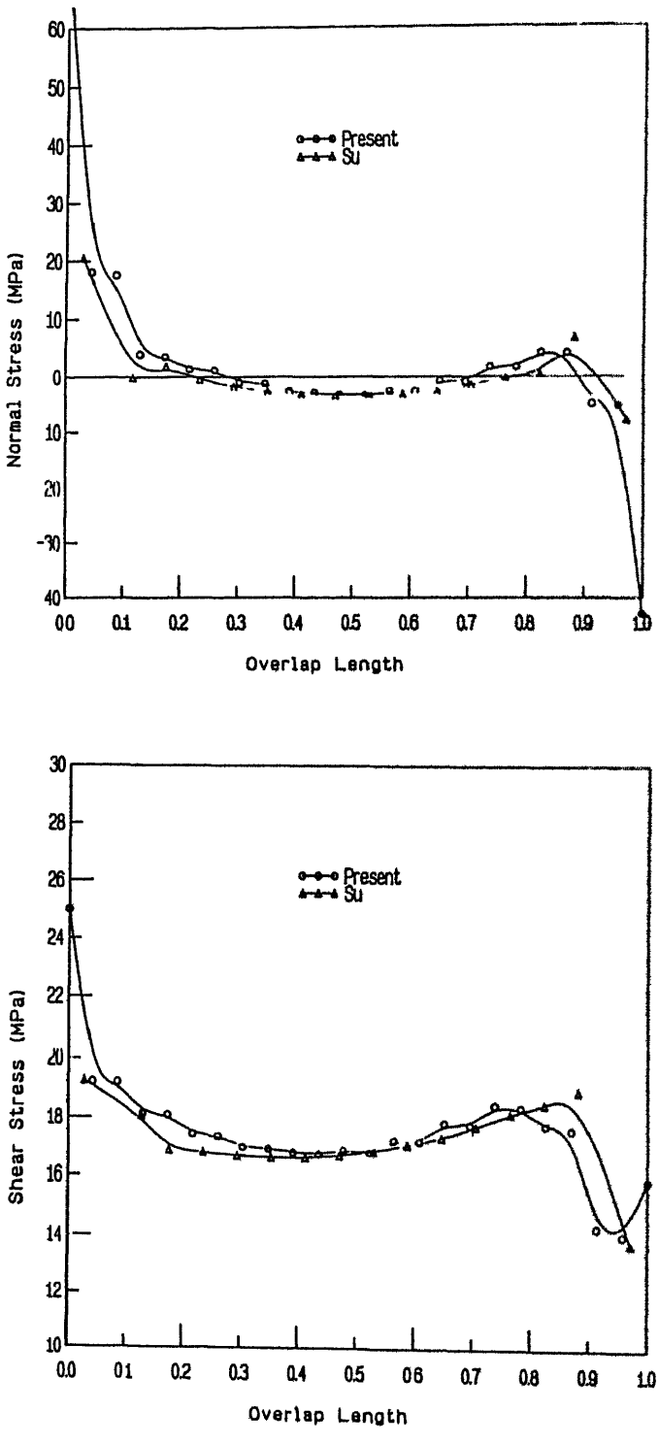

Figure 2 8 Comparison of stress distribution along the overlap length at interface of adherend and adhesive of the stepped lap joint

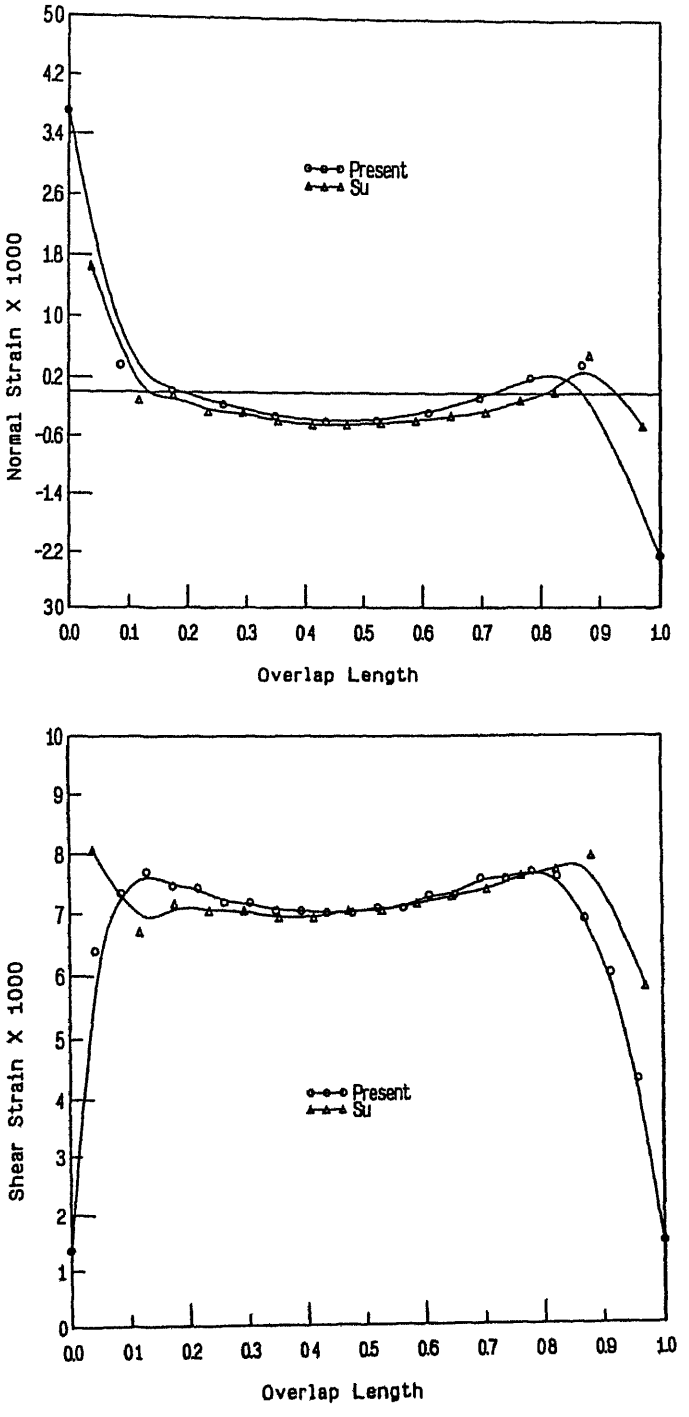

Figure 2 9 Comparison of strain distribution along the overlap length at interface of adherend and adhesive of the stepped lap joint

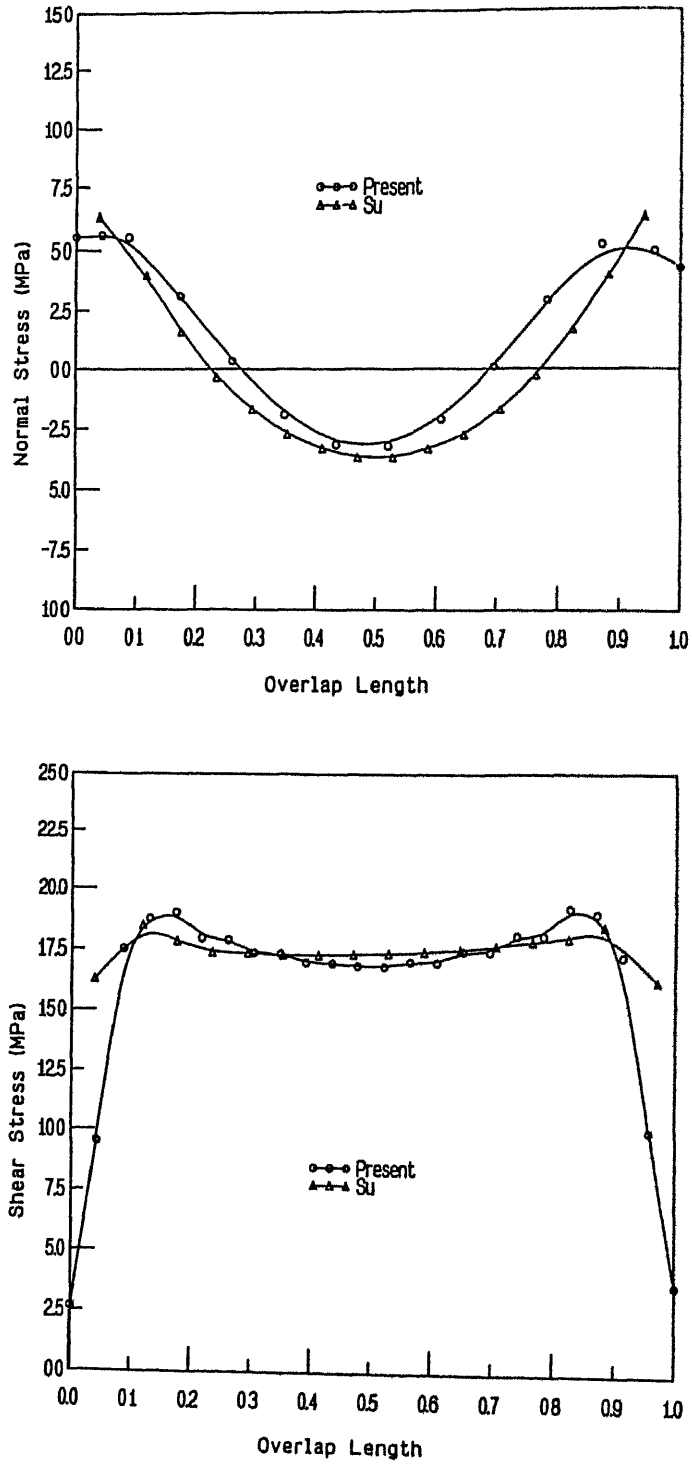

Figure 2 10. Comparison of stress distribution along the overlap length at midline of adhesive of the stepped lap joint

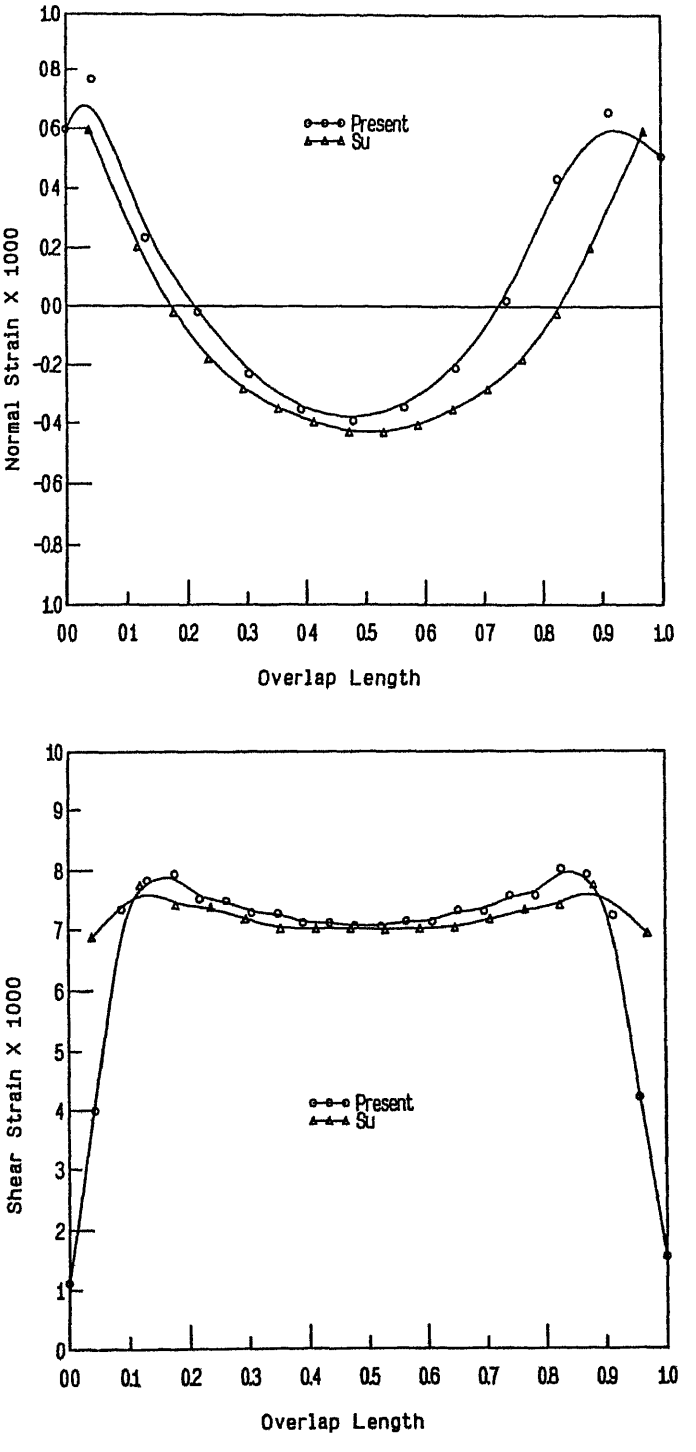

Figure 2.11 Comparison of strain distribution along the overlap length at midline of adhesive of the stepped lap joint

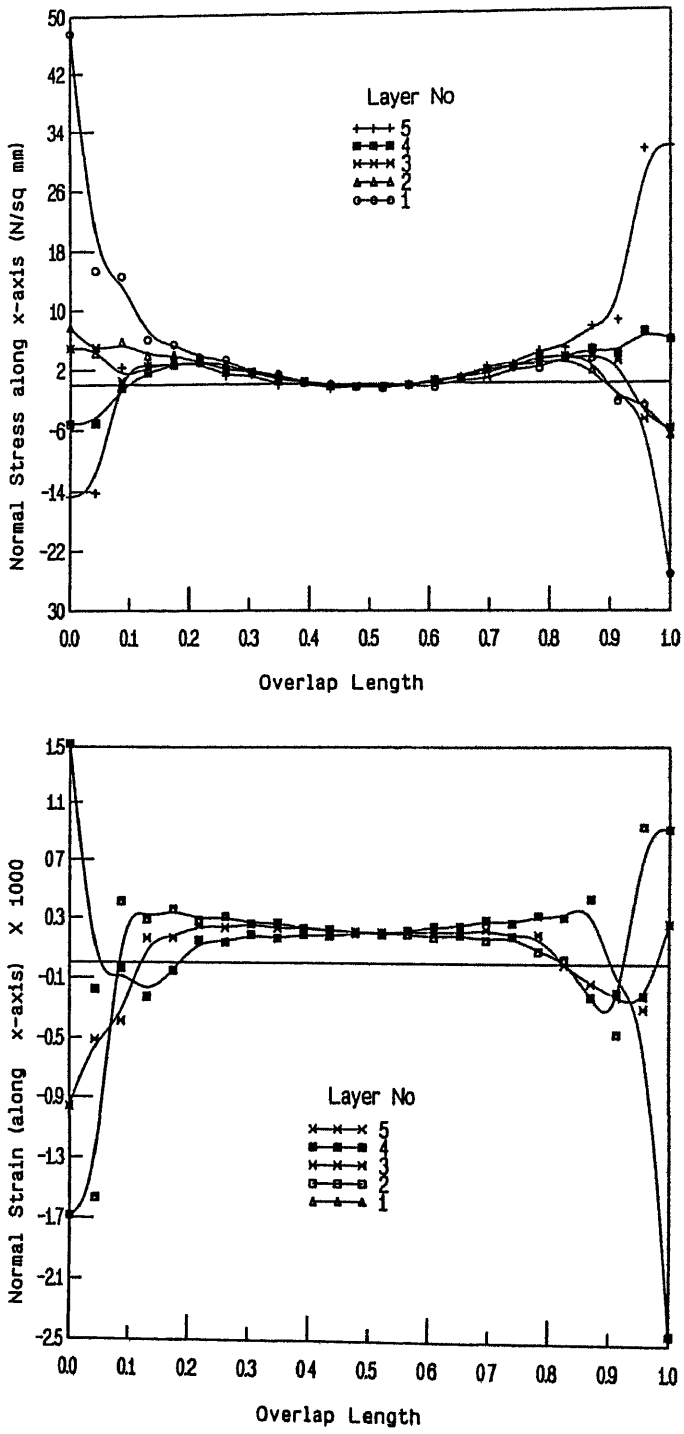

Figure 2.12 Normal stress σ_x, and strain ϵ_x, distributions along the overlap length and across the adhesive thickness of the stepped lap joint

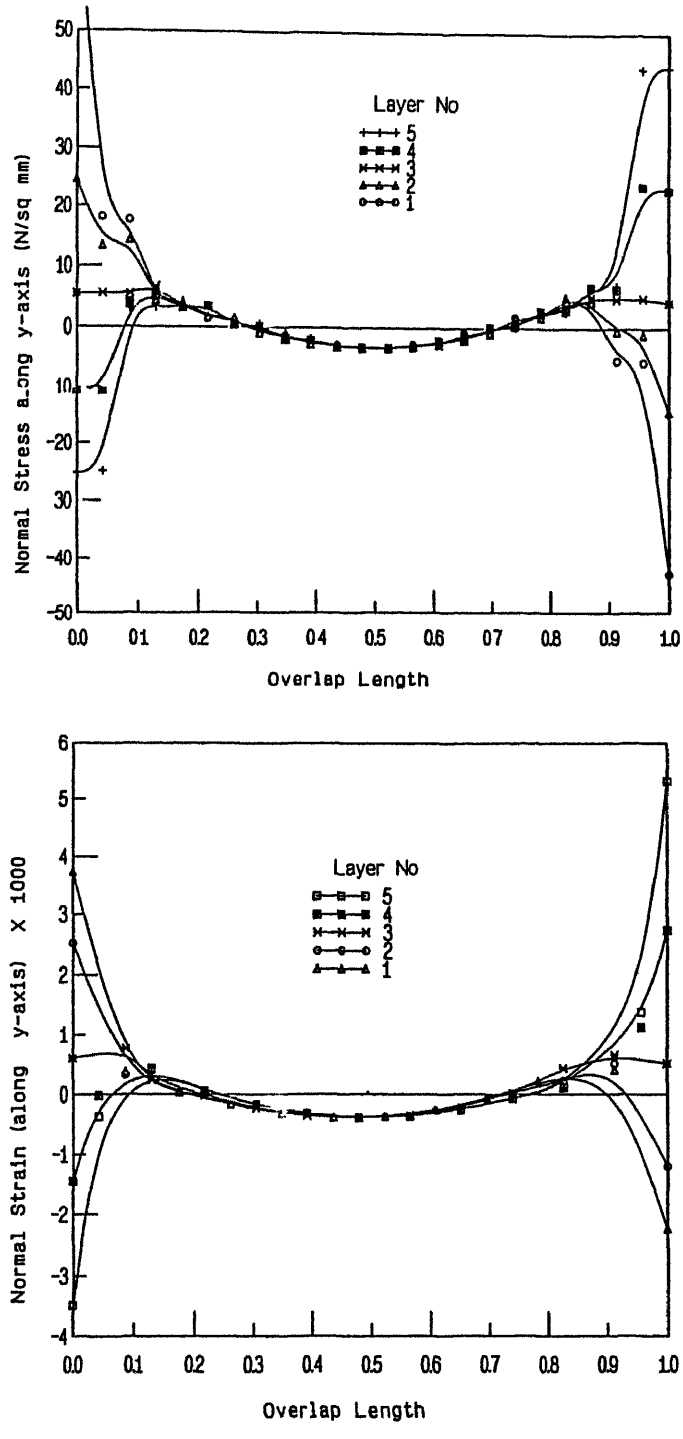

Figure 2 13: Normal stress σ_y, and strain ϵ_y, distributions along the overlap length and across the adhesive thickness of the stepped lap joint

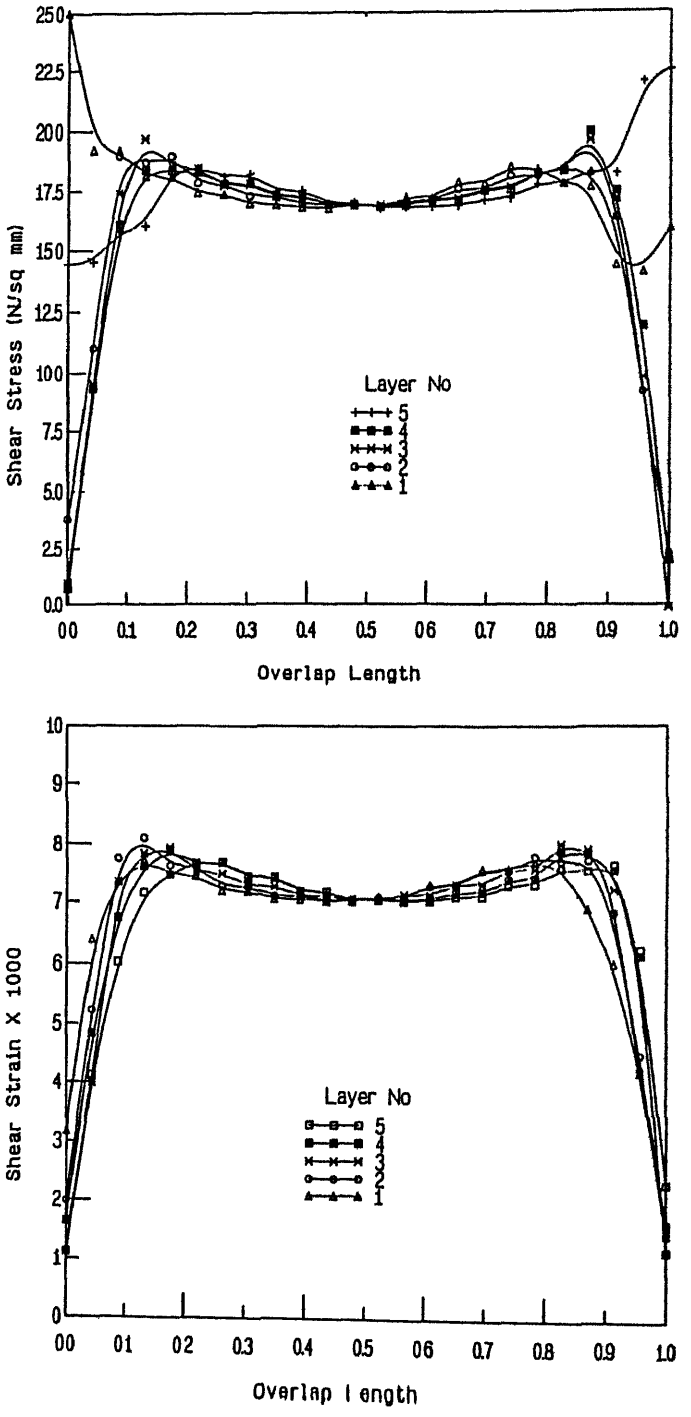

Figure 2 14 Shear stress and strain distributions along the overlap length and across the adhesive thickness of the stepped lap joint

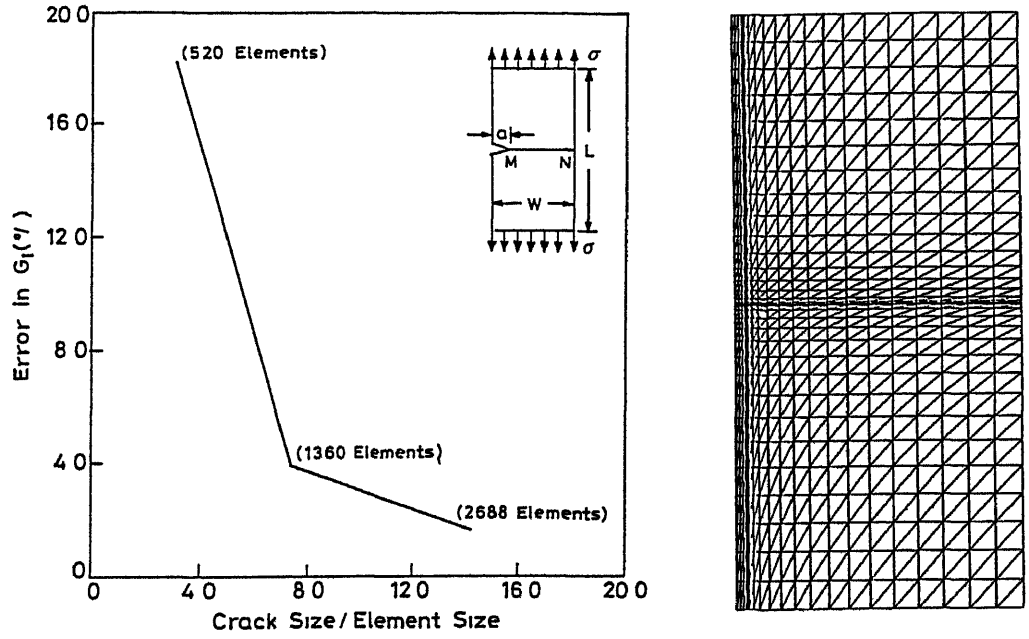

Figure 2 15 Error estimation in strain energy release rate for single edge notch (SEN) specimen and the finite element mesh consists of 1360 elements

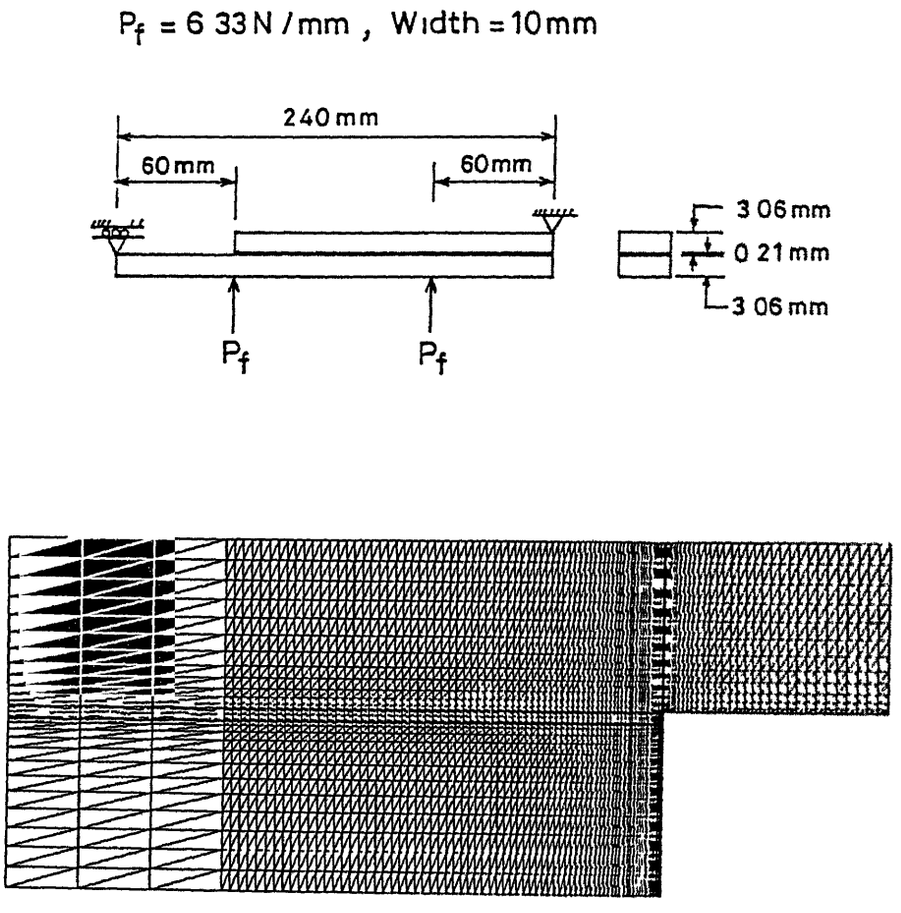

Figure 2 16 Schematic representation of cracked lap shear (CLS) specimen under four-point bending and the finite element mesh consists of 2180 elements

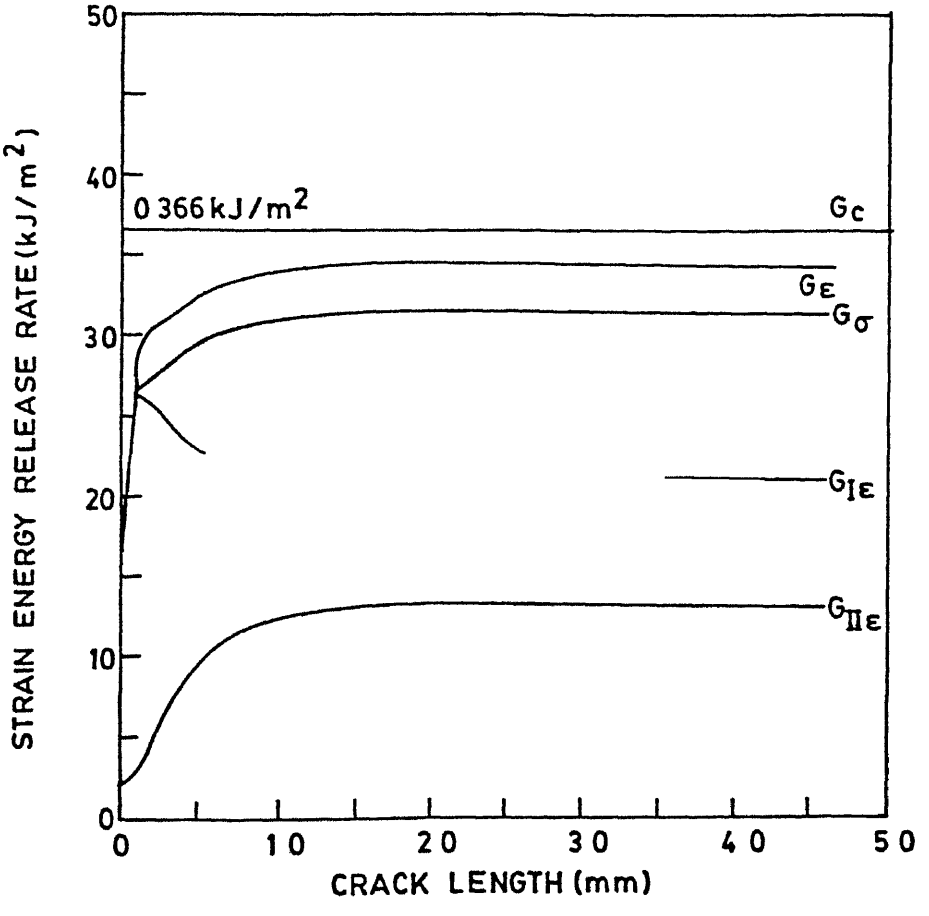

Figure 2 17 Variation of strain energy release rates with crack length for plane stress and plane strain models of the cracked lap shear (CLS) specimen

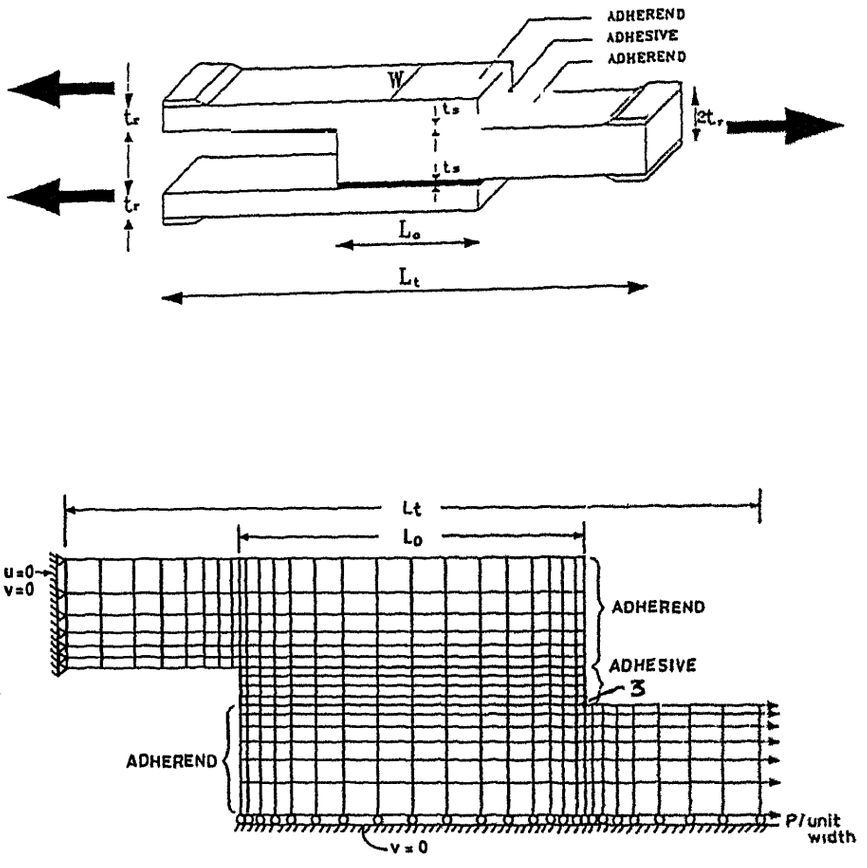

Figure 2 18. Schematic of adhesively bonded double lap joint and the finite element mesh showing the crack location at '3'

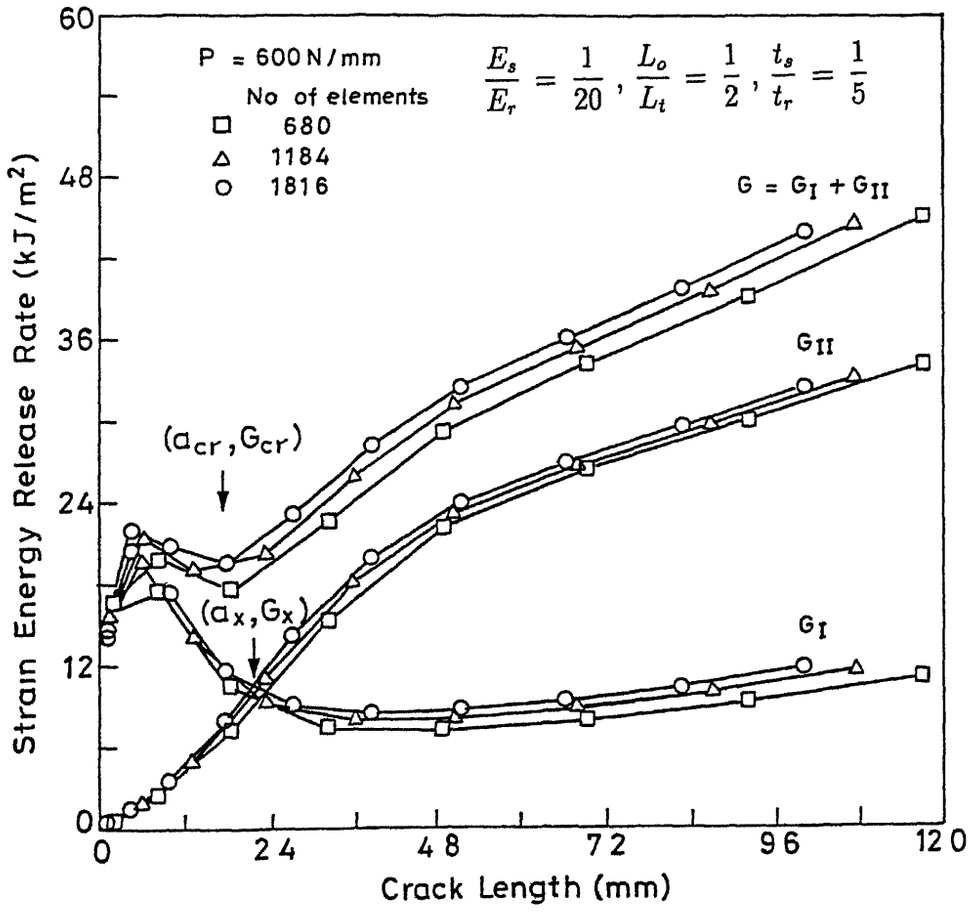

Figure 2 19. Comparison of strain energy release rates for three different refined meshes

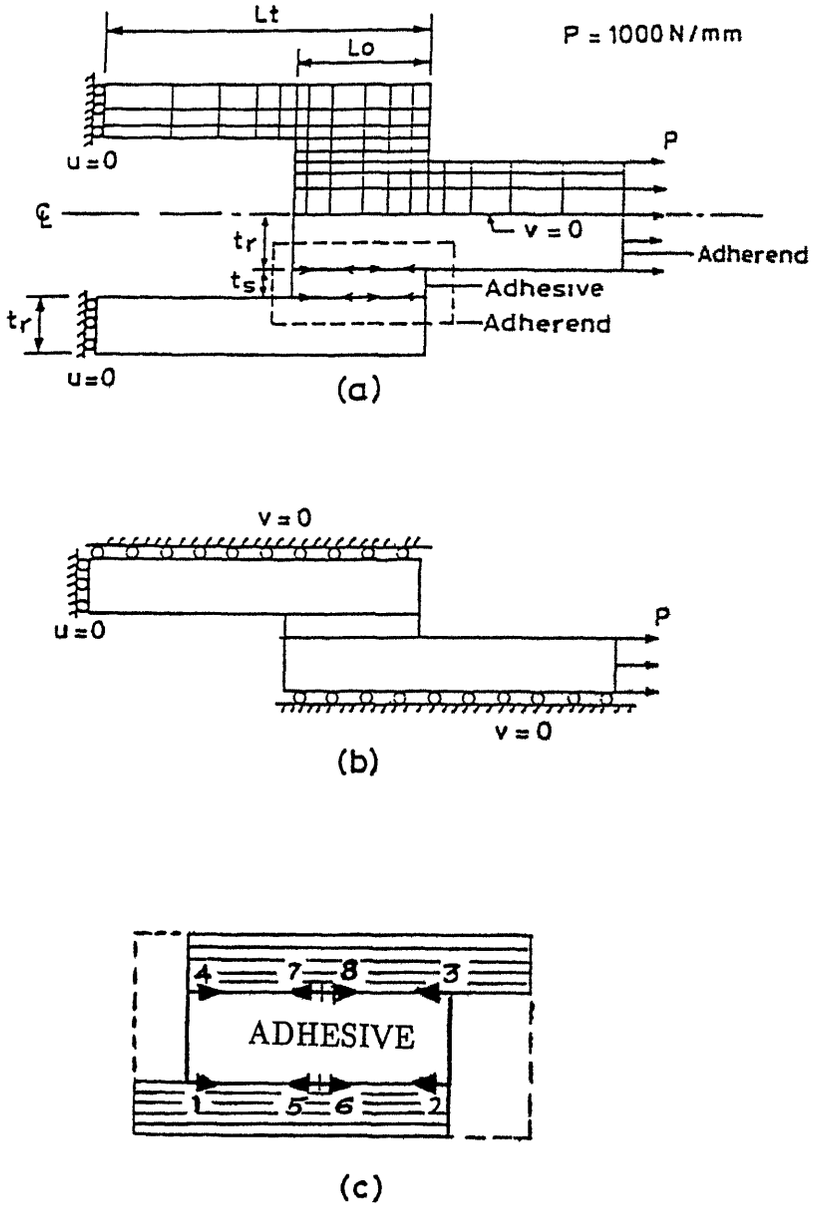

Figure 2 20 Schematic of (**a**) free edge boundary condition (in double lap joint), (**b**) constrained edge boundary condition and (**c**) eight different crack locations

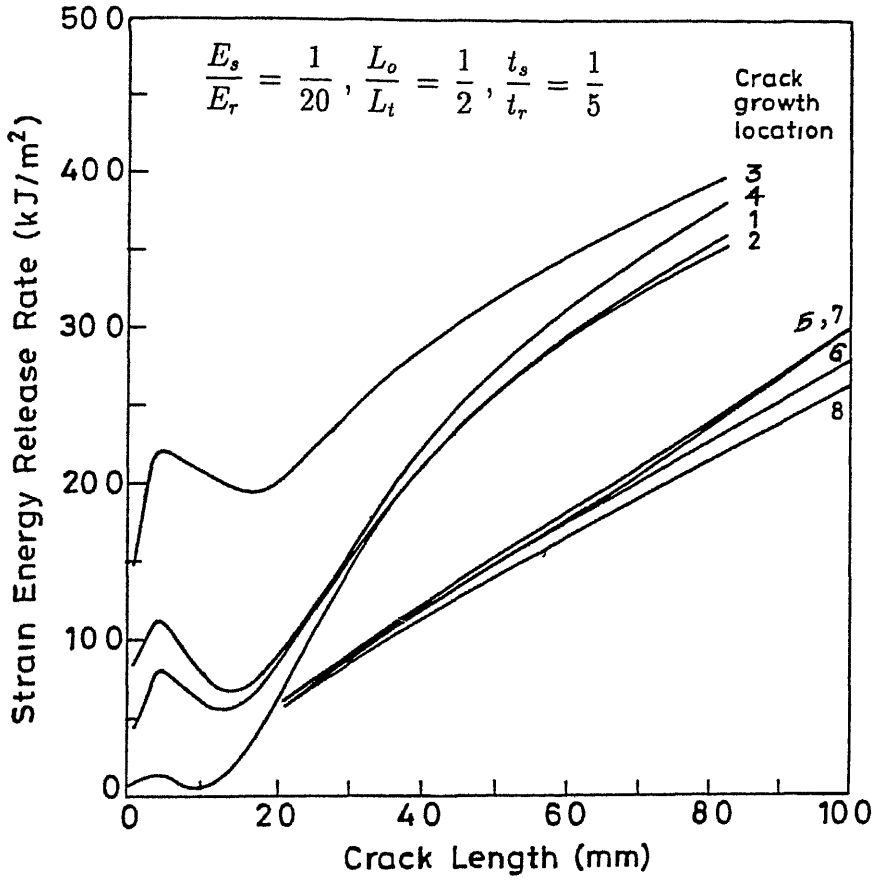

Figure 2 21 Variation of strain energy release rate with crack length for crack growths at eight different locations (Figure 2 20c) for free side type boundary condition

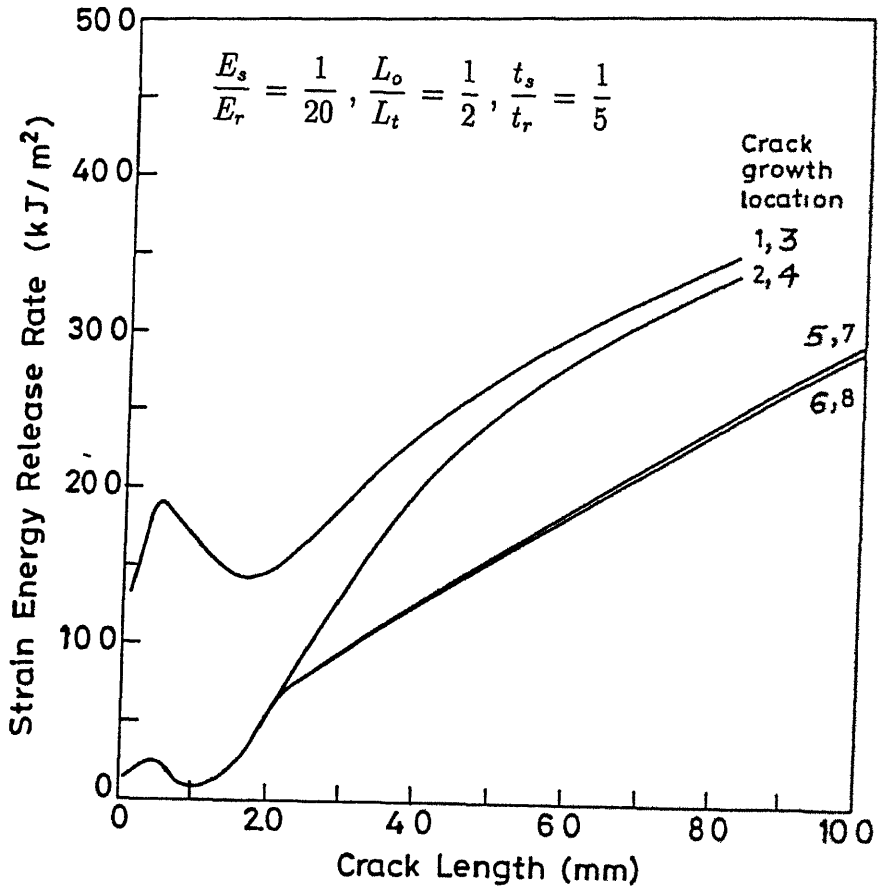

Figure 2 22 Variation of strain energy release rate with crack length for crack growths at eight different locations (Figure 2 20c) for constrained side type boundary condition

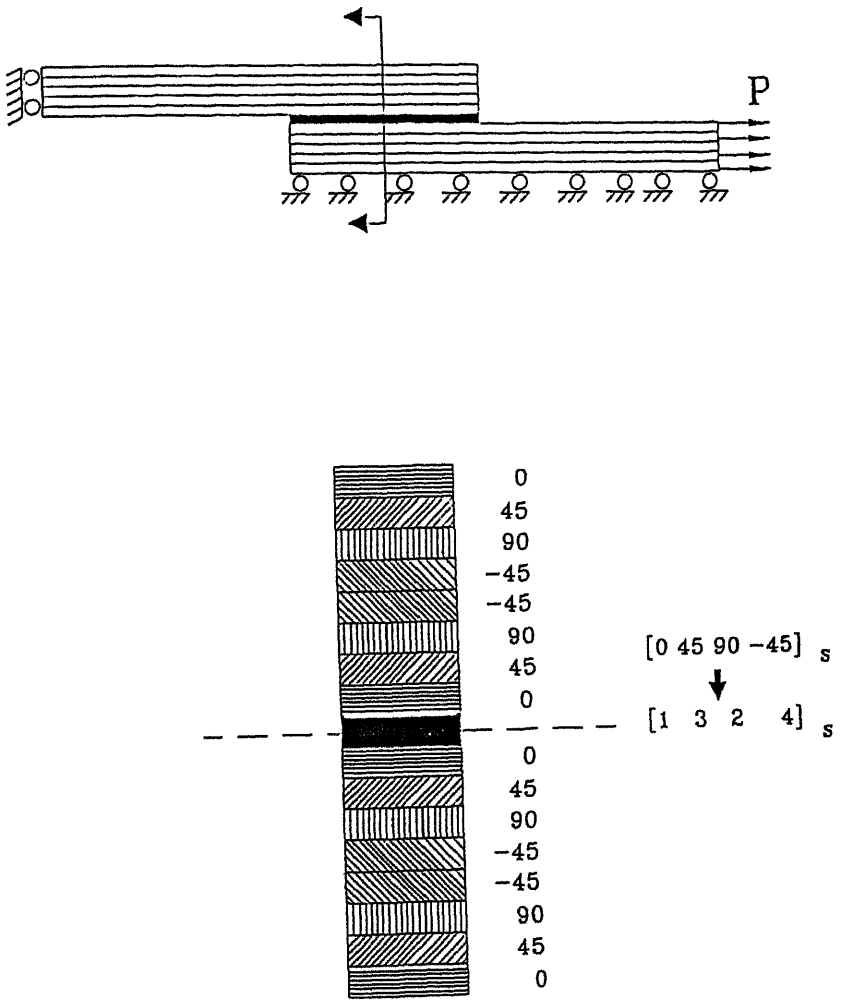

Figure 2.23 Schematic of double lap joint of composite adherends [1324_S, 1324_S] with a magnified section view

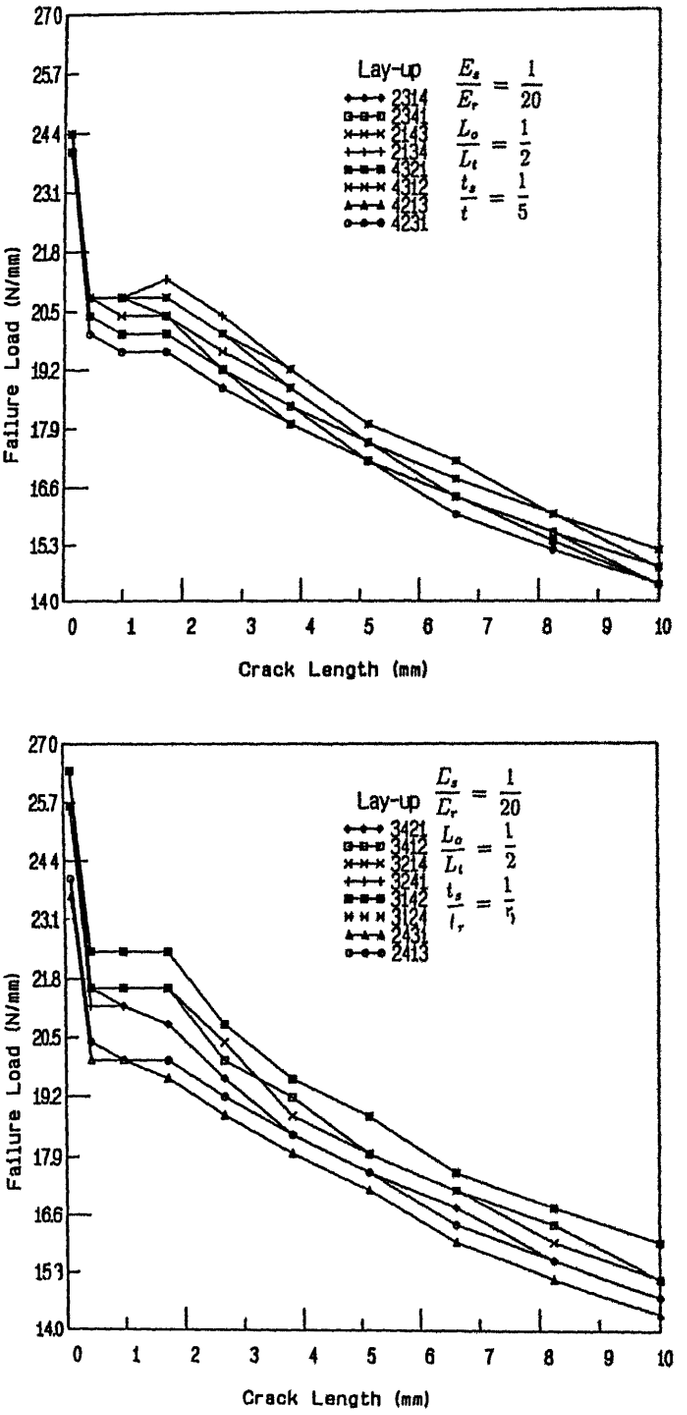

Figure 2.24 Variation of failure load with crack length for symmetric combinations of 0°, 45°, 90° and −45° layups in composite adherends, and for crack location at '3'

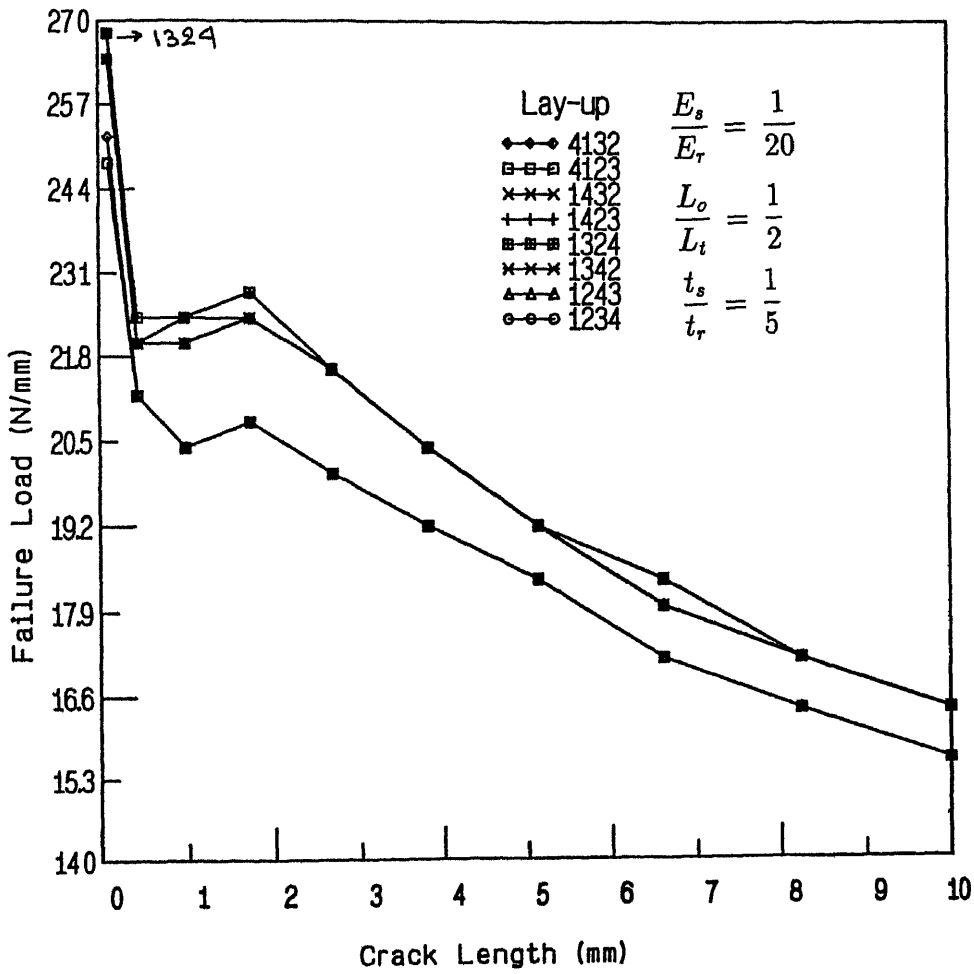

Figure 2.25 Variation of failure load with crack length for various symmetric combinations of 0°, 45°, 90° and −45° layups in composite adheren-ds, with 0° layups being present in the immediate neighbourhood of the adhesive and, for crack location at '3'

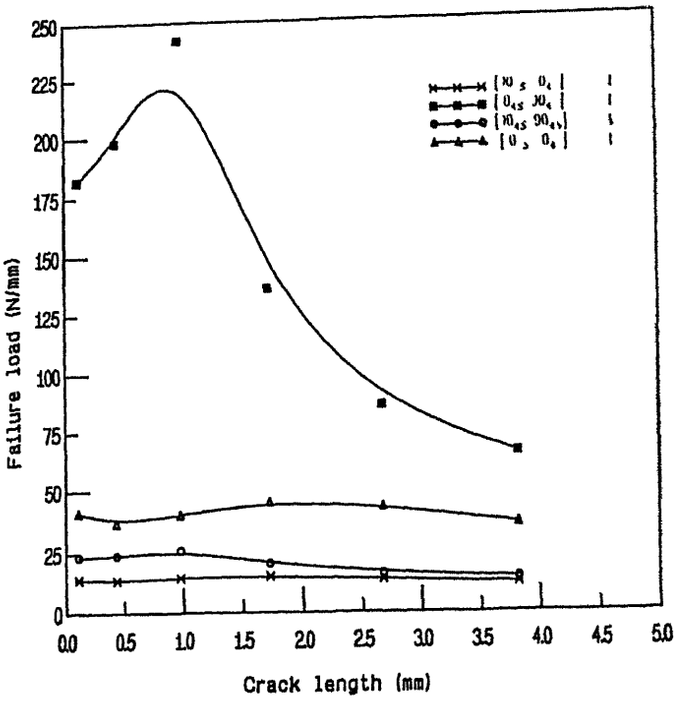

Figure 2 26 Variation of failure load with crack length for $[0^\circ_{4S}, 0^\circ_{4S}]$, $[90^\circ_{4S}, 90^\circ_{4S}]$, $[0^\circ_{4S}, 90^\circ_{4S}]$, $[90^\circ_{4S}, 0^\circ_{4S}]$ laminate pairs for crack location at '1'

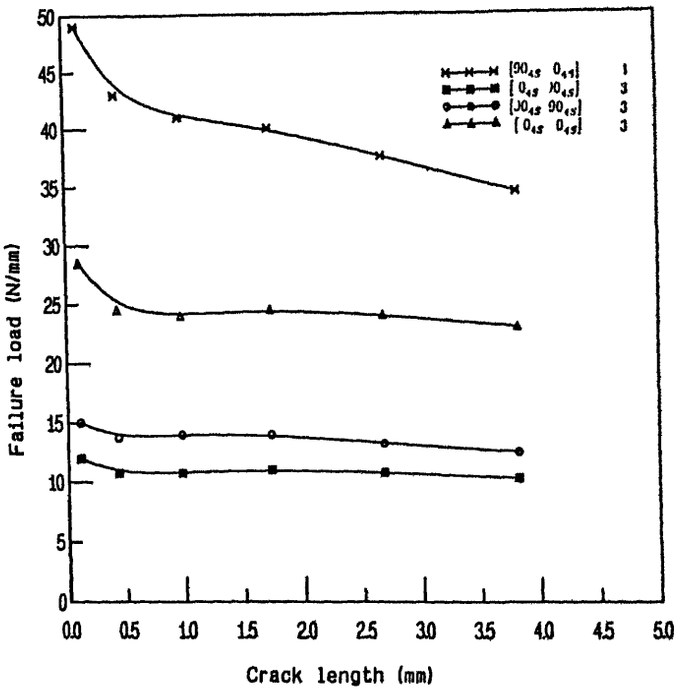

Figure 2 27 Variation of failure load with crack length for $[0^\circ_{4S}, 0^\circ_{4S}]$, $[90^\circ_{4S}, 90^\circ_{4S}]$, $[0^\circ_{4S}, 90^\circ_{4S}]$, $[90^\circ_{4S}, 0^\circ_{4S}]$ laminate pairs for crack location at '3'

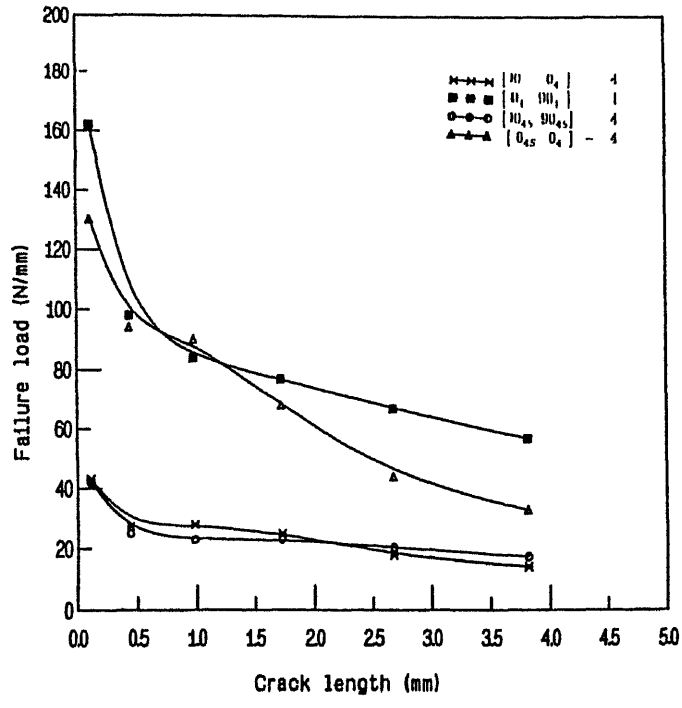

Figure 2 28 Variation of failure load with crack length for $[0^\circ_{4S}, 0^\circ_{4S}]$, $[90^\circ_{4S}, 90^\circ_{4S}]$, $[0^\circ_{4S}, 90^\circ_{4S}]$, $[90^\circ_{4S}, 0^\circ_{4S}]$ laminate pairs for crack location at '4'

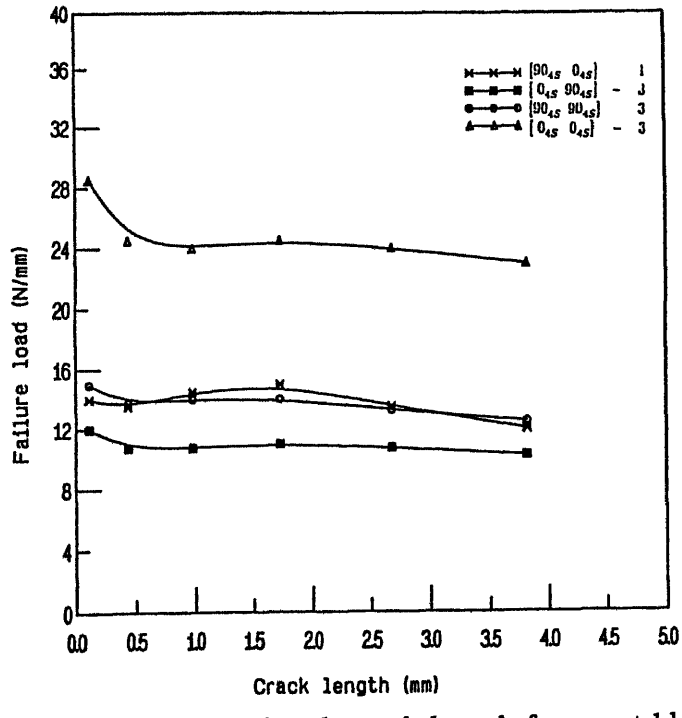

Figure 2 29 Variation of failure load with crack length for most likely interface edge crack growths in CFRP unidirectional (0°_{4S} and 90°_{4S}) laminate pairs

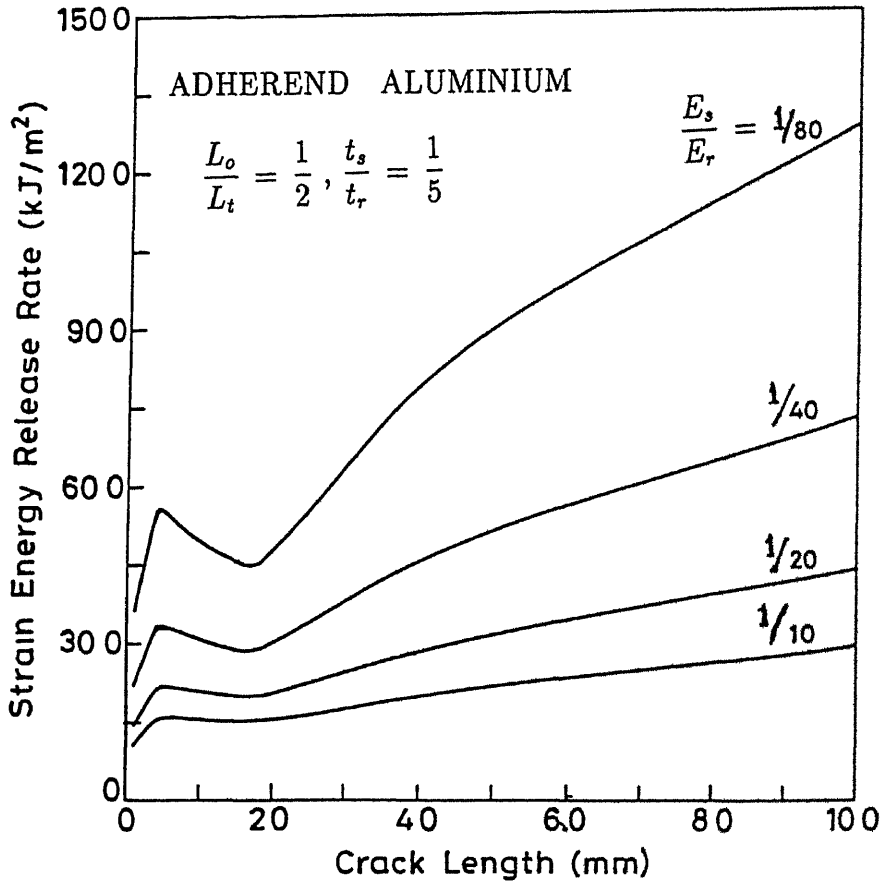

Figure 2 30 Variation of total strain energy release rate with crack length for crack initiation at location '3' and different e ($= E_s/E_r$) values in aluminium to aluminium joints

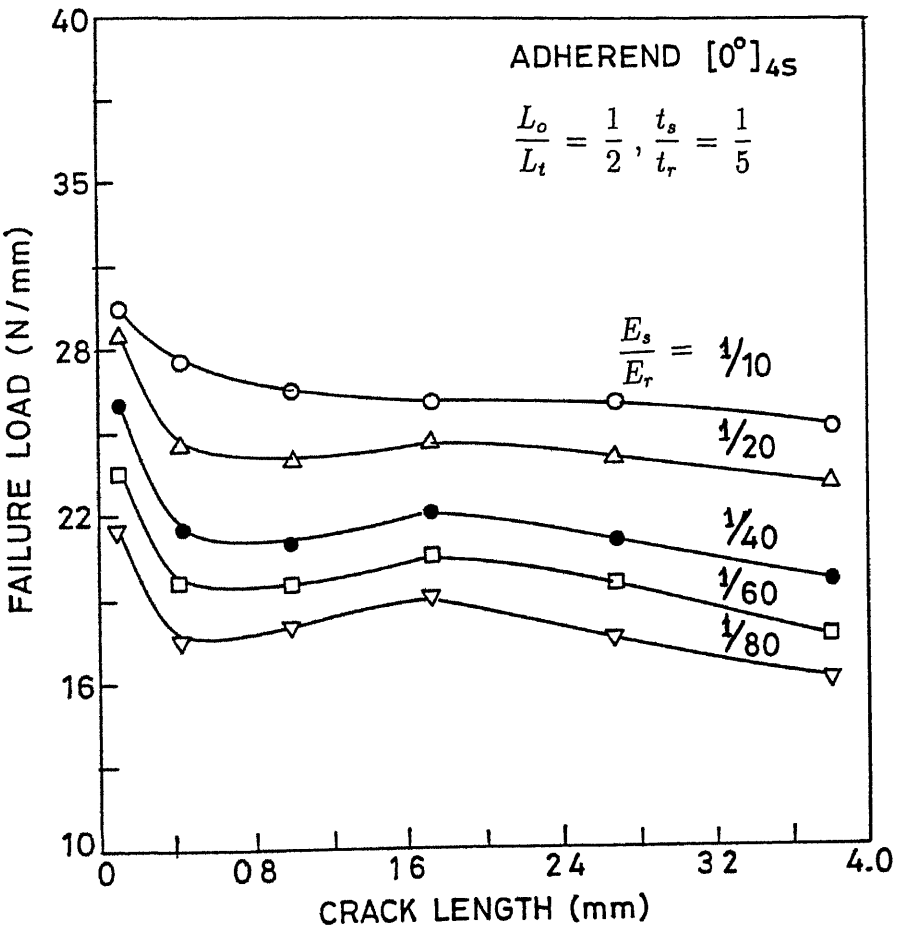

Figure 2 31 Variation of failure load with crack length for crack initiation at location '3' and different e (= E_s/E_r) values in $[0^\circ_{4S}, 0^\circ_{4S}]$ CFRP laminates

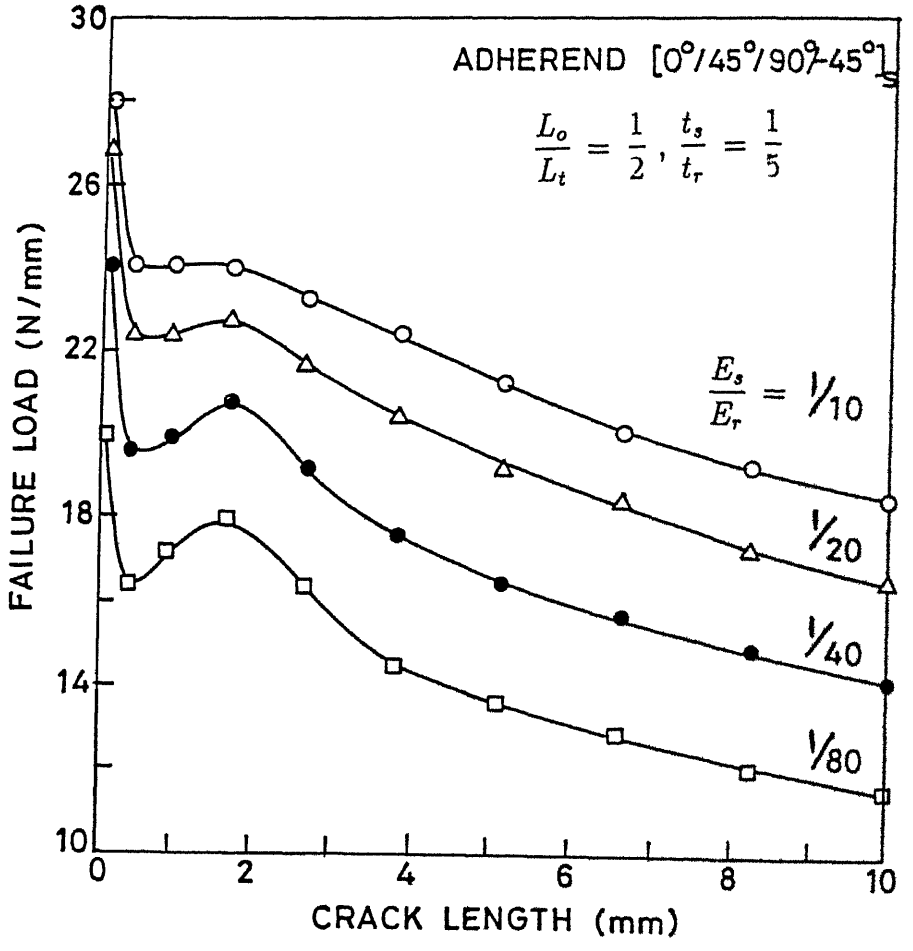

Figure 2.32 Variation of failure load with crack length for crack initiation at location '3' and different e (= E_s/E_r) values in [1324_S, 1324_S] (optimal) CFRP laminates

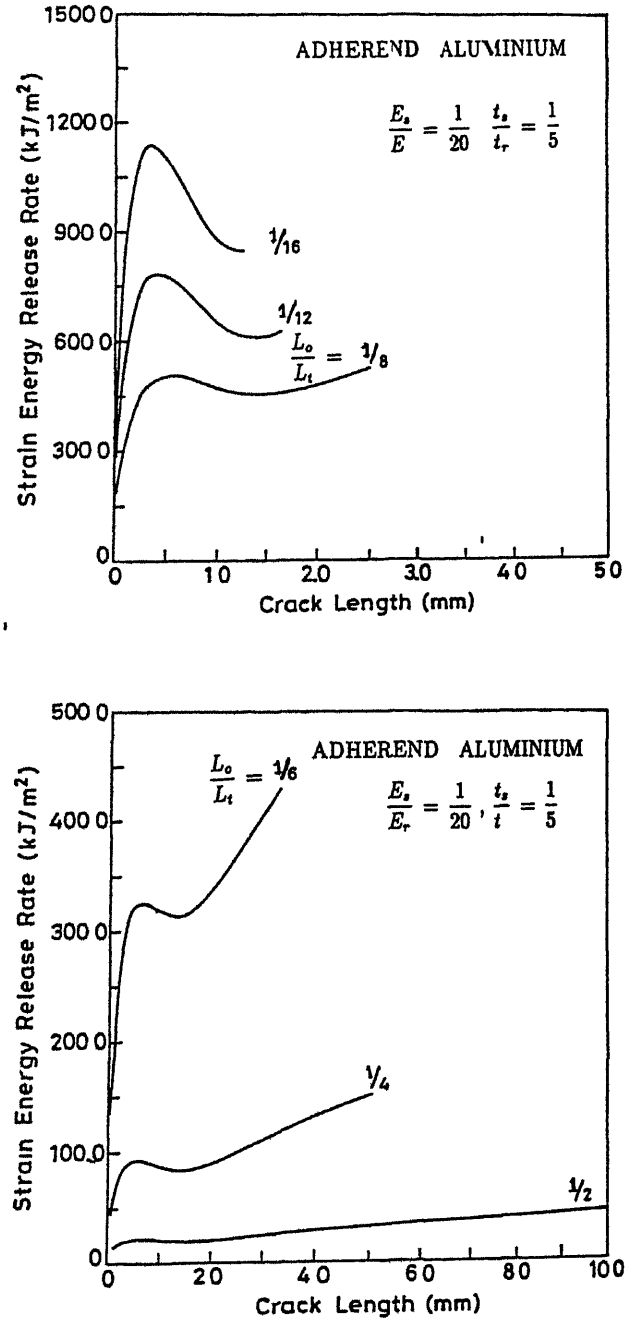

Figure 2 33 Variation of total strain energy release rate with crack length for crack initiation at location '3' and different l (= L_o/L_t) values in aluminium to aluminium joints

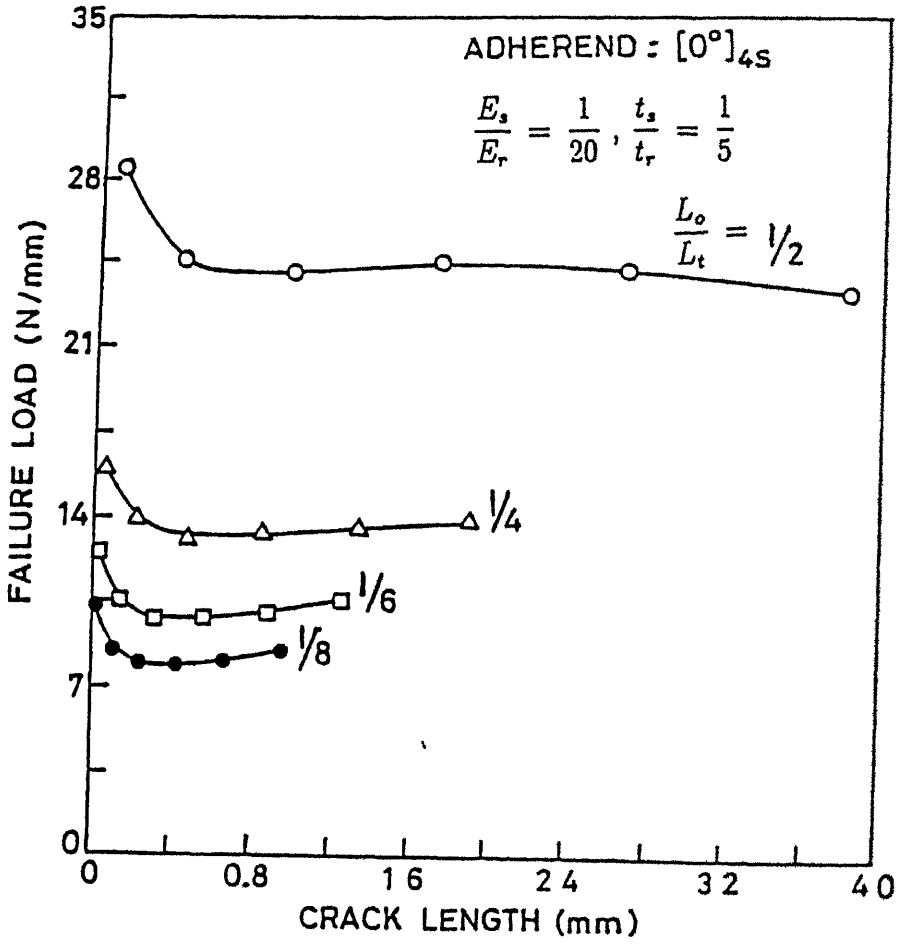

Figure 2 34 Variation of failure load with crack length for crack initiation at location '3' and different l (= L_o/L_t) values in $[0^\circ_{4S}, 0^\circ_{4S}]$ CFRP laminates

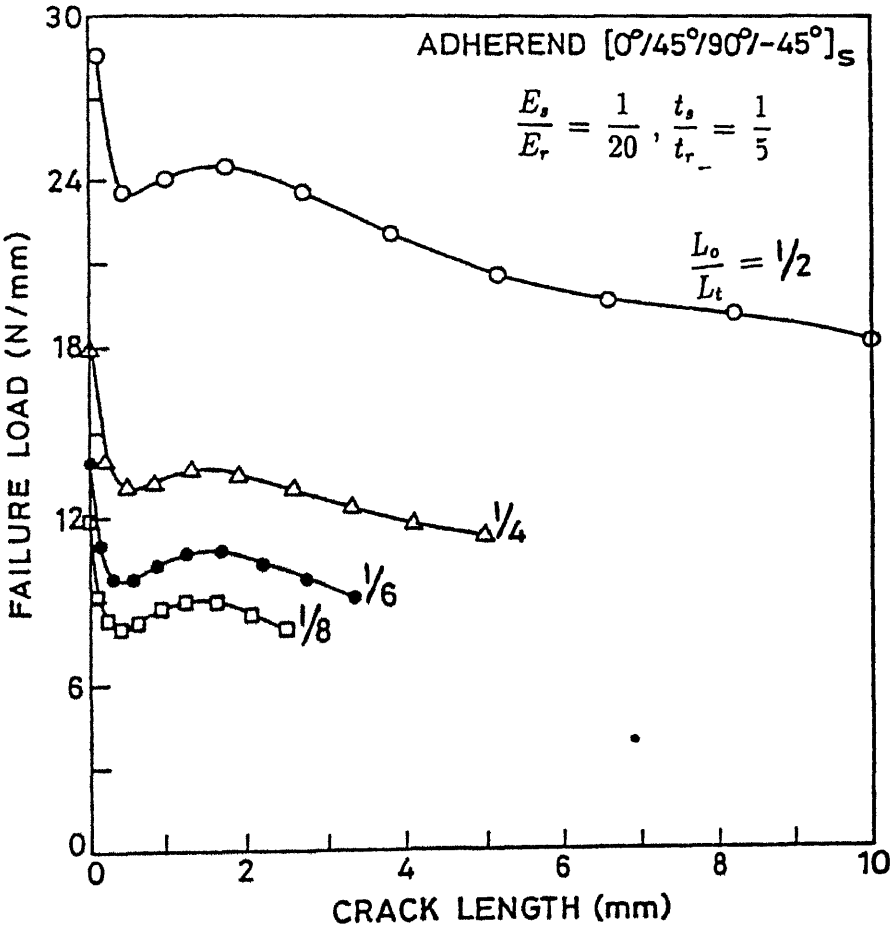

Figure 2.35 Variation of failure load with crack length for crack initiation at location '3' and different l (= L_o/L_t) values in [1324_S, 1324_S] (optimal) CFRP laminates

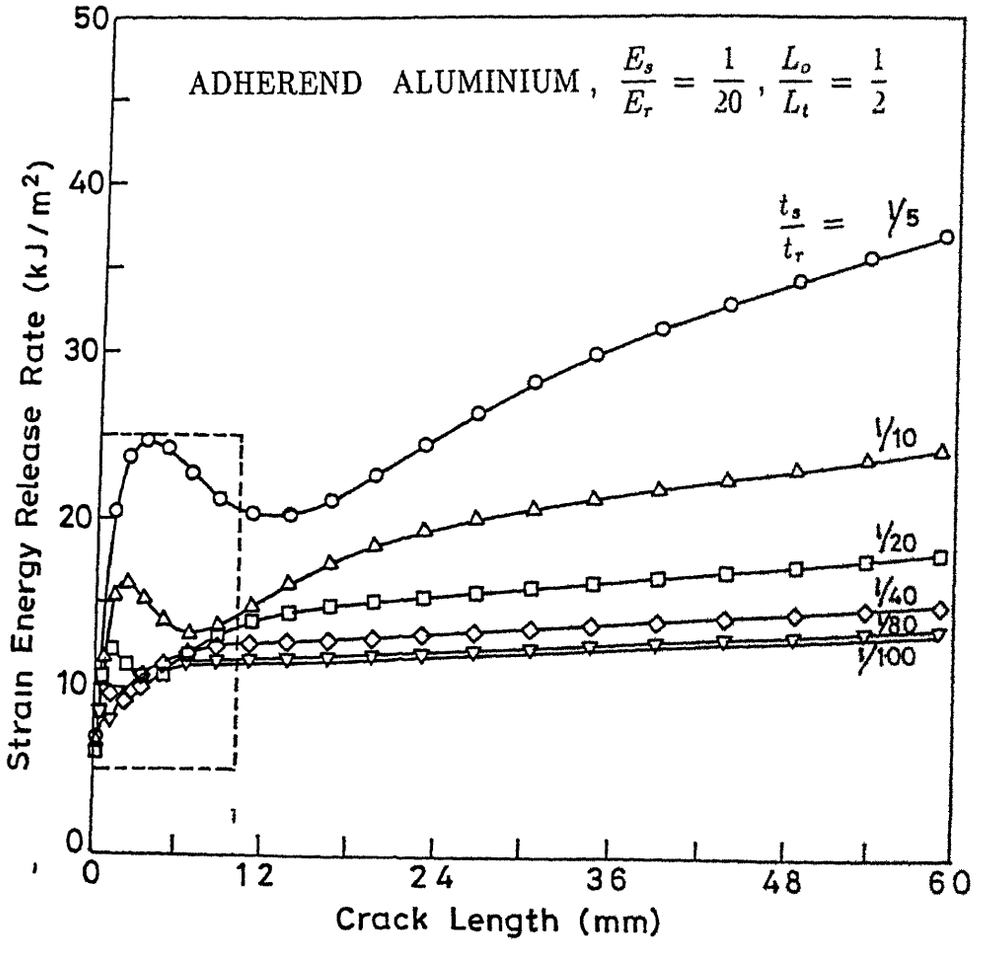

Figure 2 36. Variation of total strain energy release rate with crack length for crack initiation at location '3' and different **t** (= t_s/t_r) values in aluminium to aluminium joints

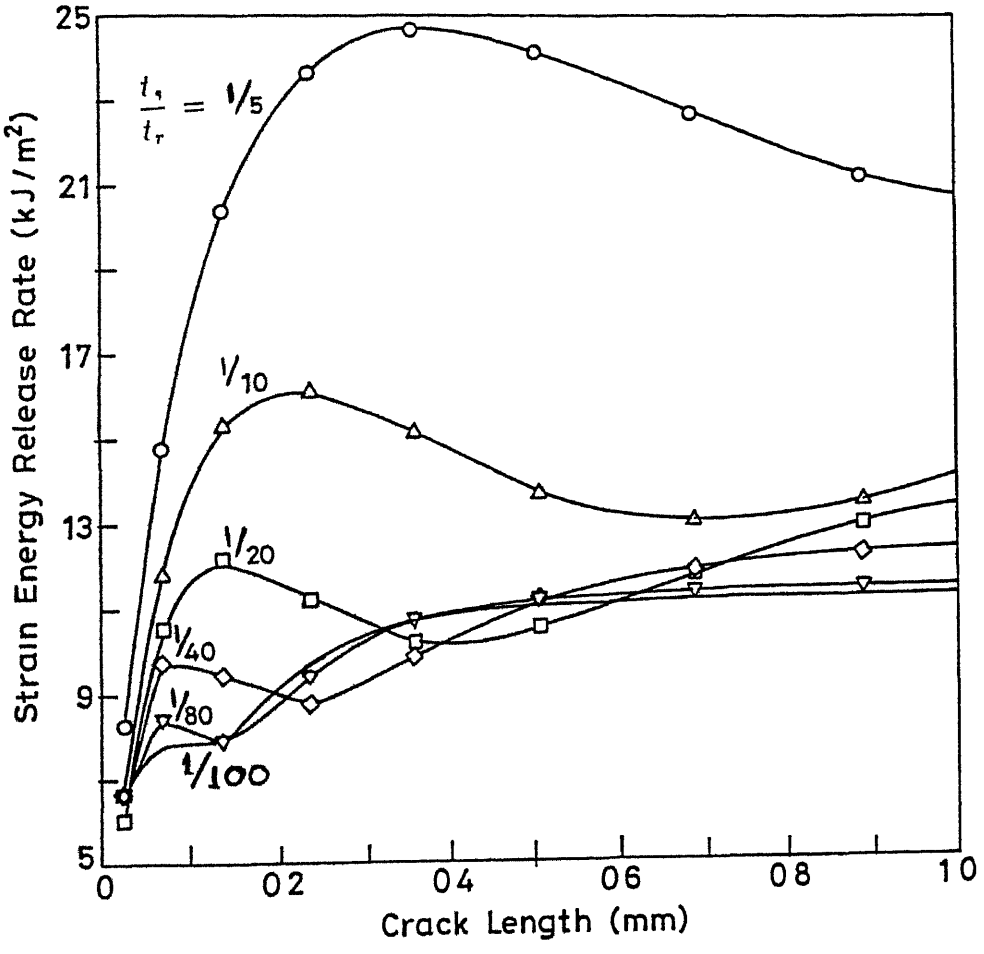

Figure 2 37: Variation of total strain energy release rate with crack length for crack initiation at location '3' and different **t** (= t_s/t_r) values in aluminium to aluminium joints with very fine mesh refinement

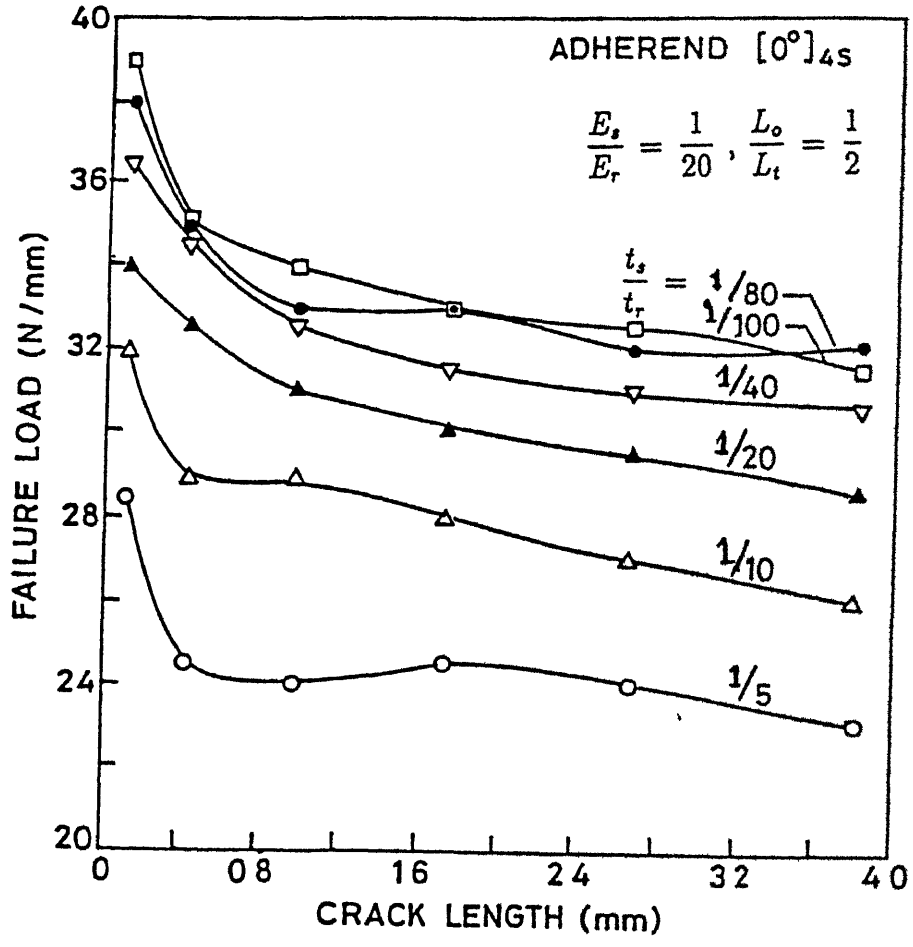

Figure 2 38 Variation of failure load with crack length for crack initiation at location '3' and different **t** ($= t_s/t_r$) values in $[0^\circ_{4S}, 0^\circ_{4S}]$ CFRP laminates

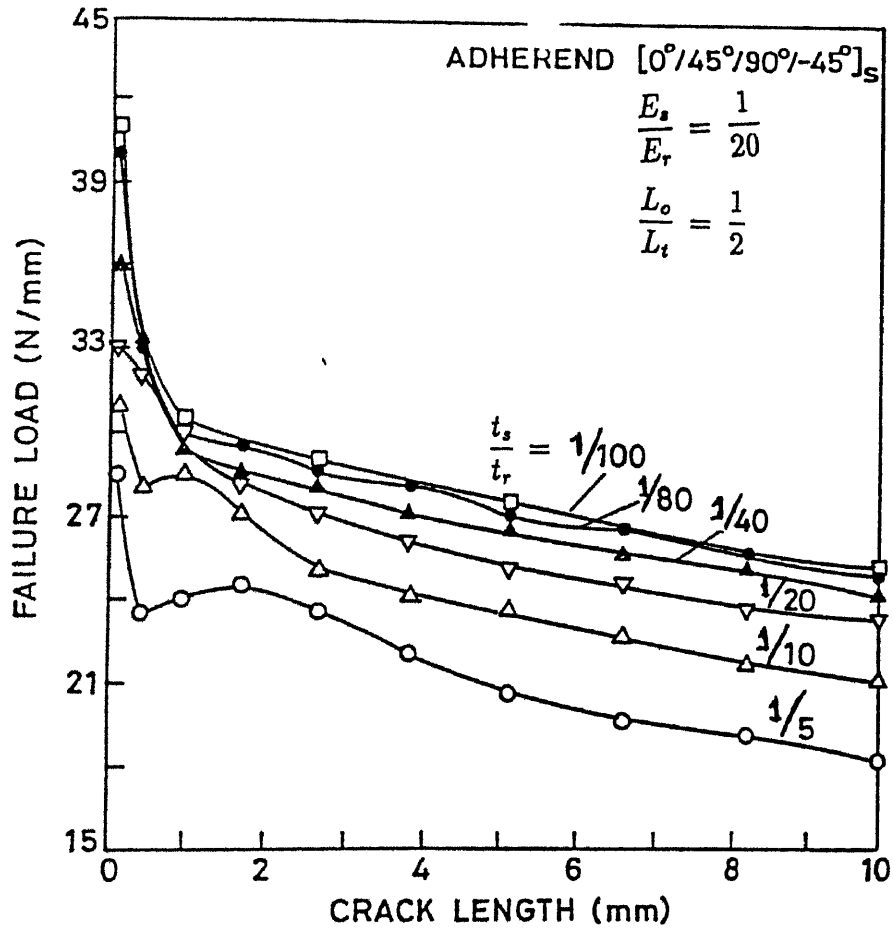

Figure 2.39 Variation of failure load with crack length for crack initiation at location '3' and different t (= t_s/t_r) values in [1324_S, 1324_S] (optimal) CFRP laminates

Chapter 3

Elasto-plastic analysis

3.1 Introduction

Adhesive materials play a major role in the load transfer mechanism of bonded joints These are mostly polymeric materials and exhibit material non-linearities em viz elasto-plastic and visco-plastic Therefore, it is important to consider the non-linear behaviour of the adhesive for a more realistic analysis In this Chapter, adhesive is considered to be elasto-plastic in behaviour, and adherend is considered to be linear elastic Finite element code with material non-linearity (elasto-plastic behaviour), is developed and validated with existing results from the literature Elasto-plastic analyses of double lap joint are carried out Growths of plastic zones are studied In addition, influence of various parameters, such as (i) stacking sequence in composite adherends, (ii) fracture toughness of the adhesive, (iii) overlap length of the joint, and (iv) thickness of adhesive on the strength of adhesively bonded joints, are investigated

3.2 Formulation

Yamada, et al (1968) presented a classical solution for continuum elasto-plastic problems by means of finite element approach This method is based on a plastic stress-strain matrix, which is derived by inverting the Prandtl-Reuss equations of theory of plasticity Zienkiewicz, et al (1969) suggested an initial stress computational process, which showed rapid convergence than other alternative approaches This also permits large load increments without violating the yield criterion They presented a general formulation for the elasto-plastic matrix for evaluating stress increments with an associated flow rule Several solutions showing stress distribution, strain development and growth of plastic enclaves are given for both the von Mises and Coulomb (Drucker) type yield surface Owen and Hinton (1980) explained in detail the finite element approach to material non-linearities (elasto-plastic and visco-plasticity) Whitcomb and Dattaguru (1984) developed a general computer code for the geometrical and material non-linear analyses of structures (GAMNAS)

3.2.1 Constitutive relations

In non-linear elastic behaviour, the stresses can be expresses as a function of strain as $\sigma = \sigma(\epsilon)$ The main difference of plastic formulation from non-linear elastic formulation is that such a unique relationship between stress and strain is not available Although the stresses at any level of strain have to lie on or, within the current yield surface, it is difficult to determine the exact value of each component

Theoretical as well as practical interest in plasticity has stimulated much work in the numerical solution of elasto-plastic problems by finite element method and other procedures Small strain displacement elasto-plastic solution

using finite element method is discussed by Yamada, et al (1968) The difference in elasto-plastic analyses reported by other researchers lie between the apparent forms of non-linear solution algorithms used, and the form of constitutive relations postulated Some common computational approachs used with incremental theory of plasticity in finite element method are (i) incremental tangent stiffness, (ii) initial strain and (iii) initial stress methods

In incremental tangent stiffness method the change of material constitutive matrix forming element stiffness, assembling and inverting an overall stiffness matrix for each step of analysis is carried out In the initial strain and the initial stress approaches, in all the iterations a simple resolution of constant linear elastic problem is carried out The initial stress method is found suitable for solving problems with ideal plasticity or with strain hardening

Yield criteria

A yield criterion is a hypothesis concerning the limit of elasticity under any possible combination of stresses The suitability of any proposed yield criterion should be validated by conducting experiments Yielding occurs when some scalar function of the principal stress differences reaches a critical magnitude, mathematically it can be expressed as

$$f(\sigma_1 - \sigma_2,\ \sigma_2 - \sigma_3,\ \sigma_3 - \sigma_1) = constant \qquad (3\ 1)$$

Two different yielding criteria namely (i) Tresca and (ii) von-Mises criteria are described in brief

Tresca yield criterion Perhaps the simplest function, which satisfies the Equation (3 1) is of the form

$$\sigma_i - \sigma_j = constant \tag{3 2}$$

Above equation can be interpreted as, when largest of the three stresses $(\sigma_1 - \sigma_2)$, $(\sigma_2 - \sigma_3)$, and $(\sigma_3 - \sigma_1)$ attains a critical constant value, (for a given material) yielding occurs

von Mises yield criterion Another admissible function, which satisfies Equation (3 1) is of the form

$$(\sigma_1 - \sigma_2)^2 + (\sigma_2 - \sigma_3)^2 + (\sigma_3 - \sigma_1)^2 = constant \tag{3 3}$$

In this type of function, each of the principal stresses contributes to yielding This criterion can also be interpreted as, when the shear strain energy reaches a critical constant value, yielding occurs

$$\sqrt{((\sigma_x - \sigma_y)^2 + (\sigma_y - \sigma_z)^2 + (\sigma_z - \sigma_x)^2 + 6(\tau_{xy}^2 + \tau_{yz}^2 + \tau_{zx}^2))/2\,0} = \sigma_0 \tag{3 4}$$

Stress-strain relation

Hooke's law for an isotropic elastic material can be written as

$$\{\sigma\} = [D]\{\epsilon\} \tag{3 5}$$

where $[D]$ is the material matrix An equivalent relation in plasticity is dependent on present state of stress and deformation Yamada, et al (1968) have developed a plastic stress-strain relation and presented in a matrix, which is termed as Elasto-plastic matrix This matrix is derived by inverting Prandtl-Reuss equations obeying von Mises yield criterion For a two dimensional plane strain model this matrix is written as

$$[D_{ep}] = \frac{E}{1+\nu}\begin{bmatrix} \frac{1-\nu}{1-2\nu} - \frac{\sigma_x'\sigma_x'}{S} & \frac{\nu}{1-2\nu} - \frac{\sigma_x'\sigma_y'}{S} & -\frac{\sigma_x'\tau_{xy}}{S} \\ \frac{\nu}{1-2\nu} - \frac{\sigma_x'\sigma_y'}{S} & \frac{1-\nu}{1-2\nu} - \frac{\sigma_y'\sigma_y'}{S} & -\frac{\sigma_y'\tau_{xy}}{S} \\ -\frac{\sigma_x'\tau_{xy}}{S} & -\frac{\sigma_y'\tau_{xy}}{S} & \frac{1}{2} - \frac{\tau_{xy}^2}{S} \end{bmatrix} \tag{3 6}$$

Primes represent the deviatoric stress components and

$$S = \frac{2\bar{\sigma}^2}{3}\left[1 + \frac{E_T}{\frac{3E}{2(1+\nu)}}\right] \tag{3 7}$$

where, E_T and $\bar{\sigma}$ are the tangent modulus and effective stress, respectively According to von Mises criterion, effective stress for two dimensional problems is written as

$$\bar{\sigma} \geq \sigma_0 \tag{3 8}$$

$$\bar{\sigma} = \sqrt{\sigma_x^2 + \sigma_y^2 - \sigma_x\sigma_y + 3\tau_{xy}^2} \tag{3 9}$$

where, σ_0 represents yield stress of the material

3.2.2 Finite element technique

Similar to the computer codes developed by Owen and Hinton (1980) and Whitcomb and Dattaguru (1984), a new code is written to predict the failure load, which is explained in the flow diagram given in Figure 3 1 The module, which takes into account the non-linear (plastic) behaviour of the material is indicated by the dashed portion in the Figure Details of the elastic and plastic analyses are explained in the main algorithm in Section 2 2 and plastic algorithm of this Section, respectively

■ *Non-linear plastic algorithm*

step 01 compute the followings

$$D_{ep} = D_{ep}(\delta^n)$$

$$B^n = B_0 + B_{NL}(\delta^n)$$

$$K^n = \int_{\Omega} [B^n]^T D_{ep} B d\Omega$$

step 02 : calculate proportionality factor H

$$H = \frac{\sigma^{n+1} - \sigma^n}{\sigma_0 - \sigma^n}$$

step 03 : compute residual stress to be compensated

$$\sigma_R = H\sigma^{n+1}$$

step 04 : update stress

$$\sigma^{n+1} = (1 - H)\sigma^{n+1}$$

step 05 · calculate residual forces

$$\Delta\psi_{ep} = \int_{\Omega} [B^n]^T \sigma_R d\Omega + \Delta f$$

where

Δf represents nodal forces

step 06 check for convergence

$|\Delta\psi_{ep}| \leq$ tolerance

if converged go to *step 07 of main algorithm* in Section 2.2

else continue

step 07 solve for displacement

$\Delta\delta = [K]^{-1}\Delta P$

step 08 calculate incremental stresses and strains

$\Delta\epsilon = [B^n]^T\Delta\delta$

$\Delta\sigma = [D_{ep}]\Delta\epsilon$

step 09 update displacements, strains and stresses

$\delta^{n+1} = \delta^n + C_0\Delta\delta^n$

$\epsilon^{n+1} = \epsilon^n + \Delta\epsilon^n$

$\sigma^{n+1} = \sigma^n + \Delta\sigma^n$

step 10 . go to step 01

As mentioned in *step* 01, D_{ep}, B^n and K^n are functions of the displacement vector of n^{th} iteration. One is expected to update these values in every iteration. But there is a possibility of divergence in results using these K^n values. However, using constant values of these parameters and Newton Raphson's modified approximation (Owen and Hinton, 1980 and Zienkiewicz and Taylor, 1991) convergence is assured. In addition, this reduces substantially the computational time and memory.

If the effective stress $\bar{\sigma}$ of any element in the adhesive, exceeds the yield value of the material σ_0, then the material behaves elasto-plastic and elasto-plastic analysis is to be carried out. Module, which takes care of plastic part of elasto-plastic analysis, is indicated by dashed box of Figure 3.1.

Elasto-plastic calculations are iterated till the elasto-plastic residual (out-of-balance) force $\Delta\psi_{ep}$ becomes smaller than a prescribed tolerance value Strain energy release rates are calculated and, as mentioned earlier in Chapter 2 and the fracture criterion $G_I + G_{II} \geq G_{IC} + G_{IIC}$ is employed to predict the failure load A comparison of these loads, for linear elastic model and plastic models with various tolerance values, and the effect of strain hardening are discussed below

Convergence criterion

Elasto-plastic analysis predicts a relatively higher failure load in comparison with that of linear elastic analysis This might be due to the fact that elasto-plastic analysis results in a considerable reduction in peak stresses as compared with elastic analysis This agrees with the finite element solutions obtained by Thomsen (1992) The failure load increases with the decrease in tolerance value and saturates for a tolerance value $\simeq$ 0 15 percent (Figure 3 2)

Strain hardening

Figure 3 3 represents the strain hardening behaviour of the adhesive material Predicted failure loads remains same for strain hardening parameter κ is in the range 0 2 to 0 8 Hart-Smith (1973) also observed that arbitrary bi-linear representations leads to the same result It can be concluded that, little accuracy could be be gained by more complex representation of adhesive characteristics However, in the elasto-plastic analysis size of plastic zone is reduced rapidly, with the increase in hardening parameter κ

3.3 Validation of computer code

In order to validate the code developed the two-dimensional elasto-plastic beam problem considered by Zienkiewicz, et al (1969) is analysed using plane strain CST element undergoing small displacement Young's modulus, Poisson's ratio and yield stress of the beam are considered to be 70 GPa, 0 2 and 243 0 MPa, respectively Figure 3 4 shows the comparison of the results using 300 isoparametric quadrilateral four noded elements, 75 CST elements and 150 CST elements with that of 200 triangular elements employed by Zienkiewicz, et al (1969) It is observed that the computed load-displacement response with 150 CST elements are in fairly good agreement with that reported by Zienkiewicz, et al (1969)

3.4 Growth of plastic zone

The growth of plastic zone in the adhesive is investigated for three different displacement boundary conditions Further this growth is studied with crack propagation

3.4.1 Boundary conditions

Adhesively bonded joints with aluminium adherend and Epon VIII (Adams and Wake, 1984) adhesive (Table 3 1) are chosen for the study of the growth of plastic zone for various boundary conditions Growth of plastic zones for the boundary conditions of types- 1, 2 and 3 are illustrated in Figures 3 5a, 3 5b and 3 5c, respectively It is observed that the growths of plastic zones are sensitive to the displacement boundary conditions For type-1 boundary

condition the growths of plastic zones are along the diagonal joining the left top and right bottom corner of the adhesive layer While for types- 2 and 3 boundary conditions the growths of plastic zones are significantly different It is along the left bottom corner to the midpoint of the top adherend-adhesive interface In other words for type-1 boundary condition failure is cohesive type (limited within the adhesive only) While for types- 2 and 3 boundary conditions failure is adhesive type (not limited to the adhesive only, interface between the adherend and adhesive is also involved) Further, in type-1 boundary condition the adhesive is under pure shear leading to stronger joint, as compared to other boundary conditions where, peel stresses are present

3.4.2 Crack propagation

Double lap joint (Figure 3 6) with carbon fibre reinforced plastic CFRP adherend and Epon VIII (Adams and Wake, 1984) adhesive (Table 3 2) is considered to study the growth of plastic zone associated with crack propagation As explained earlier crack propagation is modelled by sequential opening of paired nodes at the interface of adherend and adhesive Figure 3 7 illustrates the growths of plastic zones with the crack propagation Crack location '3' is considered Size of plastic zone decreases faster as the crack propagates and plastic zone altogether disappears when the crack becomes large in size

3.5 Parametric study

Effects of stacking sequence, critical strain energy release rate of the adhesive, overlap length and thickness of the adhesive on the strength of the double lap joint (Figure 3 6) are investigated Because of symmetry only one half of the

joint is considered for the analysis The problem is treated as one of plane strain model A finite element mesh consists of 1816 CST elements is employed for the analysis

Three non-dimensional parameters are defined viz

$$\mathbf{g} = \frac{G_C'}{G_C} \tag{3 10}$$

$$\mathbf{l} = \frac{L_o}{L_t} \tag{3 11}$$

$$\mathbf{t} = \frac{t_s}{t_r} \tag{3 12}$$

where, G_C' and G_C are the critical strain energy release rates of the adhesive used and the standard adhesive (epoxy), respectively L_o and L_t denote the overlap length and the total length of the bonded joint In addition t_s and t_r represent the thicknesses of adhesive and adherend, respectively G_C' is assumed to be in multiples of G_C In addition, assuming constant critical strain energy release rate G_C of the standard (epoxy) adhesive, adherend thickness t_r and overlap length L_o, parametric study is carried out The adherends and adhesive of the joint, are considered to be carbon fibre reinforced plastics (CFRP) and Epon VIII (Table 3 3), respectively Crack located at '3' is found to be critical in subsection 2 6 2 Therefore, only crack location at '3' is considered for further discussion in this Chapter

3 5.1 Stacking sequence

A symmetric quasi-isotropic combination is considered for the analysis to investigate the effect of stacking sequence on the bond strength Most

widely used fibre orientations 0°, 45°, 90° and -45° are considered Among all the possible symmetric combinations of these plies, it is observed in subsection 2 6 3 that $[0°/45°/90°/-45°]_S$ (optimal) layup, has the maximum bond strength among its combinations Also the presence of 0°, ply in the immediate neighbourhood of the adhesive results in stronger joint than the plies of any other orientation Elasto-plastic analysis is carried out for $[0°/0°/0°/0°]_S$, $[0°/45°/90°/-45°]_S$ and $[0°/0°/90°/90°]_S$ layups of CFRP adherends It is found that employing $[0°/0°/90°/90°]_S$ layup results in a stronger joint is obtained than $[0°/0°/0°/0°]_S$ layup This combination is found to be a stronger joint than $[0°/45°/90°/-45°]_S$ layup The failure loads are computed for various adhesive critical strain energy release rate **g** $(= G_C'/G_C)$, overlap length **l** $(= L_o/L_t)$ and adhesive thickness **t** $(= t_s/t_r)$ ratios for these three layups Detail of these results are discussed in the respective subsections

3.5.2 Fracture toughness of adhesive

For various **g** $(= G_C'/G_C)$ values and layups the computed failure loads are listed in Table 3 4 It is observed that as **g** increases failure load increases for all the three layup sequences considered Adhesive with higher value of critical strain energy release rate (high **g** value) leads to a stronger joint Therefore, in order to achieve a higher fracture strength of the joints, adhesives with higher critical strain energy release rates are suggested Variation of failure load with crack length for various **g** values in $[0°/0°/0°/0°]_S$, $[0°/45°/90°/-45°]_S$ (optimal) and $[0°/0°/90°/90°]_S$ CFRP laminates are listed in Figures ~~3 8~~ 3 10, 3 9 and ~~3 10~~ 3 8, respectively

Though fracture toughness of adhesive is generally denoted by K_{IC}, the stress intensity factor for ideal plane strain adhesive material, in the present study, for convenience critical strain energy release rate G_C is also termed as

fracture toughness

3 5.3 Overlap length

For various values of l (= L_o/L_t) and the three layups chosen the computed failure loads are listed in Table 3 5 It is observed that as l increases failure load increases for all the three layup sequences For higher fracture strength of the bonds longer overlap lengths (higher l) are suggested Variation of failure load with crack length for various l values in $[0°/45°/90°/-45°]_S$ (optimal) and $[0°/0°/90°/90°]_S$ CFRP laminates are shown in Figures 3 11, 3 12 and 3 13, respectively

3.5 4 Adhesive thickness

For various t (= t_s/t_r) values and layups the computed failure loads are listed in Table 3 6 It is observed that as t increases failure load decreases for all the three layup sequences For higher fracture strength of the bonded joints, small thicknesses of the adhesives (lower t) are suggested Variation of failure load with crack length for various t values in $[0°/45°/90°/-45°]_S$ (optimal) and $[0°/0°/90°/90°]_S$ CFRP laminates are illustrated in Figures 3 14, 3 15 and 3 16, respectively

3.6 Conclusions

On the basis of elasto-plastic analysis carried out in this chapter, the following conclusions are drawn

- The elastic analysis predicts lower failure loads as compared to the elasto-plastic analysis Therefore, for a realistic analysis elasto-plastic behaviour is suggested to be considered
- Strain hardening (20–80 percent) has no significant effect on the strain energy release rate
- Growth of plastic zone is sensitive to the displacement boundary conditions The plastic zone is initiated at the free-edges and gradually spreads over the core of the adhesive Growth of plastic zone is also sensitive to the crack propagation (size of the crack)
- Strain energy release rate is sensitive to layup sequences in composite adherends A proper choice of layup sequence in the composite adherend results in an efficient bonded joint
- Use of adhesive of high fracture toughness and large overlap lengths results in stronger bonded joint, whereas, employment of small thickness of adhesive results in stronger bonded joint

Table 3.1 Specifications of double lap joint

Adherend (aluminium)

Young's modulus (E_r)	70 GPa
Poisson's ratio (ν_r)	0.33
thickness (t_r)	10 mm

Adhesive (Epon VIII)

Young's modulus (E_s)	3.5 GPa
Poisson's ratio (ν_s)	0.41
thickness (t_s)	2 mm
yield stress (σ_o)	51.5 MPa

Table 3.2 Specifications of double lap joint

Adherend (CFRP)

longitudinal modulus (E_l)	137 GPa
transverse modulus (E_t)	7 GPa
Poisson's ratio (ν_{lt})	0.3
thickness (t_r)	10 mm

Adhesive (Epon VIII)

Young's modulus (E_s)	3.5 GPa
Poisson's ratio (ν_s)	0.41
thickness (t_s)	2 mm
yield stress (σ_o)	51.5 MPa
fracture toughness (G_C)	0.36 kJ/m^2

Table 3 3 Specifications of double lap joint

Double lap joint	
overlap length (L_o)	40 mm
total length (L_t)	80 mm
Adherend (carbon fibre reinforced plastic)	
longitudinal modulus (E_l)	137 GPa
transverse modulus (E_t)	7 GPa
shear modulus G_{lt}	4 5 GPa
Poisson's ratio (ν_{lt})	0 3
adherend thickness (t_r)	10 mm
Adhesive (Epon VIII)	
Young's modulus (E_s)	3 5 GPa
Poisson's ratio (ν_s)	0 41
thickness (t_s)	2 mm
fracture toughness (G_C)	0 36 kJ/m^2

fracture criterion $G_I + G_{II} \geq G_C$

Table 3 4 Computed failure loads (P_f's) for various g (= G_C'/G_C) values and different laminae combinations

		Failure loads in N/mm for L_o/L_t = 0 50 & t_s/t_r = 0 20		
G_C'/G_C	a_{cr} (mm)	$[0°/0°/0°/0°]_S$	$[0°/45°/90°/-45°]_S$	$[0°/0°/90°/90°]_S$
0 80	0 117	22 000	22 750	21 250
0 85	0 117	23 125	23 500	22 375
0 90	0 117	26 125	24 250	22 750
0 95	0 117	25 000	25 000	23 125
1 00	0 117	25 750	26 125	24 125
1 05	0 117	26 500	26 500	24 625
1 10	0 117	27 250	27 250	25 000
1 15	0 117	28 000	29 500	26 875
1 20	0 117	28 750	29 500	26 500

Table 3 5 Computed failure loads (P_f's) for various l (= L_o/L_t) values and different laminae combinations

		Failure loads in N/mm for G_C'/G_C = 1 00 & t_s/t_r = 0 20		
L_o/L_t	a_{cr} (mm)	$[0°/0°/0°/0°]_S$	$[0°/45°/90°/-45°]_S$	$[0°/0°/90°/90°]_S$
0 250	0 087	16 375	16 375	16 375
0 277	0 091	15 250	14 875	15 250
0 312	0 095	15 250	15 625	15 625
0 357	0 100	17 125	16 937	17 500
0 416	0 107	19 000	19 375	19 000
0 500	0 117	25 750	26 125	24 250

Table 3 6 Computed failure loads (P_f's) for various **t** (= t_s/t_r)values and different laminae combinations

		Failure loads in N/mm for G_C'/G_C= 1 00 & L_o/L_t= 0 50		
t_s/t_r	a_{cr} (mm)	$[0°/0°/0°/0°]_S$	$[0°/45°/90°/-45°]_S$	$[0°/0°/90°/90°]_S$
0 0125	0 117	47 50	41 500	56 50
0 0250	0 117	31 75	29 500	31 00
0 0500	0 117	29 50	30 250	26 50
0 1000	0 117	28 75	28 000	25 75
0 2000	0 117	25 75	26 125	24 25

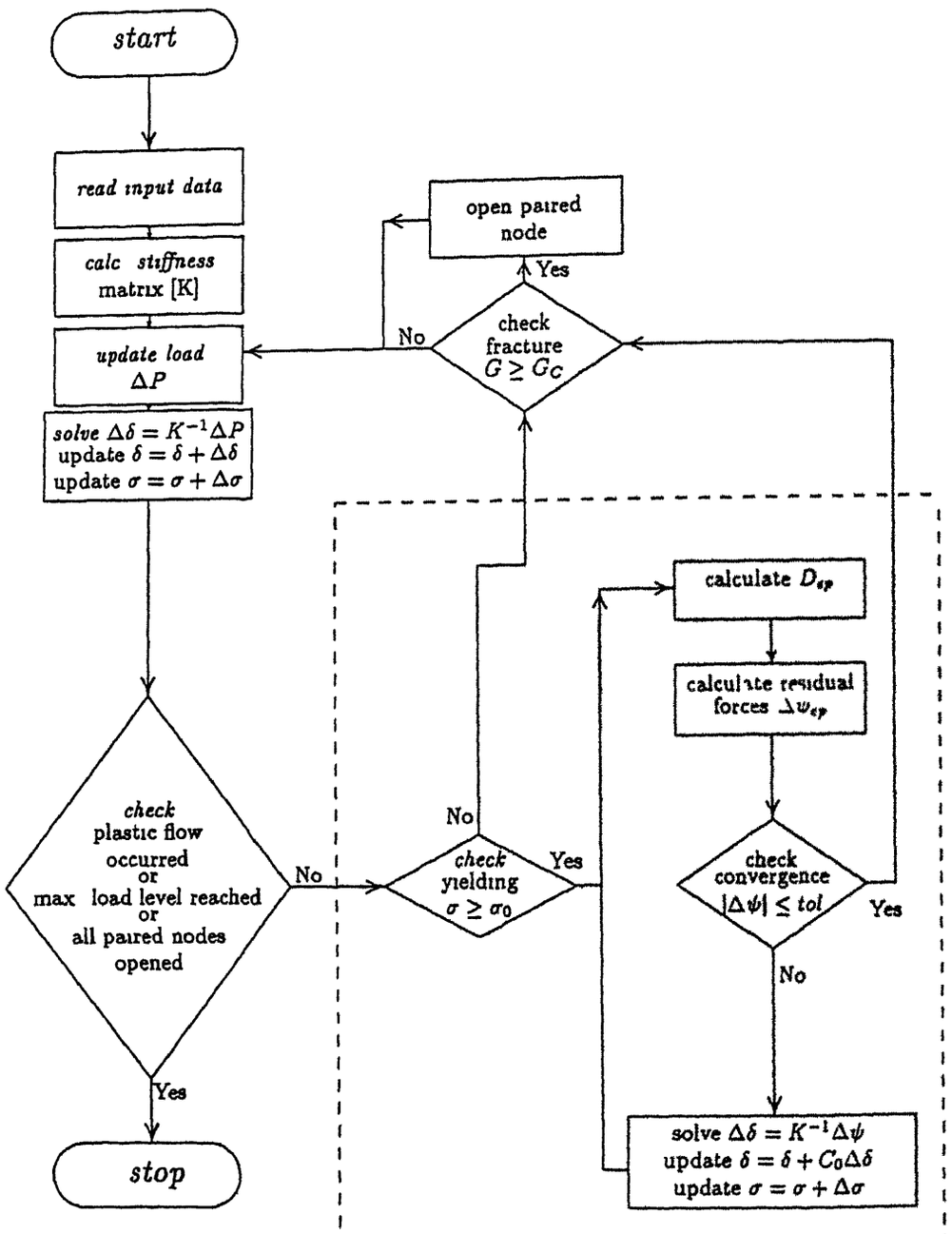

Figure 3 1 Flow chart of elasto-plastic finite element analysis

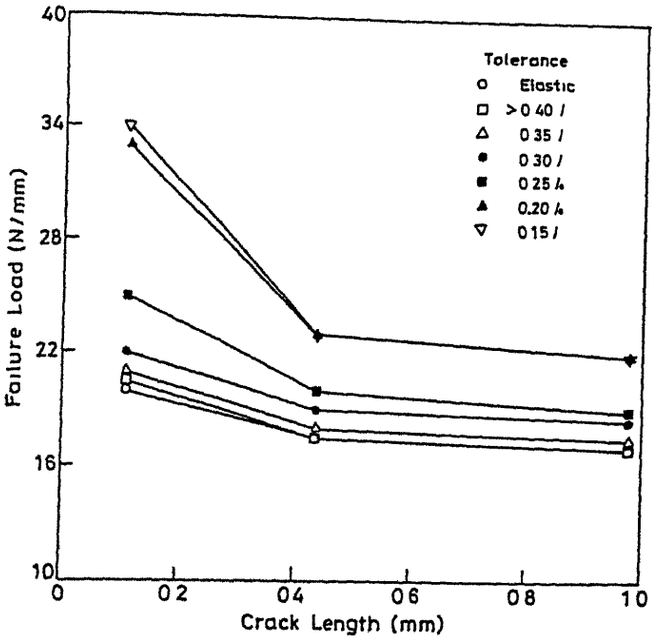

Figure 3 2 Schematic of convergence of failure loads for various tolerance values

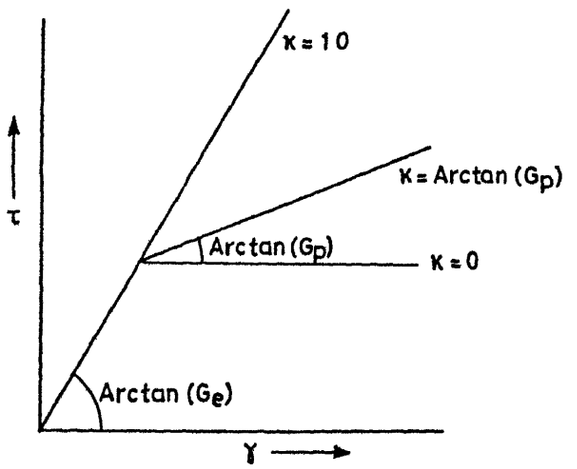

Figure 3.3 Schematic of hardening parameter κ

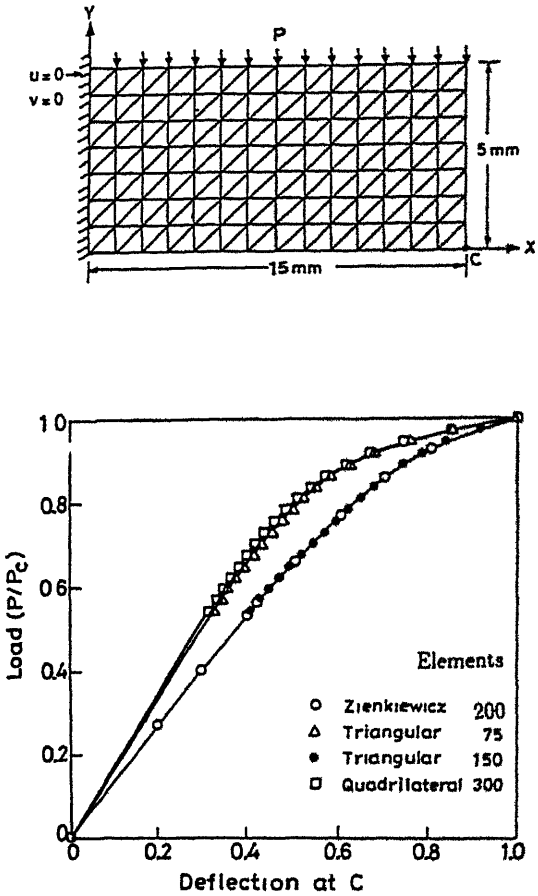

Figure 3.4 Comparison of deflections at location 'C' of cantilever beam (Zienkiewicz, et al., 1969)

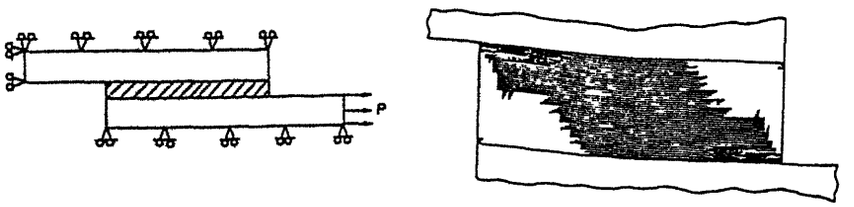

(a) Type - 1 Boundary Condition

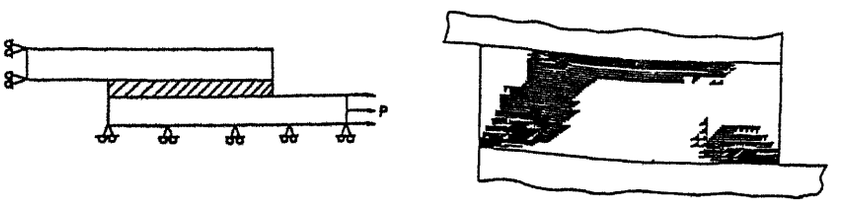

(b) Type - 2 Boundary Condition

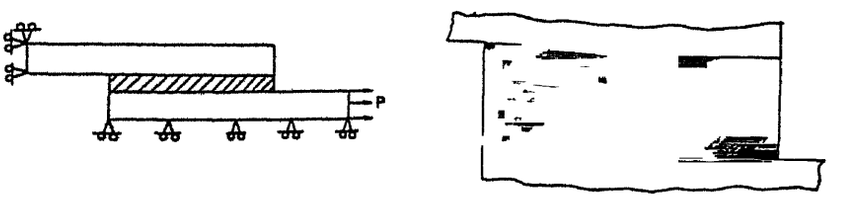

(c) Type - 3 Boundary Condition

Figure 3 5: Boundary conditions and the corresponding growth of plastic zones in the adhesive material

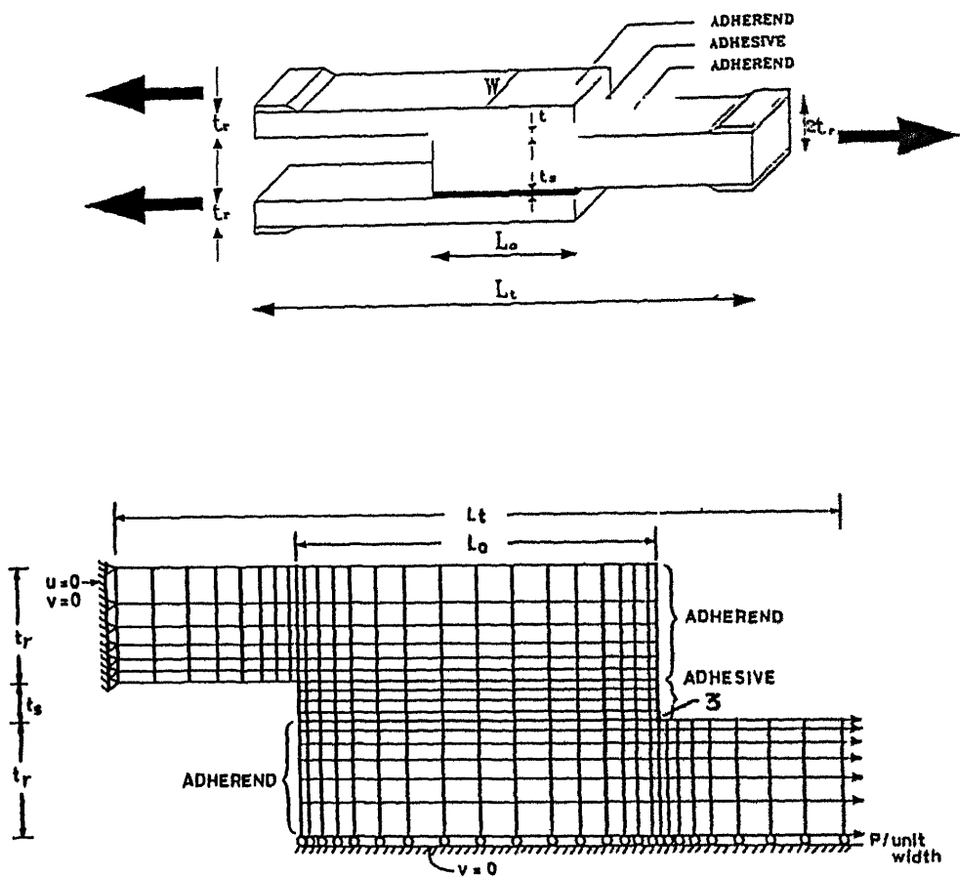

Figure 3 6 Schematic of adhesively bonded double lap joint and the finite element mesh showing the crack location '3'

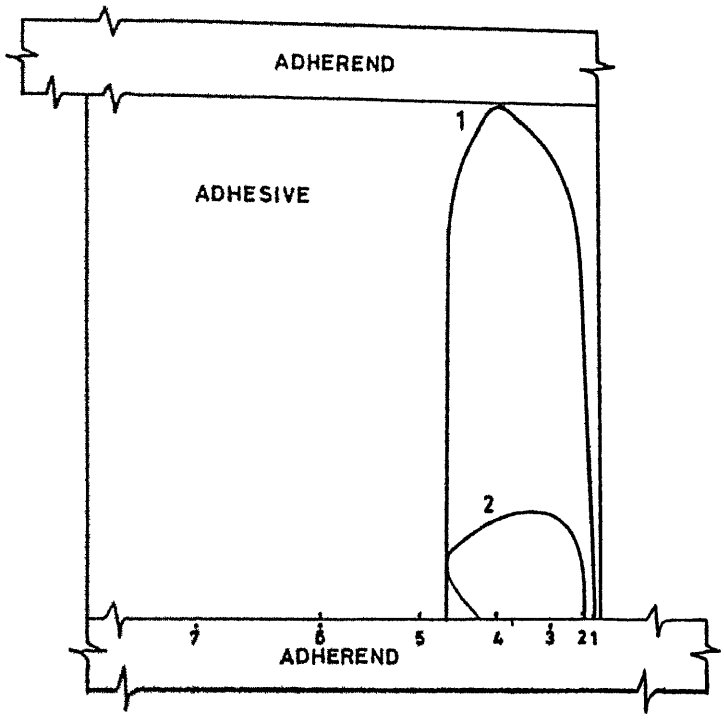

Figure 3 7 Growth of plastic zone with crack propagation

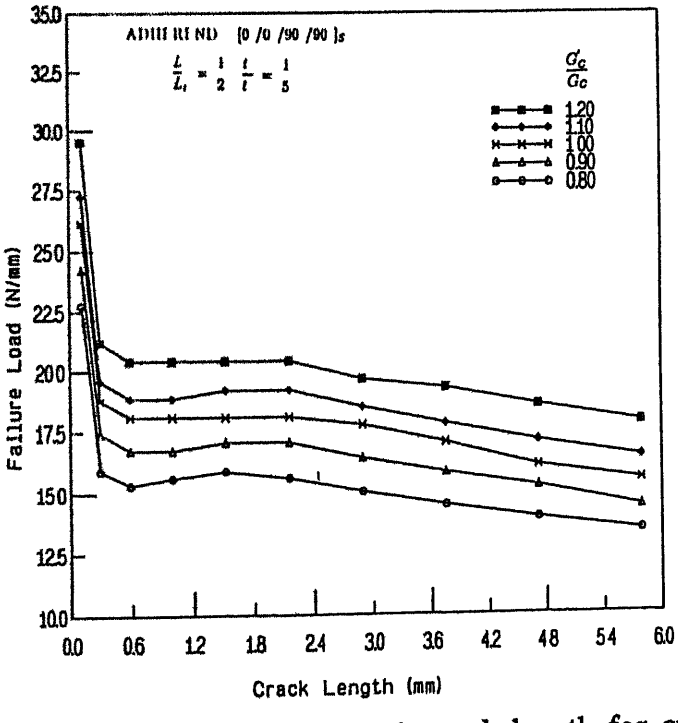

Figure 3 8 Variation of failure load with crack length for crack initiation at location '3' and different g (= G_C'/G_C) values in $[0°/0°/\emptyset°/\emptyset°]_S$ CFRP laminates

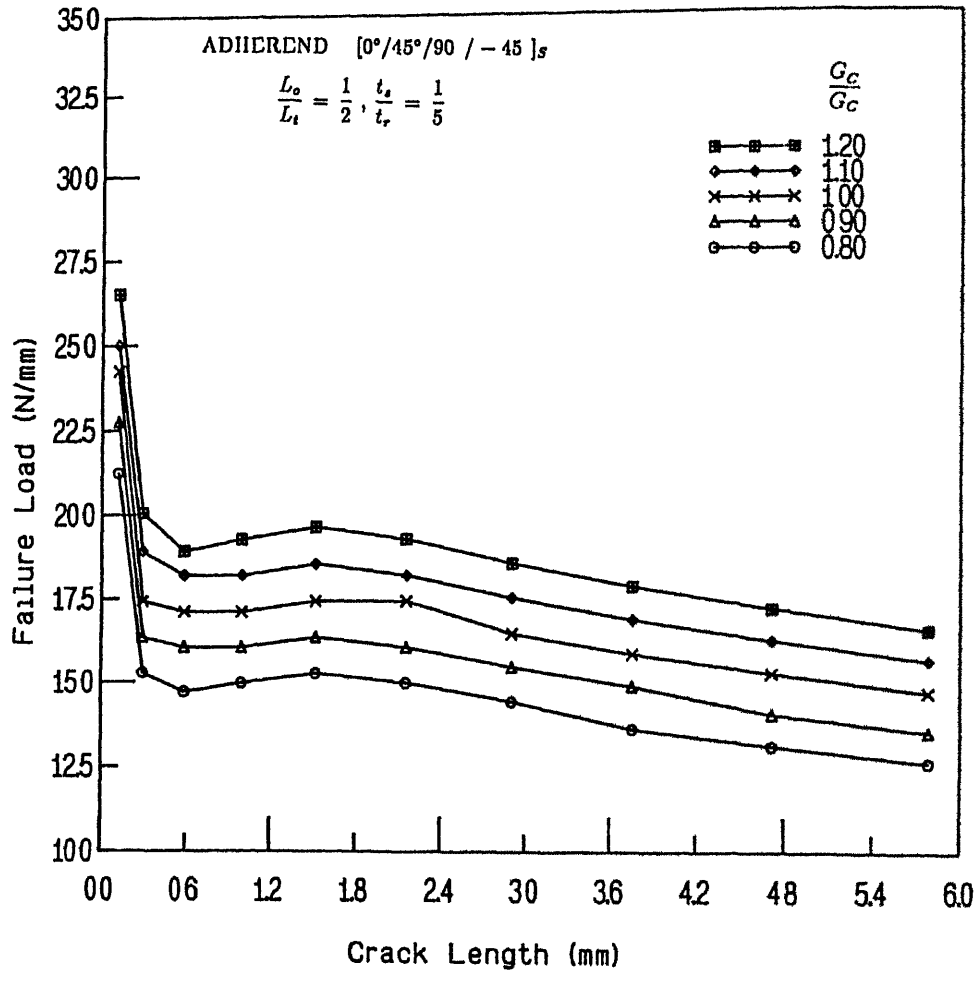

Figure 3 9 Variation of failure load with crack length for crack initiation at location '3' and different g (= G_C'/G_C) values in $[0°/45°/90°/-45°]_S$ (optimal) CFRP laminates

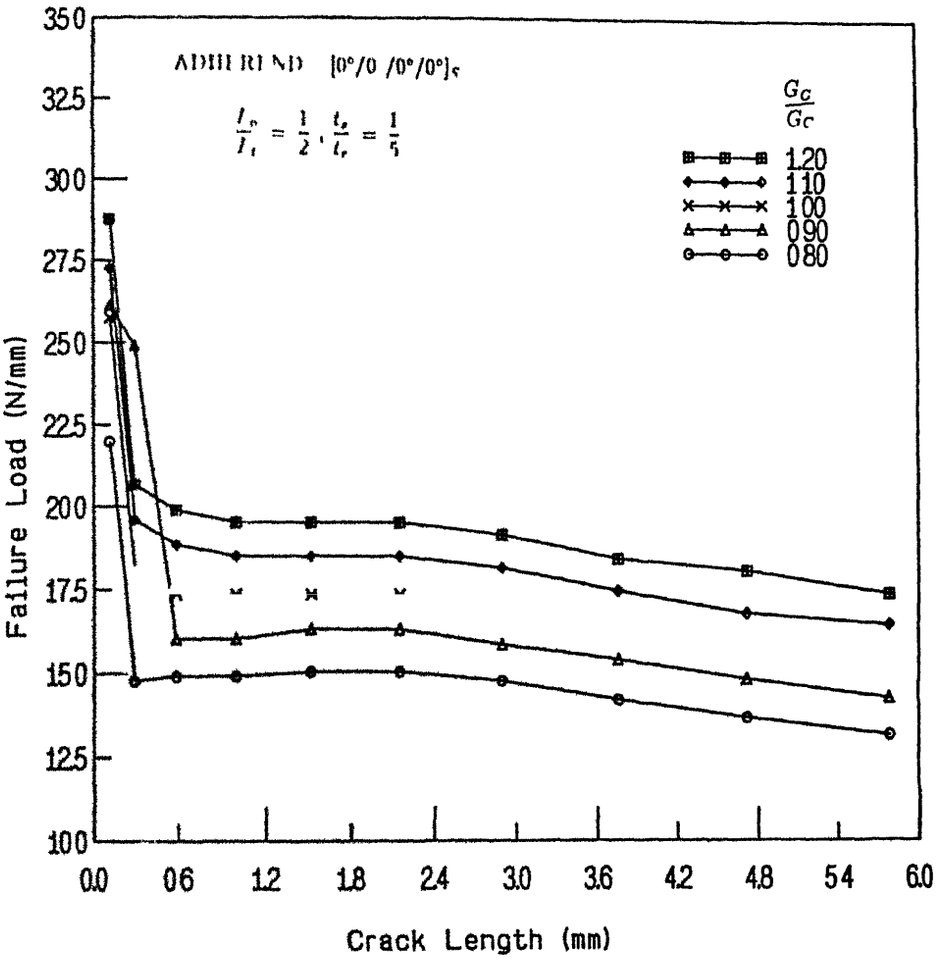

Figure 3.10. Variation of failure load with crack length for crack initiation at location '3' and different g (= G_C'/G_C) values in $[0°/0°/90°/90°]_S$ CFRP laminates

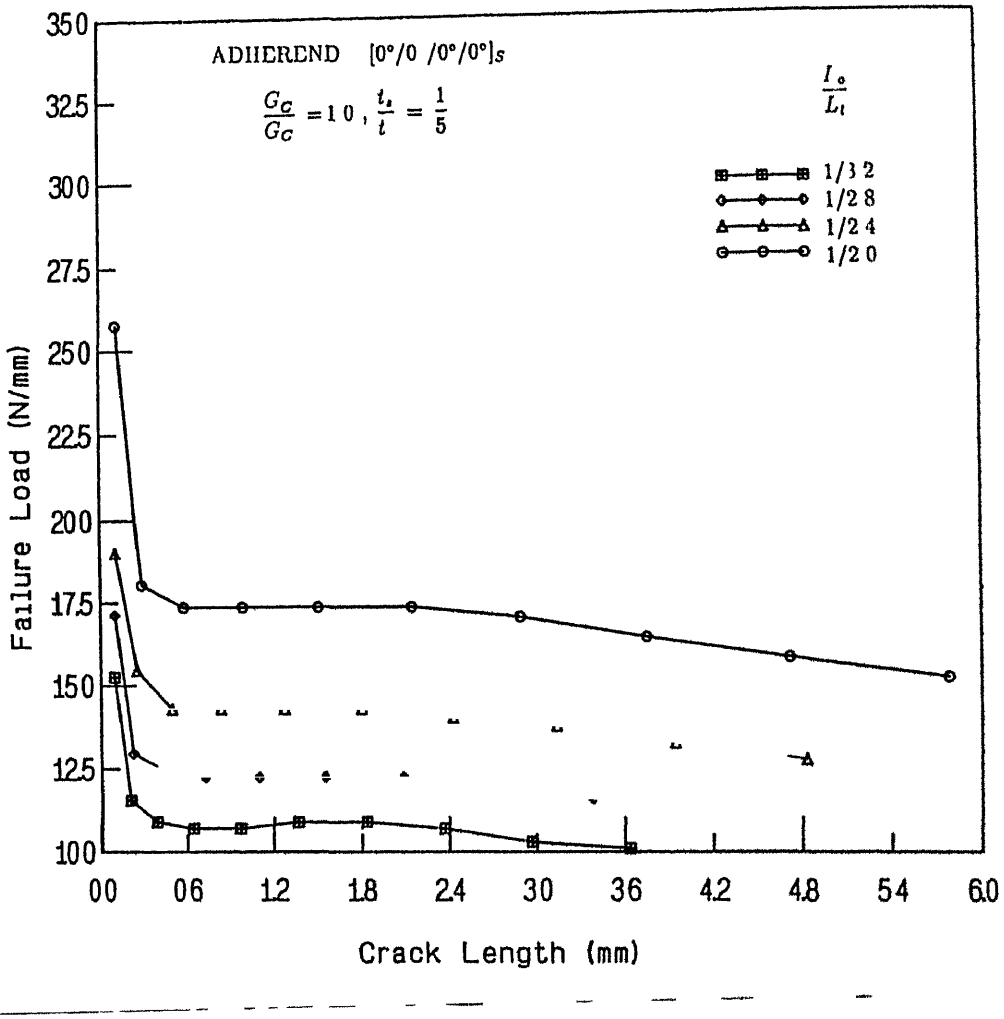

Figure 3.11 Variation of failure load with crack length for crack initiation at location 3 and different l (= L_o/L_t) values in $[0°/0°/0°/0°]_S$ CFRP laminates

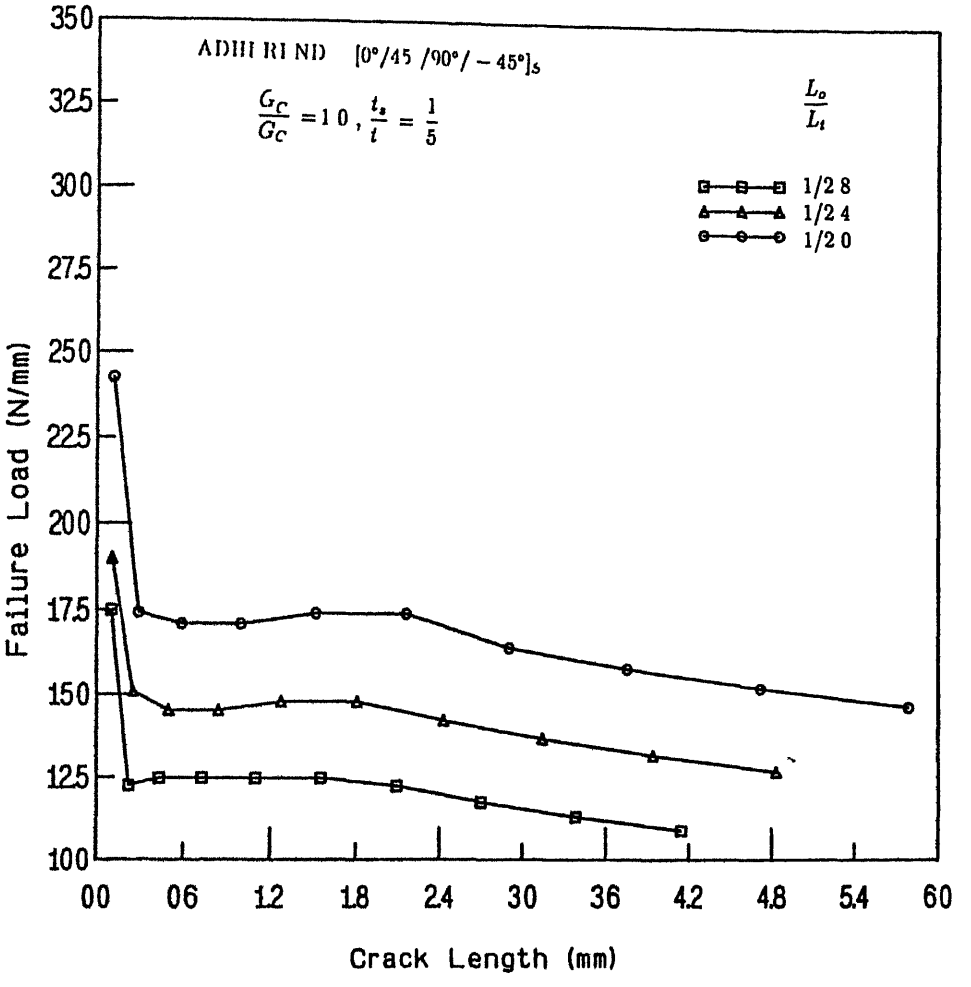

Figure 3 12 Variation of failure load with crack length for crack initiation at location 3 and different l (= L_o/L_t) values in $[0°/45°/90°/-45°]_S$ (optimal) CFRP laminates

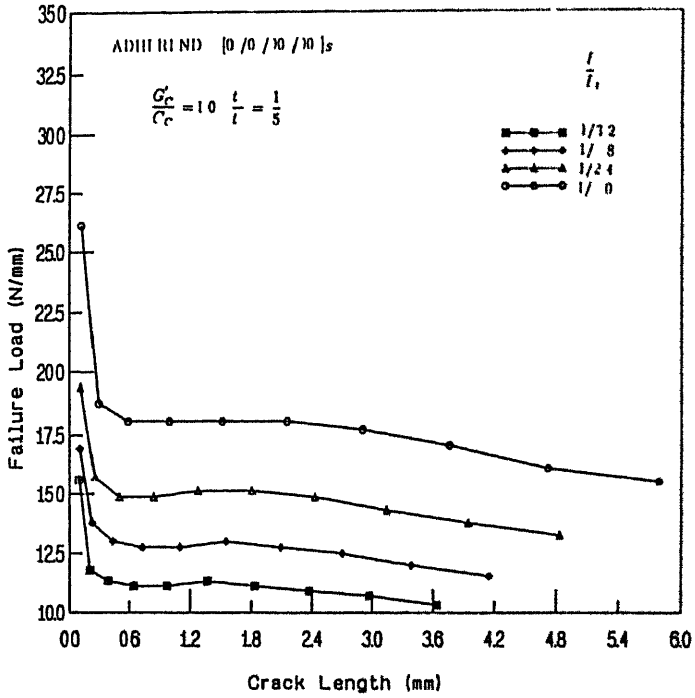

Figure 3 13 Variation of failure load with crack length for crack initiation at location 3 and different l (= L_o/L_t) values in $[0°/0°/90°/90°]_S$ CFRP laminates

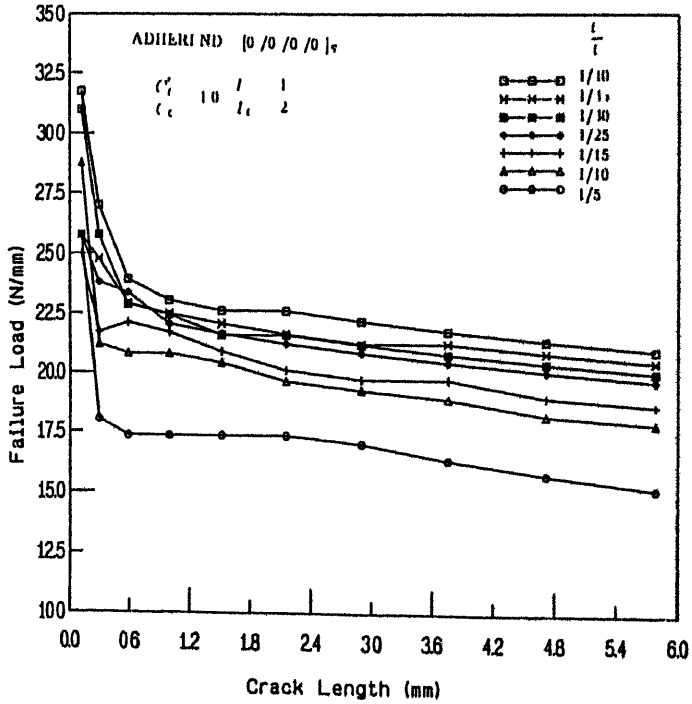

Figure 3 14 Variation of failure load with crack length for crack initiation at location '3' and different t (= t_s/t_r) values in $[0°/0°/0°/0°]_S$ CFRP laminates

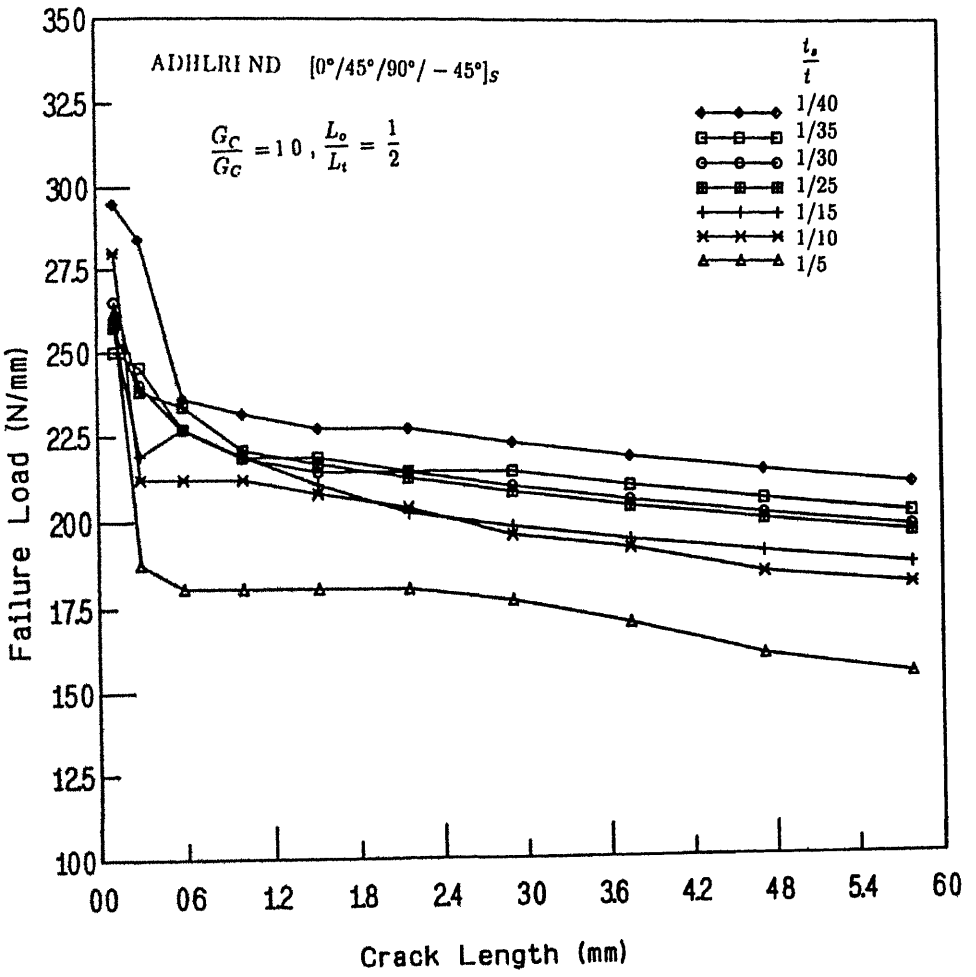

Figure 3 15 Variation of failure load with crack length for crack initiation at location '3' and different t (= t_s/t_r) values in $[0°/45°/90°/-45°]_S$ (optimal) CFRP laminates

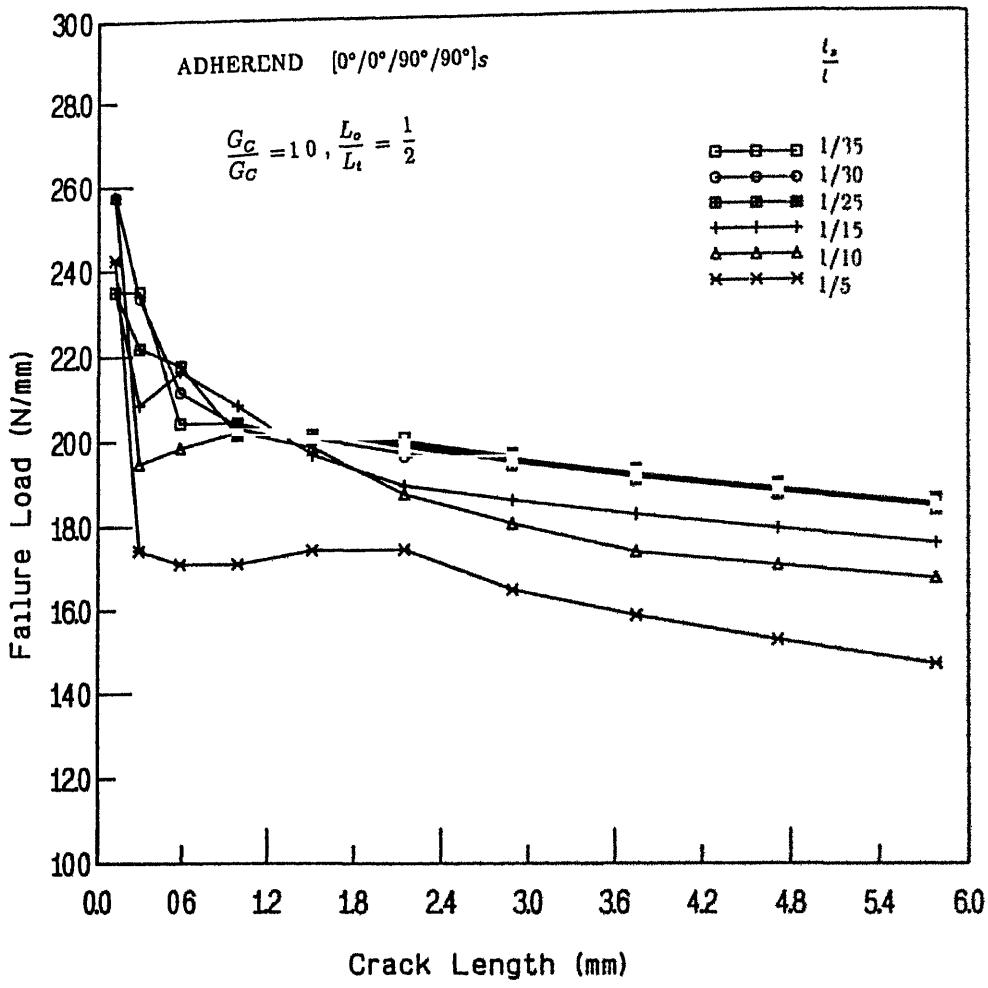

Figure 3 16 Variation of failure load with crack length for crack initiation at location '3' and different **t** ($= t_s/t_r$) values in $[0°/0°/90°/90°]_S$ CFRP laminates

Chapter 4

Visco-plastic analysis

4.1 Introduction

Adhesives are mostly polymeric materials and their responses are time dependent Groth (1986) concluded that events like moisture diffusion, delayed failure are necessary and should be taken into account for an accurate analysis of adhesively bonded joints At high stress levels, the non-linear visco-plastic effects could include creep strains These would lead to significantly different results from the linear predictions and therefore, these effects are important to be included With the increase in load level, generally, adhesive layers become visco-plastic earlier than the adherends Therefore, in this analysis, adhesive is considered as visco-plastic in behaviour, while adherends are considered to be linear elastic

Finite element code, with elasto-visco-plastic behaviour, is developed and validated with the available results from the literature Visco-plastic analyses of single lap, stepped lap, and double lap joints are carried out Influences of various parameters, such as (i) stacking sequence in composite adherends, (ii) critical strain energy release rate of the adhesive, (iii) overlap length and (iv) thickness of the adhesive on the strength of the adhesively bonded joints,

are also investigated

4.2 Formulation

Biot (1954) has derived equations to represent visco-elastic and relaxation responses by employing potential and dissipation functions A large number of phenomena involving interaction of diffusion, chemical reaction, heat transfer, mechanical deformation etc are included in this theory Zienkiewicz and Cormeau (1974) developed an elasto-visco-plastic algorithm, which is found to be an efficient tool and is applicable to a wide range of non-linear (material) problems The solution technique developed for visco-elastic behaviour and could be coupled with visco-plastic phenomenon with series However, most efficient way of dealing with large deformation and dynamic effects is not resolved Zienkiewicz, et al (1974) discussed the finite element method of solution of elasto-visco-plastic engineering problems For the computational convenience, bulk material is considered to be composed of several layers, where each layer might have different material characteristics This model was limited to isotropic and includes few material laws Kanchi, et al (1978) discussed a visco-plastic technique and employed this to study the problems of plastic and creep instability Schapery (1984) discussed pertinent aspects of J integral and energy release rate theory for non-linear elastic media He developed methods of quasi-static deformation and fracture analysis for non-linear visco-elastic media The corresponding principles, which provide the basis for the analysis are applicable to crack growth, crack closing and other problems such as ablation and interfacial contact and separation

Strain rate

Groth (1990) presented expressions for visco-elastic, visco-plastic and visco-elasto-plastic strain rate as written in Equations (4 1), (4 2) and (4 4), respectively, for the one dimensional models of adhesive material under pure shear as shown in Figure 4 1

$$\epsilon_{ve} = \gamma_{xy}[\tau_{xy} - G_{xy}\epsilon_{ve}] \tag{4 1}$$

$$\epsilon_{vp} = \gamma_{xy}[\tau_{xy} - \tau_0] \quad \text{if } \tau_{xy} > \tau_0 \tag{4 2}$$

$$= 0 \quad \text{if } \tau_{xy} \leq \tau_0 \tag{4 3}$$

$$\epsilon_{vep} = \gamma_{xy}[\tau_{xy} - G_{xy}\epsilon_{ve}] + \gamma_{xy}[\tau_{xy} - \tau_0] \quad \text{if } \tau_{xy} > \tau_0 \tag{4 4}$$

$$= \gamma_{xy}[\tau_{xy} - G_{xy}\epsilon_{ve}] \quad \text{if } \tau_{xy} \leq \tau_0 \tag{4 5}$$

From the above Equations (4 1), (4 2) and (4 4), it is observed that, the expressions for strain rates are different for different adhesive models Visco-plastic strain rate ϵ_{vp} for two dimensional problems is expressed as

$$\epsilon_{vp} = \gamma\langle\Phi\rangle\hat{a} \tag{4 6}$$

where, γ, Φ and $\hat{a}$ are fluidity parameter, visco-plastic flow function and flow vector, respectively $\langle\Phi\rangle$ indicates for positive values of Φ Fluidity parameter is a material constant Different choices are recommended (Owen and Hinton, 1980 and Zienkiewicz and Taylor, 1991) for the function Φ and three most common representations are

$$\Phi = e^{M}\left(\frac{F-\sigma_0}{\sigma_0}\right)-1 \tag{4 7}$$

$$\Phi = \left(\frac{F-\sigma_0}{\sigma_0}\right)^{N}-1 \tag{4 8}$$

$$\Phi = \frac{F}{\sigma_0} \tag{4 9}$$

where, M and N are material constants and σ_0 is yield stress Flow rule F, is assumed as

$$F = \sqrt{\sigma_x^2+\sigma_y^2-\sigma_x\sigma_y+3\tau_{xy}^2} \tag{4 10}$$

Flow vector ($\hat{a}$) is given as

$$\hat{a} = \frac{\sqrt{3}}{2J_2'}\begin{Bmatrix}\sigma_x'\\ \sigma_y'\\ 2\tau_{xy}'\end{Bmatrix} \tag{4 11}$$

Deviatoric stress components are denoted by primes and these are obtained by

$$\sigma_{ij}' = \sigma_{ij}-\frac{\delta_{ij}\sigma_{kk}}{3} \tag{4 12}$$

J_2' represents the second invariant of deviatoric stresses and written as

$$J_2' = \frac{1}{2}(\sigma_x'\sigma_x' + \sigma_y'\sigma_y') + \tau_{xy}^2 \tag{4 13}$$

Visco-plastic constitutive relation

The visco-plastic stress-strain relation is written as

$$D_{vp} = \left[D^{-1} + C^n\right]^{-1} \tag{4 14}$$

D is the material matrix of linear elastic material and C^n is given as

$$C^n = \Theta \Delta t_n H^n \tag{4 15}$$

where, Θ is a constant, Δt_n is the incremental time of nth interval and H^n is given as

$$H^n = p_1 m_1 + p_2 m_2 \tag{4 16}$$

where, p_1, p_2, m_1 and m_2 are expressed as

$$p_1 = \gamma \left\langle \frac{\sqrt{3}}{2(J_2')^{1/2}} \Phi \right\rangle \tag{4 17}$$

$$p_2 = \gamma \left\langle \frac{3}{4(J_2')} \frac{d\Phi}{dF} - \frac{\sqrt{3}\Phi}{4(J_2')^{3/2}} \right\rangle \tag{4 18}$$

$$m_1 = \begin{bmatrix} 2/3 & -1/3 & 0 \\ -1/3 & 2/3 & 0 \\ 0 & 0 & 2 \end{bmatrix} \tag{4 19}$$

$$m_2 = \begin{bmatrix} \sigma'_x\sigma'_x & \sigma'_x\sigma'_y & 2\sigma'_x\tau_{xy} \\ \sigma'_x\sigma'_y & \sigma'_y\sigma'_y & 2\sigma'_y\tau_{xy} \\ 2\sigma'_x\tau_{xy} & 2\sigma'_y\tau_{xy} & 4\tau^2_{xy} \end{bmatrix} \tag{4 20}$$

4.2.1 Finite element technique

A computer code, similar to one developed by Owen and Hinton (1980), is written to predict the failure load, which is explained in the Figure 4 2 The module, which takes into account the non-linear visco-plastic behaviour of the material is indicated by the dashed portion in the flow chart Detail of the elastic and visco-plastic analyses are explained in the main algorithm of Chapter 2 and the following visco-plastic algorithm, respectively Visco-plastic algorithm is explained as follows

- *Non-linear (visco-plastic) algorithm*

step 01 at $t = t_n$ find the following

$$B^n = B_0 + B_{NL}(\delta^n)$$

$$C^n = C^n(\sigma^n, \Delta t_n)$$

$$D^n_{vp} = [D^{-1} + C^n]^{-1}$$

$$K^n_T = \int_\Omega [B^n]^T D^n_{vp} B^n d\Omega$$

$$\epsilon^n_{vp} = \gamma\langle\Phi\rangle\hat{a}^n$$

step 02 compute incremental displacements and stresses

(if $t = t_0$ *calc* $\Delta\psi^n_{vp} = \int_\Omega [B^n]^T D^n_{vp}\epsilon^n_{vp}\Delta t_n d\Omega + \Delta f^n$)

$$\Delta\delta^n = [K^n{}_T]^{-1}\Delta\psi^n_{vp}$$

$$\Delta\sigma^n = D_{vp}(B^n\Delta\delta^n - \epsilon^n_{vp}\Delta t^n)$$

step 03 update displacements and stresses

$$\delta^{n+1} = \delta^n + C_0\Delta\delta^n$$

$$\sigma^{n+1} = \sigma^n + \Delta\sigma^n$$

step 04 calculate visco-plastic strain

$$\epsilon^{n+1}_{vp} = \gamma\langle\Phi\rangle\hat{a}^{n+1}$$

step 05 calculate proportionality factor H

$$H = \frac{\sigma^{n+1} - \sigma^n}{\sigma_0 - \sigma^n}$$

step 06 compute residual stress to be compensated

$$\sigma_R = H\sigma^{n+1}$$

step 07 update stress

$$\sigma^{n+1} = (1 - H)\sigma^{n+1}$$

step 08 • apply equilibrium correction

$$\Delta\psi^{n+1}_{vp} = \int_\Omega [B^{n+1}]^T D^{n+1}_{vp}\epsilon^{n+1}_{vp}\Delta t_{n+1}d\Omega + \Delta f^{n+1} + \psi^{n+1}$$

where

$$\psi^{n+1} = \int_\Omega [B^{n+1}]^T\sigma^{n+1}_R d\Omega + f^{n+1}$$

where

f^{n+1} represents nodal forces

step 09 • check if visco-plastic strain rate is close to steady state value

$|\epsilon^{n+1}_{vp}| \leq \epsilon_{ss}$ i e tolerance

if steady state is reached go to step 07 of *main algorithm* in Section 2 2

else go to step 01

B^n, σ^n, D_{vp}, K^n, and ϵ^n_{vp} represent strain displacement matrix, stress tensor, visco-plastic stress-strain relation and stiffness matrix, respectively of n^{th} iteration

B^n, σ^n, C^n, D_{vp}, and K^n are functions of the displacement vector of n^{th} iteration One is supposed to update these values in every iteration But there is a possibility of divergence in the results by using the K^n values Using constant values of B^n and K^n and Newton Raphson's modified approximation (Owen and Hinton, 1980 and Zienkiewicz and Taylor, 1991) one can achieve convergence Further, this reduces substantially the computational time and memory However, ϵ_{vp}^n and D_{vp}^n are updated in each time step

If the effective stress $\bar{\sigma}$ of any element in the adhesive, exceeds the yield value of the material σ_0, then the material state becomes visco-plastic and visco-plastic analysis is carried out Visco-plastic module of elasto-visco-plastic analysis is indicated by dashed box of Figure 4 2

Visco-plastic calculations are repeated until the strain rate has reached a steady state value Then strain energy release rates are calculated and, as mentioned earlier in Chapter 2 The fracture criterion $G_I + G_{II} \geq G_{IC} + G_{IIC}$ is employed to predict the failure loads

The developed code is quite general, and could be used for visco-elastic, visco-plastic and elasto-visco-plastic models of adhesive materials One needs to incorporate the corresponding behaviour of the models for adhesives in the expression for strain rate

4.3 Validation of computer code

4.3 1 Perforated plate

In order to validate the developed computer code the two dimensional visco-plastic perforated plate problem considered by Zienkiewicz, *et al* (1974) is considered Schematic of this plate is shown in Figure 4 3 The physical dimensions and the material properties of the plate are listed in Table 4 1 The

stress level is plotted in Figure 4 4 against the time for an element P, which is in plastic range The result is in fairly good agreement with that by Zienkiewicz, et al (1974)

Further, to check the accuracy of the computer code developed, a single lap joint and a stepped lap joint are investigated Stress and strain distributions along the overlap lengths of these joints are compared with those available in open literature

4.3.2 Single lap joint

To check the accuracy of computer code of visco-plastic finite element analysis a single lap joint (Figure 4 5) is employed Details of the joint are listed in Table 4 2 Stresses, along the overlap length of single lap joint (Hiregoudar, 1993), are computed from elastic and visco-plastic analyses and these results are compared in Figure 4 6 The maximum difference in the computed peel stress along the overlap length of the single lap joint is less than 3 6 percent only While, this difference for shear stress is less than 11 4 percent Stresses predicted by the present visco-plastic analysis and visco-plastic analysis done by Hiregoudar (1993) are also compared in Figure 4 7 The difference in the computed peel stress along the overlap length of the single lap joint is of the order of 11 percent It is also observed that this difference is maximum near the edges and gradually reduces to a minimum towards the central part of the overlap Because of the proper refinement in the finite element mesh near the edges, stress distributions are expected to be more accurate

4.3.3 Stepped lap joint

Further, validation of the computer code of finite element developed is carried out on a stepped lap joint (Figure 4.8). Joint specifications are listed in Table 4.3. In Figures 4.9 the shear stress and shear strain distributions, in the adhesive along the overlap and near the interface of adherend and adhesive, are compared in Figure 4.9 with those of Su and Mackie (1993). The difference is found to be of the order of 11.7 percent. It is also observed that this difference is maximum near the edges and gradually reduces to a minimum towards the central part of the overlap length. Because of the more refined mesh near the edges as compared to Su and Mackie (1993), present results are expected to be accurate.

4.4 Parametric study

Effects of crack location, stacking sequence, critical strain energy release rate of adhesive material, overlap length and adhesive thickness on the strength of the double lap joint (Figure 4.10) are investigated. Because of symmetry only one half of the joint is considered for the analysis. The problem is treated as one of plane strain model and a finite element mesh consisting of 1816 CST elements is employed for the analysis.

Three non-dimensional parameters are defined viz.

$$\mathbf{g} = \frac{G_C'}{G_C} \tag{4.21}$$

$$\mathbf{l} = \frac{L_o}{L_t} \tag{4.22}$$

$$\mathbf{t} = \frac{t_s}{t_r} \tag{4 23}$$

where, G_C' and G_C are the fracture toughnesses of the adhesive used and the standard adhesive (epoxy), respectively L_o and L_t denote the overlap length and the total length of the bonded joint In addition t_s and t_r represent the thicknesses of adhesive and adherend, respectively G_C' is considered to be in multiples of G_C Assuming constant fracture toughness of the adhesive (G_C), adherend thickness t_r and overlap length L_o parametric study is carried out The adherends and adhesive of the joint, are considered to be carbon fibre reinforced plastics (CFRP) and Epon VIII (Table 4 4), respectively Critical crack location '3' is considered for further discussion in this Chapter

4.4.1 Stacking sequence

Symmetric quasi-isotropic combinations are considered to investigate the effect of stacking sequence on the bond strength Four fibre orientations are considered They are 0°, 45°, 90° and -45° Among all the possible symmetric combinations, it was observed in Chapter 2 (elastic analysis) that $[0°/45°/90°/-45°]_S$ has the maximum bond strength among its combinations Also the presence of 0°, ply in the immediate neighbourhood of the adhesive results in stronger joint Visco-plastic analysis is carried out for $[0°/0°/0°/0°]_S$, $[0°/45°/90°/-45°]_S$ and $[0°/0°/90°/90°]_S$ layups of CFRP adherends It is found that employing $[0°/0°/90°/90°]_S$ layup results in a stronger joint is obtained than $[0°/0°/0°/0°]_S$ layup This combination is found to be a stronger joint than $[0°/45°/90°/-45°]_S$ layup The failures loads are computed for various adhesive fracture toughnesses ratio **g** ($= G_C'/G_C$), overlap lengths **l** ($= L_o/L_t$) and adhesive thickness ratio **t** ($= t_s/t_r$) for these three layups Detail of these results are discussed in the respective sections

4 4.2 Fracture toughness of adhesive

For various g (= G_C'/G_C) values and layups the computed failure loads are listed in Table 4 5 It is observed that as g increases failure load increases for all the three layup sequences considered Adhesives with higher critical strain energy release rate (high g value) lead to a stronger joint Therefore, in order to achieve a higher fracture strength of the joint, adhesives with higher critical strain energy release rate are suggested Variation of failure load with crack length for various g values in $[0°/0°/0°/0°]_S$, $[0°/45°/90°/-45°]_S$ (optimal) and $[0°/0°/90°/90°]_S$ CFRP laminates are listed in Figures 4 11, 4 13 and 4 12, respectively

Though fracture toughness of adhesive is generally denoted by K_{IC}, the stress intensity factor for ideal plane strain adhesive material, in the present study, for convenience critical strain energy release rate G_C is also termed as fracture toughness

4.4.3 Overlap length

For various values of l (= L_o/L_t) and the three layups chosen the computed failure loads are listed in Table 4 6 It is observed that as l increases failure load increases for all the three layup sequences For higher fracture strength of the bond larger overlap length (high l) is suggested Variation of failure load with crack length for various l values in $[0°/45°/90°/-45°]_S$ (optimal) and $[0°/0°/90°/90°]_S$ CFRP laminates are shown in Figures 4 14, 4 16 and 4 15, respectively

4 4 4 Adhesive thickness

For various t (= t_a/t_r) values and layups the computed failure loads are listed in Table 4 7 It is observed that as t increases failure load decreases for the three layup sequences For higher fracture strength of the bond small thickness of the adhesive (low t) is suggested Variation of failure load with crack length for various t values in $[0°/45°/90°/-45°]_S$ (optimal) and $[0°/0°/90°/90°]_S$ CFRP laminates are listed in Figures 4 17, 4 19 and 4 18, respectively

4.5 Conclusions

On the basis of elasto-visco-plastic analysis carried out in this chapter, the following conclusions are drawn

- The elastic analysis predicts lower failure loads as compared to the elasto-visco-plastic analysis Therefore, for a realistic analysis elasto-visco-plastic behaviour is suggested to be considered
- Strain energy release rate is highly influenced by the adhesive properties such as fluidity parameter and flow rule
- Stress distributions, along the overlap length of the single lap joint, are predicted by the present elasto-visco-plastic analysis and the results are found to agree with the those reported by Hiregoudar (1993)
- Stress distributions along the overlap length and across the adhesive thickness of the stepped lap joint, are predicted by the elasto-visco-plastic and the results agree with the those reported for thick adherend shear test (TAST) specimen by Su and Mackie (1993)

- Strain energy release rate is sensitive to layup sequences in composite adherends A proper choice of layup sequence in the composite adherend results in an efficient bonded joint
- Use of adhesive of high fracture toughness and large overlap lengths results in stronger bonded joint, whereas, employment of small thickness of adhesive results in stronger bonded joint

Table 4 1 Specifications of the perforated plate problem (Zienkiewicz, et al , 1974)

Perforated plate

dimension of plate	36 mm X 20 mm
diameter of the circular cut out	10 mm
Young's modulus (E)	70 Gpa
Poisson's ration (ν)	0 2
stress applied (σ)	95 MPa
yield stress (σ_o)	243 Mpa
fluidity parameter (γ)	0 01 Sec^{-1}

Table 4.2 Specifications of single lap joint (Hiregoudar, 1993)

Single lap joint

overlap length (L_o)	16 mm
total length (L_t)	80 mm
applied stress (σ)	200 MPa
adhesive thickness (t_s)	0.30 mm
adherend thickness (t_r)	1.60 mm

Adhesive (FM 73)

Young's modulus (E_s)	2.21 Gpa
Poisson's ratio (ν_s)	0.43
yield stress (σ_o)	40 Mpa
fluidity parameter (γ)	$4.495\ 10^{-3}\ Sec^{-1}$
constant N	1.426
constant λ	1.4
flow function (Φ)	$\left[\frac{F - F_o}{F_o}\right]^N$

Adherend (Steel)

Young's modulus (E_r)	211.3 GPa
Poisson's ratio (ν_r)	0.33
yield stress (σ_o)	∞

Table 4 3. Specifications of stepped lap joint (thick adherend shear test specimen) of Su and Mackie (1993)

Joint configuration	
overlap length (L_o)	8 mm
total length (L_t)	125 mm
applied load (P)	3 5 kN
total joint thickness (t)	13 35 mm
width of the joint (W)	25 4 mm
Adhesive (rubber-toughened epoxy)	
Young's modulus (E_a)	6 60 Gpa
Poisson's ratio (ν_a)	0 38
thickness of adhesive (t_a)	0 65 mm
Adherend (Steel)	
Young's modulus (E_r)	210 Gpa
Poisson's ratio (ν_r)	0 3
thickness of adherend (t_r)	6 35 mm

Table 4 4 Specifications of double lap joint

Double lap joint	
overlap length (L_o)	40 mm
total length (L_t)	80 mm
Adherend (carbon fibre reinforced plastic)	
longitudinal modulus (E_l)	137 GPa
transverse modulus (E_t)	7 GPa
shear modulus G_{lt}	4 5 GPa
Poisson's ratio (ν_{lt})	0 3
adherend thickness (t_r)	10 mm
Adhesive (Epon VIII)	
Young's modulus (E_s)	3 5 GPa
Poisson's ratio (ν_s)	0 41
thickness (t_s)	2 mm
fracture toughness (G_C)	0 36 kJ/m^2

fracture criterion $G_I + G_{II} \geq G_C$

Table 4 5 Computed failure loads (P_f's) for various g (= G_C'/G_C) values and different laminae combinations

		Failure loads in N/mm for L_o/L_t = 0 50 & t_s/t_r = 0 20		
G_C'/G_C	a_{cr} (mm)	$[0/0°/0°/0°]_S$	$[0°/0°/90°/90°]_S$	$[0°/45°/90°/-45°]_S$
0 1	0 164	5 760	5 984	5 696
0 2	0 164	8 096	8 416	8 032
0 3	0 164	9 920	10 304	9 856
0 4	0 164	11 520	11 904	11 392
0 5	0 164	12 800	13 312	12 672
0 6	0 164	14 080	14 592	14 016
0 7	0 164	15 232	15 872	15 168
0 8	0 164	16 384	17 024	25 472
0 9	0 164	17 472	18 304	16 192
1 0	0 164	18 560	19 456	17 408
1 1	0 164	19 840	20 736	18 944
1 2	0 164	20 992	22 016	20 096
1 3	0 164	22 400	23 296	21 632
1 4	0 164	23 552	24 576	23 040
1 5	0.164	24 704	25 984	24 320

Table 4.6: Computed failure loads (P_f's) for various l (= L_o/L_t) values and different laminae combinations

		Failure loads in N/mm for G_C'/G_C = 0 40 & t_s/t_r = 0 20		
L_o/L_t	a_{cr} (mm)	$[0°/0°/0°/0°]_S$	$[0°/0°/90°/90°]_S$	$[0°/45°/90°/-45°]_S$
0 307	0 050	4 463	–	–
0 333	0 054	4 752	4 607	4 271
0 363	0 059	5 112	4 968	4 607
0 400	0 065	5 472	5 448	5 040
0 444	0 073	5 832	5 880	5 520
0 500	0 164	11 616	12 048	11 472

– plastic flow

Table 4 7. Computed failure loads (P_f's) for various t (= t_s/t_r) values and different laminae combinations

		Failure loads in N/mm for G_C'/G_C = 0 40 & L_o/L_t = 0 50		
t_s/t_r	a_{cr} (mm)	$[0°/0°/0°/0°]_S$	$[0°/0°/90°/90°]_S$	$[0°/45°/90°/-45°]_S$
0 012	0 164	16 384	17 792	16 128
0 025	0 164	15 488	16 000	14 848
0 033	0 164	15 040	15 296	14 528
0 050	0 164	14 336	14 592	13 696
0 100	0 164	13 056	13 440	12 672
0 200	0 164	11 616	12 048	11 472

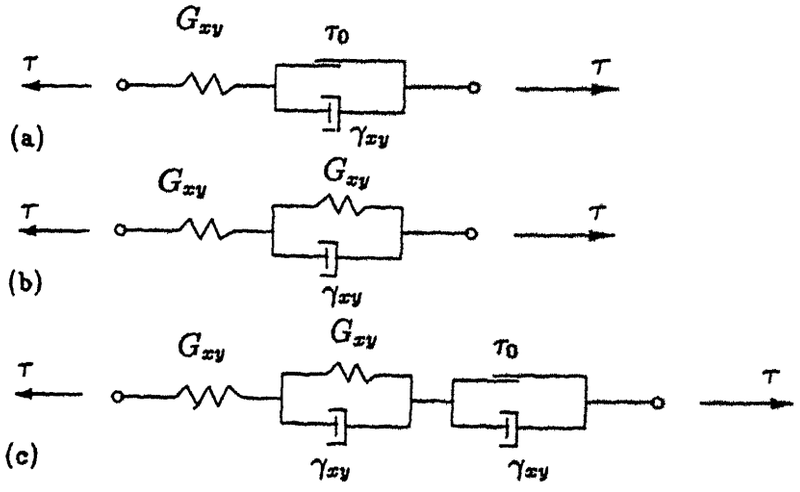

Figure 4 1 Adhesive material models (a) the three parameter solid model, (b) the Bingham visco-plastic model, and (c) the five parameter viscoelastic-viscoplastic model

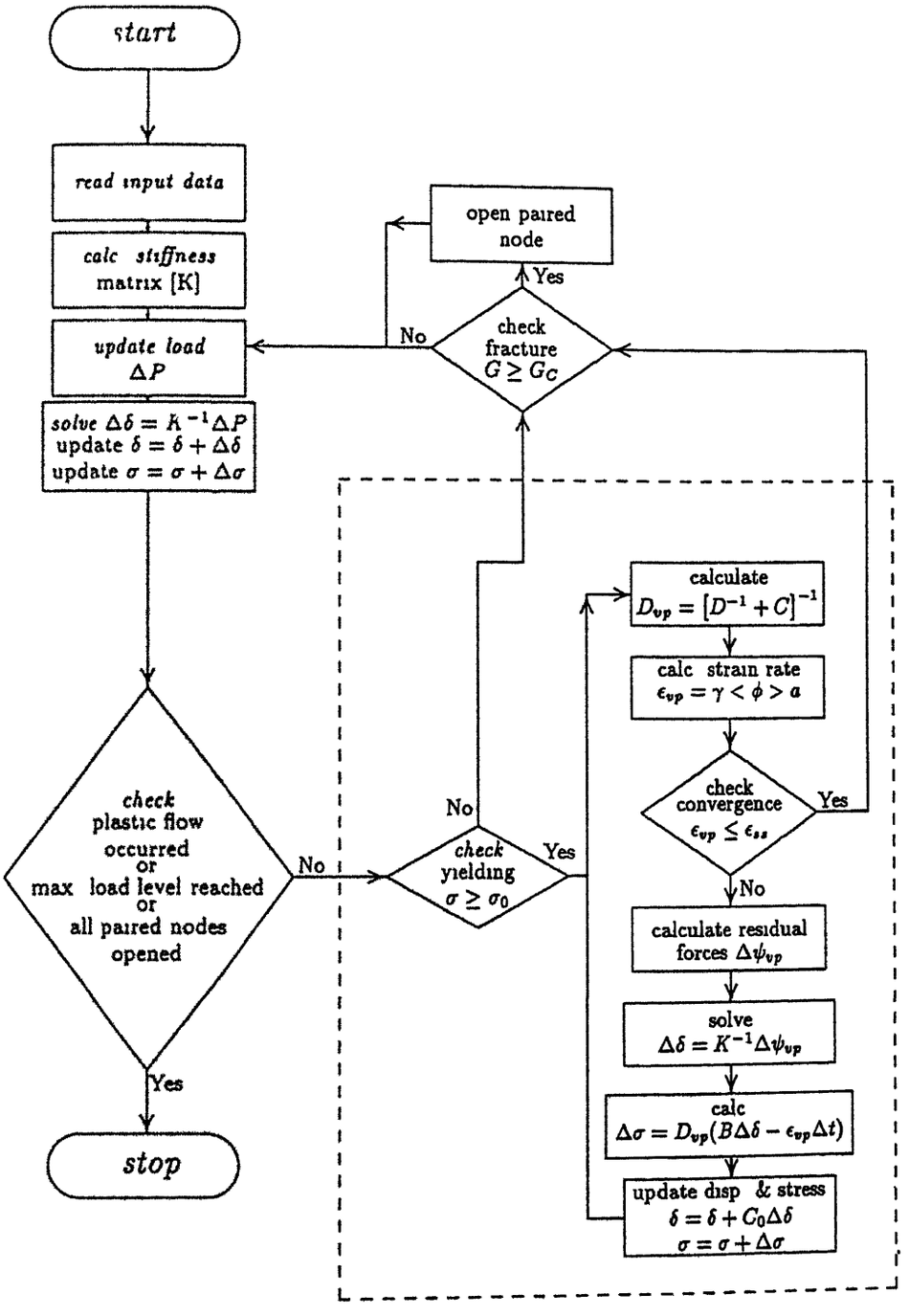

Figure 4 2: Flow chart of visco-plastic finite element analysis

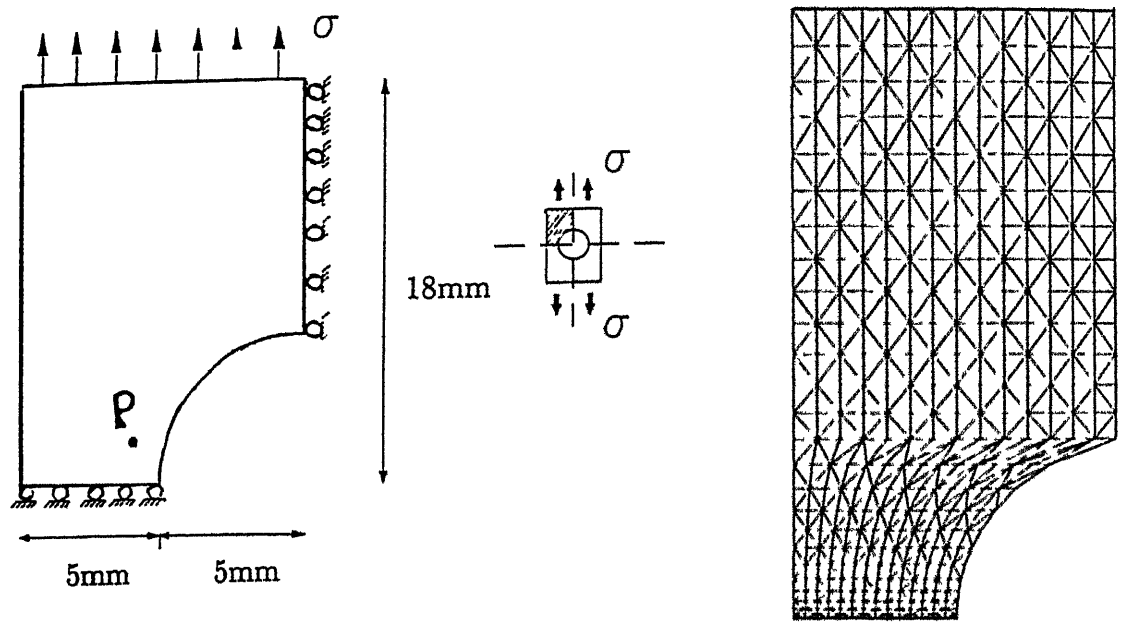

Figure 4.3 Schematic of perforated plate under uniform tension (Zienkiewicz, et al , 1974) showing the plastic element $\mathcal{P}$ and the finite element mesh of the plate

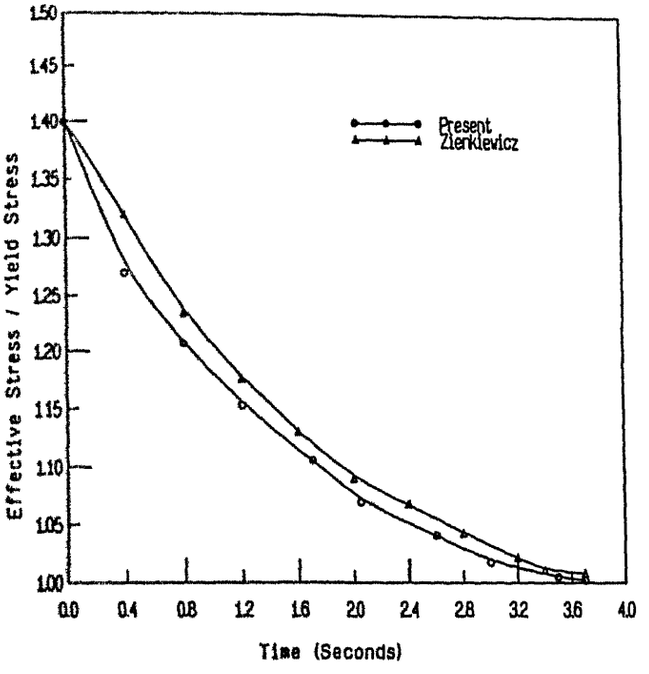

Figure 4 4 Variation of stress with time for plastic element $\mathcal{P}$ of the perforated plate (Figure 4 3)

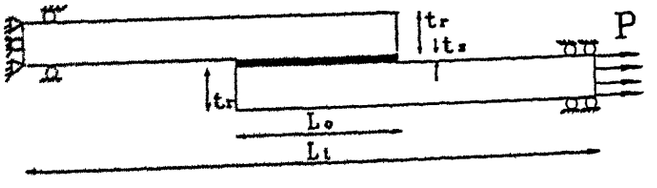

Figure 4 5. Schematic of single lap joint considered by Hiregoudar (1993)

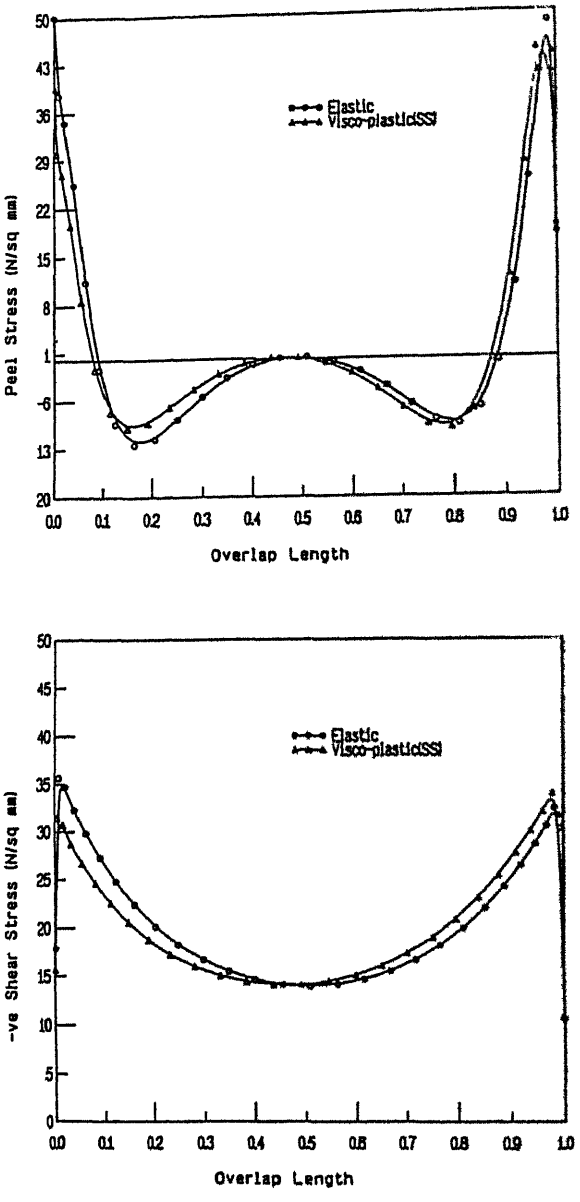

Figure 4 6 Comparison of elastic and visco-plastic stress distribution along the overlap length of single lap joint (Hiregoudar, 1993)

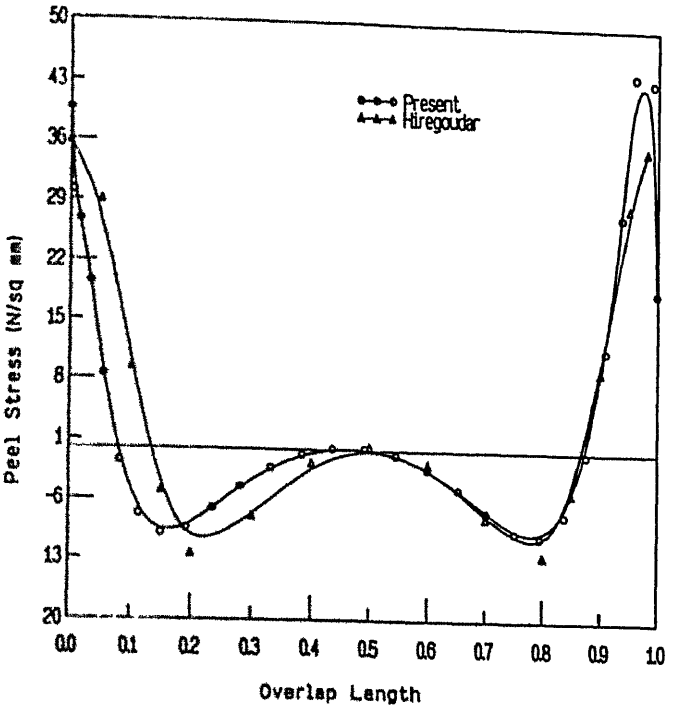

Figure 4.7: Comparison of peel stress distribution along the overlap length of single lap joint (Hiregoudar, 1993)

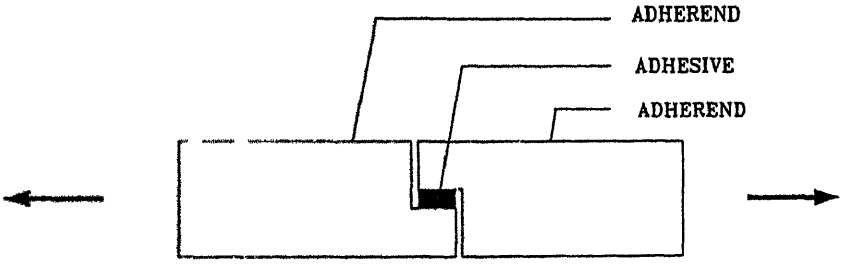

Figure 4.8: Schematic of the stepped lap joint (thick adherend shear test TAST specimen considered by Su and Mackie, 1993)

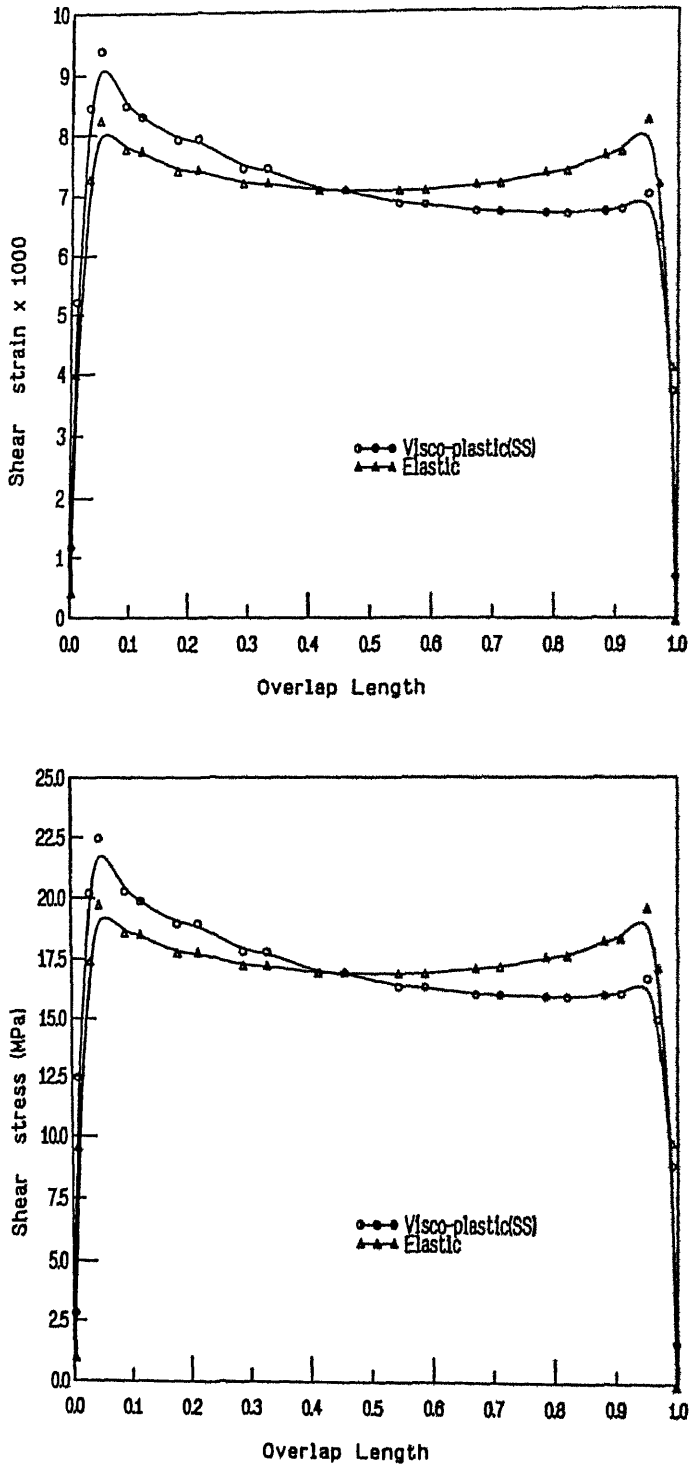

Figure 4 9 Comparison of shear stress and strain distribution along the overlap length at interface of adherend and adhesive of the stepped lap joint

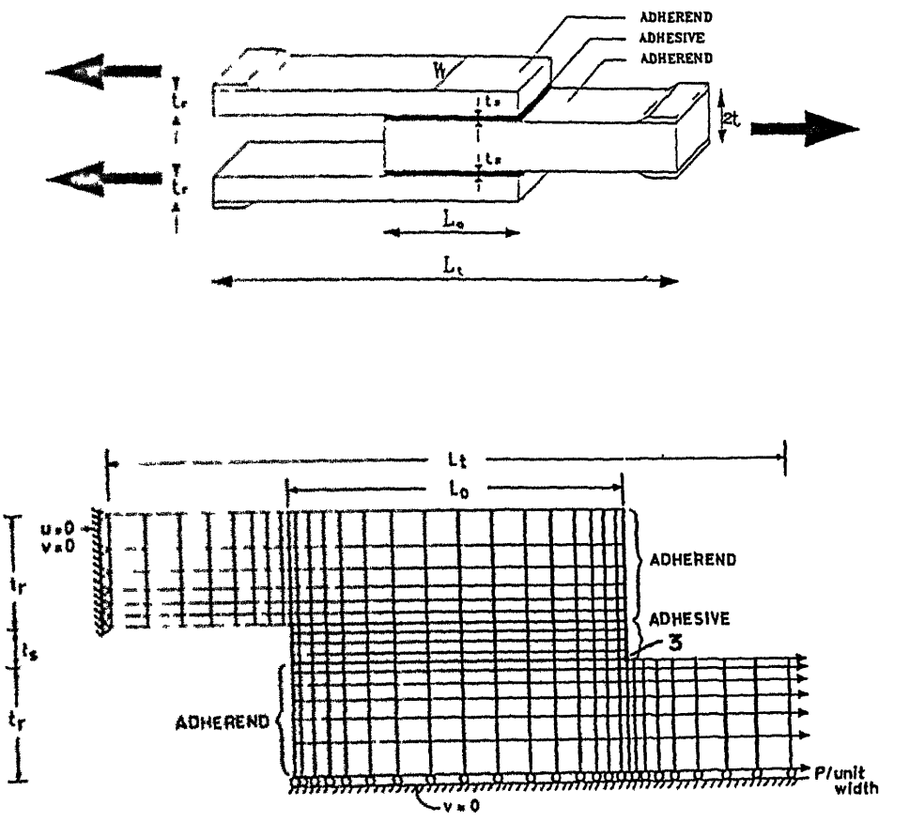

Figure 4 10. Schematic of adhesively bonded double lap joint and the finite element mesh showing the crack location '3'

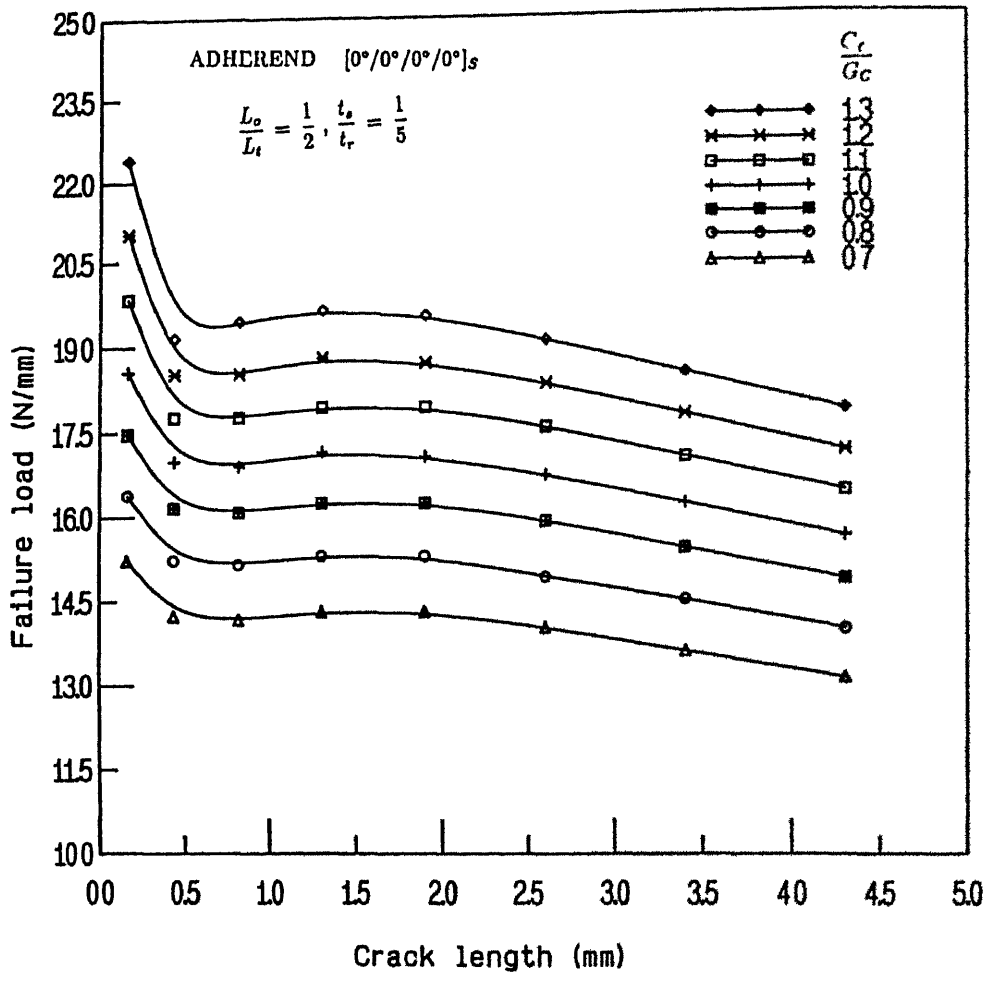

Figure 4.11 Variation of failure load with crack length for crack initiation at location '3' and different g (= G_C'/G_C) values in $[0°/0°/0°/0°]_S$ CFRP laminates

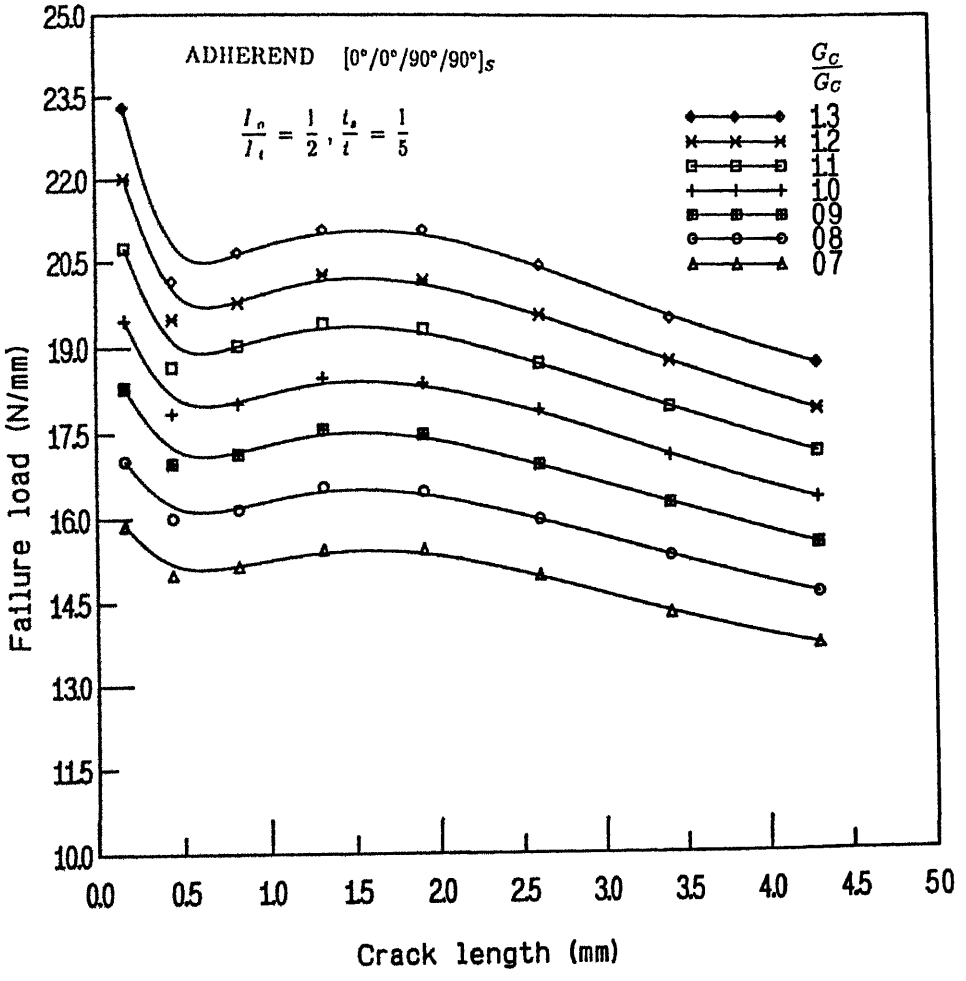

Figure 4.12 Variation of failure load with crack length for crack initiation at location '3' and different g (= G_C'/G_C) values in $[0°/0°/90°/90°]_S$ CFRP laminates

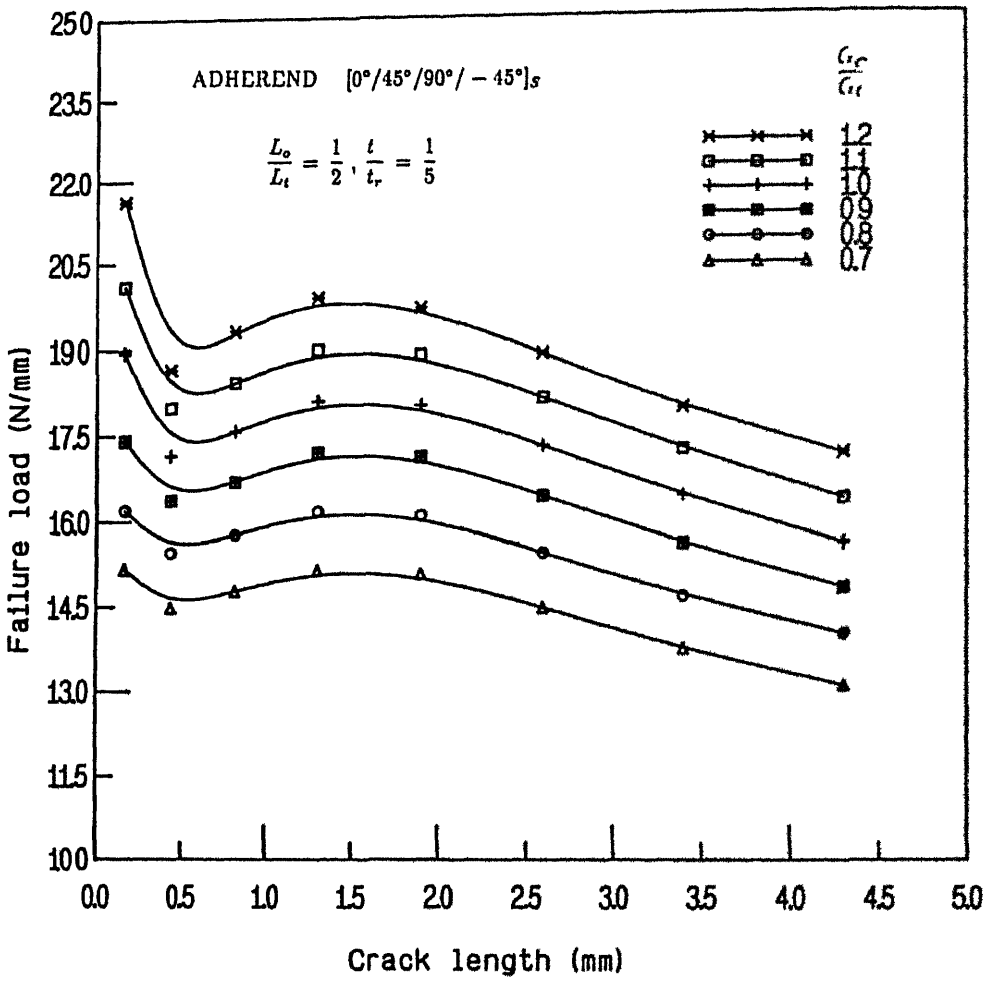

Figure 4.13 Variation of failure load with crack length for crack initiation at location '3' and different g (= G_C'/G_C) values in $[0°/45°/90°/-45°]_S$ (optimal) CFRP laminates

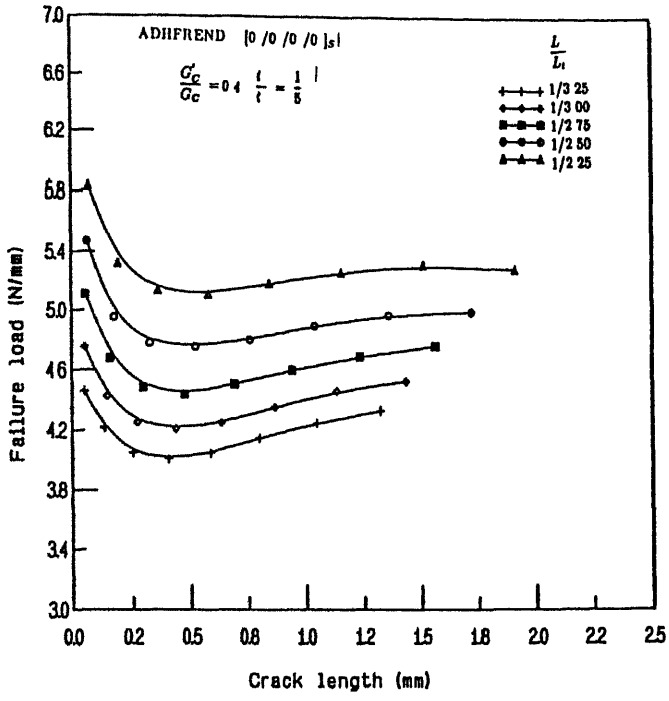

Figure 4 14 Variation of failure load with crack length for crack initiation at location '3' and different l (= L_o/L_t) values in $[0°/0°/0°/0°]_S$ CFRP laminates

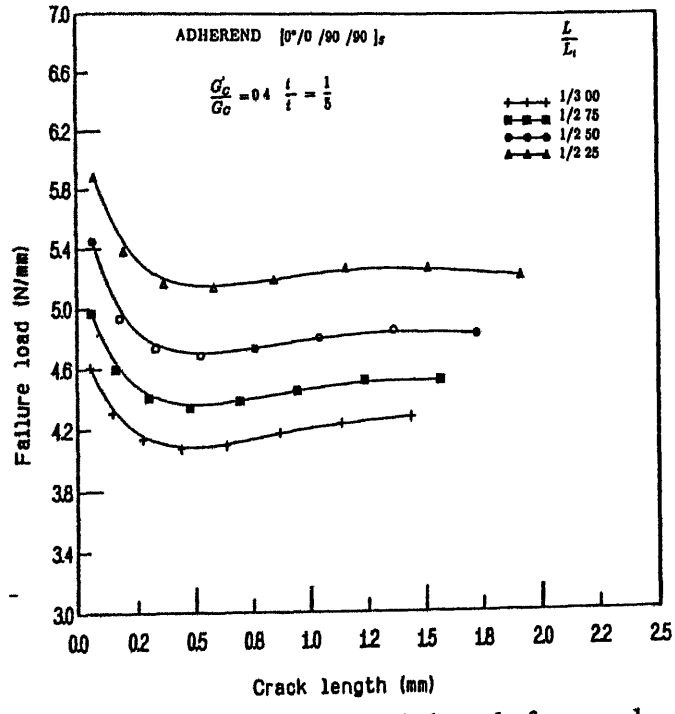

Figure 4 15. Variation of failure load with crack length for crack initiation at location '3' and different l (= L_o/L_t) values in $[0°/0°/90°/90°]_S$ CFRP laminates

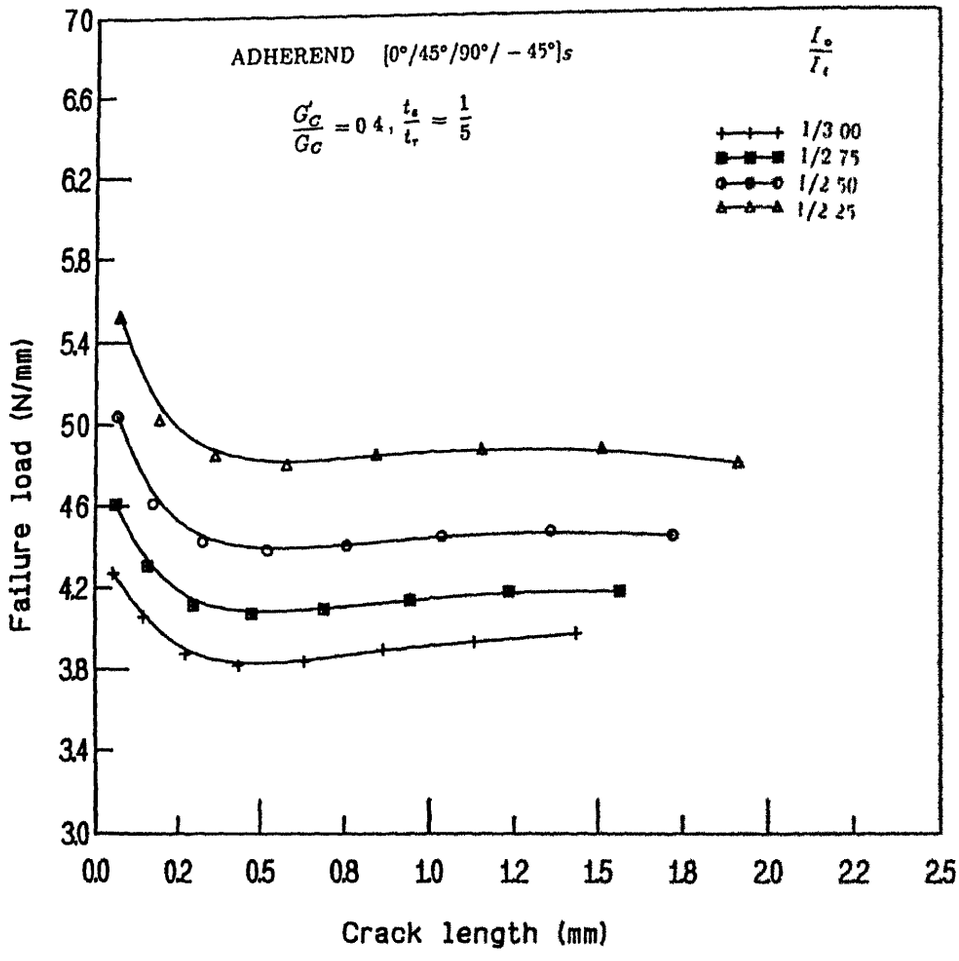

Figure 4.16 Variation of failure load with crack length for crack initiation at location '3' and different l (= L_o/L_t) values in $[0°/45°/90°/-45°]_S$ (optimal) CFRP laminates

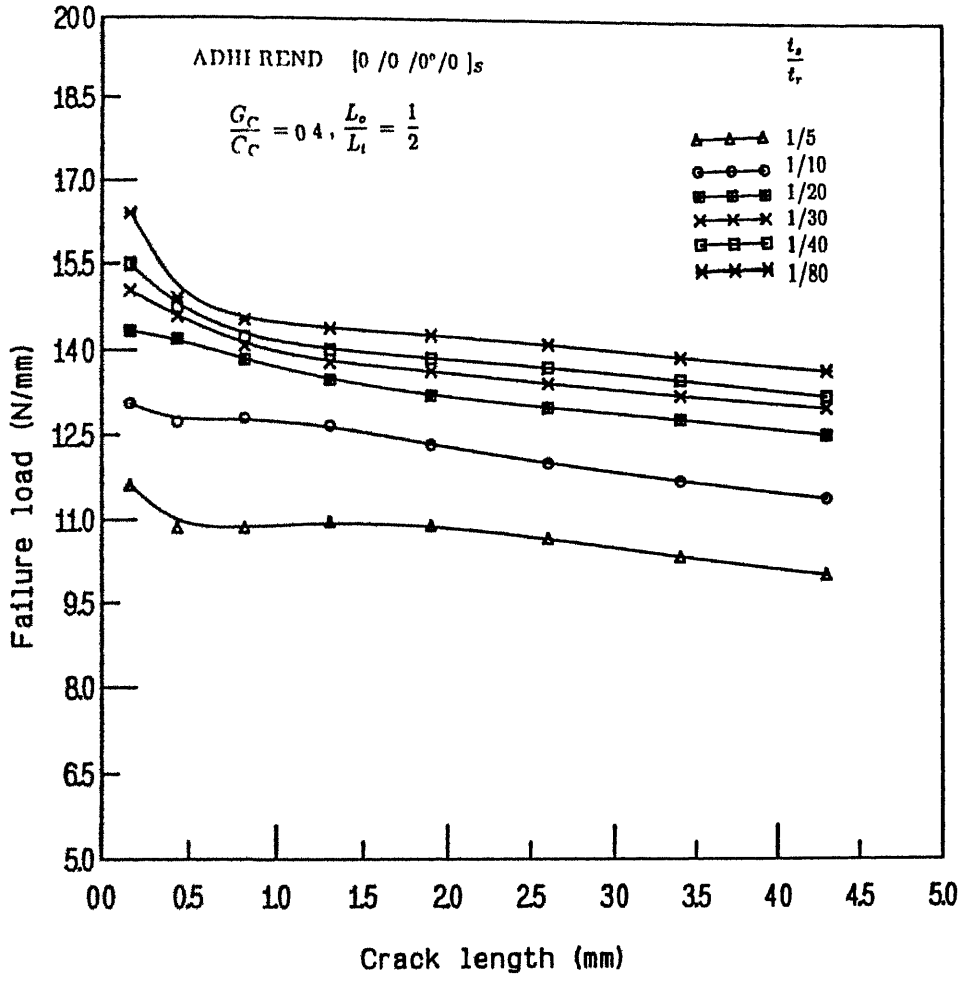

Figure 4.17. Variation of failure load with crack length for crack initiation at location '3' and different t ($= t_s/t_r$) values in $[0°/0°/0°/0°]_S$ CFRP laminates

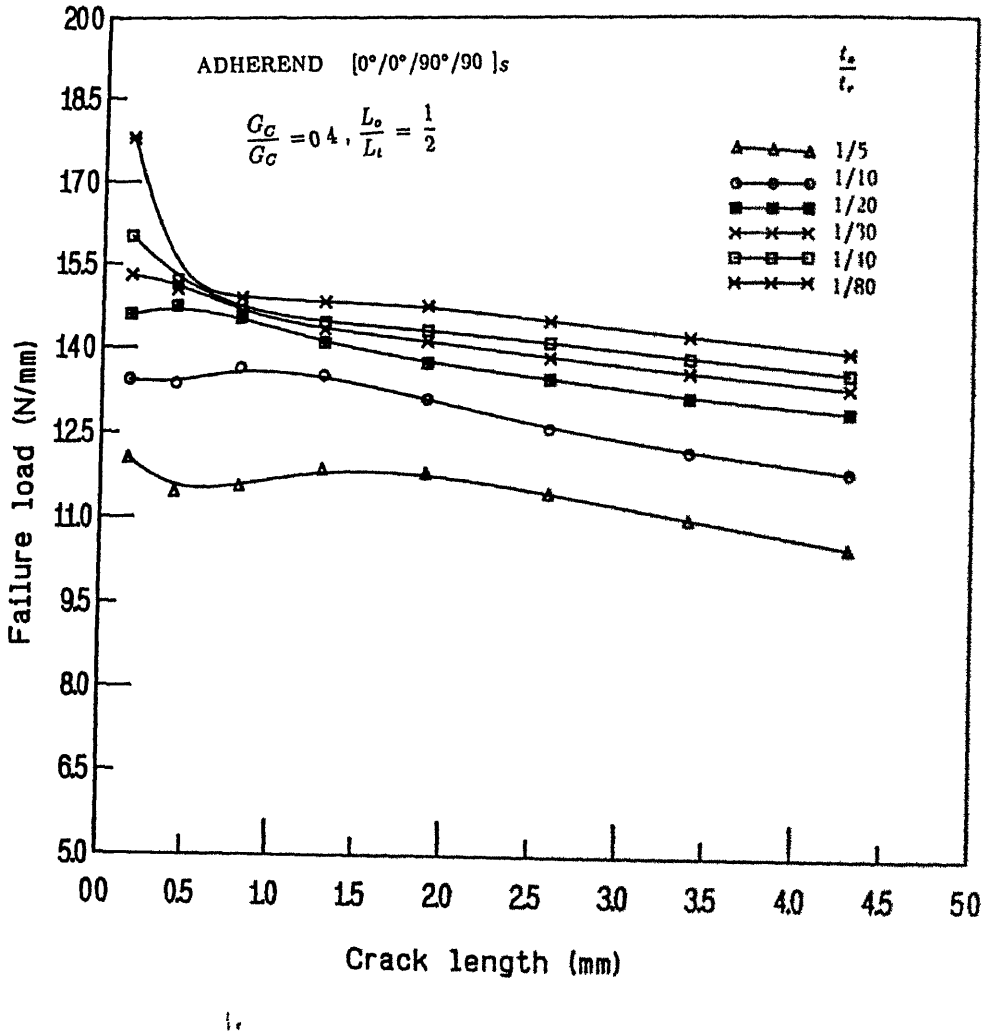

Figure 4.18 Variation of failure load with crack length for crack initiation at location '3' and different t (= t_s/t_r) values in $[0°/0°/90°/90°]_S$ CFRP laminates

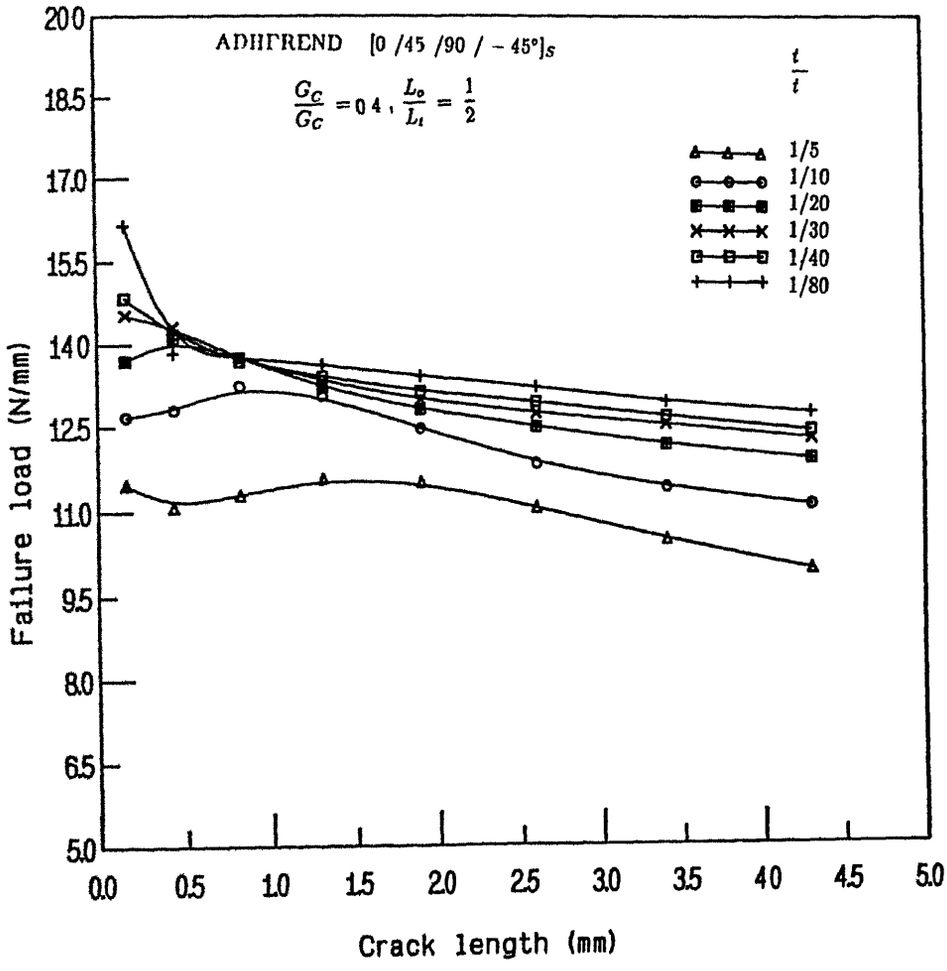

Figure 4.19: Variation of failure load with crack length for crack initiation at location '3' and different t (= t_s/t_r) values in $[0°/45°/90°/-45°]_S$ (optimal) CFRP laminates

Chapter 5

Experiments

5.1 Introduction

The fracture criteria employed in structural analyses are based on pure modes I and II and various combinations of them Davies, et al (1992) discussed interlaminar fracture testing of carbon fibre reinforced epoxy and PEEK composites They found large amount of scatter in the results of strain energy release rates in modes I and II, respectively Therefore, these fracture parameters are required to be determined experimentally Also, accuracy in the testing would reflect in the estimation of the strength of a bonded joint

In this Chapter experimental determination of critical strain energy release rates in modes I and II, and the necessary theory is explained Also, the strengths of the double lap bonded joints are determined experimentally and compared with those obtained from the finite element analysis considering various fracture criteria With the limited observations, the most critical fracture criterion is suggested

5.2 Strain energy release rate in mode I

The energy approach discussed by Carlsson and Pipes (1987) is based on a thermodynamic criterion for fracture by considering the energy available for crack growth of the system, and the surface energy required to extend an existing crack Energy balance of a cracked body can be represented as

$$\bar{H} = \bar{U} - \bar{W} \tag{5 1}$$

where $\bar{H}$, $\bar{U}$ and $\bar{W}$ represents the potential energy, the elastic strain energy stored in the body and the work done by the movement of external forces, respectively The strain energy release rate in defined as

$$G_I = -\frac{\partial \bar{H}}{\partial A} \tag{5 2}$$

where, ∂A is the newly created cracked area Figure 5 1 shows a typical load versus displacement response for a cracked body Assuming that crack growth is under constant load (fixed load) P and the vertical displacement is v

- *For contant load*

$$\partial \bar{W} = P \Delta v \tag{5 3}$$

$$\partial \bar{U} = \text{area } ADE - \text{area } ABC \tag{5 4}$$

$$= \frac{1}{2}P(v + \Delta v) - \frac{1}{2}Pv \tag{5 5}$$

$$= \frac{1}{2}P\Delta v \tag{5 6}$$

$$\partial\bar{H} = -\frac{1}{2}P\Delta v \tag{5 7}$$

For linear elastic body, the reactions between the load and displacement may be expressed as

$$v = CP \tag{5 8}$$

where, C is the compliance of the specimen Using Equations (5 7) and (5 8) in Equation (5 2), the strain energy release rate under constant load is written as

$$G_I = \frac{P^2}{2}\frac{\partial C}{\partial A} \tag{5 9}$$

▮ *For contant displacement*

Similarly, for crack groth under constant displacement condition (fixed grip) work done $\bar{W}$ vanishes and

$$\partial\bar{U} = \text{area } AFC - \text{area } ABC \tag{5 10}$$

$$= \frac{1}{2}(P - \Delta P)v - \frac{1}{2}Pv \tag{5 11}$$

$$= -\frac{1}{2}v\Delta P \tag{5 12}$$

and

$$G_I = \frac{1}{2}v\frac{\partial P}{\partial A} \tag{5 13}$$

Substituting Equation (5 8) in Equations (5 9) and (5 13), respectively one can obtain

$$G_I = \frac{v^2}{2C^2}\frac{\partial C}{\partial A} \tag{5 14}$$

$$G_I = \frac{P^2}{2}\frac{\partial C}{\partial A} \tag{5 15}$$

From Equations (5 9) and (5 15), crack growths under constant load and constant displacement yields the same expression for mode I strain energy release rate Therefore, depending on the convenience one can conduct the experiment either under constant load or constant displacement Several methods have been adapted to experimentally determine the mode I critical strain energy release rate These include

- Compliance method using DCB specimen
- area method

- modified area method
- method using theoretical formulae
- method using non-linear beam theory

Compliance method using DCB specimen is widely used in the case of metals and also in composites because of the following features

- crack growth is stable under constant displacement loading (fixed grip)
- error introduced in analysing data is small
- each DCB specimen will provide a G_{IC} value

Wilkins, et al (1982) discussed the characterisation of delamination growth in graphite epoxy Further, description on various factors that might affect the load displacement response of slender DCB specimen under mode I testing of compliance method is given by Keary, et al (1985) Following precautions are to be taken while conducting the experiment

- the crack remains in a plane
- crack-tip plane is perpendicular to the length of the DCB specimen
- crack plane is perpendicular to the load line
- the cantilevers of the specimens are thin plates and the contribution of shear stress developed due to bending moment is negligible in comparison to bending loads
- large deflections in beam bending, which could generate geometrical non-linearity is avoided

From elastic beam theory the displacement can be written as

$$v = \frac{2Pa^3}{3EI} \tag{5 16}$$

where, E, I and a represent the Young's modulus, moment of inertia of cross section and the crack length of the cantilever, respectively Using the compliance as expressed in Equation (5 8) and substituting for v as expressed in Equation (5 16)

$$C = \frac{v}{P} \tag{5 17}$$

$$C = \frac{2a^3}{3EI} \tag{5 18}$$

$$C = A_1 a^3 \tag{5 19}$$

$$A_1 = \frac{2}{3EI} \tag{5 20}$$

A_1 is a constant for a given specimen Also, the above equation could be rewritten in logarithm form as

$$ln\, C = ln\, A_1 + 3\, ln\, a \tag{5 21}$$

$$G_I = \frac{P^2}{2}\frac{\partial C}{\partial A} \tag{5 22}$$

$$= \frac{P^2}{2W}\frac{\partial C}{\partial a} \tag{5 23}$$

$$= \frac{P^2 a^2}{EIW} \tag{5 24}$$

where, W represents the width of the DCB specimen Since, critical load P_C corresponds to critical strain energy release rate G_{IC}, above equation is rewritten as

$$G_{IC} = \frac{P_C^2 a^2}{EIW} \tag{5 25}$$

$$P_C = \sqrt{G_{IC} EIW}\, a^{-1} \tag{5 26}$$

$$P_C = A_2 a^{-1} \tag{5 27}$$

$$A_2 = \sqrt{G_{IC} EIW} \tag{5 28}$$

A_2 is a constant for a given specimen Also Equation (5 27) could be rewritten in logarithm form as

$$ln\, P_C = ln\, A_2 - ln\, a \tag{5 29}$$

Eliminating EI from Equations (5 20) and (5 28), the critical strain energy release rate in mode I G_{IC} is expressed as

$$G_{IC} = \frac{3A_1A_2^2}{2W} \tag{5 30}$$

The unidirectional composite laminates are prepared by hand layup technique on flat steel plates with carbon fibre (G-808) with a warp to weft ratio of 91 9 and area density 220 gm/m^2 (manufacturer Brochier SA, France) and the resin Resin is prepared by mixing Araldite LY 556 and Hardener HY 951 (manufacturer Ciba-Geigy Ltd, India) with a weight ratio 10 1 These composite laminates are cut to 30 mm width strips Each pair of strip is glued with epoxy resin with bi-axially oriented polypropylene (BOPP) filler of thickness 20 μm is embedded at one end This BOPP membrane provides opening space to attach the fixture with hinge facilities for mode I loading condition and a sharp through width crack After curing BOPP strip is removed, holes are made and the fixture is fitted with screws To measure the crack length at each load increment, on the thickness sides thin strips of graph paper are glued Specimen is loaded in mode I loading as shown in Figure 5 2 Experiment is carried out in displacement control condition (fixed grip) with a cross head speed of 1 mm per minute Initially it was loaded till the crack just begins to grow and unloaded till the load level comes down to zero value Loading and unloading cycles were repeated for 5 to 8 times till the crack grows to half of the length of the specimen At the end of each loading cycle, the crack sizes were noted from either sides of the DCB specimen with the help of a magnifying lens and a torch Average value of these crack lengths were considered for the calculation of G_{IC}

Load versus displacement curves for all 8 specimens are obtained A typical load versus displacement curves for loading and unloading cycles is shown in

Figure 5 3 For crack length corresponding compliance C are calculated from loading cycle of the graph and the corresponding critical loads P_C are noted From Equation (5 30) it is clear that knowing A_1 and A_2 one can find G_{IC} for a DCB specimen The values of A_1 and A_2 can be found out graphically from the logarithm plots of P_C vs a and C vs a, respectively Also, these values could be determined by linear regression of data, which is given as

$$ln\, A_1 = \frac{1}{n}\sum_{i=1}^{n}\{ln\, C_i + 3\, ln\, a_i\} \tag{5 31}$$

$$ln\, A_2 = \frac{1}{n}\sum_{i=1}^{n}\{ln\, P_{C_i} - ln\, a_i\} \tag{5 32}$$

where, n represents the number of load cycles Thus, using the above linear regression method, critical strain energy release rate for mode I (G_{IC}) is calculated for the SEN specimens and listed in Table 5 1 The average value of G_{IC} ($0\,446\,kJ/m^2$) is considered to predict the strength of bonded joints

These G_{IC} values are not close a single value The reasons could be non-uniform thicknesses of the adherends and adhesives, defects in adherend and adhesive, uneven surface preparation, improper gluing etc

5.3 Strain energy release rate in mode II

For the determination of critical strain energy release rate in mode II loading, standard experimental procedure using ENF specimen and the necessary theory

is explained by Carlsson, et al (1986) In the present work, an ENF specimen is employed for the experimental determination of critical strain energy release rate in mode II condition This is a three point bending flexure specimen (Figure 5 4) with an embedded through width crack at the interface of two laminates The specimen has been found to produce shear loading at the crack-tip without much friction between the surfaces (fretting) From the beam theory an expression for the strain energy release rate in mode II is explained by Carlsson, et al (1986) The expression is written as

$$G_{IIC} = \frac{9P^2Ca^2}{2W(2L^3 + 3a^3)} \tag{5 33}$$

where, C, P, a, W, and L represents the the compliance, the applied load, the crack length, the width and the semi-span length of the specimen, respectively (Figure 5 4) This expression does not include the action of shear surfaces and the surface of friction between crack surfaces (fretting) They also derived the condition for stable crack growth, which is expressed as

$$a \geq 0\,7L \tag{5 34}$$

But usually the crack length a is of the order of $\simeq 0\,5L$ leading to unstable crack growth A load displacement curve is obtained for each specimen The specimen under three point bending is shown in Figure 5 4 A cross head speed of 1 mm per minute was maintained during the loading Seven such specimens were tested and the critical strain energy release rates for mode II are determined and listed on Table 5 2 The average of these values ($0\,664\,kJ/m^2$) is considered for the prediction of the joint strength

5.4 Strength of adhesively bonded joints

Composite laminates are prepared as mentioned earlier These are cut to 30 mm, 20 mm and 15 mm width strips With proper surface preparation end tabs are glued Further surfaces are prepared to make the double lap joints (Figure 5 5) After curing tensile strength of these bonded joints are determined experimentally and compared with those obtained from the elastic finite element analysis with various fracture criteria Details of the failure criteria are listed in Chapter 2 Also a comparison of failure load vs crack length curves based on these failure criteria for the same specimen are illustrated

The physical dimensions of the double lap bonded joints are listed in Table 5 3 Failure loads (P_f) of these joints from testing and finite element analysis with various fracture criteria are presented in Table 5 4 In some joints failure occurred at the interface (adhesive), while in some it occurred in the adherend and for others the failure was a combination of both interface (adhesive) failure and adherend failure Types of failure occurred in the specimens are given in the Table 5 4

5.5 Conclusions

On the basis of experimental study and comparison of results of finite element analysis following conclusions are drawn

- It is observed that the experimental results are close to those results based on following fracture criterion

$$G_I + G_{II} \geq G_{IC} + G_{IIC} \tag{5 35}$$

where G_{Ic} and G_{IIc} are critical strain energy release rates in modes I and II, respectively

- The difference in critical strain energy release rate results, might be due to non-uniform thickness of the composite adherends and adhesive during specimen (joint) preparation

Table 5 1 Experimental results for mode I critical strain energy release rate G_{Ic}

Specimen No	fracture toughness (kJ/m^2)	average value (kJ/m^2)
1	0 726	
2	0 638	
3	0 642	
4	0 148	0 446
5	0 246	
6	0 529	
7	0 233	
8	0 411	

Table 5 2 Experimental results for mode II critical strain energy release rate G_{IIc}

Specimen No	fracture toughness (kJ/m^2)	average value (kJ/m^2)
1	0 623	
2	0 778	
3	0 666	0 664
4	0 722	
5	0 587	
6	0 736	
7	0 536	

Table 5 3 Various dimensions of double lap joint specimens (Figure 5 5)

Specimen Number	L_o (mm)	L_t (mm)	Width (mm)	t_r(Lower) (mm)	t_s (mm)	t_r(Upper) (mm)
1	103	353	19 13	1 66	0 09	2 35
2	121	339	17 62	1 26	0 10	1 75
3	102	353	17 65	1 12	0 10	1 80
4	134	325	17 96	1 19	0 09	1 73
5	121	341	17 66	1 66	0 10	1 91
6	102	217	29 5	1 72	0 10	1 66
7	101	215	29 0	1 67	0 09	1 80
8	101	216	29 0	1 63	0 10	1 76
9	98	216	28 5	1 83	0 10	1 82
10	101	217	29 0	1 85	0 09	1 82
11	97	220	28 5	1 64	0 10	1 79
12	98	220	29 0	1 67	0 09	1 68
13	98	220	29 0	1 66	0 10	1 66
14	102	220	28 5	1 71	0 10	1 69
15	90	295	18 9	1 35	0 10	2 44
16	89	296	19 1	1 33	0 10	2 53
17	100	332	13 8	1 68	0 10	1 75
18	98	336	13 6	1 70	0 10	1 65

Table 5 4 Comparison of experimental and finite element technique (elastic analysis) results for various fracture criteria

	experiment	finite element analysis					
		failure loads (P_f's)					
			criterion type 1	criterion type 4	criterion type 5	criterion type 6	criterion type 7
specimen number	failure type	(10^5N)	(10^5N)	(10^5N)	(10^5N)	(10^5N)	(10^5N)
1	adhesive	0 1569	0 1250	0 0791	0 0978	0 0875	0 1043
2	both	0 1550	0 1482	0 0939	0 1143	0 1025	0 1208
3	both	0 1467	0 1503	0 0958	0 1153	0 1050	0 1237
4	adhesive	0 1434	0 1506	0 0958	0 0895	0 1066	0 1249
5	adhesive	0 1359	0 1355	0 0856	0 1040	0 0927	0 1084
6	both	0 1538	0 1382	0 0881	0 1089	0 0968	0 1131
7	both	0 1397	0 1370	0 0868	0 1069	0 0939	0 1111
8	both	0 1571	0 1383	0 0880	0 1074	0 0952	0 1123
9	both	0 1675	0 1232	0 0784	0 9564	0 8483	0 0999
10	both	0 1561	0 1215	0 0773	0 0943	0 0836	0 0985
11	both	0 1369	0 1369	0 0874	0 1063	0 0942	0 1111
12	adherend	0 1336	0 1400	0 0887	0 1073	0 0955	0 1124
13	adherend	0 1402	0 1408	0 0893	0 1080	0 0961	0 1131
14	both	0 1351	0 1390	0 0874	0 1071	0 0957	0 1123
15	adhesive	0 2089	0 1670	0 1063	0 1297	0 1150	0 1355
16	adhesive	0 1962	0.1695	0 1079	0 1316	0 1167	0 1376
17	adhesive	0.1569	0 1364	0 0859	0 1054	0 0929	0 1108
18	adhesive	0 1628	0 1374	0 0862	0 1067	0 0945	0 1115

where, P_f failure load, both both interface (adhesive) and adherend
criterion type 1 $G_I + G_{II} \geq G_{IC} + G_{IIC}$, criterion type 4 $G_I + G_{II} \geq G_{IC}$
criterion type 5 $G_I + G_{II} \geq G_{IIC}$, criterion type 6 $\frac{G_I}{G_{IC}} + \frac{G_{II}}{G_{IIC}} \geq 1$
criterion type 7 . $\left(\frac{G_I}{G_{IC}}\right)^2 + \left(\frac{G_{II}}{G_{IIC}}\right)^2 \geq 1$

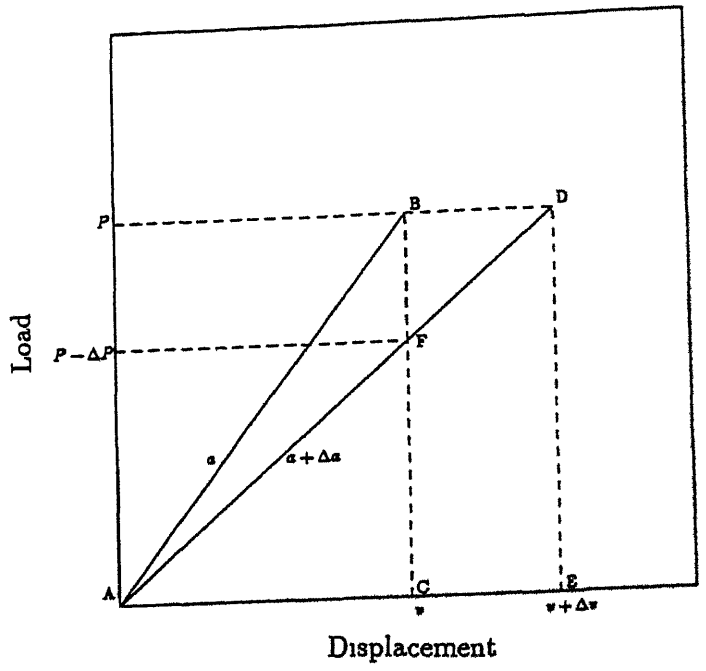

Figure 5 1 Load-displacement behaviour for a cracked body under constant load and constant displacement

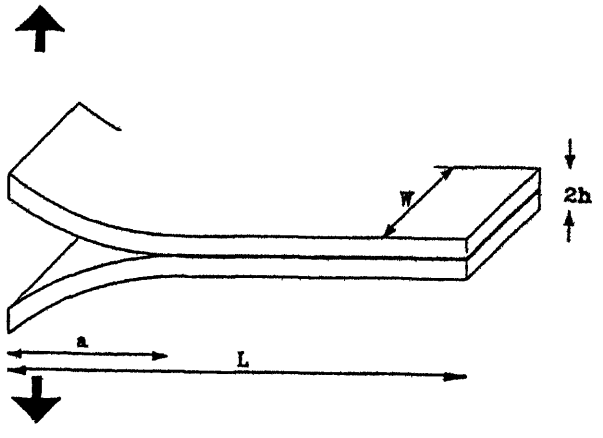

Figure 5.2 Double cantilever beam (DCB) specimen under mode I loading

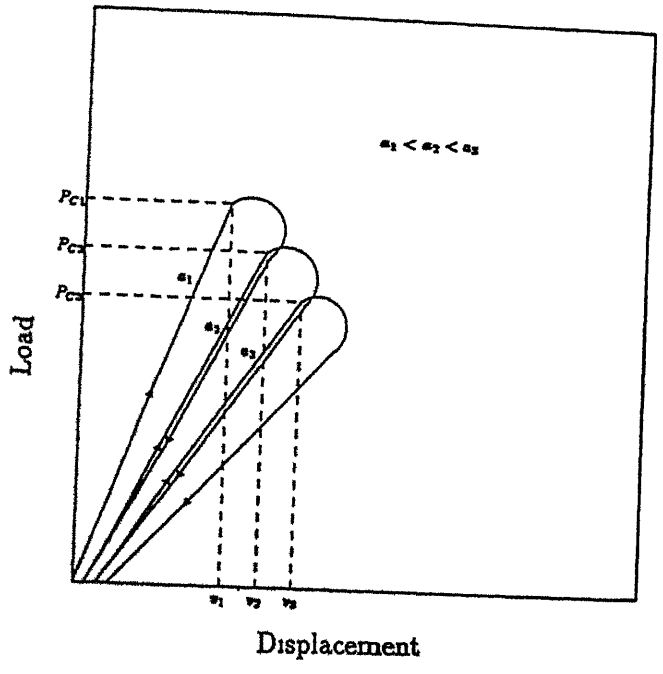

Figure 5.3: A schematic of load-displacement (crack opening displacement) responses of double cantilever beam (DCB) specimen under mode I loading

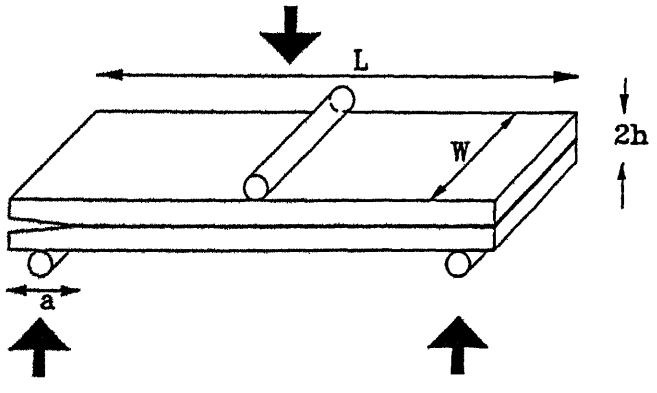

Figure 5 4: End notch flexure (ENF) specimen under mode II loading

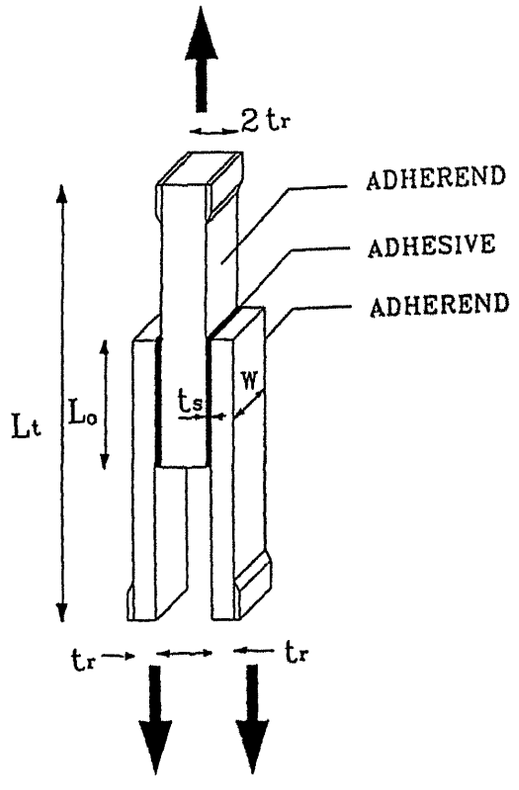

Figure 5 5 Double lap joint under tensile loading

Chapter 6

General Conclusions

In this Chapter, general conclusions, from linear elastic, elasto-plastic, elasto-visco-plastic analyses and experimental study, are listed A comparison of computation time for different analyses are made Limitations of the present work and the future scope of this work are also discussed

6.1 Results and discussion

6.1.1 Comparison of results

Execution time taken for linear elastic, elasto-plastic and elasto-visco-plastic analyses to open three pairs of nodes in the computer CONVEX C 220, are compared in Table 6 1 The starting load level, material properties, physical dimensions, mesh refinement and crack location are maintained identical for all the three analyses Adhesive and adherends are considered to be Epon VIII and CFRP laminate, respectively The non-dimensional ratios g (= G_C'/G_C), l (= L_o/L_t) and t (= t_s/t_r) are assumed to be 0 4, 1/2 and 1/5, respectively The convergence tolerance value, fracture toughness tolerance value, fracture

toughness, fluidity parameter and the flow rate function employed are 1 percent, 1 percent, 0 15 kJm^{-2}, 4 495 10^{-3}/Sec and Equation (6 2), respectively From the comparison of the results it is observed that the linear elastic analysis predicts a lower failure load as compared to both elasto-plastic and the elasto-visco-plastic analyses This might be due to the peak stresses calculated from elasto-plastic and elasto-visco-plastic analyses are reduced

$$\Phi = \left(\frac{F - \sigma_0}{\sigma_0}\right)^N - 1 \tag{6 1}$$

$$= \frac{F}{\sigma_0} \tag{6 2}$$

where, N is 1 426, σ_0 is the yield stress and the flow rule F is expressed as

$$F = \sqrt{\sigma_x^2 + \sigma_y^2 - \sigma_x\sigma_y + 3\tau_{xy}^2} \tag{6 3}$$

On the basis of elastic, elasto-plastic and elasto-visco-plastic analyses carried out, the following general conclusions are made

- The finite element approach with paired nodes modelling the crack provides a simple computational tool to predict joint failure However, fine grids near the crack-tip are necessary for accurate estimation of strain energy release rates

- The elastic analysis predicts a lower failure load as compared to the elasto-plastic and elasto-visco-plastic analyses Therefore, for a realistic analysis elasto-plastic and elasto-visco-plastic behaviour are necessary to be included

- The general computer code developed, can model fairly accurately the elastic, elasto-plastic and elasto-visco-plastic behaviour of adhesively bonded joint
- Stress distributions, along the overlap length of the single lap joint, are predicted by the present elastic and elasto-visco-plastic analysis and the results agree with those reported by Hiregoudar (1993)
- Stress distributions, along the overlap length and across the adhesive thickness of thick adherend shear test (TAST) specimen (stepped lap joint) are predicted by the elastic and elasto-visco-plastic analysis and the results agree with the those reported by Su and Mackie (1993)
- In case of single edge notch (SEN) specimen, with 2688 elements and proper mesh refinement, error estimated in the value of fracture parameter is less than 1 6 percent (as compared with close form solution)
- Strain energy release rate predicted by finite element analysis with fracture mechanics approach agreed well with the experimental result reported by Fernlund and Spelt (1991c) for cracked lap shear (CLS) specimen The difference is less than 2 7 percent
- Growth of plastic zone is influenced by the displacement boundary conditions and the size of the crack
- Cracks occurring at the edges are more critical than those at the central part of the overlap region Further, in symmetric boundary conditions the diagonally opposite cracks are equally prone to failure
- In case of composite laminates, introduction of 0° ply in the immediate neighbourhood of adhesive results in a stronger joint Further, a proper choice of layup sequence results in an efficient bonded joint
- The results obtained from parametric study are similar for linear elastic, elasto-plastic and elasto-visco-plastic analyses

- Use of adhesive of high Young's modulus, high fracture toughness and large overlap length results in a stronger bonded joint
- Use of small thickness of adhesive results in stronger bonded joint Free-edge effects are significant for joints with very thin adhesive For the analysis of bonded joints having very small adhesive thickness, more refined mesh is preferable to account for the free-edge effect
- Following fracture criterion is observed to predict bond strength better than other basic criteria (as compared with the experimental results)

$$G_I + G_{II} \geq G_{IC} + G_{IIC} \tag{6 4}$$

where G_{IC} and G_{IIC} are critical strain energy release rates in modes I and II, respectively

- The computed bond strengths employing elastic behaviour for the adhesive are in good comparison with those obtained from the experiments The difference in fracture toughness results, might be due to non-uniform thickness of the composite adherends and adhesive during specimen (joint) preparation

6.2 Limitations of the present work

In the present work, the bonded joints are modelled as two-dimensional plane stress and/or plane strain models It is assumed that the adhesive in bulk adhesive sample specimen and very thin layer of adhesive in the bonded joint, have same material properties In the non-linear analyses only adhesive material is considered to be either elasto-plastic and elasto-visco-plastic Linear elastic

fracture mechanics (LEFM) is employed The cracks are assumed to be quasi-static and through width type and the crack growth is assumed to occur along the interface of adhesive and adherend (adhesive type failure)

6.3 Suggestions for future work

Present two-dimensional finite element analysis could be extended to three-dimensional one Thumb nail cracks could be employed Cohesive and mixed (both cohesive and adhesive) type of failure could be included Similar to overlap length, area of adhesive in contact with the adherends could be a more realistic parameter to study for the prediction of strength of bonded joints Geometrical non-linearity could be included More number of experiments could help to find fracture toughnesses in pure modes (I, II and III) and mixed modes Prediction of failure load under adverse environmental conditions needs to be looked into Incorporation of non-linear fracture mechanics might be rational, particularly when the adhesive exhibit non-linear behaviour Studies on use of primers in bonded joints could help to analyse very strong adhesive joints

Table 6 1 Comparison of results obtained from linear elastic, elasto-plastic and elasto-visco-plastic analyses

crack length (mm)	failure loads in kN/mm		
	elastic	elasto-plastic	elasto-visco-plastic
0 055	13 824	14 496	14 400
0 219	11 612	11 379	11 592
0 492	10 886	10 867	10 896
execution time (Seconds) in Convex C 220			
	2 432	3 574	4 513

References

Adams, R D (1989) Strength prediction for lap joints, especially with composite adherends, a review Journal of *Adhesion*, **30** 219–242

Adams, R D (1992) Strength predicted in bonded joints current thoughts and research at the university of Bristol, U K Journal of *Adhesion*, **37** 47–50

Adams, R D and Harris, J A (1987) The influence of local geometry on the strength of adhesive joints International Journal of *Adhesion and Adhesives*, **7**(2) 69–80

Adams, R D and Mallick, V (1993) The effect of temperature on the strength of adhesively–bonded composite-aluminium joints Journal of *Adhesion*, **43** 17–33

Adams, R D and Wake, W C (1984) Structural adhesive joints in engineering Elsevier Applied Science Publishers London and New York

Adams, R D, Coppendale, J, Mallick, V and H, Al-Halman (1992) The effect of temperature on the strength of adhesive joints International Journal of *Adhesion and Adhesives*, **12**(3) 185–190

Aivazzadeh, S and Verchery, G (1986) Stress analysis at the interface adhesive joints by special finite elements International Journal of *Adhesion and Adhesives*, **6**(4) 185–188

Aivazzadeh, S, Bichara, M, Ghazal, A and Verchery, G (1988) Special mixed finite elements for interfacial stress analysis of adhesively bonded joints *Adhesively Bonded Joints Testing, Analysis and Design*, W S Johnson, Ed, ASTM STP, **981** 133–144

Allen, K W and Shanahan, M E R (1975) The creep behaviour of structural adhesive joints I Journal of *Adhesion*, **7** 161–174

Allen, K W and Shanahan, M E R (1976) The creep behaviour of structural adhesive joints II Journal of *Adhesion*, **8** 43–56

Alwar, R S and Nagaraja, Y R (1976) Elastic analysis of adhesive butt joints Journal of Adhesion, **6** 279–287

Bassani, J L and Qu, J (1989) Finite crack on bimaterial and bicrystal interfaces Journal of Mechanical Physics and Solids, **37**(4) 435–453

Bigwood, D A and Crocombe, A D (1989a) Bonded joint design analysis Adhesion – 13 Ed K W Allen, Chapter – 11, Elsevier Applied Science Publishers New York 163–187

Bigwood, D A and Crocombe, A D (1989b) Elastic analysis and engineering design formulae for bonded joints International Journal of Adhesion and Adhesives, **9**(4) 229–242

Bigwood, D A and Crocombe, A D (1990) Non-linear adhesive bonded joint design analyses International Journal of Adhesion and Adhesives, **10**(1) 31–41

Biot, M A (1954) Theory of stress–strain relations in anisotropic viscoelasticity and relaxation phenomena Journal of Applied Physics, **25**(11) 1385–1391

Bishopp, J A (1992) The chemistry and properties of a new generation of toughened epoxy matrices International Journal of Adhesion and Adhesives, **12**(3) 178–184

Broek, D (1984) Elementary Engineering Fracture Mechanics Martinus Nijhoff Publishers Boston

Brust, F W, Nakagami, M and Gilles, P (1990) Comparison of elastic–plastic fracture mechanics techniques Fracture Mechanics Tenty-first Symposium, J P Gudas, J.A Joyce and E M Hackett, Eds ASTM STP, **1074** 448–469

Carlsson, L A and Pipes, R B (1987) Experimental characterisation of advanced composite materials Prentice-Hall Inc

Carlsson, L A , Gillespie, J W (Jr) and Pipes, R B (1986) On the design and analysis of end notched specimen (ENF) specimen for mode II testing Journal of Composite Materials, **20** 594–604

Chai, H (1986) Bond thickness effect in adhesive joints and its significance for mode I interlaminar fracture of composites Composite Materials Testing and Design (Seventh Conference), J M Whitney, Ed , ASTM STP, **893** 209–231

Chai, H (1992) Experimental evaluation of mixed–mode fracture in adhesive bonds Experimental Mechanics, **32**(2) 296–303

Chai, H (1993) Observation of deformation and damage at the tip of cracks in adhesive bonds loaded in shear and assessment of a criterion for fracture International Journal of Fracture, **60**(4) 311–326

Chalkley, P D and Chiu, W K (1993) An improved method for testing the shear stress/strain behaviour of adhesives International Journal of *Adhesion and Adhesives*, **13**(4) 237–242

Chen, D and Cheng, S (1983) An analysis of adhesive–bonded single–lap joints Trans *ASME Journal of Applied Mechanics*, **50** 109–115

Chen, D and Cheng, S (1990) Stress distribution in plane scarf and butt joints Trans *ASME Journal of Applied Mechanics*, **57** 78–83

Chen, D and Cheng, S (1992) Torsional stress in tubular lap joints *International Journal Solids Structures*, **29**(7) 845–853

Cheng, S, Chen, D and Shi, Y (1991) Analysis of adhesive–bonded joints with nonidentical adherends Journal of Engineering Mechanics, **117**(3) 605–623

Cherry, B W and Ye, Y Q (1992) The behaviour of high–temperature anaerobic adhesives International Journal of *Adhesion and Adhesives*, **12**(3) 206–210

Choi, H J and Thangjitham, S (1993) Thermally–induced interlaminar crack–tip singularities in laminated anisotropic composites International Journal of Fracture, **60**(4) 349–361

Conley, K M, Gu, W, Ritter, J E and Lardner, T J (1992) Observations on finger–like crack growths at a urethane acrylate/glass interface Journal of *Adhesion*, **39** 173–184

Conley, K M, Ritter, J E and Lardner, T J (1992) Subcritical crack growth along epoxy/glass interfaces Journal of material Research, 7(9) 2621–2629

Crocombe, A D and Bigwood, D A (1992) Development of full elasto–plastic adhesive joint design analysis Journal of *Strain Analysis*, **27**(4) 211–218

Crocombe, A D and Evan, I E J (1988) The interaction of adhesive joint strength of adherend cladding Journal of *Adhesion*, **26** 199–213

Crocombe, A D, Bigwood, D A and Richardson, G (1990) Analysing structural adhesive joints for failure International Journal of *Adhesion and Adhesives*, **10**(3) 167–178

Crompton, J S and Clark, J D (1989) Finite element modelling applied to crack propagation studies in bonded components *Adhesion - 13* Ed K W Allen, Chapter-12, Elsevier Applied Science Publishers New York 188–200

Czarnocki, P and Piekarski, K (1986) Non-linear numerical stress analysis of a symmetric adhesive bonded lap joint International Journal of *Adhesion and Adhesives*, **6**(3) 157–160

Davies, P, Kausch, H H, Williams, J G and Kinloch, A J (1992) Round-robin interlaminar fracture testing of carbon-fibre-reinforced epoxy and PEEK composites Composite Structures, **43**(2) 129–136

Davies, R and Khalil, A A (1990) Design and analysis of bonded double containment corner joints International Journal of *Adhesion and Adhesives*, **1**(1) 25–30

Devitt, D F, Schapery, R A and Bradley, W L (1980) A method for determining the mode I delamination fracture toughness of elastic and viscoelastic composite materials Journal of Composite Materials, **14** 270–285

Dorn, L and Weiping, L (1993) The stress state and failure properties of adhesive-bonded plastic/metal joints International Journal of *Adhesion and Adhesives*, **13**(1) 21–31

Dung, N L (1992) Three-dimensional void growth in plastic materials Mechanics Research Communications, **19**(3) 227–235

Edde, F and Verreman, Y (1992) On the fracture parameters in a clamped cracked lap shear adhesive joint International Journal of *Adhesion and Adhesives*, **12**(1) 43–48

Edlund, U and Warbring, A (1990) Analysis of elastic and elastic-plastic adhesive joints using a mathematical programming approach Computer Methods in Applied Mechanics and Engineering, **78** 19–47

Felippa, C A (1975) Solution of linear equations with skyline stored symmetric matrix Computers and Structers, **5**(1) 13–28

Fernlund, G and Spelt, J K (1991a) Analytical method for calculating adhesive joint fracture parameters Engineering Fracture Mechanics, **40**(1) 119–132

Fernlund, G and Spelt, J K (1991b) Failure load prediction of structural adhesive joints part 1. Analytical method International Journal of *Adhesion and Adhesives*, **11**(4) 213–220

Fernlund, G and Spelt, J K (1991c) Failure load prediction of structural adhesive joints part 2 experimental study International Journal of Adhesion and Adhesives, **11**(4) 221–227

Findlater, D (1987) A preliminary design approach for adhesively bonded joints International Journal of Adhesion and Adhesives, **7**(3) 129–134

Fujii, T (1993). Dynamic response of sandwich beams with an adhesive damping layer (general Maxwell method for a viscoelastic adhesive layer) International Journal of Adhesion and Adhesives, **13**(3) 201–209

Gilchrist, M D and Smith, R A (1993) Fatigue growth of cohesive defects in T-peel joints Journal of Adhesion, **42** 179–190

Goland, M and Reissner, E (1944) The stresses in cemented joints Trans ASME Journal of Applied Mechanics, **11**(1) A17–A27

Groth, H L (1986) Calculation of stresses in bonded joints using the substructuring technique International Journal of Adhesion and Adhesives, **6**(1) 31–35

Groth, H L (1988a) Prediction of failure loads of adhesive joints using the singular intensity factor Fracture Mechanics Eighteenth Symposium, D T Read and R P Reed, Eds , ASTM STP, **945** 278–284

Groth, H L (1988b) A test specimen with constant stress intensity factor Adhesively Bonded Joints Testing, Analysis and Design, W S Johnson, Ed , ASTM STP, **981** 98–104

Groth, H L (1990) Viscoelastic and viscoplastic stress analysis of adhesive joints International Journal of Adhesion and Adhesives, **10**(3) 207–213

Groth, H L and Brottare, I (1988) Evaluation of stress intensity factors in elastic–plastic materials Journal of Testing and Evaluation, **16**(3) 291–297

Groth, H L and Brottare, I (1989) Apparent stiffness of a butt joints with a thick adhesive layer and elastic–plastic adhesives Journal of Testing and Evaluation, **17**(2) 131–134

Groth, H L and Nordlund, P (1991) Shape optimization of bonded joints International Journal of Adhesion and Adhesives, **11**(4) 204–211

Habib, M , Aivazzadeh, S and Verchery, G (1988) Edge effect analysis in adhesively bonded composite tubes using axisymmetric interface elements Proceedings International Conference Southampton, on Computer Aided Desi Composite Material Technology, Eds C A Brebbia, W P deWilde and W R 415–428

Hanneman, S E and Kınra, V K (1992a) A new technique for ultrasonic nondestructive evaluation of adhesive joints Part I theory Experimental Mechanics, **32**(2) 323–331

Hanneman, S E and Kınra, V K (1992b) A new technique for ultrasonic nondestructive evaluation of adhesive joints Part II experiment Experimental Mechanics, **32**(2) 332–339

Harj-Rabab, Y, Aıvazzadah, S and Verchery, G (1990) Edge effect analysis and influence of defects in adhesively bonded composite joints using interface finite elements Development and Design with Advanced Materials, Eds G C Sih, S V Hoa and J J Pindera, Elsevier Science Publishers B V, The Netherlands 129–136

Harris, J A and Adams, R D (1985) An assessment of the impact performance of bonded joints for use in high energy absorbing structures Proceedings of the Institution of Mechanical Engineers, **199**(C2) 121–131

Hart-Smith, L J (1973) Adhesive-bonded double-lap joints NASA Technical Report, CR 112235

Hart-Smith, L J (1981) Stress analysis a continuum mechanics approach Developments in Adhesives–2, Ed A J Kinloch, Applied Science Publishers London

Hashim, S A, Cowling, M J and Winkle, I E (1990) Design and assessment methodologies for adhesively bonded structural connections International Journal of Adhesion and Adhesives, **10**(3) 139–145

Hattori, T (1991) A stress–singularity–parameter approach for evaluating the adhesive strength of single–lap joints JSME International Journal Series I, **34**(3) 326–331

Hattori, T, Sakata, S and Murakami, G (1989) A stress singularity parameter approach for evaluating the interfacial reliability of plastic encapsulated LSI devices Journal of Electronic Packaging, **111** 243–248

Henriksen, M (1984) Nonlinear viscoelastic stress analysis – a finite element approach Computers and Structers, **18**(1) 133–139

Hiregoudar, S (1993) Viscoplastic and geometric nonlinear finite element analysis of adhesively bonded lap joint M Sc Thesis Report, Dept of Civil Engineering, Indian Institute of Science, Bangalore

Ikegami, K, Takeshita, T, Mastruo, K and Sugibayashi, T (1990) Strength of adhesively bonded scarf joints between glass-reinforced plastics and metals International Journal of Adhesion and Adhesives, **10**(3) 199–206

Imanaka, M, Kishimoto, W, Okita, K, Nakayama, H and Nagai, H (1989) Fatigue life estimation of adhesive bonded shaft joints *International Journal of Fracture*, **41** 223–234

Ishikawa, H, Yuuki, R, Chung, N Y and Nakano, S (1991) Mixed mode fracture criteria on adhesive joints Proceedings of International Symposium on Mixed-Mode Fracture and Fatigue at *Vienna* AUSTRIA, during July 15–19, 1991

Janardhana, M N, Brown, K C, Jones, R and Paul, J (1986) Effect of debonding adhesively bonded composite to metal joints in compression *Composite Structures*, **5**(1) 1–14

Jeandrau, J P (1986) Intrinsic mechanical characterization of structural adhesives *International Journal of Adhesion and Adhesives*, **6**(4) 229–231

Jeandrau, J P (1991) Analysis and design data for adhesively bonded joints *International Journal of Adhesion and Adhesives*, **11**(2) 71–79

Jiao, D and Rose, J L (1991) An ultrasonic interface layer model for bond evaluation Journal of *Adhesion Science and Technology*, **5**(8) 631–646

Johnson, W S (1987) Stress analysis of the cracked-lap-shear specimen An ASTM round-robin Journal of Testing and Evaluation, **15**(6) 303–324

Jones, R M (1975) Mechanics of Composite Materials Scripta Book Comapany Washington D C

Kairouz, k C and Matthews, F L (1990) Mechanisms of failure in bonded CFRP single lap joints with different stacking sequences Proceedings of the Institution of Mechanical Engineers, FRC' (1990), Fourth International Conference, C400/014 47–59

Kanchi, M B, Zienkiewicz, O C and Owen, D R J (1978) The visco-plastic approach to problems of plasticity and creep involving geometrical nonlinear effects *International Journal for Numerical Methods in Engineering*, **12** 169–181

Keary, P E, Ilcewicz, L B, Shaar, C and Trostle, J (1985) Mode I interlaminar fracture toughness of composites using slender double cantilever beam specimens Journal of *Composite Materials*, **19** 154–176

Khalil, A A and Bayoumi, M R (1991) Effect of loading rate on fracture toughness of bonded joints *International Journal of Adhesion and Adhesives*, **11**(1) 25–29

Kim, K S, Kim, W T, Lee, D G and Jun, E J (1992) Optimal tubular adhesive-bonded lap joint of the carbon fiber epoxy composite shaft Composite *Structures*, **21**(3) 163–176

Krenk, S (1992) Energy release rate of symmetric adhesive joints Engineering Fracture Mechanics, **43**(4) 549–559

Lee, A W and Selby, J S (1992) Adhesive selection by means of the pal program Computerisation and Networking of Materials Databases Third Volume, T I Barry and K W Reynard, Eds, *ASTM STP*, **1140**

Lee, R J, Davidson, R and McCarthy, J C (1989) Composite to metal joining for transport application *Adhesion* – 13 Ed K W Allen, Chapter–10, Elsevier Applied Science Publishers New York 142–162

Liechti, K M and Chai, Y S (1991) Biaxial loading experiments for determining interfacial fracture toughness *Trans ASME Journal of Applied Mechanics*, **58** 680–687

Long, R S (1991) Static strength of adhesively bonded ARALL–1 joints *Journal of Composite Materials*, **25** 391–415

Mackie, R I and Vardy, A E (1990) Applying the coin–tap test to adhesives in civil engineering a numerical study *International Journal of Adhesion and Adhesives*, **10**(3) 215–220

Mall, S and Johnson, W S (1986) Characterization of mode I and mixed–mode failure of adhesive bonds between composite adherends *Composite Materials Testing and Design (Seventh Conference)*, J M Whitney, Ed, ASTM STP, **893** 322–334

Mall, S and Ramamurthy, G (1989) Effect of bond thickness on fracture and fatigue strength of adhesively bonded composite joints *International Journal of Adhesion and Adhesives*, **9**(1) 33–37

Marcolefas, S, Kostopoulos, V and paipetis, S A (1991) Non–linear analysis of a metal–to–composite scarf joint *International Journal of Mechanical Science*, **33**(12) 961–973

Mecklenburg, M F, Arah, C O, McNamara, D, Hand, H and Joyce, J A (1990) Adhesive fracture testing *Fracture Mechanics Tenty-first Symposium*, J P Gudas, J A Joyce and E M Hackett, Eds *ASTM STP*, **1074** 307–321

Miskioglu, I, Villmann, C R, Pawloski, J S and Pariseau, D (1991) A photoelastic and FEM analysis of interfacial crack propagation *Experimental Mechanics*, **31** 135–139

Munz, D and Yang, Y Y (1992) Stress singularities at the interface in bonded dissimilar materials under mechanical and thermal loading *Trans ASME Journal of Applied Mechanics*, **59** 857–861

Nagaraja, Y N and Alwar, R S (1980) Viscoelastic analysis of an adhesive-bonded plane lap joint Computers and Structers, **11** 621–627

Needleman, A (1990) Analysis of interfacial failure Applied Mechanics Review, **43**(5) S274–S275

Ojalvo, I U and Eidinoff, H L (1978) Bond thickness effects upon stresses in single-lap adhesive joints *AIAA Journal*, **16**(3) 204–211

Owen, D R J and Hinton, E (1980) Finite elements in plasticity Pineridge Press, Swansea U K

Parker, B M (1990) The strength of bonded carbon fibre composite joints exposed to high humidity International Journal of Adhesion and Adhesives, **10**(3) 187–191

Parker, B M (1993) Environmental durability of aluminium joints with different pretreatments International Journal of Adhesion and Adhesives, **13**(1) 47–51

Pilarski, A and Rose, J L (1988) A transverse-wave ultrasonic oblique-incidence technique for interfacial weakness detection in adhesive bonds Journal of Applied Physics, **63**(2) 300–307

Pindera, J T and Wang, G (1990) Criticality of local three dimensional stresses on a symmetric adhesive bonded joint Development and Design with Advanced Materials, Eds G C Sih, S V Hoa and J J Pindera, Elsevier Science Publishers B V 119–128

Qu, J and Bassani, J L (1989) Crack on bimaterial and bicrystal interfaces Journal of Mechanical Physics and Solids, **37**(4) 417–433

Qu, J and Bassani, J L (1993) Interface fracture mechanics for anisotropic materials Trans ASME Journal of Applied Mechanics, **60** 422–431

Qu, J and Li, Q (1991) Interfacial dislocation and its applications to interface cracks in anisotropic bimaterials Journal of Elasticity, **26** 169–195

Ramamurthy, T S and Rao, A K (1984) Analysis of bonded joints with arbitrary adherend shapes and adhesive non-linearities Journal of the Aeronautical Society of India, **36**(1) 29–36

Rao, M D and Crocker, M J (1990) Analytical and experimental study of the vibration of bonded beams with a lap joint Trans ASME Journal of Vibrations and Acoustics, **112** 444–451

Ratwani, M M and Kan, H (1986) Analysis of delamination propagation in composite layer of metal-to-composite stepped-lap joints Composite Materials Testing and Design (Seventh Conference), J M Whitney, Ed, ASTM STP, **893** 308–321

Ratwani, M M, Kan, H P and Liu, D D (1982) Time-dependent adhesive behavior effects in a stepped lap joint *AIAA Journal*, **20**(5) 734–736

Reddy, J N and Roy, S (1988) Non-linear analysis of adhesively bonded joints International Journal of Non-Linear Mechanics, **23**(2) 97–112

Richardson, G, Crocombe, A D and Smith, P A (1993) A comparison of two- and three-dimensional finite element analyses of adhesive joints International Journal of Adhesion and Adhesives, **13**(3) 193–200

Ritter, J E and Conley, K (1992) Moisture-assisted crack propagation at polymer/glass interfaces International Journal of Adhesion and Adhesives, **12**(4) 245–250

Rossettos, J N and Zang, E (1993) On the peak shear stress in adhesive joint with voids Trans ASME Journal of Applied Mechanics, **60** 559–560

Roy, S and Reddy, J N (1988a) Finite-element models of viscoelasticity and diffusion in adhesively bonded joints International Journal for Numerical Methods in Engineering, **26** 2531–2546

Roy, S and Reddy, J N (1988b) A finite element analysis of adhesively bonded composite joints with moisture diffusion and delayed failure Computers and Structers, **29**(6) 1011–1031

Rybicki, E F and Kanninen, M F (1977) A finite element calculation of stress intensity factors a modified crack closure integral Engineering Fracture Mechanics, **9** 931–938

Sawa, T and Kobayashi, T (1988) The strength of joints combining an adhesive with a bolt Journal of Adhesion, **25** 269–280

Sawa, T, Ishikawa, H and Muto, K (1992) The strength of joints combining adhesives with bolts JSME International Journal Series I, **35**(1) 38–44

Sawa, T, Temma, K and Ishikawa, H (1989) Three-dimensional stress analysis of adhesive butt joints of solid cylinders subjected to external tensile loads Journal of Adhesion, **31** 33–43

Sawa, T, Temma, K and Tsunoda, Y (1989) Axisymmetric stress analysis of adhesive butt joints of dissimilar solid cylinders subjected to external tensile loads International Journal of Adhesion and Adhesives, **9**(3) 161–169

Schapery, R A (1984) Correspondence principles and a generalized J integral for large deformation and fracture analysis of viscoelastic media International Journal of Fracture, **25** 195–223

Sen, J K and Jones, R M (1980a) Stresses in double-lap joints bonded with a viscoelastic adhesive part I theory and experimental corroboration *AIAA Journal*, **18**(10) 1237–1244

Sen, J K and Jones, R M (1980b) Stresses in double-lap joints bonded with a viscoelastic adhesive part II parametric study and joint design *AIAA Journal*, **18**(11) 1376–1382

Sethuraman, R and Maiti, S K (1989) Finite element analysis of doubly bonded crack-stiffened panels under mode I or mode II loading Engineering Fracture Mechanics, **34**(2) 465–475

Su, N and Mackie, R I (1993) Two-dimensional creep analysis of structural adhesive joints International Journal of *Adhesion and Adhesives*, **13**(1) 33–40

Su, N, Mackie, R I and Harvey, W J (1992) The effects of aging and environment on the fatigue life of adhesive joints International Journal of *Adhesion and Adhesives*, **12**(2) 85–93

Suo, Z (1990) Failure of brittle adhesive joints *Applied Mechanics Review*, **43**(5) S276–S279

Temma, K, Sawa, T and Iwata, A (1990) Two-dimensional stress analysis of adhesive butt joints subjected to cleavage loads International Journal of *Adhesion and Adhesives*, **10**(4) 285–293

Temma, K, Sawa, T and Tsunoda, Y (1990) Three-dimensional stress analysis of adhesive butt joints with disbonded areas and spew fillets International Journal of *Adhesion and Adhesives*, **10**(4) 294–300

Temma, K, Sawa, T, Uchida, H and Nakano, Y (1991) A two-dimensional stress analysis of butt adhesive joints having a circular hole defect in the adhesive subjected to external bending moments Journal of *Adhesion*, **33** 133–147

Thomsen, O T (1992) Elasto-static and elasto-plastic stress analysis of adhesive bonded tubular lap joints Composite Structures, **21**(4) 249–259

Thomson, R B and Thomson, D O (1991) Past experiences in the development of tests for adhesive bond strength Journal of Adhesion Science and Technology, **5**(8) 683–599

Tiwari, A, Hienneke, I, Edmund, G and Duke, J C (1991) Acousto-ultrasonic(AU) technique for assuring adhesive bond quality Journal of Adhesion, **34** 1–15

Volkerson, O (1938) Rivet strength distribution in tensile stressed rivet joints with butt strap cross-section Luftahforschung, **15** 41–47

Wang, A S D and Crossman, F W (1982) Fracture mechanics of sub-laminate cracks Technical Report F 49620-79-C-0206, AFOSR, Drexel Univ, Philadelphia

Wassell, G C, Clark, J D, Crompton, J S and Dickson, R F (1991) Fatigue within adhesive bonds International Journal of Adhesion and Adhesives, **11**(2) 117–120

Whitcomb, J D and Dattaguru, B (1984) User's manual for GAMNAS-Geometrical and Material Nonlinear Analysis of Structures NASA Technical Memorandum, **85734**

Whitcomb, J D and Woo, K (1993) Analysis of debond growth in tubular joints subjected to tension of flexural loads Computers and Structers, **46**(2) 323–329

Wilkins, D J, Eisenmann, J R, Camin, R A, Margolis, W S and Benson, R A (1982) Characterizing delamination growth in graphite epoxy Characterizing Delamination Growth in Graphite Epoxy, K L Reifsnider, Ed, ASTM STP, **775** 168–183

Wingfield, J R J (1993) Treatment of composite surfaces for adhesive bonding International Journal of Adhesion and Adhesives, **13**(3) 151–156

Yadagiri, S, Reddy, C P and Reddy, T S (1987) Viscoelastic analysis of adhesively bonded joints Computers and Structers, **27**(4) 445–454

Yamada, Y, Yoshimura, N and Sakuri, T (1968) Plastic stress-strain matrix and its application for the solution of elastic-plastic problems by the finite element method International Journal of Science, **10** 343–354

Zenkert, D (1991) Strength of sandwich beams with interface debondings Composite Structures, **17**(4) 331–350

Zienkiewicz, O C and Cormeau, I C (1974) Visco-plasticity-plasticity and creep in elastic solids – A unified numerical solution approach International Journal for Numerical Methods in Engineering, **8** 821–845

Zienkiewicz, O C and Taylor, R L (1989) The finite element method, volume 1 McGraw-Hill Book Co New York, fourth edition

Zienkiewicz, O C and Taylor, R L (1991) The finite element method, volume 2 McGraw-Hill Book Co New York, fourth edition

Zienkiewicz, O C, Owen, D R J and Cormeau, I C (1974) Analysis of viscoplastic effects in pressure vessels by the finite element method Nuclear Engineering and Design, **28** 278–288

Zienkiewicz, O C, Valliappan, S and King, I S (1969) Elasto-plastic solutions of engineering problems 'initial stress', finite element approach International Journal for Numerical Methods in Engineering, **1** 75–100